

Physics is the marriage between reality and imagination -

Anyons are attracting a lot of recognition in the scientific community – from condensed matter to quantum information. Such quasiparticles have the remarkable features of carrying fractional charges and exhibiting fractional statistics. Craze to use anyons in building topological quantum computers is one of the active current research directions. This thesis investigates anyons in strongly correlated quantum many-body systems on lattices having topological orders including fractional quantum Hall systems, fractional Chern insulators, and Kitaev's toric code model.

You will not get the second chance to create the first impression -

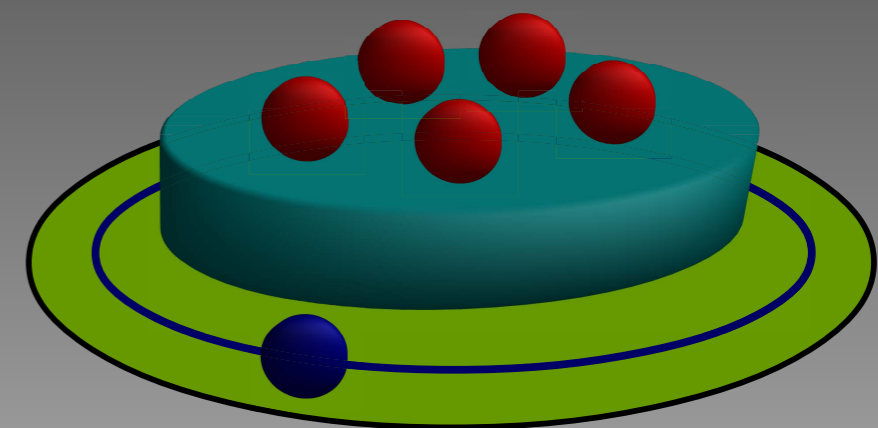
The author pursued Bsc. in Physics (Hons.) from Ramakrishna Mission Residential College, Narendrapur (Autonomous) under Calcutta University in 2011-2014. He completed Msc. from Indian Institute of Technology, Kanpur in 2014-2016. This book is his PhD thesis at Max-Planck-Institut für Physik Komplexer Systeme under Technische Universität Dresden, Germany in 2016-2020.

*I, a universe of atoms, an atom in the universe
- Richard P. Feynman*

Sourav Manna

Quasiparticles in Quantum Many-Body Systems

Quasiparticles in Quantum Many-Body Systems



Any **Anyon** Anywhere? Anyone?

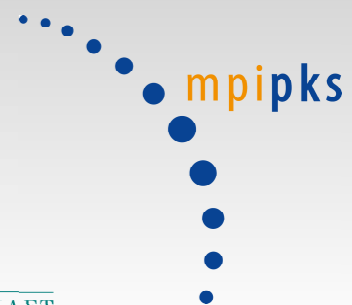
Sourav Manna



TECHNISCHE
UNIVERSITÄT
DRESDEN



MAX-PLANCK-GESELLSCHAFT



**Max-Planck-Institut für Physik
Komplexer Systeme**

Technische Universität Dresden

**Quasiparticles in Quantum
Many-Body Systems**

DISSERTATION

zur Erlangung des akademischen Grades

Doctor of Philosophy

(Ph.D.)

vorgelegt

dem Bereich Mathematik und Naturwissenschaften

von

SOURAV MANNA

geboren am 21st September in 1993 in India

*Die Dissertation wurde in der Zeit von August/2016 bis
May/2020 angefertigt*



**TECHNISCHE
UNIVERSITÄT
DRESDEN**



MAX-PLANCK-GESELLSCHAFT



Eingereicht am 06.05.2020

Betreuer : 1. Prof. Dr. Anne E. B. Nielsen
 2. Prof. Dr. Roderich Moessner

Vorsitzender : 1. Prof. Dr. Kai Zuber

Gutachter : 1. Prof. Dr. Roderich Moessner
 2. Prof. Dr. Jan C. Budich
 3. Prof. Dr. Simon Trebst

Rigorosum : 1. Prof. Dr. Holger kantz
 2. Prof. Dr. Carsten Timm

Protokollant : 1. Dr. Aniket Patra

Verteidigt am 28.07.2020

*Dedicated to my beloved mother and younger
sister*

Biographical Sketch

” *Education is the manifestation of the perfection already in man. Religion is the manifestation of the Divinity already in man.*

— **Swami Vivekananda**

Sourav Manna graduated from Ramakrishna Mission Residential College, Narendrapur (Autonomous) under Calcutta University, India in 2014 with a BSc. in physics Honors. He subsequently joined Indian Institute of Technology Kanpur from 2014-2016 and completed his MSc. degree. Thereafter he joined Max-Planck-Institut für Physik Komplexer Systeme and Technische Universität Dresden in Dresden, Germany as a PhD fellow. His next destination to pursue his postdoctoral studies is Université de Sherbrooke in Québec, Canada where he has been selected for the prestigious international prize postdoctoral fellowship in quantum science and technology at Institut Quantique. He was awarded Prof. K. P. Ghosh memorial prize for securing first class first position in BSc. with physics Honors in 2014. He was recognized as a Jagadis Bose National Science Talent Search scholar in 2011. He was awarded DST-INSPIRE scholarship from 2011-2016.

Acknowledgments

” *A journey of a thousand miles begins with a single step.*

— **Lao Tzu**

Oops!!! I have arrived at the end of my doctoral studies and am writing thesis—hard to believe!!! I feel like yesterday that I stepped to MPIPKS, Dresden in 2016, August on a sunny day for the first time. Indeed it is unbelievable that all these years of incredible experiences are already behind me. I realize what I am today, from my personal to professional life, is due to the constant supports, inspiring discussions and endless love of some truly remarkable people. My dissertation is the opportunity to thank and to express my sincere gratitude to some of these remarkable persons, together with the words ‘as one journey ends, so another begins’. Onwards still!

First and foremost, I owe an immense debt of gratitude to my doctoral supervisor, Dr. Anne E. B. Nielsen, for her guidance through my graduate years, for introducing me to the exciting field of anyons in strongly correlated quantum many-body systems, and for her kind and generous supports all the time. Right from the time she took me on as a graduate student to the patience she showed while I was floundering at research during my first year. I had the privilege of learning from watching Anne in making concrete inevitable arguments unlike the hand-waving, uncertain and jaded arguments elsewhere.

I convey my heartfelt gratitude to all my collaborators without whom this thesis is incomplete. Dr. Julia Wildeboer helped me a lot in learning C++ and in introducing me the field of frustrated quantum magnets, Prof. German Sierra shared his vast knowledge in improving my concepts in spin models and the fractional quantum Hall systems, Prof. Bitan Roy provided me the golden opportunity to work with him and to learn from him the field of topological materials, and Dumitru Calugaru, Biplab Pal, Wei Wang, Callum Duncan discussed many aspects with me on our collaborative projects. Special thanks goes to N. S. Srivatsa and Dr. Snehasish Nandy. You guys are more my friends than my collaborators. I owe you a lot for our precious time from sitting down to do calculations to plan sudden parties and weekend-tours. You guys were with me all the time from fundamental discussions to technical details. I really enjoyed a lot in working with you and a big thanks to you all.

I express my cordial thanks to all the MPIPKS members, for giving me such an outstanding environment of doing research and of flourishing myself, including our formal and current group members with whom I learned a lot during the meetings, my office-mates particularly Dr. Lucas Wetzel and Dr. Bernhard Frank for giving me a great company during the office hours, our visitors program-administrative staff-IT department

especially Dr. Regine Schuppe, Dr. Hubert Paulus and Dr. Thomas Muller for helping me from finding my apartment to taking care of my travels—both within and outside Europe, to maintaining the computing facilities. I owe a tremendous debt of gratitude to Prof. Roderich Moessner for considering my application when I first emailed him with my will of joining MPIPKS as a PhD fellow and for giving me the opportunity to visit here as an applicant for which I am here today. A big hug goes to all my MPIPKS friends and colleagues—both formal and current. There are too many to name but you guys know who you are. In particular I convey a lot of thanks to Sebastian Mantilla and Daniele Trapin with whom many of my days became joyful. After the whole week of hard-work, my weekend became refreshing and I gathered a lot of energy to work hard in the next days with the homemade weekend-parties which started with Sajal K. Giri who is my all-time partner in parties and has an immense importance in my life—from research motivations to personal, Himangsu P. Goswami, Satya N. Guin from MPICPFS Dresden, and Abhisek Nag from TU Dresden. I spent some of the most precious moments in my life with you guys from fighting on physics problems to sharing happiness and sad moments of my life with the 'Cheers' of our wine glasses and the smoke-rings of cigarettes and especially Sajal, I owe you a lot. I am very thankful to IFW, Dresden for giving me the chance in joining the ongoing classes there and to TU Dresden for giving me the opportunity to supervise the Bachelor students there in one semester Experimental course where I spent joyful moments with Yuliia Tymoshenko.

I am highly obliged to Prof. Didier Poilblanc at Laboratoire de Physique Théorique, Toulouse in France and to Prof. Ady Stern and Prof. David Mross at Weizmann Institute of Science in Israel for giving me the great opportunities of visiting there where I discussed my research interests and came to know about theirs.

I convey my sincere acknowledgment to all my professors and teachers from my Bachelors, Masters and High Schools, where the base of my interests in physics were endowed. I thank all my friends, colleagues and seniors-juniors there for your endless support in any occasion and for being with me in my triumph and disaster. Again I will not make any list of names but you guys know whom I am talking about. Especially a big hug goes to Sagar Paul, Pratap C. Adak, and Satyaki Sasmal—my partners in chess. I would like to convey my sincere obligation to Swami Suparnananda Maharaj (*Satya Da*), who is one of the greatest human being and personalities I have ever met.

I would like to thank my parents Lakshmi Kanta Manna (*baba*) and Pinku Rani Manna (*ma*) and my sister Shreyasi Manna (*bon*) for their hard work, endless support, boundless love and innumerable sacrifices they made for my sake and which are the reasons I am able to write this thesis today. Graduate school appeared with its own bittersweet moments of ups and downs, and you have patiently stood by my side all the time and always encouraged me to achieve my goals. Everything that I am today, I owe to my parents and my sister. This dissertation is dedicated to them.

I thank all my nearest-dearest family members for their unconditional love and endless supports. I want to remember my all-time cheerful maternal uncle cum friend Santu Bera (*mama*), who sadly passed on to glory around December, 2018. You left a vacuum in my heart, *Mama*. I really miss you!

Abstract

” *The most exciting phrase to hear in science, the one that heralds new discoveries, is not 'Eureka!' but 'That's funny...'*

— **Isaac Asimov**

Topologically ordered phases flaunt a cornucopia of intriguing phenomena that cannot be perceived in the conventional phases including the most striking property of hosting anyon quasiparticles having fractional charges and fractional statistics. Such phases were discovered with the remarkable experiment of the fractional quantum Hall effect and are drawing a lot of recognition.

Realization of these phases on lattice systems and study of the anyon quasiparticles there are important and interesting avenue to research in unraveling new physics, which can not be found in the continuum, and this thesis is an important contribution in that direction. Also such lattice models hosting anyons are particularly important to control the movement of anyons while experimentally implemented with ultra-cold atoms in optical lattices. We construct lattice models by implementing analytical states and parent Hamiltonians on two-dimensional plane hosting non-Abelian anyons, which are proposed candidates for quantum computations. Such lattice models are suitable to create both quasiholes and quasielectrons in the similar way and thereby avoiding the singularity problem for the quasielectrons in continuum. Anyons in these models are found to be well-screened with proper charges and right statistics. Going beyond two dimensions, we unravel the intriguing physics of topologically ordered phases of matter in fractional dimensions such as in the fractal lattices by employing our model constructions of analytical states and parent Hamiltonians there. We find the anyons to be well-screened with right charges and statistics for all dimensions. Our work takes the first step in bridging the gap between two dimensions and one dimension in addressing topological phases which reveal new physics. Our constructions are particularly important in this context since such lattices lack translational symmetry and hence become unsuitable for the fractional Chern insulator implementations. The special features of topologically ordered phases make these difficult to probe and hence the detection of topological quantum phase transitions becomes challenging. The existing probes suffer from shortcomings up to a large extent and therefore construction of new type of probes become important and are on high demand. The robustness of anyon properties draw our attention to propose these as detector of topological quantum phase transitions with significant advantages including the facts that these are numerically cheaper probes and are independent of the boundary conditions. We test our probe in three different examples and find that simple properties like anyon charges detect the transitions.

Zusammenfassung

“ *When you change the way you look at things, the things you look at change.*

— **Max Planck**

Topologisch geordnete Phasen extravagieren ein Füllhorn faszinierender Phänomene, die in den herkömmlichen Phasen nicht wahrgenommen werden können, einschließlich der auffälligsten Eigenschaft, Quasiteilchen mit fraktionierten Ladungen und fraktionierten Statistiken aufzunehmen. Solche Phasen wurden mit dem bemerkenswerten Experiment des fraktionierten Quanten-Hall-Effekts entdeckt und finden viel Anerkennung.

Die Realisierung dieser Phasen auf Gittersystemen und die Untersuchung der Anyon-Quasiteilchen sind wichtige und interessante Wege zur Erforschung der Entschlüsselung neuer Physik, die im Kontinuum nicht zu finden sind, und diese These ist ein wichtiger Beitrag in diese Richtung. Auch solche Gittermodelle, die Anyons enthalten, sind besonders wichtig, um die Bewegung von Anyons zu steuern, während sie experimentell mit ultrakalten Atomen in optischen Gittern implementiert werden. Wir konstruieren Gittermodelle, indem wir analytische Zustände und Eltern-Hamiltonianer auf einer zweidimensionalen Ebene implementieren, die nicht-abelsche Anyons enthält, die als Kandidaten für Quantenberechnungen vorgeschlagen werden. Solche Gittermodelle sind geeignet, sowohl Quasi-Löcher als auch Quasielektronen auf ähnliche Weise zu erzeugen und dadurch das Singularitätsproblem für die Quasielektronen im Kontinuum zu vermeiden. Jeder in diesen Modellen wird mit angemessenen Gebühren und richtigen Statistiken gut überprüft. Über zwei Dimensionen hinaus enträtseln wir die faszinierende Physik topologisch geordneter Phasen der Materie in fraktionierten Dimensionen wie in den fraktalen Gittern, indem wir dort unsere Modellkonstruktionen von analytischen Zuständen und Eltern-Hamiltonianern verwenden. Wir finden, dass die Anyons mit den richtigen Gebühren und Statistiken für alle Dimensionen gut überprüft werden. Unsere Arbeit macht den ersten Schritt, um die Lücke zwischen zwei Dimensionen und einer Dimension zu schließen und topologische Phasen anzugehen, die neue Physik enthüllen. Unsere Konstruktionen sind in diesem Zusammenhang besonders wichtig, da solche Gitter keine Translationssymmetrie aufweisen und daher für die fraktionierten Chern-Isolatorimplementierungen ungeeignet werden. Die besonderen Merkmale topologisch geordneter Phasen machen es schwierig, diese zu untersuchen, und daher wird die Detektion topologischer Quantenphasenübergänge schwierig. Die vorhandenen Sonden leiden in hohem Maße unter Mängeln, weshalb die Konstruktion neuer Sondenarten wichtig wird und eine hohe Nachfrage besteht. Die Robustheit der Anyon-Eigenschaften lenkt unsere Aufmerksamkeit darauf, diese als Detektor für topologische Quantenphasenübergänge mit signifikanten Vorteilen vorzuschlagen, einschließlich der Tatsache, dass dies numerisch

billigere Sonden sind und von den Randbedingungen unabhängig sind. Wir testen unsere Sonde in drei verschiedenen Beispielen und stellen fest, dass einfache Eigenschaften wie Ladungen die Übergänge erfassen.

Publications

” *Question - What is featuring a good scientist in your estimation?*
Answer - Well, I guess it requires different values but one of them I think that is very important is not to follow trends. So not to do what everybody says that one has to do but to go in different directions and so when you see that everybody is working on something, so may be turn a little bit and explore directions even though at the beginning they are not trendy, they are not what everybody is doing...

— **J. Ignacio Cirac**

List of publications covered in this thesis

[1] : Callum Duncan, **Sourav Manna** and Anne E. B. Nielsen, "Topological models in rotationally symmetric quasicrystals", *Physical Review B* **101**, 115413 (2020) [*Editors' Suggestion*]

[2] : **Sourav Manna**, N. S. Srivatsa, Julia Wildeboer and Anne E. B. Nielsen, "Quasi-particles as detector of quantum phase transitions", [submitted to *Physical Review Research* (Rapid Com.)], arXiv:1909.02046 (2019)

[3] : **Sourav Manna***, Biplab Pal*, Wei Wang* and Anne E. B. Nielsen, "Anyons and fractional quantum Hall effect in fractal dimensions", *Physical Review Research* **2**, 023401 (2020) [* authors equally contributed to this work]

[4] : **Sourav Manna**, Julia Wildeboer and Anne E. B. Nielsen, "Quasielectrons in lattice Moore-Read models", *Physical Review B* **99**, 045147 (2019)

[5] : **Sourav Manna**, Julia Wildeboer, Germán Sierra and Anne E. B. Nielsen, "Non-Abelian quasiholes in lattice Moore-Read states and parent Hamiltonians", *Physical Review B* **98**, 165147 (2018)

[6] : Julia Wildeboer, Aniket Patra, **Sourav Manna** and Anne E. B. Nielsen, "Anyonic quasiparticles of hardcore anyons", Physical Review B **102**, 125117 (2020)

[7] : **Sourav Manna** and Anne E. B. Nielsen, "Chain and ladder models with two-body interactions and analytical ground states", Physical Review B **97**, 195143 (2018)

Further publications (not covered in this thesis)

[8] : Snehasish Nandy, **Sourav Manna**, Dumitru Calugaru and Bitan Roy, "Generalized Triple-Component Fermions: Lattice Model, Fermi arcs and Anomalous Transport", Physical Review B **100**, 235201 (2019)

Contents

1	Introduction	1
1.1	Motivations	1
1.2	Thesis structure : purposes and findings	2
1.2.1	Chapter 3 : Construction of the anyonic lattice fractional quantum Hall states	2
1.2.2	Chapter 4 : Investigations of non-Abelian anyons in lattice Moore-Read models	3
1.2.3	Chapter 5 : Exploring anyons and topological order in quasicrystals and in fractal spaces	4
1.2.4	Chapter 6 : Anyonic quasiparticles from the systems of hardcore anyons	5
1.2.5	Chapter 7 : Quasiparticles as detector of topological quantum phase transitions	5
1.2.6	Chapter 8 : Constructions and investigations of the spin-1/2 chain and ladder models	6
2	Topology, Fractional Quantum Hall Effect and Anyons	7
2.1	Topological phases of matter	7
2.2	The fractional quantum Hall effect	9
2.3	Anyons	13
3	Lattice Fractional Quantum Hall States Containing Anyons	17
3.1	Conformal field theory description of the states	18
3.1.1	The free, massless boson	18
	(a). Radial quantization	19
	(b). Mode expansion	20
3.1.2	Conformal transformations and primary fields	20
3.1.3	Primary fields of the free, massless boson	21
3.2	Continuum fractional quantum Hall states	22
3.2.1	Quasielectron states and the singularity problem	24
3.3	Anyonic lattice fractional quantum Hall states	25
3.3.1	Lattice Laughlin states on a plane	26
	(a). States without anyons	27
	(b). States with anyons	28
3.3.2	Lattice Moore-Read states on a plane	29
	(a). States without anyons	29
	(b). States with non-Abelian or Ising anyons	30
	(c). States with Abelian anyons	33

3.3.3	Quasielectron states and avoiding the singularity problem	33
3.3.4	Continuum limit of the lattice states	34
3.4	Conclusions	35
4	Non-Abelian Anyons in Lattice Moore-Read Models	37
4.1	Density profiles and charges of the anyons	38
4.1.1	Density profiles of anyons	38
(a)	Charges at infinity	41
4.1.2	Charges of anyons	42
4.2	Fractional braiding statistics of anyons	43
4.2.1	Two anyons scenario	46
(a)	Berry matrix	46
(b)	Monodromy matrix	48
(c)	Aharonov-Bohm phase	48
4.2.2	Four anyons scenario	48
(a)	Berry matrix	49
(b)	Monodromy matrix	52
(c)	Aharonov-Bohm phase	53
4.3	Parent Hamiltonians	53
4.3.1	Parent Hamiltonians for the states containing quasiholes	54
(a)	Parent Hamiltonians for $\eta = 1$	54
(b)	Parent Hamiltonians for $\eta < 1$	55
4.3.2	Parent Hamiltonians for the states containing quasielectrons	57
4.4	Anyons in the Kapit-Mueller model	59
4.4.1	The Kapit-Mueller Hamiltonian	60
4.4.2	Creation of anyons in the ground state	61
4.4.3	Density profiles and charges of anyons	63
4.5	Conclusions	64
5	Anyons and Fractional Quantum Hall Physics in Quasicrystals and in Fractal Lattices	67
5.1	Quasicrystals	68
5.1.1	Examples as the Penrose tiling and the Ammann-Beenker tiling	70
5.2	Fractal lattices and fractional dimensions	70
5.2.1	Example as the Sierpinski gasket of dimension $\simeq 1.585$	72
5.3	Anyon density profiles and charges	73
5.3.1	Anyons in quasicrystals	74
5.3.2	Anyons in the Sierpinski gasket of dimension $\simeq 1.585$	74
5.3.3	Anyons in other fractal dimensions $0 < \text{dimension} \leq 2$	78
5.4	Braiding statistics of anyons	81
5.5	Parent Hamiltonians	84
5.6	Conclusions	85
6	Anyonic Quasiparticles of Hardcore Anyons	87
6.1	Model of the hardcore anyons	88
6.2	Anyon density profiles and charges	88
6.3	Braiding statistics of anyons	92

6.4	Conclusions	93
7	Quasiparticles Detect Topological Quantum Phase Transitions	95
7.1	Detection of a topological quantum phase transition in a Moore-Read state on a square lattice	98
7.1.1	Topological properties	99
7.1.2	Excess charges and the topological quantum phase transition detection	100
7.2	Detection of a topological quantum phase transition in a Moore-Read state on a fractal lattice	102
7.3	Detection of a topological quantum phase transition in an interacting Hofstadter model	103
7.3.1	Interacting Hofstadter model	103
7.3.2	Creation of anyons in the ground state	104
7.3.3	Excess charges and the topological quantum phase transition detection	105
7.4	Detection of a topological quantum phase transition in a disordered interacting Hofstadter model	107
7.5	Detection of a topological quantum phase transition in the Kitaev's toric code model	108
7.5.1	The Kitaev's toric code model	108
7.5.2	Creation of anyons in the ground state	109
7.5.3	Detection of the topological quantum phase transition	110
	(a). Case when $k = z$	112
	(b). Case when $k = y$	113
7.6	Conclusions	113
8	Spin-1/2 Chain and Ladder Models with Two-Body Interactions and Analytical Ground States	115
8.1	The two-dimensional Haldane-Shastry model	118
8.2	The one-dimensional Haldane-Shastry model	119
8.3	Two-body chain and ladder models	121
8.3.1	Symmetries	122
8.3.2	Spin-spin correlations and Renyi entropy	122
8.3.3	Small Λ limit and the decoupling of the legs	123
8.3.4	Large Λ limit and the product of singlets	124
8.4	Uniform one-dimensional spin chain	124
8.4.1	Spin-spin correlations	125
8.4.2	Renyi Entropy of order two	130
8.4.3	Strengths of the spin-spin interactions	133
	(a). Behavior for small and large λ with N fixed	133
	(b). Numerical results	134
8.4.4	Spin chains with an odd number of spins	136
8.5	Uniform ladder model	137
8.5.1	Strengths of the spin-spin interactions	137
8.5.2	Weak coupling	138
8.5.3	Spin-spin correlations	139

8.5.4	Renyi Entropy of order two	140
8.6	Conclusions	142
9	Conclusions	145
10	Future Directions	149
A	Numerical Techniques	153
A.1	Exact diagonalization	153
A.1.1	Creation of the blocks with fixed number of particles	155
(a)	Example	156
A.2	The Metropolis-Hastings Monte-Carlo technique	157
A.2.1	Algorithm	157
A.2.2	Error estimation	158
A.2.3	Example	159
(a)	Error estimation	160
B	Null Fields of the Underlying Conformal Field Theory	161
B.1	Null field $\chi^q(v)$	162
B.2	Null field $\chi^{q-1}(v)$	163
B.3	Null fields $\chi^p(v)$, $p \in \{0, 1, \dots, q-2\}$	164
C	Operators Annihilating the Lattice Moore-Read States with Quasi-holes	165
C.1	$\eta = 1$ and occupancy $n_j \in \{0, 1, 2\}$	165
C.2	$\eta = 1$ and occupancy $n_j \in \{0, 1\}$	170
C.3	Condition on η	171
D	Wavefunction in the Limit of Small Λ	175
E	Wavefunction in the Limit of Large Λ	177
F	Derivation of an Inequality	179
	Bibliography	183

Introduction

” *Imagination is more important than knowledge. Knowledge is limited. Imagination encircles the world.*

— **Albert Einstein**

Topologically ordered phases of matter [252, 251] are of immense importance, since these go beyond the description of local order parameters in conventional phases, from both fundamental theoretical slants and experimental point of view and thereby have stood up as an active research area both in theoretical grounds and in practical applications. An exotic feature of these phases is the ability to host peculiar quasiparticles, which are known as anyons exhibiting fractional charges and fractional statistics [141, 255], which are proposed potential ingredients for the fault-tolerant topological quantum computations [165, 200]. Fractional quantum Hall effect is very special in this context since it is the first experimentally realized topologically ordered phase that can host such exotic quasiparticles. However investigation of these phases and manipulation of such quasiparticles remain a challenge, since large resources are needed for the numerical computations in tackling the large Hilbert space sizes of strongly interacting quantum many-body systems. This thesis is devoted to study such quasiparticles in topologically ordered phases in lattice systems using both analytical tools and numerical techniques.

1.1 Motivations

New phases of matter emerged a few decades ago with the remarkable experimental discovery of the fractional quantum Hall effect phenomenon in two-dimensional electron gas under magnetic field. Such phases host low-energy anyon quasiparticles carrying fractional charges and fractional statistics. To describe such phases and their quasiparticles in the continuum, many-body ansatz states were proposed by physicists including Laughlin, Moore and Read, Halperin, Read and Rezayi. Later Jain proposed another theory based on the composite fermion picture to describe the similar physics. However continuum systems gave rise to shortcomings including the ill-defined negatively charged anyonic fractional quantum Hall states and the requirement of large physical magnetic field. Therefore realization of the similar physics in two-dimensional lattices became particularly important to reveal new physics where the first step was taken by Kalmeyer and Laughlin to construct the trial fractional quantum Hall like state and by Haldane to construct the Chern insulator models, where physical magnetic field was cleverly skipped.

Later such constructions were extended to describe other fractional quantum Hall states hosting Abelian anyons and to construct different fractional Chern insulator models.

The journey of this thesis commence by addressing the important cutting-edge open questions in this field after the progress as briefly outlined above. Previous studies on the lattice fractional quantum Hall models hosting Abelian anyons provided the hint to construct the more challenging and more important lattice models hosting non-Abelian anyons, which are potential ingredients for quantum computations. Such lattice models turn out to be suitable to create both positively charged and negatively charged anyons on equal footing and thereby revealing new physics which we did not find in the continuum. Also such non-Abelian lattice models carrying anyons are important to get control over anyons if these could be experimentally implemented with ultra-cold atoms in optical lattices. Having understood the construction of topologically ordered models and the behavior of anyons in two-dimensional lattices we uncover the intriguing physics of topological phases of matter in fractional dimensions such as in the fractal lattices. Thereby we bridge the gap between two dimensions and one dimension by placing our model constructions on fractal lattices which reveal new physics. Our constructions are particularly relevant in this context since such lattices lack translational symmetry and hence become unsuitable for the fractional Chern insulator constructions. Now we have the methodology to construct anyons and to study those in different systems. Our investigations show the robustness of the properties of anyons which draw our attention to propose those as the detector of topological quantum phase transitions with significant advantages. Our findings overcome the shortcomings of the existing probes up-to a large extent and become important to set up the bigger picture of using quasiparticles, which may not be anyonic, as detector of quantum phase transitions in other systems like in frustrated quantum magnets.

1.2 Thesis structure : purposes and findings

In this thesis, we research quasiparticles in strongly correlated quantum many-body systems described on lattices with an emphasis on the topologically ordered phases of matter which includes the lattice fractional quantum Hall models, the fractional Chern insulator models, and the \mathbb{Z}_2 quantum spin liquid phases. A chapter-wise guide in nutshell of the thesis, after providing the short background on the relevant topics in Chapter-2, is structured as follows.

1.2.1 Chapter 3 : Construction of the anyonic lattice fractional quantum Hall states

Fractional quantum Hall effect is very important phenomenon since this is the first ever experimentally demonstrated topological phases of matter. The fractional quantum Hall states in continuum have been explored earlier in the literature, where the major shortcoming is the fact that the states with quasiholes are well-behaved but the states

containing quasielectrons give rise to the singularity and thereby result in complicated states. Translating fractional quantum Hall states in lattices come up with new avenues and reveal new physics including the scenario that the singularity problem, as appeared in the continuum systems, with the quasielectrons does not appear in the lattice systems and the quasielectron states are similar to those of the quasihole state. Also the analytical forms of the states are suitable to study the topological properties, such as the entanglement entropy, of the systems and the anyon properties for large system sizes by using Monte-Carlo simulations. The purposes of this chapter is to construct the lattice fractional quantum Hall states containing anyons by using the representation of the infinite-dimensional matrix product states as the correlators of the fields of the underlying conformal field theory.

We commence by deriving the correlators of primary fields of the free, massless bosons of the underlying conformal field theory, which correspond to the description of the fractional quantum Hall states in Sec. 3.1. We point out the singularity problem of the quasielectron states in continuum fractional quantum Hall effect in Sec. 3.2. We construct the lattice fractional quantum Hall states containing anyons, as the conformal field correlators acting on the lattice sites and on the anyon positions, in Sec. 3.3 where we explicitly derive the lattice Laughlin states and the lattice Moore-Read states on the plane.

1.2.2 Chapter 4 : Investigations of non-Abelian anyons in lattice Moore-Read models

Anyons are important blessings of topologically ordered phases of matter since these are neither fermions nor bosons, rather carry fractional charges and fractional statistics. Study of non-Abelian anyons are particularly important for topological quantum computations. Anyons have been investigated in earlier studies in continuum systems, where the quasiholes are easier to describe than the quasielectrons. Realizing anyons in lattice systems become important to uncover new physics and to get more control over these. In this prospect recently Abelian anyons in the lattice Laughlin states have been investigated. The purposes of this chapter is to research more difficult scenario as the non-Abelian anyons in the lattice Moore-Read fractional quantum Hall models. We also derive the parent Hamiltonians for which the lattice Moore-Read states, containing anyons as provided in Chapter-3, are the ground states.

We investigate density profiles, shapes, excess charge distributions and compute charges of the non-Abelian Ising anyons in the lattice Moore-Read states at the Landau level filling factor $5/2$ in Sec. 4.1 by using Monte-Carlo technique. Thereby we show that the quasielectrons can be created in a similar way that of the quasiholes. We find that the anyons are screened well with radii of a few lattice constants and approach charges $\simeq 0.25$ for the quasiholes and charges $\simeq -0.25$ for the quasielectrons. We research fractional braiding statistics of the anyons in Sec. 4.2 and show that the anyons are non-Abelian and find that the braiding statistics are the same as expected from the continuum. In Sec. 4.3 we derive the parent Hamiltonians for which the lattice Moore-Read states are the exact ground states. We find that the parent Hamiltonians are long-range and contain

few-body interactions which may be a starting point to search for the local Hamiltonians with practically the same ground state physics.

We create non-Abelian anyons in the Kapit-Mueller model, which is simpler and experimentally relevant and which shows an exact equivalence between a realistic lattice system and the lowest Landau level of the fractional quantum Hall effect, in Sec. 4.4 and show that the quasielectrons can be created in the same fashion as that of the quasiholes. By using exact diagonalizations we find that the anyons in this model are well-screened and have right charges. We find that anyons in the lattice Moore-Read states and anyons in the Kapit-Mueller model display similar density profiles and similar shapes, which make our analytical states to be relevant for this simpler model.

1.2.3 Chapter 5 : Exploring anyons and topological order in quasicrystals and in fractal spaces

Quasicrystals provide a wealth of intriguing phenomena due to long-range order and non-periodic structure of atoms. Such constructions are also motivated by the experimental progress in discovering the eight-fold rotationally symmetric optical lattice, realizing a two-dimensional quasicrystalline potential [239] for ultra-cold atoms. Fractal lattices give rise to the possibilities in exploring interesting physics in non-integer dimensions, known as the fractal dimensions or the Hausdorff dimensions such as between 0 and 2, which act as the bridge to reveal new phenomenon between integer dimensions. In this prospect recently non-interacting topological phases of matter in fractal spaces have been investigated. The purposes of this chapter is to take the first step to address strongly interacting topologically ordered phases such as anyons and the fractional quantum Hall physics in quasicrystals and in fractal spaces. We emphasis on an important common point for the investigations in quasicrystals and in fractal lattices is that we can use our construction to obtain anyons and fractional quantum Hall physics to directly probe the topological order on lattices, where one can not easily construct a topological flat band due to the lack of translational symmetry.

We start by introducing quasicrystals and fractal lattices with fractal dimensions, with a particular example as the Sierpinski gasket, in Sec. 5.2. We focus on the anyonic Laughlin states and we show in Sec. 5.3 the existence of well-screened anyons in two types of quasicrystals and in fractal lattices with fractal dimension $\simeq 1.585$ on the Sierpinski gasket fractal geometry. On the contrary of the well-known fact that anyons do not exist in one-dimensional linear system, since the model is critical, we find that anyons can exist in one dimension on fractal space. Also we show that anyons exist in dimension less than one such as in dimension $\ln(4)/\ln(5) \simeq 0.86$. We conclude that anyons and the fractional quantum Hall physics can be obtained in all dimensions $1 \leq \text{dimension} \leq 2$ and the shape of the fractal is important for this purpose. Our findings reveal that the lattice points distributions are more important in hosting anyons and the fractional quantum Hall physics rather than the Hausdorff dimensions of the fractal spaces. By computing braiding statistics of anyons in Sec. 5.4, we show that the systems have right topological order. In Sec. 5.5 we construct parent Hamiltonians of our lattice models.

1.2.4 Chapter 6 : Anyonic quasiparticles from the systems of hardcore anyons

So far the fractional quantum Hall systems of bosons or fermions are known to host anyon quasiparticles. This gives rise to an interesting question about the possibility of model systems where the original particles are anyonic. The purposes of this chapter is to show that the lattice fractional quantum Hall systems consisting of hardcore anyons can give rise to their own anyonic quasiparticles. These studies give rise to the new type of lattice fractional quantum Hall models.

In Sec. 6.1 we introduce the Laughlin type states of hardcore anyons containing anyonic quasiparticles. We study density profiles and charges of the emergent anyons in Sec. 6.2 which show that the anyonic quasiparticles are well-screened and exhibit right charges. In Sec. 6.3 we compute braiding statistics of the anyonic quasiparticles and show that it is different from the statistics of the elementary anyons which constitute the systems.

1.2.5 Chapter 7 : Quasiparticles as detector of topological quantum phase transitions

Topological phases of matter, and hence the topological quantum phase transitions, breaks the notion of local order parameters and therefore demand for new kind of probes to detect. A few probes, including ground state degeneracy, topological entanglement entropy, many-body Chern number, spectral flow, and the entanglement spectrum have been developed earlier to detect the topological quantum phase transitions but these are numerically expensive and often depend on the specific boundary conditions. Therefore the existing probes suffer from shortcomings up-to a large extent and the shortage of suitable detectors of topological quantum phase transition become prominent. The purposes of this chapter is to demonstrate that the quasiparticles can be used as a powerful and a numerically cheaper tool to detect the topological quantum phase transitions. We support our claim by testing the method on five concrete examples. In all the cases we trap anyons in the ground states of the systems. We look at the simple properties of anyons like the anyon charges and we change the parameter, which drives the system from topological to non-topological phase, and thereby we detect different phases.

In Sec. 7.1 we consider a lattice Moore-Read state on a square lattice and in Sec. 7.2 on a fractal lattice, which undergoes a topological quantum phase transition as a function of the lattice filling factor as shown in earlier studies. We show that the anyon charges detect the topological quantum phase transition. In Sec. 7.3, we investigate an interacting Hofstadter model in the absence of disorder, which has a Laughlin type ground state, and which undergoes a topological quantum phase transition as a function of the lattice filling factor as found in earlier investigations. We consider this model in the presence of disorder in Sec. 7.4. We find that the anyon charges detect the topological quantum phase transition. In Sec. 7.5, we study the Kitaev's toric code model, which undergoes a topological quantum phase transition when a sufficiently strong external magnetic field is applied. We create anyons in the ground state and show that the anyons dictate the

topological quantum phase transition. In all these examples we find that it is sufficient to compute the anyon charges to determine the phase transition point and therefore the method is numerically cheap.

1.2.6 Chapter 8 : Constructions and investigations of the spin-1/2 chain and ladder models

Exactly solvable quantum many-body systems are important due to their own right. The spin-1/2 one-dimensional Haldane-Shastry model is one of the examples among them. Here we consider a family of spin-1/2 models with few-body, $SU(2)$ invariant Hamiltonians and analytical ground states related to the one-dimensional Haldane-Shastry wavefunction. The spins are placed on the surface of a cylinder, and the standard one-dimensional Haldane-Shastry model is obtained by placing the spins with equal spacing in a circle around the cylinder. The purpose of this chapter is to show that another interesting family of models with two-body exchange interactions is obtained if we instead place the spins along one or two lines parallel to the cylinder axis, giving rise to chain and ladder models, respectively.

We briefly recall the two-dimensional Haldane-Shastry model for spins on an arbitrary lattice on the cylinder in Sec. 8.1. We discuss the one-dimensional Haldane-Shastry model on the circle in Sec. 8.2. We show that the two-dimensional Haldane-Shastry model reduces to a two-body model for particular choices of the lattice in Sec. 8.3. Special cases include spin chain models, which we analyze in Sec. 8.4, and ladder models, which we analyze in Sec. 8.5. We find that depending on the length scales the models show critical behavior, with power-law decaying correlations and logarithmic law maintaining Renyi entanglement entropy, in one limit and show product of singlets behavior, with exponentially decaying correlations and area law maintaining Renyi entanglement entropy, in another limit. In between more complicated behaviors are found.

Topology, Fractional Quantum Hall Effect and Anyons

” *Living is worthwhile if one can contribute in some small way to this endless chain of progress.*

— Paul Dirac

2.1 Topological phases of matter

Physicists’ understanding of the quantum phases has undergone major revolutions precipitated by experimental discoveries and by profound theoretical revelations. Landmarks include the Landau-Ginzburg-Wilson theory which describes the second order quantum phase transitions [198] among conventional phases in terms of symmetry breaking. This theory characterizes phase transitions by defining local order parameters which vanish in one phase and acquire non-zero values in the other phase and thereby break symmetry. This concept is known as the spontaneous symmetry breaking. For example ferromagnet to paramagnet transition at zero temperature where total magnetization plays the role of local order parameter.

However not all phases can be fully characterized by symmetries and therefore not all quantum phase transitions can be described by local order parameters. Some quantum systems, for example the fractional quantum Hall phase, do not admit symmetry breaking local order parameters and therefore go beyond the painting of Landau’s theory. These systems are characterized by global properties such as topology of the system and hence display a new kind of order that goes beyond the conventional classification of phases of matter. This new type of order is called as the topological order [112, 176, 251] which cannot be transformed into a conventional product state through a local unitary transformation. Topologically ordered phases are short-range correlated, where correlation function decays exponentially, and possess long-range entanglement. The entanglement entropy follows the area-law behavior with the sub-system size and displays a finite sub-leading correction in the scaling which is known as the topological entanglement entropy [142, 127, 112]. Such kind of system exhibits an energy gap above the ground state and is associated with a ground state degeneracy [79, 217] that depends on the topology of the space, such as genus of the torus, on which the system is defined. The energy gap and the ground state degeneracy are not protected by symmetry and can

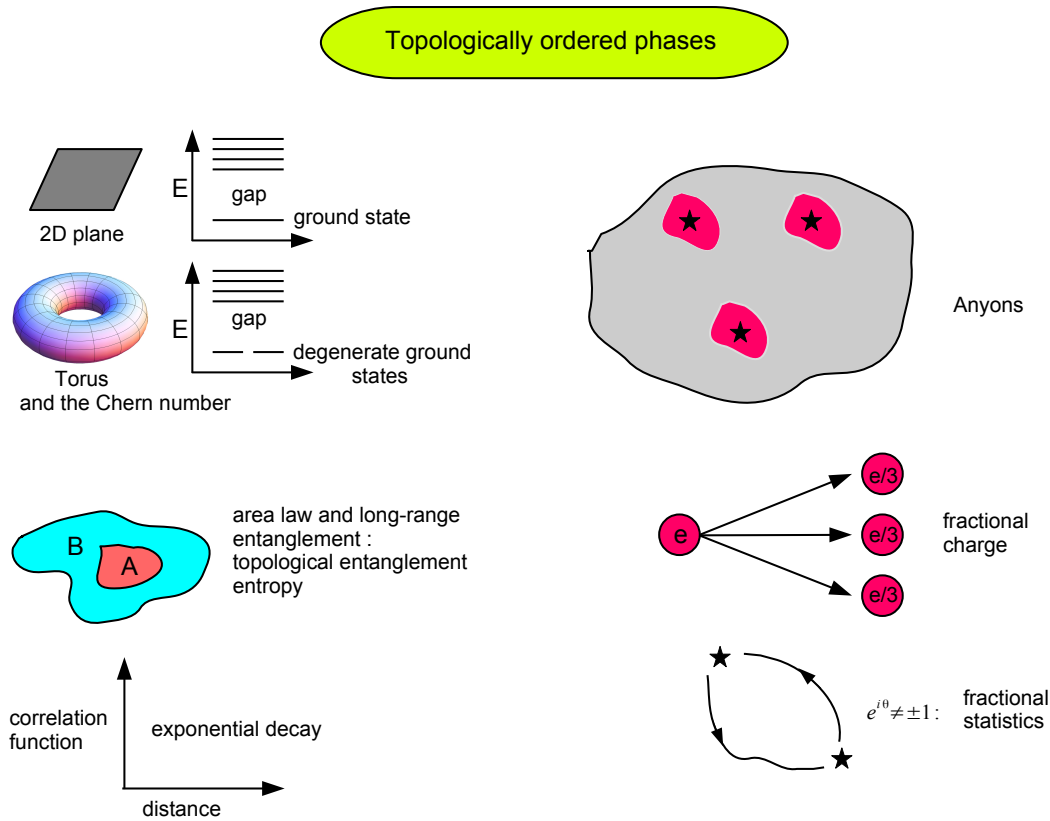


Figure 2.1.: Topologically ordered phases show an energy gap to the excited states and exhibit degeneracy in the ground state spectrum while defined on the non-trivial surfaces such as on the torus. These phases are described by the exponentially decaying short-range correlations and by the area-law obeying long-range entanglement with a finite sub-leading correction term known as the topological entanglement entropy. Existence of the anyonic quasiparticle excitations, above the ground state and carrying fractional charges and fractional statistics, are one of the signature properties of the topologically ordered phases of matter.

not be lifted by any local perturbation. Therefore such phases are robust to noise and become suitable for storing quantum informations. The quasiparticle excitations above the ground state are neither fermions nor bosons and show fractional charges and fractional statistics [10, 178, 164]. These quasiparticles are potential candidates for performing fault-tolerant topological quantum computations [218, 50, 159, 200, 30, 121, 43, 138, 208, 124]. We display a pictorial sketch of the topologically ordered phases of matter in Fig. 2.1. In searching for the topologically ordered states, fractional quantum Hall phenomena [225, 130] is a prominent example which is described by the chiral spin liquid ground states [140] and breaks the time reversal symmetry.

Apart from the chiral spin liquid states, there are \mathbb{Z}_2 topologically ordered states [186]. An exactly solvable model of such order was developed by Alexei Kitaev, which is known as the Kitaev's toric code model [126]. Also frustrated quantum magnet models [184, 40, 276, 232, 204, 104, 147, 39, 277, 229, 243, 19, 230, 245, 74, 122, 213, 52, 15] are potential candidates to realize quantum spin liquid phases [202] and sometimes

they exhibit \mathbb{Z}_2 topologically ordered gapped quantum spin liquid states as the ground states. Examples include the spin-1/2 Heisenberg model on the Kagome lattice [91, 92], and the spin-1/2 Heisenberg J_1 - J_2 model on square lattice [73, 113, 242, 38] etc. Recently, experimentally discovered layered magnet Herbertsmithite, having the chemical composition as $\text{ZnCu}_3(\text{OH})_6\text{Cl}_2$, becomes the potential candidate for the theoretical model of the Heisenberg interaction on the Kagome lattice and for realizing quantum spin liquid phases. Also the rare-earth pyrochlore magnets in three-dimensions are drawing a lot of recognition in realizing quantum spin liquid phases [105, 7, 207, 272].

Along with the topologically ordered phases, there exist symmetry protected topological phases which are not-long range entangled but show topological properties. Topological behavior of such systems are protected by symmetry. Examples include the quantum spin Hall systems [97, 100, 117, 118, 12, 27] and topological insulators [26, 9, 88] in which topological properties are protected by the time-reversal symmetry.

2.2 The fractional quantum Hall effect

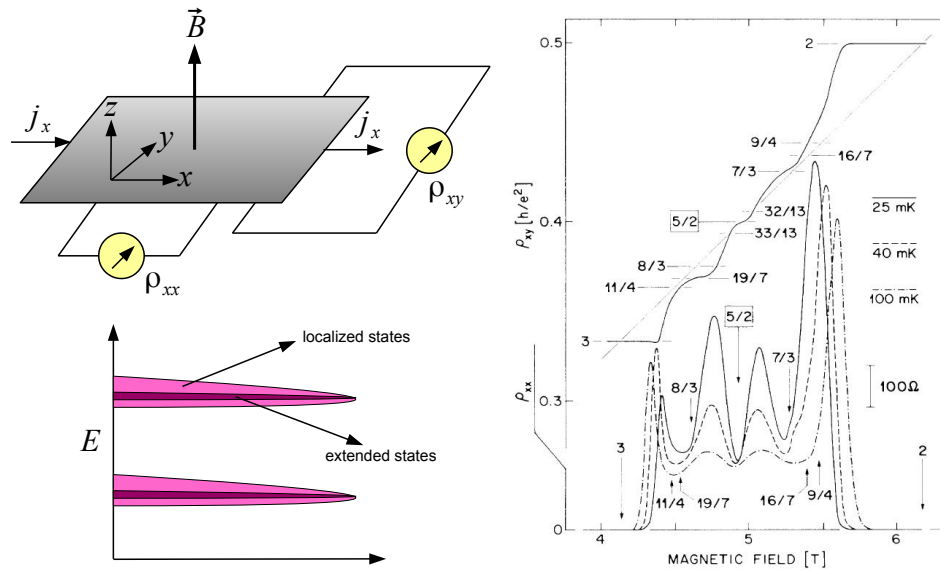


Figure 2.2.: Left upper figure : Experimental demonstration of the Hall effect and the transport measurements are shown where the electron gas is confined in a two-dimensional plane. A current j_x is driven in the x -direction and an external magnetic field \vec{B} is applied in the z -direction. The longitudinal resistivity ρ_{xx} is measured in the x -direction and the Hall resistivity ρ_{xy} is measured in the y -direction. Left lower figure : Pictorially we show the effect of impurities of the sample on the density of states, which is known as the Landau levels. The impurities make the states which are close to the center of the band to be extended and make the states which are at the far edge of the band to be localized. Right figure : Experimental data of ρ_{xy} and of ρ_{xx} as a function of B are shown (Picture Courtesy - Wikipedia).

Over the past three decades, one of the most important playgrounds in revealing topological order becomes the fractional quantum Hall physics which is important both from fundamental viewpoint as well as for their potential applications in quantum information processing. The importance of this phenomenon lies in the fact that it has been realized experimentally. The nomenclature comes from the classical Hall effect [224], which is the generation of a transverse voltage V_H , known as the Hall voltage, in conductors placed in crossed electric and magnetic fields. It was discovered by Edwin Hall in 1879. This voltage, which arises from the accumulation of charges due to the bending of paths of the charge carriers from the magnetic field, can be used to define a transverse electrical conductivity σ_{xy} which is written to be the ratio of the applied current to the Hall voltage.

Just after the hundredth anniversary of the Edwin Hall's discovery, the discovery of the integer quantum Hall effect [130] by Klaus von Klitzing *et al.* in 1980 and the disclosure of the fractional quantum Hall effect [225, 258] by Tsui-Stormer-Gossard in 1982 paved the path for one of the most important developments in topological phases of matter. The quantum Hall phases take place when a two-dimensional electron gas is subjected to a perpendicular high magnetic field at low temperature and thereby Landau levels are formed. Low temperature is needed to ensure the physics to come from the quantum fluctuations. And the thermal energy KT must be very less than the gap between the Landau levels, where K is the Boltzmann constant and T is the temperature. The magnetic field breaks the time-reversal and the parity symmetry, and the ground state is known as the chiral topological state and is associated with the chiral edge states which have preferred directions along the edges of the sample. The term "chiral" corresponds to the time-reversal symmetry breaking scenario. Experimentally the electrons are confined at the interface of two semiconductors. As displayed in Fig. 2.2 (left upper), the key experimental signature of the quantum Hall effect is the behavior of the transverse Hall resistivity ρ_{xy} and the longitudinal Hall resistivity ρ_{xx} as a function of the perpendicular magnetic field B . The quantities ρ_{xy} and ρ_{xx} are computed in transport measurements and we show the data for ρ_{xy} as a function of B for the fractional quantum Hall effect in Fig. 2.2 (right). The quantum Hall effect is characterized by the formation of plateaus, where ρ_{xx} vanishes and ρ_{xy} is constant which takes the values [224]

$$\rho_{xy} = \frac{1}{\nu} \frac{h}{e^2}, \text{ and } \sigma_{xy} = \frac{1}{\rho_{xy}}, \quad (2.1)$$

where h is the Planck's constant, e is the electron charge, and ν is a rational number which is known to be the Landau level filling fraction of the quantum Hall state. The quantity ν corresponds to the number of particles per magnetic flux in the system.

In the integer quantum Hall effect [194, 224], the Landau levels are fully filled which correspond to ν to be integers. This phenomena can be understood by considering the single-particle picture. And the development of plateaus, in ρ_{xy} for a range of B , can be explained by considering the effect of impurities. Impurities turn many of the quantum states from extended to localized. In general the extended states are spread throughout the whole system while the localized states are restricted to lie in some region of space. The effect of impurities lead to the fact that the states which are close to the center of the band become extended and the states which are at the far edge of the band will be

localized [224]. We show this schematically in Fig. 2.2 (left lower). It is to be noted that only the extended states take part in the transport and therefore the localized states do not contribute to the conductivity. Now if the Fermi energy lies in the gap between two Landau levels, which in turn corresponds to the scenario of the fully filled Landau levels, then there exists no state close to the Fermi energy and thereby the system becomes gapped. In that case all the extended states in a given Landau level are filled. Now if we increase the magnetic field, it will change the Fermi energy. But before jumping to the next Landau level, the localized states will be populated. This corresponds to the conductivity to be unchanged, which leads to the observation of having plateaus.

When B is high then the magnetic length $l_B \propto 1/\sqrt{B}$ becomes small and therefore the particles come closer which corresponds to the interaction to be stronger. The single-particle picture breaks down for the fractional quantum Hall effect and the Landau levels are partially filled. Hence the interactions among the particles are the key ingredients for the fractional quantum Hall effect which are incompressible and gapped phases of matter. Strong particle-particle interactions invalidate the perturbative treatment and make the investigations of the fractional quantum Hall effect challenging [25]. Remarkably a breakthrough happened by the Laughlin's ansatz [140] for the trial states in the theoretical description of the fractional quantum Hall effect. The Laughlin states provide paradigmatic model states which give the effective descriptions of the complex strongly interacting physical phenomenon by cleverly skipping a direct microscopic solution of the quantum many-body problem. The Laughlin states describe the fractional quantum Hall phases with the lowest Landau level filling fraction $\nu = 1/q$, where $q \in \{1, 3, 5, \dots\}$. It is to be noted that $q = 1$ Laughlin state recovers the Slater determinant for the single electron case. It was shown that the trial states exhibit excitations, which are neither fermions nor bosons, with fractional charges and fractional statistics.

Laughlin states were later generalized to the states of other filling fractions with odd denominators through a hierarchy construction, which were recognized to be the composite fermion theory of the fractional quantum Hall effect as coined by J. K. Jain [106]. This theory sells the fractional quantum Hall states as the integer quantum Hall states of composite fermions [16, 84, 85, 111, 109, 259, 221, 220], which are described to be the bound states of electrons and magnetic fluxes. Later further generalizations of the Laughlin states were done to describe the physics of the higher Landau levels. Examples include the Moore-Read state [162, 191, 69, 275, 17, 157, 156, 93, 49] and Read-Rezayi state [192, 160] at the Landau level fillings factors $5/2$ and $12/5$ respectively, which correspond to the physics of the second Landau level at filling fractions $1/2$ and $2/5$ respectively.

The theoretical support of the experimentally observed fractional quantum Hall effect has been provided by constructing ansatz states. Craze to realize the similar physics in lattices [131] has the motivation for experiments with ultra-cold atoms in optical lattices. Lattice systems can reveal new behavior which can not be perceived in the continuum. Also manipulation of the quasiparticles in fractional quantum Hall states remain a challenge. Finding other systems exhibiting the same physics is an important step towards a better understanding of these phenomena as well as towards the practical applications in quantum computing. Also realizing fractional quantum Hall physics in ultra-cold atoms would open up new possibilities for doing measurements on the

systems. Kalmeyer and Laughlin stepped first in this direction where they proposed a lattice version of the continuum Laughlin state for $q = 2$ and thereby corresponds to the bosonic fractional quantum Hall phase [115]. This can be characterized as the chiral spin liquids where the term "spin liquid", as first coined by Phil Anderson, refers to the strongly correlated low temperature phase having no magnetic order [6].

Lattice models displaying the integer quantum Hall physics, known to be the Chern insulator models, were first constructed by Duncan Haldane, where the time reversal symmetry is not broken through an external magnetic field, rather is broken by the presence of complex phases in the hopping terms of the Hamiltonian [81]. Later this concept was generalized to the interacting models which are known to be the fractional Chern insulator models [76, 163, 193]. Usually two approaches draw a lot of interests in constructing the lattice models. The first approach deals with the construction of the non-interacting Chern insulator models [271, 22, 108, 216, 246, 247, 214]. And interactions become important to have fractional filling factor for the flat band which mimic the lowest Landau level. This approach gives rise to different fractional Chern insulator models [79, 210, 260, 149, 148, 47, 166] having flat bands. In the second approach, one mimics the interaction of the fractional quantum Hall systems in the continuum and translate the states on the lattices [256, 175, 197, 69, 169, 227, 173, 170, 157, 156].

Lattice models show the avenue to realize the fractional quantum Hall physics even in the room temperature. We explain this possibility as follows. We require low enough temperature to get the physics from quantum fluctuations. Now the thermal energy is proportional to the temperature and the gap between the Landau levels is proportional to the square root of the magnetic field. Therefore we need very low temperature and high magnetic field to keep the thermal energy small enough compared to the gap. To realize the fractional quantum Hall physics we require strong interactions among the particles which in turn requires high magnetic field since the length scale between two particles becomes smaller when we have higher magnetic field. In continuum systems, like in the two-dimensional electron gas, the fractional quantum Hall physics is obtained by applying the external magnetic field, which has the limitation up to a few Tesla. In lattice systems, we have the possibility of generating artificial magnetic fields or artificial gauge fields, which are larger than the external magnetic field. Therefore it is possible to satisfy the condition of having the thermal energy small enough compared to the gap in moderate temperature, such as in the room temperature. Hence if one finds a material with the right combination of properties, one may be able to realize the fractional quantum Hall physics at room temperature.

Lattice models are often suitable to be realized in experiments with ultra-cold atoms [29, 72] in optical lattices, where interactions can be engineered. The experimental realization of the Hofstadter model [95], which corresponds to the integer quantum Hall physics, with ultra-cold atoms [4, 158] is an example in that direction. Proposals to realize fractional quantum Hall physics with ultra-cold atoms are discussed in different literature [79, 210, 45, 265].

2.3 Anyons

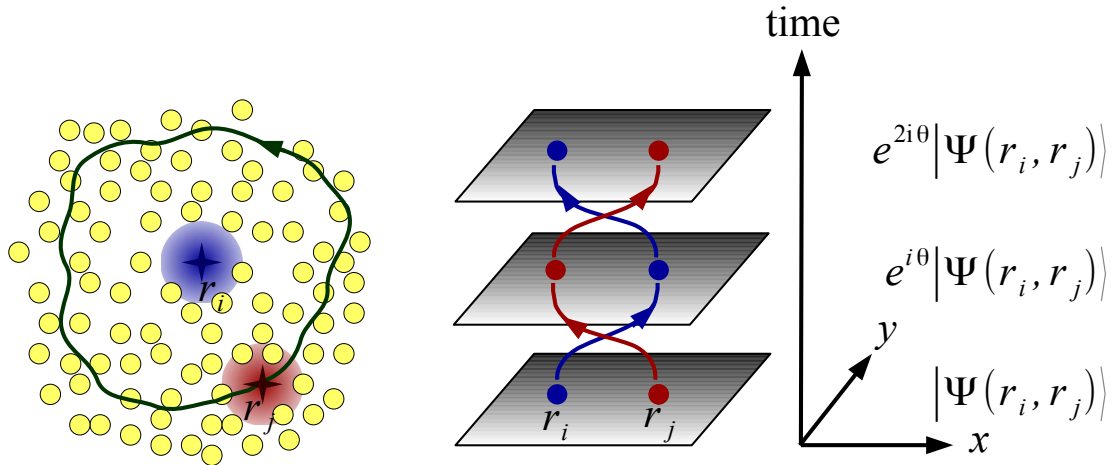


Figure 2.3.: Pictorial representation of the anyon braiding and the fractional statistics are shown. In the left figure we display the blue blob and the red blob as anyons and the yellow circles as particles. One anyon at position r_j is braiding around another anyon at position r_i in the two-dimensional plane. In the right figure we show the different time slices for the anyon movement of the left figure. When the anyons are exchanged, the many-body state $|\Psi(r_i, r_j)\rangle$ acquires a phase $e^{i\theta} \neq \pm 1$ and when one anyon braids around another anyon the phase factor becomes $e^{2i\theta} \neq 1$.

Quantum statistics provides the pillar of quantum mechanical viewpoint of the world. Our three-dimensional world, that is $3 + 1$ -dimensional world, consists of the two types of elementary particles which are classified into bosons and fermions as distinguished by their quantum statistics. The state of a collection of bosons or fermions satisfy the proper symmetry, when a pair of them are exchanged. The state acquires a phase factor $+1$ or -1 , and hence the state is symmetric or anti-symmetric, when two bosons or two fermions are exchanged respectively. This limitation comes from the fact that the process in which two particles are exchanged twice is equivalent to the process in which one particle is braided around another particle. In three-dimensions, braiding one particle around another particle is the same as doing no movement of the particles and therefore the state should be left unchanged after that process. Hence there exist only two possibilities to pick up a factor of either $+1$ or -1 by the state after a single exchange. While bosons were discovered by Bose and Einstein obeying Bose-Einstein statistics, Fermi and Dirac discovered fermions which obey Fermi-Dirac statistics. These particles are responsible for fascinating phenomena like Bose-Einstein condensation at very low temperature where all bosons occupy the lowest state and exhibit superfluidity. Also conductivity, magnetism and superconductivity are given rise to by fermions.

The above mentioned phenomenon are however independent of the topology of the systems. Topology is a branch of mathematics which dictates the system properties those are preserved under the smooth deformations like stretching or twisting but not tearing. For example a coffee cup and a doughnut (or donut if the reader is from United States) are topologically equivalent systems. In physics the concept of topology entered with the

discovery of the Aharonov-Bohm effect [3]. Here a charge q circulates around a magnetic flux Φ and thereby the state picks up a phase factor $e^{inq\Phi}$, where n is the number of times the charge circulates the flux. It is to be noted that this phase factor is independent of the nature of the path and depends only on the circulation number.

In two-dimensions, that is in $2 + 1$ -dimension, theoretical studies into other possibilities revealed that there exist particles which break the dichotomy of particle classification into bosons or fermions in three-dimensions. A particle loop which braids around another particle can not be deformed into a point without crossing through the other particle. These particles exhibit non-trivial exchange statistics. That is when one particle at position r_i is exchanged with another particle at position r_j in counter-clockwise manner, then the many-particle state picks up an arbitrary complex phase factor as

$$|\Psi(r_i, r_j)\rangle \rightarrow e^{i\theta} |\Psi(r_i, r_j)\rangle, \text{ where } e^{i\theta} \neq \pm 1. \quad (2.2)$$

The phase is not merely a \pm sign because a second counter-clockwise exchange, or equivalently braiding one particle at position r_i around another particle at position r_j , does not need to bring the state back to the initial state but can result in a non-trivial phase as

$$|\Psi(r_i, r_j)\rangle \rightarrow e^{2i\theta} |\Psi(r_i, r_j)\rangle, \text{ where } e^{2i\theta} \neq 1, \quad (2.3)$$

as shown in Fig. 2.3. This difference between two-dimensions and three-dimensions was first realized by Leinaas and Myrheim [141] and by Wilczek [255]. When $\theta = 0$ or $\theta = \pi$ the particles are bosons or fermions respectively and when $\theta = \pi/2$, the particles are especially named as semions.

As the state can pick up any phase factor after the particle exchange, hence the particles are nomenclature as anyons [190, 10, 48]. In analogy with the Aharonov-Bohm effect, this exchange is independent of the nature of the traversed path and depends only on the winding number. Thereby the systems of anyons are topological. Different exchanges give rise to different phase factors and those phase factors commute. Therefore they serve as the member of the Abelian braid group and the anyons are Abelian anyons [140]. The topological classes of trajectories which take the particles from the initial positions to the final positions are in one-to-one correspondence with the elements of the braid group. An element of the braid group can be visualized by thinking of the trajectories of particles as world-lines or as strands in $2 + 1$ -dimensional space-time originating at the initial positions and terminating at the final positions, as shown in Fig. 2.3 (right).

More dramatic scenario happens if the ground state manifold is degenerate. In that case the set of ground states acquires a unitary matrix \hat{U} under two particles exchange. And the ground states rotate among themselves as

$$\begin{bmatrix} \Psi_1(r_i, r_j) \\ \Psi_2(r_i, r_j) \\ \cdot \\ \cdot \\ \cdot \end{bmatrix} \rightarrow \hat{U} \begin{bmatrix} \Psi_1(r_i, r_j) \\ \Psi_2(r_i, r_j) \\ \cdot \\ \cdot \\ \cdot \end{bmatrix}. \quad (2.4)$$

Different exchanges give rise to different unitary matrices and those matrices do not commute. Therefore they serve as the member of the non-Abelian braid group and the anyons are non-Abelian anyons [162, 28, 42, 201, 145, 101].

From the viewpoint of charges, anyons come in two flavors as the positively charged anyons are called the quasiholes and the negatively charged anyons are called the quasi-electrons. These discoveries pave the path of many new research directions. Examples include the exposure of new phases of matter and the possibility of building the fault-tolerant topological quantum computer by using non-Abelian anyons. Systems that can host anyons are, for example, the fractional quantum Hall systems and two-dimensional quantum spin liquids [140, 162, 126, 202, 91, 92, 73, 113, 242, 38].

Lattice Fractional Quantum Hall States Containing Anyons

” *Nature is filled with a limitless number of wonderful things which have causes and reasons like anything else but nonetheless cannot be foreseen but must be discovered, for their subtlety and complexity transcends the present state of science.*

— **Robert B. Laughlin**

In the fractional quantum Hall systems, gapless edge states are described by the 1+1-dimensional low-energy conformal field theory [64]. However Moore and Read showed [162] that the same theory can be used to describe the 2+1-dimensional gapped bulk of the fractional quantum Hall systems, which is known to be the bulk-boundary correspondence. The infinite-dimensional matrix product states [182, 177, 174] play an important role, to construct the lattice fractional quantum Hall models, because of their representation with respect to the correlators of the fields of the underlying conformal field theory. In this chapter we analytically construct the lattice versions of the continuum fractional quantum Hall states hosting anyons.

In Sec. 3.1 we discuss the primary fields and the conformal transformations. We write the primary fields of the free, massless bosons and derive their correlator. In Sec. 3.2 we describe the fractional quantum Hall states in continuum and discuss the topological entanglement entropy. We point out the singularity problem of the quasielectron states in continuum. We construct the lattice Laughlin and the lattice Moore-Read fractional quantum Hall states on the plane in the presence and in the absence of anyons in Sec. 3.3. We show that the singularity problem with the quasielectrons, in continuum, can be avoided in the lattice systems. We display the continuum limit of our lattice states. And in Sec. 3.4 we draw the conclusions. This chapter is based on parts of the following Refs. [57, 155, 180, 156, 157, 256]:

[1] : **Sourav Manna**, Julia Wildeboer, Germán Sierra and Anne E. B. Nielsen, "Non-Abelian quasiholes in lattice Moore-Read states and parent Hamiltonians", *Physical Review B* **98**, 165147 (2018)

[2] : **Sourav Manna**, Julia Wildeboer and Anne E. B. Nielsen, "Quasielectrons in lattice Moore-Read models", *Physical Review B* **99**, 045147 (2019)

[3] : **Sourav Manna***, Biplab Pal*, Wei Wang* and Anne E. B. Nielsen, "Anyons and fractional quantum Hall effect in fractal dimensions", *Physical Review Research* **2**, 023401 (2020) [* authors equally contributed to this work]

[4] : **Sourav Manna**, N. S. Srivatsa, Julia Wildeboer and Anne E. B. Nielsen, "Quasiparticles as detector of quantum phase transitions", [submitted to *Physical Review Research* (Rapid Com.)], arXiv:1909.02046 (2019)

[5] : Julia Wildeboer, Aniket Patra, **Sourav Manna** and Anne E. B. Nielsen, "Anyonic quasiparticles of hardcore anyons", *Physical Review B* **102**, 125117 (2020)

[6] : Callum Duncan, **Sourav Manna** and Anne E. B. Nielsen, "Topological models in rotationally symmetric quasicrystals", *Physical Review B* **101**, 115413 (2020) [*Editors' Suggestion*]

3.1 Conformal field theory description of the states

The fractional quantum Hall states can be written as the correlator of the field operators of the underlying conformal field theory as [162, 174, 60]

$$|\Psi\rangle = \sum_{n_1, \dots, n_N} \langle 0 | V_{n_1}(z_1) V_{n_2}(z_2), \dots, V_{n_{N-1}}(z_{N-1}) V_{n_N}(z_N) | 0 \rangle | n_1, \dots, n_N \rangle, \quad (3.1)$$

where $\langle 0 | \dots | 0 \rangle$ denotes the vacuum expectation value and $V_{n_i}(z_i)$ is the field operator at the i th lattice site z_i having degrees of freedom n_i . Appropriate choices of these field operators lead to the analytical expressions of the wavefunctions. We particularly focus on a free, massless bosonic field theory of primary fields where the operators are expressed in terms of the bosonic creation and annihilation operators. Therefore we discuss below the essential features of such fields.

3.1.1 The free, massless boson

We consider the free, massless bosonic conformal field theory in 1 + 1-space-time dimensions [64] with x and t as the spatial and the temporal coordinates respectively. We choose the free massless bosonic field $\phi(x, t)$ and hence the action is

$$\mathcal{S} = \frac{1}{8\pi} \int [(\partial_t \phi(x, t))^2 - (\partial_x \phi(x, t))^2] dx dt. \quad (3.2)$$

This action is scale invariant, that is \mathcal{S} is invariant under the following transformation as

$$(x, t) \rightarrow (ax, at), \text{ with } a > 0. \quad (3.3)$$

Since we will construct the analytical states on the two-dimensional complex plane, therefore we show how the space-time coordinate of a particle is related to the coordinate of that particle on the complex plane as follows.

(a). Radial quantization

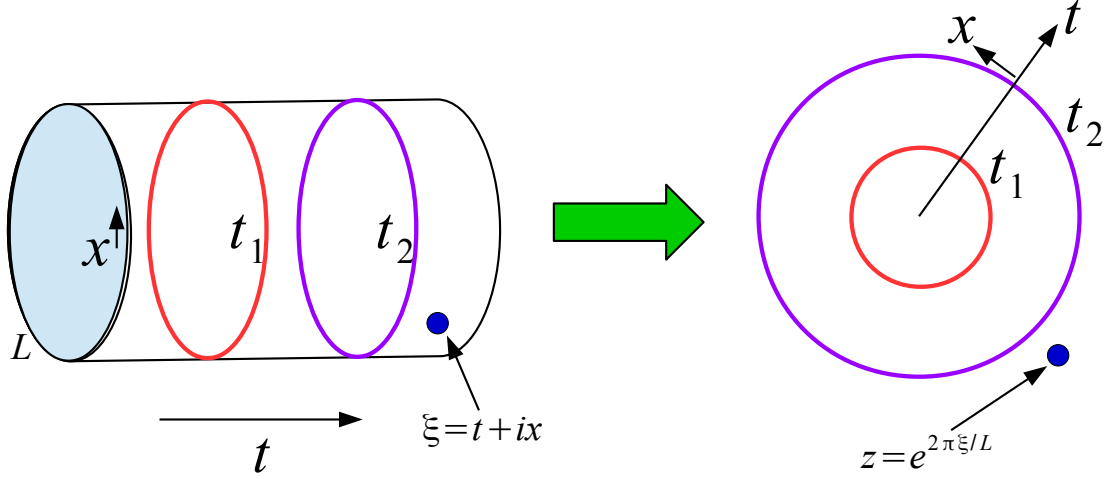


Figure 3.1.: We show the mapping from the cylinder to the complex plane, which is called as the radial quantization. On the cylinder of length L the spatial coordinate x is along the circumference of the cylinder and the temporal coordinate t is along the axis of the cylinder. The position ξ of a particle is shown by the blue circle on the surface of the cylinder. And the different time slices are shown by red and violet circles. We perform the mapping on the plane where x and t are along the angular and the radial directions respectively. We show the position z of the particle by the blue circle. The different time slices on the cylinder become the concentric circles as shown by red and violet circles.

We define a space-time cylinder with the circumference L such that

$$\phi(x + L, t) = \phi(x, t). \quad (3.4)$$

The time $t \in \{-\infty, +\infty\}$ is along the cylinder axis and $x \in \{0, L\}$ is along the circumference of the cylinder. Therefore any point on the cylinder is described by the complex coordinate

$$\xi = t + ix. \quad (3.5)$$

We map the cylinder on a complex plane z , or on a Riemann sphere, through the mapping

$$z = e^{2\pi\xi/L} \quad (3.6)$$

which is known as the radial quantization [64] as shown in Fig. 3.1. Therefore each transverse slice of the cylinder forms a circle on the complex plane and different such slices constitute concentric circles, which are centered at the origin and each having a particular t . Therefore x is along the angular direction on the plane and t is along the radial direction on the plane. And the remote past, as defined by $t \rightarrow -\infty$, is placed at the origin $z = 0$ and the remote future, as defined by $t \rightarrow +\infty$, approach the point at infinity on the plane or on the Riemann sphere. And in terms of the coordinates (z, \bar{z}) the action in Eq. (3.2) can be written as

$$\mathcal{S} = \frac{1}{4\pi} \int \partial_z \phi(z, \bar{z}) \partial_{\bar{z}} \phi(z, \bar{z}) dz d\bar{z} \quad (3.7)$$

(b). Mode expansion

To construct the analytical states, we have to evaluate the correlator which requires to express the field in terms of the modes of the bosonic creation and annihilation operators. And the mode expansion of the field $\phi(z, \bar{z})$ is expressed as [64]

$$\phi(z, \bar{z}) = \phi_0 - i\pi_0 \ln(|z|^2) + \sum_{n=1}^{\infty} \frac{i}{\sqrt{n}} \left(a_n z^{-n} - a_n^\dagger z^n \right) + \left(a_{-n} \bar{z}^{-n} - a_{-n}^\dagger \bar{z}^n \right), \quad (3.8)$$

where a_n and a_n^\dagger are the bosonic annihilation and creation operators for the n th mode respectively, \bar{z} is the complex conjugate of z and π_0 is the canonical momentum conjugate of $\phi_0(z, \bar{z})$ in the zeroth-mode, that is for the $n = 0$ mode, satisfying the following relations

$$[\phi_0, \pi_0] = i \text{ and } [a_n, a_m^\dagger] = \delta_{nm}, \quad (3.9)$$

where δ_{nm} is the Kronecker delta function.

3.1.2 Conformal transformations and primary fields

We consider primary fields of free, massless bosons while constructing the states. A primary field satisfies a particular transformation property under the mapping of the coordinates, known to be the conformal map. Hence we first introduce the mapping and then describe the transformation of the primary field under such mapping. Conformal transformations are the holomorphic maps

$$z \rightarrow w = f(z) \quad (3.10)$$

and correspondingly the anti-holomorphic maps

$$\bar{z} \rightarrow \bar{w} = \bar{f}(\bar{z}) \quad (3.11)$$

which preserve the angles. On the complex plane, the global conformal transformations are given by the so called Möbius transformations [64] as

$$w = \frac{az + b}{cz + d}, \text{ with } ad - bc \neq 0, \quad (3.12)$$

where a, b, c, d are complex numbers. These transformations include translation, rotation, dilation, and inversion.

Now a primary field, say Θ , is defined to be the field which transforms under Eq. (3.12) as

$$\Theta(z, \bar{z}) \rightarrow \tilde{\Theta}(w, \bar{w}) = \left(\frac{\partial w}{\partial z} \right)^{-h} \left(\frac{\partial \bar{w}}{\partial \bar{z}} \right)^{-\bar{h}} \Theta(z, \bar{z}), \quad (3.13)$$

where h and \bar{h} are real numbers, which are called as the conformal scaling dimensions of Θ . Generators of the conformal transformations of the primary fields satisfy the Virasoro algebra and give rise to the central charge, which is a key feature of the conformal field theory. Two-point correlations of the primary fields follow the relation

$$\langle \Theta(z_1, \bar{z}_1) \Theta(z_2, \bar{z}_2) \rangle \propto \frac{1}{(z_1 - z_2)^{h_1+h_2} (\bar{z}_1 - \bar{z}_2)^{\bar{h}_1+\bar{h}_2}}, \quad (3.14)$$

which is reminiscent of the scale invariant decay of the correlations in gapless systems.

3.1.3 Primary fields of the free, massless boson

As we are using 1 + 1-dimensional conformal field theory, therefore the field operators have to be conformal invariant and accordingly the wavefunctions are invariant under conformal transformations. This in turn means that the field operators have to be primary fields maintaining the conformal transformations. We note that the bosonic field ϕ is not a primary field since the two-point correlator takes the form

$$\langle \phi(z_1) \phi(z_2) \rangle \propto -\ln(z_1 - z_2), \quad (3.15)$$

which is not the same as Eq. (3.14).

However we can construct primary fields for the free, massless bosons by using ϕ . We write the primary fields, which are known as the vertex operators, as

$$V_\gamma(z, \bar{z}) =: e^{i\gamma\phi(z, \bar{z})} :, \gamma \in \mathbb{R}, \quad (3.16)$$

where $: \dots :$ denotes the normal ordering. Since the underlying theory is massless hence we can decompose the non-chiral bosonic field $\phi(z, \bar{z})$ into its holomorphic or chiral part $\phi(z)$ and its anti-holomorphic or anti-chiral part $\phi(\bar{z})$. Therefore we have

$$\phi(z, \bar{z}) = \phi(z) + \phi(\bar{z}). \quad (3.17)$$

This licenses us to decouple the non-chiral vertex operator as

$$V_\gamma(z, \bar{z}) = V_\gamma(z) \times V_\gamma(\bar{z}) \quad (3.18)$$

into its chiral and anti-chiral parts. And the coefficients of the chiral wavefunction in Eq. (3.1) can be evaluated from their non-chiral part as

$$\left| \langle 0 | V_{\gamma_1}(z_1), \dots, V_{\gamma_N}(z_N) | 0 \rangle \right|^2 = \langle 0 | V_{\gamma_1}(z_1, \bar{z}_1), \dots, V_{\gamma_N}(z_N, \bar{z}_N) | 0 \rangle, \quad (3.19)$$

where the specific choices of $V_{\gamma_i}(z_i)$ lead to the desired analytical forms of the wavefunctions. The vacuum correlation function of the chiral vertex operators evaluates to

$$\langle 0 | V_{\gamma_1}(z_1), \dots, V_{\gamma_N}(z_N) | 0 \rangle = \Xi \delta_\gamma \prod_{j < k}^N (z_j - z_k)^{\gamma_j \gamma_k}, \quad (3.20)$$

where Ξ is a phase factor which can be chosen at will. And we have

$$\delta_\gamma = 1 \text{ if } \sum_{j=1}^N \gamma_j = 0, \quad (3.21)$$

which is called the charge neutrality condition [64]. This Eq. (3.20) is the key to construct the analytical wavefunctions by using conformal field theory.

3.2 Continuum fractional quantum Hall states

In the fractional quantum Hall effect the particles are subjected to the external magnetic field and are strongly correlated through the Coulomb interactions. Therefore diagonalization of the Hamiltonian to get the ground state is very difficult. Instead, being motivated by the physical insights, Laughlin simply wrote down an ansatz for the state [140]. He described the physics at the lowest Landau level at filling fraction $\nu = 1/q$, where q is an odd integer, by the following state as

$$\Psi_L(n_1, \dots, n_M) = \prod_{j < k}^M (Z_j - Z_k)^q e^{-\frac{1}{4} \sum_{j=1}^M |Z_j|^2}, \quad (3.22)$$

where Z_j are the positions of M particles on a complex plane and the magnetic length is set to be unity. The state is anti-symmetric and hence defines fermions, as for example electrons. The Gaussian factor appears by solving the single particle problem in the lowest Landau level. The pre-factor, which is called as the Jastrow factor vanishes with a zero of order q whenever two electrons are at the same position, as guaranteed by the Pauli exclusion principle. The state has a very high overlap with the ground state of the exact Hamiltonian with Coulomb interactions.

Later it was realized that the guessed state in Eq. (3.22) can be written as the conformal field correlator with the vertex operators

$$V(Z_j) =: e^{i\sqrt{q}\phi(Z_j)} : \quad (3.23)$$

of the conformal field theory as [162]

$$\Psi_L(n_1, \dots, n_M) = \langle 0 | \prod_{j=1}^M : e^{i\sqrt{q}\phi(Z_j)} :: e^{-i\sqrt{q} \int \rho \phi(Z) d^2Z} : | 0 \rangle, \quad (3.24)$$

where

$$\rho = \frac{1}{2\pi q} \quad (3.25)$$

is the electron density and the term in Eq. (3.24) involving ρ satisfies the charge neutrality condition.

The filling fraction ν is defined as the number of particles per magnetic flux as

$$\nu = \frac{M}{N_\phi}. \quad (3.26)$$

Now a gapped excitation above the ground state of Eq. (3.22) can be obtained by adding a flux quantum to the system. That is by inserting positive flux tubes. Experimentally this can be obtained by slightly increasing the magnetic field in the system. The wavefunction with a well-screened excitation at position $\eta \in \mathbb{C}$ is [224]

$$\Psi_L^h(n_1, \dots, n_M) = \prod_{i=1}^M (Z_i - \eta) \prod_{j < k}^M (Z_j - Z_k)^q e^{-\frac{1}{4} \sum_{j=1}^M |Z_j|^2}. \quad (3.27)$$

We note that the wavefunction vanishes at point η . That is a "hole" is created in the electron liquid. This "hole" has a remarkable property of carrying fractional charge and of obeying fractional statistics which are distinguishable from the elementary particle properties. And the "hole" is called the quasihole. We can estimate the charge of the quasihole as follows. We place q quasiholes at point η and therefore write the state as

$$\Psi_L^{h\{q\}}(n_1, \dots, n_M) = \prod_{i=1}^M (Z_i - \eta)^q \prod_{j < k}^M (Z_j - Z_k)^q e^{-\frac{1}{4} \sum_{j=1}^M |Z_j|^2}. \quad (3.28)$$

This state describes the Laughlin state of Eq. (3.22) with the deficit of an electron at position η . That is q number of quasiholes are responsible to take one electron out of the system. Therefore each quasihole carries a fraction $1/q$ of the electron charge.

Similar to Eq. (3.24), the state in Eq. (3.28) can be expressed with the vertex operators

$$V(\eta_k) =: e^{\frac{i}{\sqrt{q}}\phi(w_k)} : \quad (3.29)$$

for $k \in \{1, \dots, Q\}$ number of quasiholes. As opposed to the elementary particles as fermions and bosons in three-dimensions, these quasiparticle excitations in two-dimensions follow any statistics between the Fermi-Dirac statistics and the Bose-Einstein statistics. Hence these quasiparticles are nomenclature as anyons. For example the Laughlin quasiholes acquire a phase $e^{i\pi/q}$ under an anti-clockwise exchange.

Beyond the hierarchical construction based on the Laughlin state, another candidate of the fractional quantum Hall effect has gained a lot of recognition since its discovery. This is the Moore-Read Pfaffian state [162] at the Landau level filling factor $5/2$ which can be thought to consist of the fully filled lowest Landau level with both spin up-spin down electrons and followed by the spin polarised second Landau level at $1/2$ filling. The state reads as

$$\Psi_{\text{MR}}(n_1, \dots, n_M) = \text{Pf} \left(\frac{1}{Z_i - Z_j} \right) \prod_{j < k}^M (Z_j - Z_k)^q e^{-\frac{1}{4} \sum_{j=1}^M |Z_j|^2}, \quad (3.30)$$

where 'Pf' stands for the Pfaffian which is the square root of the determinant, with proper sign, of an anti-symmetric matrix of even order. We define the Pfaffian of an anti-symmetric matrix \mathcal{M}_{ij} of order $\mathcal{N} \times \mathcal{N}$ as

$$\text{Pf}(\mathcal{M}) = \frac{1}{2^{\mathcal{N}/2} (\mathcal{N}/2)!} \sum_{\sigma} \text{sign}(\sigma) \prod_{k=1}^{\mathcal{N}/2} \mathcal{M}_{\sigma(2k-1), \sigma(2k)}, \quad (3.31)$$

where σ denotes the symmetric group of dimension \mathcal{N} and $\text{sign}(\sigma)$ is the signature of σ . Therefore the state in Eq. (3.30) defines fermions for q even and defines bosons for q odd. This state can be expressed with the vertex operators

$$V(Z_j) = \psi(Z_j) : e^{i\sqrt{q}\phi(Z_j)} : \quad (3.32)$$

in a similar manner as before, where $\psi(Z_j)$ is the Majorana field [31] at the j th particle position Z_j . The quasiholes in the Moore-Read state carry a charge $1/2q$ of the electron charge.

3.2.1 Quasielectron states and the singularity problem

We have talked about the quasiholes so far. Now the quasiparticles with opposite charges of the quasiholes are expected to be created by inserting negative flux tubes in the systems and thereby slightly decreasing the magnetic field. These are termed as the quasielectrons. Experimentally the quasiholes and the quasielectrons play a very similar role, however the quasielectrons are much harder to describe theoretically in parallel to that of the quasiholes. Because it is easier to reduce the electron density locally than to increase it due to the Pauli exclusion principle.

In the same spirit of Eq. (3.27) if we want to increase the electron density, and thereby to decrease the angular momentum, then we need to multiply Eq. (3.22) by the factor

$$\prod_{i=1}^M (Z_i - \eta)^{-1}. \quad (3.33)$$

But we note that the wavefunction is now singular and hence is ill-defined. Instead Laughlin proposed to decrease the angular momentum by differentiation and wrote the state for the quasielectron at η in the Laughlin state as [224]

$$\Psi_L^e(n_1, \dots, n_M) = e^{-\frac{1}{4} \sum_{j=1}^M |Z_j|^2} \prod_{i=1}^M \left(2 \frac{\partial}{\partial Z_i} - \bar{\eta} \right) \prod_{j < k}^M (Z_j - Z_k)^q. \quad (3.34)$$

This state is much harder to deal with both analytically and numerically in comparison to the Laughlin state containing quasiholes, as shown in Eq. (3.28). In addition, this state does not properly describe a quasielectron [110]. In the same way the quasielectrons in other states, like the Moore-Read states, are more difficult to handle with respect to their quasihole counterparts.

3.3 Anyonic lattice fractional quantum Hall states

Mainly two approaches are taken to realize the continuum fractional quantum Hall physics on the lattices. One approach is to mimic the Landau level by constructing the flat-band fractional Chern insulator models [271, 22, 108, 216, 246, 247, 214, 79, 63]. Here the real background magnetic field is replaced by the complex hopping terms in the Hamiltonian and thereby breaking the time-reversal symmetry. These flat-band models provide an exact equivalence between the Landau level and the lattice systems. The other approach is to mimic the interactions directly to construct the lattice chiral spin liquid states [256, 197, 69, 169, 227, 173, 170, 157, 156, 175] which have the same topological properties as those of the continuum fractional quantum Hall states. An example of the latter approach was first done by Kalmeyer and Laughlin [115] to propose the Laughlin type states on the lattices for bosons, that is for $\nu = 1/2$. This state has the similar expression as the state in Eq. (3.22) but now with $q = 2$ and the particles are placed on the lattice sites, that is Z_i denotes the i th lattice site position. Some recent works [70, 71, 69, 169] in this direction show that the topological properties remain same while translating the states in the lattice systems. Also the realization of anyons is possible in the lattice models and the quasielectron state can be constructed in a similar fashion to that of the quasihole state [175, 156]. In this section, by following this latter approach, we derive the analytical forms of the anyonic lattice Laughlin and lattice Moore-Read states on a plane with particular choices of the vertex operators, and by restricting the magnetic flux to only go through the lattice sites.

We note that the continuum model is rotationally invariant for any amount of rotation, whereas the lattice model breaks the continuous rotational symmetry but possesses the discrete rotational symmetry. This can be thought of as an anisotropy in the system due

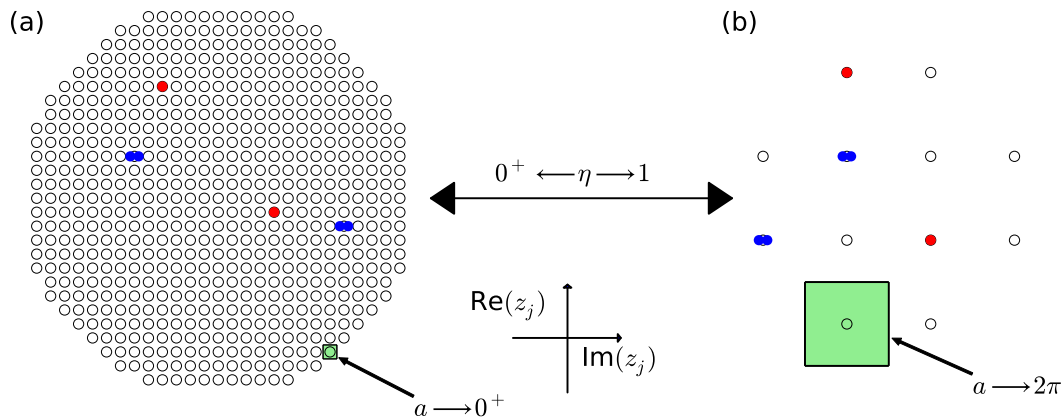


Figure 3.2.: We define the lattice on a two-dimensional complex plane, as defined by $[\text{Re}(z_j), \text{Im}(z_j)]$, and on a disk shaped geometry. Each lattice site is either empty, as pictured by the black circles, or singly occupied, as pictured by the red filled circles, or doubly occupied, as pictured by the blue filled circles, respectively. We mark the area a of a lattice site with a green square where $a \rightarrow 0^+$ in the continuum limit, as shown in (a), and where $a \rightarrow 2\pi$ in the lattice limit, as shown in (b). We take N number of lattice sites and we define $\eta = a/2\pi$. We illustrate the transformation between the continuum limit, that is the scenario $\eta \rightarrow 0^+, N \rightarrow \infty$ in (a) and the lattice limit, that is the scenario $\eta \rightarrow 1$ in (b) by varying η between 0 and 1. The interpolation is performed by keeping ηN fixed throughout.

to the underlying lattice structure. As for example the square lattice without any anyon preserves C_4 symmetry, and hence it is invariant under a $\pi/2$ rotation. By choosing different kinds of lattice structures one can import further anisotropies, like C_2 symmetry, and therefore a π rotation invariance, for a rectangular lattice etc. We point out that here the absence of the continuous rotational symmetry is solely due to the underlying lattice structure and is completely different from the continuous rotational symmetry, under the Mobius transformations, of the primary fields. The vertex operators maintain the Mobius transformations and therefore the constructed analytical states exhibit continuous rotational symmetry.

3.3.1 Lattice Laughlin states on a plane

On the two-dimensional complex plane we construct family of the Laughlin states at the Landau level filling factor $1/q$ and of arbitrary lattice filling factor, in the presence and in the absence of anyons, as follows.

(a). States without anyons

We consider an arbitrary lattice with N lattice sites at positions z_j , $j \in \{1, \dots, N\}$. Specific choices of z_j lead to the different types of lattices, for example square lattice etc. Let us define a local basis state at the j th lattice site as $|n_j\rangle$, where n_j defines the number of particles at site j . We take the local basis states as $n_j \in \{0, 1, \dots, p\}$ denoting the lattice occupancy at the j th site. For example with $n_j \in \{0, 1\}$ maximum one boson, that is the hardcore limit or one fermion is allowed at each site, with $n_j \in \{0, 1, 2\}$ at most two bosons or two fermions of different types are allowed at each site. Therefore the total Hilbert space dimension becomes $(p+1)^N$.

We take a as the average area per lattice site and define

$$\eta = \frac{a}{2\pi}. \quad (3.35)$$

Hence we set the magnetic length to be unity. The parameter η allows us to interpolate between the lattice limit and the continuum limit. We keep ηN fixed throughout this interpolation and take $\eta \rightarrow 1$ to be the lattice limit and take

$$\eta \rightarrow 0^+, N \rightarrow \infty \quad (3.36)$$

as the continuum limit. We see below that this in turn keeps the particle number per area fixed in the system while interpolating the number of lattice sites per particle from q in the lattice limit to infinite in the continuum limit. We show in Fig. 3.2 such an example with $q = 2$ and with $n_j \in \{0, 1, 2\}$.

We describe the state on the lattice as

$$|\Psi\rangle = \frac{1}{C} \sum_{n_1, \dots, n_N} \Psi |n_1, \dots, n_N\rangle \text{ with } C^2 = \sum_{n_1, \dots, n_N} |\Psi|^2, \quad (3.37)$$

where C is a real constant. And Ψ can be obtained by following the conformal field theory construction of the states as shown in Eq. (3.1) and thereby using the correlators of the vertex operators $V_{n_j}(z_j)$ of the underlying conformal field theory as [256, 175, 197, 169, 180]

$$\Psi(\{z_j\}) = \langle \prod_{j=1}^N V_{n_j}(z_j) \rangle \text{ with } V_{n_j}(z_j) =: e^{i(qn_j - \eta)\phi(z_j)/\sqrt{q}} :, \quad (3.38)$$

where we denote Ψ as $\Psi(\{z_j\})$ and $\langle \dots \rangle$ as the vacuum expectation value. We have $\phi(z_j)$ as the chiral field of the free massless bosons of the $U(1)$ conformal field theory with central charge $c = 1$ and $: \dots :$ denotes the normal ordering. We note that the charge neutrality condition is already taken care of by suitably choosing the vertex operators in Eq. (3.38). Hence the background charge is not needed as opposed to the continuum version of the state.

The correlator in Eq. (3.38) evaluates to the Jastrow factors as

$$\Psi(\{z_j\}) = \delta_n \prod_{i<j} (z_i - z_j)^{q n_i n_j} \prod_{i \neq j} (z_i - z_j)^{-\eta n_i}, \quad (3.39)$$

where $\delta_n = 1$ if the number of particles is

$$M = \frac{\eta N}{q} \quad (3.40)$$

and otherwise $\delta_n = 0$. The lattice filling fraction is

$$\frac{M}{N} = \frac{\eta}{q} \quad (3.41)$$

which becomes the Landau level filling factor $1/q$ for $\eta = 1$. The state in Eq. (3.39) describes fermions and bosons for q odd and q even respectively. We note that the factor

$$\prod_{l<j} (z_l - z_j)^{q n_l n_j} \quad (3.42)$$

is interpreted as the attachment of q fluxes to each particle and the factor

$$\prod_{l \neq j} (z_l - z_j)^{-\eta n_l} \quad (3.43)$$

corresponds to the background charge in the lattice.

(b). States with anyons

We consider Q anyons at positions w_k , $k \in \{1, \dots, Q\}$ and define the vertex operators from $c = 1$ conformal field theory as [180, 175, 169, 197]

$$W_{p_k}(w_k) =: e^{i p_k \phi(w_k) / \sqrt{q}} : \text{ with } p_k \in \pm\{0, 1, \dots, q-1\}, \quad (3.44)$$

where w_k are not restricted to lie on the lattice sites, and hence w_k can be anywhere in the complex plane. The charge of the k th anyon is given as p_k/q where we assume the standard charge of a particle as -1 . Therefore the positive and the negative values of p_k describes the quasiholes and the quasielectrons respectively.

We write the correlator as

$$\Psi(\{z_j\}, \{w_k\}) = \langle \prod_{j=1}^N V_{n_j}(z_j) \prod_{k=1}^Q W_{p_k}(w_k) \rangle, \quad (3.45)$$

where $V_{n_j}(z_j)$ is the same as used in Eq. (3.38) and we denote Ψ as $\Psi(\{z_j\}, \{w_k\})$. We evaluate the correlator as the Jastrow factors as

$$\Psi(\{z_j\}, \{w_k\}) = \delta_n \prod_{i<j} (z_i - z_j)^{q n_i n_j} \prod_{i \neq j} (z_i - z_j)^{-\eta n_i} \prod_{i,j} (w_i - z_j)^{p_i n_j}, \quad (3.46)$$

where $\delta_n = 1$ if the number of particles is

$$M = \frac{(\eta N - \sum_k p_k)}{q} \quad (3.47)$$

and otherwise $\delta_n = 0$. Therefore a single quasihole or a single quasielectron remove or add a p_k/q fraction of particles respectively, which indicates the fractional charge of the anyon as p_k/q .

3.3.2 Lattice Moore-Read states on a plane

On the two-dimensional complex plane we construct family of the Moore-Read states at the second Landau level with filling factor $1/q$ and of arbitrary lattice filling factor, in the presence and in the absence of anyons, as follows.

(a). States without anyons

We associate the following vertex operator to each lattice site z_j , $j \in \{1, \dots, N\}$ as [69, 9]

$$V_{n_j}(z_j) = \chi_{n_j}(z_j) \psi(z_j)^{\Delta_{n_j}} : e^{i(qn_j - \eta)\phi(z_j)/\sqrt{q}} : \text{ with } \chi_{n_j}(z_j) = e^{i\pi(j-1)\eta n_j}, \quad (3.48)$$

where $\psi(z_j)$ is the holomorphic free Majorana fermion field with conformal dimension $h_\psi = 1/2$ and with central charge $c = 1/2$ of the underlying Ising conformal field theory. We define $\Delta_{n_j} = 1$ if $n_j = 1$ and $\Delta_{n_j} = 0$ otherwise. Therefore the Majorana field acts only on the singly occupied lattice sites. The phase factor $\chi_{n_j}(z_j)$ could be taken as will. We have chosen this particular form of $\chi_{n_j}(z_j)$ because it ensures that the analytical state is SU(2) invariant for $q = 1$ and in the absence of anyons. However a different choice of the single particle phase factors will not affect the topological properties of the states, for example the topological entanglement entropy, braiding statistics of the anyons etc.

The underlying conformal field theory here is with the central charge

$$c = \frac{1}{2} + 1, \quad (3.49)$$

where $c = 1/2$ part provides the Pfaffian contribution which is also known as the Ising contribution since this conformal field theory part also describes the Ising spin chain model, coming from the Majorana sector, and $c = 1$ part describes the Jastrow factors, coming from the bosonic sector, in the analytical states.

The correlator gets decoupled as a product into the two contributions as the free fermionic part and the free bosonic part as

$$\Psi(\{z_j\}) = \left\langle \prod_{j=1}^N \psi(z_j)^{\Delta_{n_j}} \right\rangle \left\langle \prod_{j=1}^N : e^{i(qn_j - \eta)\phi(z_j)/\sqrt{q}} : \right\rangle, \quad (3.50)$$

where we denote $\Psi = \Psi(\{z_j\})$. We evaluate the correlator to get the analytical state as

$$\Psi(\{z_j\}) = \delta_n \text{Pf} \left(\frac{1}{z'_i - z'_j} \right) \prod_{i < j} (z_i - z_j)^{q n_i n_j} \prod_{i \neq j} (z_i - z_j)^{-\eta n_i}, \quad (3.51)$$

where $\delta_n = 1$ if the number of particles is

$$M = \frac{\eta N}{q} \quad (3.52)$$

and otherwise $\delta_n = 0$. The symbol 'Pf' stands for the Pfaffian, which we have defined in Eq. (3.31), and which, to be non-zero, requires \mathcal{M} as even, where \mathcal{M} represents the number of singly occupied sites. We denote the singly occupied lattice sites by z' . Since the Pfaffian is antisymmetric therefore the state in Eq. (3.51) corresponds to bosons and to fermions for q odd and for q even respectively.

(b). States with non-Abelian or Ising anyons

We consider the following vertex operator at each anyon position w_k , $k \in \{1, \dots, Q\}$ as [157, 156]

$$W_{p_k}(w_k) = \sigma(w_k) : e^{i p_k \phi(w_k) / \sqrt{q}} : \text{ with } p_k = \pm 1/2, \quad (3.53)$$

where $\sigma(w_k)$ is the holomorphic spin operator of the chiral Ising conformal field theory and having the conformal dimension $h_\sigma = 1/16$. The charge of the k th anyon is p_k/q where we assume the standard charge of a particle as -1 and hence the positive and the negative values of p_k describes the quasiholes and the quasielectrons respectively.

We write the states as

$$|\Psi_\alpha\rangle = \frac{1}{C_\alpha} \sum_{n_1, \dots, n_N} \Psi_\alpha(\{z_j\}, \{w_k\}) |n_1, \dots, n_N\rangle \quad (3.54)$$

$$\text{with } C_\alpha^2 = \sum_{n_1, \dots, n_N} \left| \Psi_\alpha(\{z_j\}, \{w_k\}) \right|^2,$$

where $\Psi_\alpha(\{z_j\}, \{w_k\})$ can be expressed as the conformal blocks of the underlying conformal field theory by following the construction as shown by Moore and Read for the continuum case and its latter extensions to the lattices. We have C_α as a real constant.

We have many conformal blocks of the holomorphic spin operators σ , as given in Eq. (3.53), of the Ising conformal field theory. The number of conformal blocks depends on the number of the anyons present in the system. The total number of different labels of the conformal blocks is denoted by the vector α in Eq. (3.54). And the number of conformal blocks for each of the topological charge sectors identity I or Majorana ψ is [9, 31]

$$2^{\frac{Q}{2}-1} \quad (3.55)$$

for the Q anyons in the system. Hence we always need an even number of anyons in the systems. Therefore the wavefunctions $|\Psi_\alpha\rangle$ in Eq. (3.54) represent a degenerate set of wavefunctions for fixed anyon positions. And this scenario constitutes the basis for the non-Abelian statistics of the anyons. Now all the fields must be fused to the identity to provide a non-zero correlator and we have the following non-trivial Ising fusion algebra as

$$\psi \times \psi = I; \quad \psi \times \sigma = \sigma; \quad \sigma \times \sigma = I + \psi. \quad (3.56)$$

We specify the fusion channel of the Ising spin fields

$$\sigma(w_{2k-1}) \text{ and } \sigma(w_{2k}) \quad (3.57)$$

by the k th entry of the vector α . And we have if $\alpha_i = 0$ then these fields fuse to the identity I or correspondingly if $\alpha_i = 1$ then these fields fuse to the Majorana field ψ . Therefore depending on the number of anyons in the system the analytical forms of the states become different. And we note that the identity I and the Majorana ψ are referred to the two different topological charge sectors.

We write the correlator as

$$\begin{aligned} \Psi_\alpha(\{z_j\}, \{w_k\}) = & \left\langle \prod_{j=1}^N \psi(z_j)^{\Delta_{n_j}} \prod_{k=1}^Q \sigma(w_k) \right\rangle_\alpha \\ & \times \left\langle \prod_{j=1}^N : e^{i(qn_j - \eta)\phi(z_j)/\sqrt{q}} : \prod_{k=1}^Q : e^{ip_k\phi(w_k)/\sqrt{q}} : \right\rangle, \end{aligned} \quad (3.58)$$

where the second part provides the Jastrow factors from $c = 1$ conformal field theory and are the same for an arbitrary even number of anyons in the system. The first part comes from the $c = 1/2$ conformal field theory and gives rise to the different terms which depend on the number of anyons in the system. These anyons are often called as the Ising anyons. We explicitly write the analytical forms of the states containing two and four anyons in the systems as follows.

(1). State with two anyons: In this case we have one conformal block for each topological charge sector. Depending on the fusion channel of the two σ fields, as mentioned in Eq. (3.56), we have two independent possibilities. That is for $Q = 2$ we have one state for each of the topological charge sectors I and ψ . When two σ fields fuse to the identity I , or fused to the Majorana ψ , then we have an even, or an odd, number of the Majorana field ψ in Eq. (3.58) respectively which in turn indicates that we have an even, or an odd, number of the singly occupied lattice sites respectively. We are interested in the state corresponding to the fusion channel I , that is corresponding to the topological charge sector I , since we find the expression for the correlator is simpler.

We write the state as

$$\begin{aligned} \Psi_\alpha(\{z_j\}, \{w_k\}) &= \delta_n 2^{-\frac{M}{2}} (w_1 - w_2)^{-\frac{1}{8}} \text{Pf}(A) \prod_{i,j} (w_i - z'_j)^{-\frac{1}{2}} \prod_{i<j} (z_i - z_j)^{qn_i n_j} \\ &\times \prod_{i \neq j} (z_i - z_j)^{-\eta n_i} \prod_{i<j} (w_i - w_j)^{p_i p_j / q} \prod_{i,j} (w_i - z_j)^{p_i n_j} \prod_{i,j} (w_i - z_j)^{-\eta p_i / q} \end{aligned} \quad (3.59)$$

with

$$A_{ij} = \left(\frac{(z'_i - w_1)(z'_j - w_2) + (i \leftrightarrow j)}{z'_i - z'_j} \right), \quad (3.60)$$

where $\delta_n = 1$ if the number of particles is

$$M = \frac{(\eta N - \sum_k p_k)}{q} \quad (3.61)$$

and otherwise $\delta_n = 0$. We have \mathcal{M} as even and $\alpha = I$.

(2). States with four anyons: In this case we have two conformal blocks for each topological charge sector since we have $Q = 4$ here. This gives rise to the degeneracy in the system. We are interested in the states corresponding to the fusion channel I of the four σ fields, that is corresponding to the topological charge sector I . We denote the two conformal block indices as $m_I = 0$ and as $m_\psi = 1$.

We write the states as

$$\begin{aligned} \Psi_\alpha(\{z_j\}, \{w_k\}) &= \delta_n 2^{-\frac{M+1}{2}} (w_1 - w_2)^{-\frac{1}{8}} (w_3 - w_4)^{-\frac{1}{8}} \left((1-x)^{\frac{1}{4}} + \frac{(-1)^{m_\alpha}}{(1-x)^{\frac{1}{4}}} \right)^{-\frac{1}{2}} \\ &\times \left((1-x)^{\frac{1}{4}} \Phi_{(13)(24)} + (-1)^{m_\alpha} (1-x)^{-\frac{1}{4}} \Phi_{(14)(23)} \right) \prod_{i,j} (w_i - z'_j)^{-\frac{1}{2}} \prod_{i<j} (z_i - z_j)^{qn_i n_j} \\ &\times \prod_{i \neq j} (z_i - z_j)^{-\eta n_i} \prod_{i<j} (w_i - w_j)^{p_i p_j / q} \prod_{i,j} (w_i - z_j)^{p_i n_j} \prod_{i,j} (w_i - z_j)^{-\eta p_i / q} \end{aligned} \quad (3.62)$$

with

$$\Phi_{(k_1 k_2)(k_3 k_4)} = \text{Pf} \left(\frac{(w_{k_1} - z'_i)(w_{k_2} - z'_i)(w_{k_3} - z'_j)(w_{k_4} - z'_j) + (i \leftrightarrow j)}{(z'_i - z'_j)} \right) \quad (3.63)$$

and

$$x = \frac{(w_1 - w_2)(w_3 - w_4)}{(w_1 - w_4)(w_3 - w_2)}, \quad (3.64)$$

where \mathcal{M} is even and x is called the anharmonic ratio. We label the anyons by k_i in

$$\Phi_{(k_1 k_2)(k_3 k_4)} \text{ and we have } \alpha \in \{I, \psi\}. \quad (3.65)$$

We have $\delta_n = 1$ if the number of particles is

$$M = \frac{(\eta N - \sum_k p_k)}{q} \quad (3.66)$$

and otherwise $\delta_n = 0$.

(c). States with Abelian anyons

We associate the vertex operator from Eq. (3.48) to each lattice site and the vertex operator from Eq. (3.44) to each anyon position. These give the lattice Moore-Read state hosting the Abelian type anyons in the system. We write the correlator as

$$\Psi(\{z_j\}, \{w_k\}) = \langle \prod_{j=1}^N \psi(z_j)^{\Delta_{n_j}} \rangle \langle \prod_{j=1}^N : e^{i(qn_j - \eta)\phi(z_j)/\sqrt{q}} : \prod_{k=1}^Q : e^{ip_k\phi(w_k)/\sqrt{q}} : \rangle \quad (3.67)$$

and the analytical state reads as

$$\Psi(\{z_j\}, \{w_k\}) = \delta_n \text{Pf} \left(\frac{1}{z'_i - z'_j} \right) \prod_{i < j} (z_i - z_j)^{qn_i n_j} \prod_{i \neq j} (z_i - z_j)^{-\eta n_i} \prod_{i,j} (w_i - z_j)^{p_i n_j}, \quad (3.68)$$

where $\delta_n = 1$ if the number of particles is

$$M = \frac{(\eta N - \sum_k p_k)}{q} \quad (3.69)$$

and otherwise $\delta_n = 0$. We require \mathcal{M} as even.

3.3.3 Quasielectron states and avoiding the singularity problem

We have discussed in Sec. 3.2 about the singularity problem for the quasielectron states in the continuum. There the states correspond to the particle coordinates and the particles can be anywhere in the entire system. Now the creation of a quasielectron at a position means that the density of the particles are increased locally. This in turn corresponds that the quasielectron attracts the particles towards it. Now when a particle, say the k th one at position Z_k , coincides with the quasielectron, say the j th one at position w_j , then the factor

$$(w_j - Z_k)^{p_j}, \quad (3.70)$$

with p_j negative, creates the singularity and the state is not well defined anymore. This trouble arises if one constructs the quasielectron state in a similar manner as that of the quasihole states.

Now in the lattice systems we restrict the particles to sit only on the lattice sites and we keep the anyon positions flexible. Therefore we get the factor

$$(w_j - z_k)^{p_j n_k}, \quad (3.71)$$

with p_j negative and n_k corresponds to the occupancy of the k th lattice site at position z_k . We place the anyons anywhere in between the lattice sites and thereby we avoid the singularity since the anyon positions do not coincide with the particle positions. The placement of anyons exactly on the lattice sites is also possible. In that case the corresponding lattice site where the quasihole, or the quasielectron, is placed remains unoccupied, or occupied respectively. That is we take away the degrees of freedom of that particular lattice site by putting either no particle for the quasihole or by putting one particle for the quasielectron, while maintaining the degrees of freedom for the rest of the lattice sites as either occupied or empty. Therefore the factor

$$(w_j - z_k)^{p_j n_k}, \quad (3.72)$$

with p_j negative and for all n_k values, can be incorporated in the normalization constant in the limit $w_j \rightarrow z_k$. In this way the singularity problem does not appear and the quasielectron states can be constructed in the same way as those of the quasihole states [156, 175].

3.3.4 Continuum limit of the lattice states

We take the continuum limit of the lattice fractional quantum Hall states, by following the procedure as shown in Refs. [69, 157]. The lattice construction of the anyonic states closely resembles to the continuum states where the wavefunctions are expressed in the basis spanned by the particle coordinates and the background charge is represented by the Gaussian factors. We take the states on a two-dimensional lattice defined on a disk of radius $R_D \rightarrow \infty$. We reach the continuum limit by considering

$$\eta \rightarrow 0^+, N \rightarrow \infty \quad (3.73)$$

with ηN fixed which in turn fix the particle number M of the system as depicted in Fig. 3.2. We choose lattices such that the area per lattice sites is constant a , and thereby

$$\eta = \frac{a}{2\pi} \quad (3.74)$$

is constant, but similar outcomes hold also for other lattices where a and hence η is position dependent.

We first note that in the continuum limit we can write the factor

$$\left| \prod_{j(\neq l)} (z_l - z_j)^{-\eta} \right| \quad (3.75)$$

as

$$\left| \prod_{j(\neq l)} (z_l - z_j)^{-\eta} \right| = \left| \exp\left(-\sum_{j(\neq l)} \eta \ln(z_l - z_j)\right) \right| = \exp\left(-\int_D \ln(|z_l - z|) d^2z/2\pi\right), \quad (3.76)$$

where the notations

$$\prod_{j(\neq l)} \text{ and } \sum_{j(\neq l)} \quad (3.77)$$

represent respectively the product and the sum over the index j , which is not equal to l , only. In the continuum limit the integral in Eq. (3.76) evaluates to

$$|z_l|^2 + \text{constant}. \quad (3.78)$$

In a similar fashion the continuum limit of the factor

$$\prod_{l,j} (w_l - z_j)^{-p_l/q} \quad (3.79)$$

can be computed.

Therefore we inscribe

$$\begin{aligned} \prod_{j \neq l} (z_l - z_j)^{-\eta n_l} &\propto e^{-i \Sigma_l g_l} e^{-\Sigma_l n_l |z_l|^2/4}, \\ \prod_{l,j} (w_l - z_j)^{-p_l/q} &\propto e^{-i \Sigma_l f_l} e^{-\frac{1}{4} \frac{2\pi}{a} \Sigma_l \frac{p_l}{q} |w_l|^2}, \end{aligned} \quad (3.80)$$

where we have

$$g_l = \text{Im} \left[\eta \sum_{j(\neq l)} n_l \ln(z_l - z_j) \right] \text{ and } f_l = \text{Im} \left[\frac{1}{q} \sum_j p_l \ln(w_l - z_j) \right] \quad (3.81)$$

as real numbers which give rise to the phase factors. These overall phase factors are the gauge factors which can be transformed away if needed. And these phase factors do not hamper the properties like particle-particle correlations and the entanglement entropy of the state.

3.4 Conclusions

In this chapter we have constructed the lattice fractional quantum Hall states hosting anyons. The states are derived as the conformal field correlators acting on the lattice

sites and on the anyon positions. We have explicitly constructed the lattice Laughlin state and the lattice Moore-Read state on the plane in the presence and in the absence of anyons. We have shown that the singularity problem with the quasielectrons, as appeared in the continuum, can be avoided in the lattice systems. Thereby we have shown that the quasielectron states can be constructed in a similar way as those of the quasihole states. We introduce a parameter in the states which allows us to interpolate between the lattice models and their continuum limits.

These analytical forms of the states facilitate to investigate the properties of the states and also to compute the properties of the anyons, both quasiholes and quasielectrons, for larger system sizes using the Monte-Carlo simulations. Furthermore exact parent Hamiltonians can be derived analytically which have the derived analytical states as the ground states. We discuss these in the upcoming chapters.

Non-Abelian Anyons in Lattice Moore-Read Models

“Over coffee at the Red Door Cafe that afternoon, we bonded over our shared admiration for a visionary paper by Greg Moore and Nick Read about non-abelian anyons in fractional quantum Hall systems, though neither of us fully understood the paper (and I still don't). Maybe, we mused together, non-abelian anyons are not just a theorist's dream . . . It was the beginning of a beautiful friendship.

— John Preskill with Alexei Kitaev

Anyons appear in two flavors, as the quasiholes, which are the positively charged anyons and as the quasielectrons, which are the negatively charged anyons. While the quasiholes [261, 274, 273] are well explored, the quasielectrons are much harder to analyze [24, 86, 263, 87, 129] in the continuum as we discussed in Chapter-3. Recently it was shown that, in the lattice models, the quasielectrons can be investigated [175] in a similar way as that of the quasiholes. However the Abelian type of anyons in the Laughlin state are researched till now. In this chapter we explore the properties of the non-Abelian anyons, which are also known as the Ising anyons, in the lattice Moore-Read state at the Landau level filling factor $5/2$ for which the analytical states were derived in Chapter-3. We justify our claim that the non-Abelian quasielectrons can be created and can be investigated in a way similar as that of the non-Abelian quasiholes. We derive the parent Hamiltonians for which the analytical states are exact ground states. We also create the non-Abelian anyons in a simpler model of hardcore bosons, which is known as the Kapit-Mueller model.

In Sec. 4.1 we investigate the density profiles, shapes, excess charge distributions and charges of the non-Abelian Ising anyons in the lattice Moore-Read states. We find that the anyons are well-screened and we show that the quasielectrons can be created in a similar way as that of the quasiholes. We research the fractional braiding statistics of the anyons in Sec. 4.2 and show that the anyons are non-Abelian and the statistics are as expected from the continuum. We derive the parent Hamiltonians for our lattice models in Sec. 4.3 and find that the Hamiltonians contain few-body long-range interactions. We create anyons in the Kapit-Mueller model in Sec. 4.4 and show that the quasielectrons can be

created in the same fashion as that of the quasiholes. We find that our analytical lattice Moore-Read states are relevant to the Kapit-Mueller model. We draw the conclusions in Sec. 4.5. This chapter is based on parts of the following Refs. [156, 157]:

[1] : **Sourav Manna, Julia Wildeboer and Anne E. B. Nielsen**, "Quasielectrons in lattice Moore-Read models", *Physical Review B* **99**, 045147 (2019)

[2] : **Sourav Manna, Julia Wildeboer, Germán Sierra and Anne E. B. Nielsen**, "Non-Abelian quasiholes in lattice Moore-Read states and parent Hamiltonians", *Physical Review B* **98**, 165147 (2018)

4.1 Density profiles and charges of the anyons

In this section we investigate how the anyons influence the particle densities in the lattice sites. We analyze the shape of the anyons and compute their charges. We employ Monte-Carlo simulations [241, 199, 253, 90] and take $n_j \in \{0, 1\}$, $\eta = 1$, and $q = 2$ in the anyonic lattice Moore-Read states, as defined in Chapter-3 in Sec. 3.3 in Eqs. (3.51), (3.59), (3.62).

4.1.1 Density profiles of anyons

We define particle density of the i th lattice site for any state $|\Phi\rangle$ to be

$$\langle n(z_i) \rangle = \langle \Phi | n(z_i) | \Phi \rangle. \quad (4.1)$$

Therefore density profile of the anyons can be evaluated as

$$\rho(z_i) = \langle n(z_i) \rangle_{Q \neq 0} - \langle n(z_i) \rangle_{Q=0}, \quad (4.2)$$

where $n(z_i)$ is the particle occupation number at the i th lattice site. We have

$$\langle n(z_i) \rangle_{Q \neq 0} \text{ and } \langle n(z_i) \rangle_{Q=0} \quad (4.3)$$

as the particle densities of the i th lattice site in the presence and in the absence of anyons in the state respectively.

We note that, due to the restriction of the particle number as

$$M = \frac{\left(\eta N - \sum_{k=1}^Q p_k \right)}{q}, \quad (4.4)$$

the insertion of a quasihole or a quasielectron leads respectively to the decrement or to the increment of the total number of particles in the system by a fraction p_k/q .

Now, we require the Pfaffian factors in both the wavefunctions containing the anyons, that is Eqs. (3.59) and (3.62), and without anyons, that is Eq. (3.51), to be non-zero.

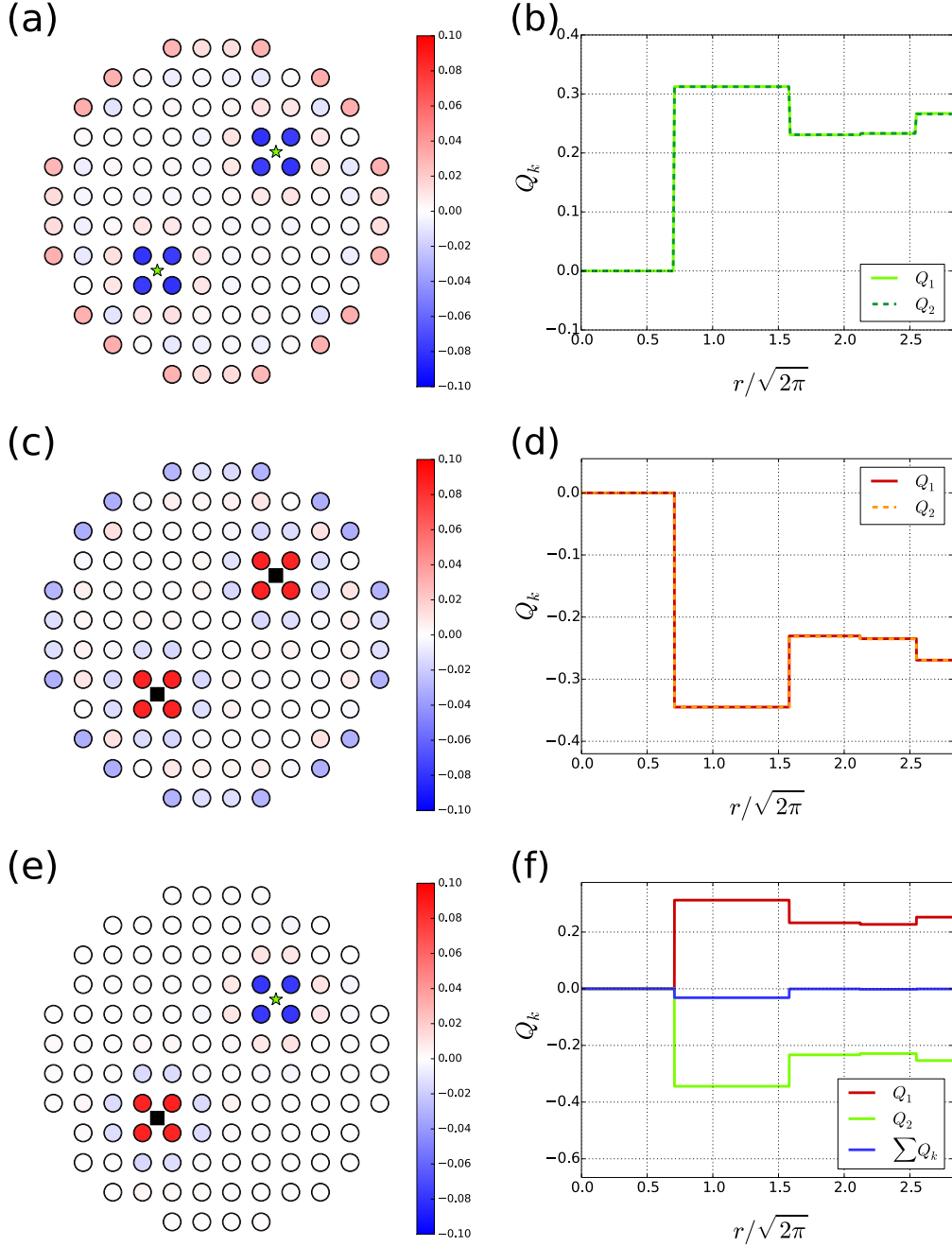


Figure 4.1.: In (a), (c), (e): We represent lattice sites, quasiholes and quasielectrons, respectively by the black circles, the green stars and the black squares. We take the number of lattice sites $N = 112$. The density profiles $\rho(z_i)$ from Eq. (4.2), defined as the particle density difference between the states in the presence and in the absence of anyons, are plotted with colorbars for the cases of (a) two quasiholes, (c) two quasielectrons, and (e) one quasihole-one quasielectron. We place the anyons in the middle of the lattice plaquette. The anyons are well-screened with the radii of a few lattice constants. The colors on the edges appear due to the charges at infinity in the state containing anyons as explained in the main text. In (b), (d), (f): The excess charge distributions Q_k with $k \in \{1, \dots, Q\}$ are computed from Eq. (4.10) and are plotted as a function of the radial distances $r/\sqrt{2\pi}$, from the anyon positions, corresponding to the above mentioned anyon configurations respectively. The anyon positions are symmetric with respect to $\pi/2$ rotation of the lattice. Therefore the excess charge plots are on top of each other. The anyon charges approach $\simeq \pm 0.25$ for large r with an errorbar of size 10^{-4} arising from the Monte-Carlo simulations. We note that the density profiles are similar for the quasiholes and the quasielectrons except for a sign as we can see from the plot of $\sum_k Q_k$ in (f).

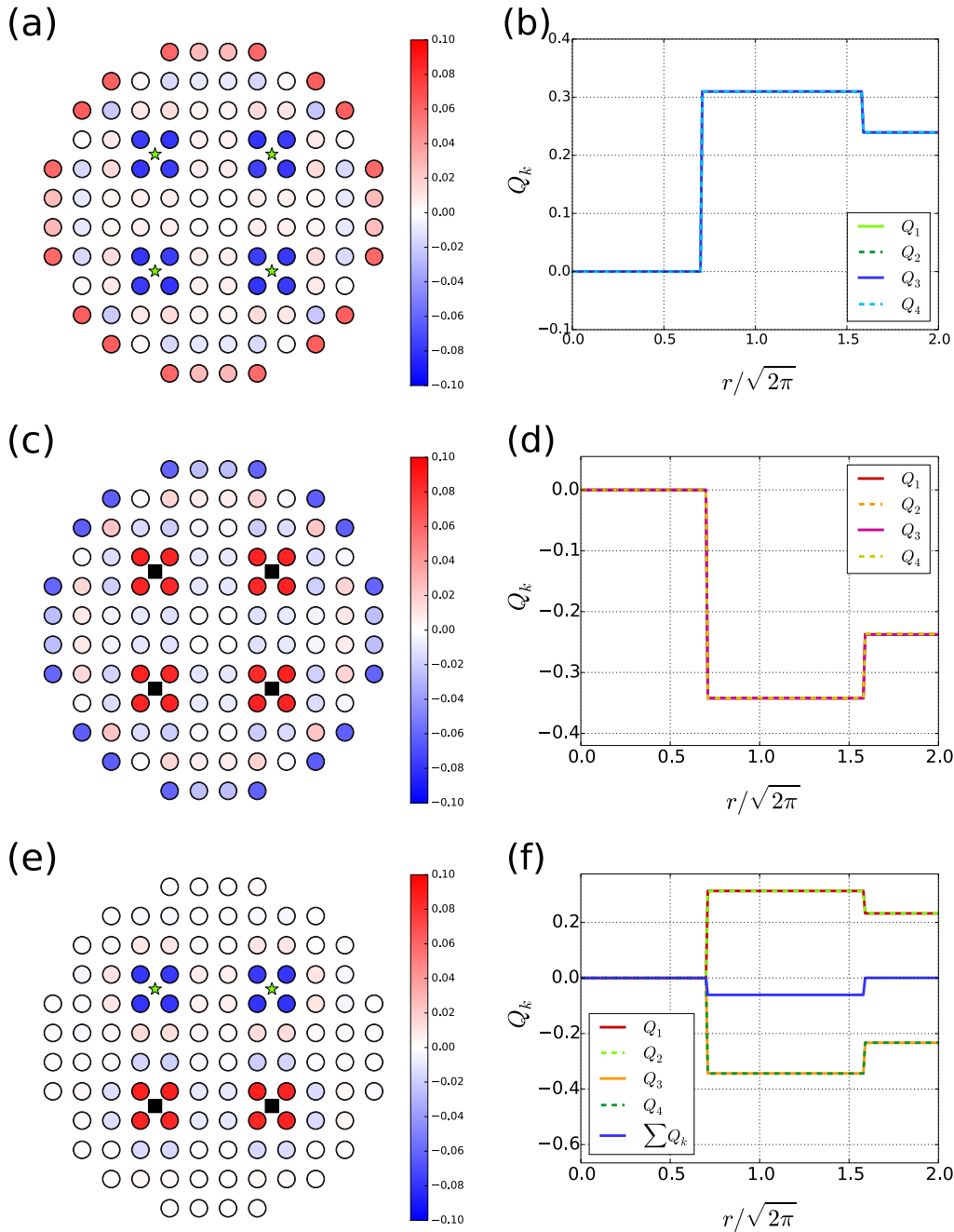


Figure 4.2.: In (a), (c), (e): We represent lattice sites, quasiholes and quasielectrons, respectively by the black circles, the green stars and the black squares. We take the number of lattice sites $N = 112$. The density profiles $\rho(z_i)$ from Eq. (4.2), defined as the particle density difference between the states in the presence and in the absence of anyons, are plotted with colorbars for the cases of (a) four quasiholes, (c) four quasielectrons, and (e) two quasiholes-two quasielectrons. We place the anyons in the middle of the lattice plaquette. The anyons are well-screened with the radii of a few lattice constants. The colors on the edges appear due to the charges at infinity in the state containing anyons as explained in the main text. In (b), (d), (f): The excess charge distributions Q_k with $k \in \{1, \dots, Q\}$ are computed from Eq. (4.10) and are plotted as a function of the radial distances $r/\sqrt{2\pi}$, from the anyon positions, corresponding to the above mentioned anyon configurations respectively. The anyon positions are symmetric with respect to $\pi/4$ rotation of the lattice. Therefore the excess charge plots are on top of each other. The anyon charges approach $\simeq \pm 0.25$ for large r with an errorbar of size 10^{-4} arising from the Monte-Carlo simulations. We note that the density profiles are similar for the quasiholes and the quasielectrons except for a sign as we can see from the plot of $\sum_k Q_k$ in (f).

Thereby we need to set the number of particles M to be even in both the cases. We inspect the conditions on M as arising from the δ_n factors in the wavefunctions and we find that we can not fulfill the condition, of having M even, simultaneously if we choose the same η value for both the cases. We point out that the factor ηN corresponds to the flux through the system and therefore we have to keep the η value same in both the cases. However we overcome this problem by proceeding as follows.

(a). Charges at infinity

We insert an extra charge \mathcal{P}/q at infinity [70]. This allows us to choose the appropriate values of this charge and thereby we can use the same η values and can get M even in both the cases. The charge at infinity is incorporated by the vertex operator

$$\Xi_{\mathcal{P}}(\infty) = : e^{i\frac{\mathcal{P}}{\sqrt{q}}\phi(\infty)} : \quad (4.5)$$

in the correlator of the wavefunction as in Eq. (3.58).

Thereby we write the correlator as

$$\begin{aligned} \Psi_{\alpha}(\{z_j\}, \{w_k\})[\mathcal{P}(\xi \rightarrow \infty)] &= \langle \prod_{j=1}^N \psi(z_j)^{\Delta_{n_j}} \prod_{k=1}^Q \sigma(w_k) \rangle_{\alpha} \\ &\times \langle \prod_{j=1}^N : e^{i(qn_j - \eta)\phi(z_j)/\sqrt{q}} : \prod_{k=1}^Q : e^{ip_k\phi(w_k)/\sqrt{q}} :: e^{i\frac{\mathcal{P}}{\sqrt{q}}\phi(\infty)} : \rangle, \end{aligned} \quad (4.6)$$

which is evaluated to provide the state as

$$\begin{aligned} \Psi_{\alpha}(\{z_j\}, \{w_k\})[\mathcal{P}(\xi \rightarrow \infty)] &= \delta'_n \langle \prod_{j=1}^N \psi(z_j)^{\Delta_{n_j}} \prod_{k=1}^Q \sigma(w_k) \rangle_{\alpha} \prod_{i < j} (z_i - z_j)^{qn_i n_j} \\ &\times \prod_{i \neq j} (z_i - z_j)^{-\eta n_i} \prod_j (\xi - z_j)^{\mathcal{P} n_j} \prod_{i, j} (w_i - z_j)^{p_i n_j} \prod_{i < j} (w_i - w_j)^{p_i p_j / q} \prod_{i, j} (w_i - z_j)^{-\eta p_i / q} \\ &= \delta'_n \langle \prod_{j=1}^N \psi(z_j)^{\Delta_{n_j}} \prod_{k=1}^Q \sigma(w_k) \rangle_{\alpha} \xi^{\mathcal{P}(N - \mathcal{P})/q} \prod_{i < j} (z_i - z_j)^{qn_i n_j} \prod_{i \neq j} (z_i - z_j)^{-\eta n_i} \\ &\times \prod_{i, j} (w_i - z_j)^{p_i n_j} \prod_{i < j} (w_i - w_j)^{p_i p_j / q} \prod_{i, j} (w_i - z_j)^{-\eta p_i / q} \\ &\propto \delta'_n \langle \prod_{j=1}^N \psi(z_j)^{\Delta_{n_j}} \prod_{k=1}^Q \sigma(w_k) \rangle_{\alpha} \prod_{i < j} (z_i - z_j)^{qn_i n_j} \prod_{i \neq j} (z_i - z_j)^{-\eta n_i} \\ &\times \prod_{i, j} (w_i - z_j)^{p_i n_j} \prod_{i < j} (w_i - w_j)^{p_i p_j / q} \prod_{i, j} (w_i - z_j)^{-\eta p_i / q}, \end{aligned} \quad (4.7)$$

where the $\langle \dots \rangle_\alpha$ part remains the same as given in Sec. 3.3 in Eq. (3.58). Here $\delta'_n = 1$ if the total number of particles is

$$M = \frac{\left(\eta N - \mathcal{P} - \sum_{k=1}^Q p_k \right)}{q} \quad (4.8)$$

and $\delta'_n = 0$ otherwise. Therefore, with $\eta = 1$, we take the number of particles $M = N/2$ for all the cases of the presence and of the absence of anyons in the states and thereby choose appropriate \mathcal{P} values. We note that the analytical form of the state in Eq. (4.7) is similar to those in Eqs. (3.59) and (3.62) apart from the particle numbers in the system.

We present the density profiles of the anyons in Fig. 4.1 and in Fig. 4.2 with $N = 112$ by placing the anyons in the bulk and sufficiently separated from one another. We take the choices of two quasiholes in Fig. 4.1 (a) [with $\mathcal{P} = -1$], two quasielectrons in Fig. 4.1 (c) [with $\mathcal{P} = -2$], one quasihole-one quasielectron in Fig. 4.1 (e) [with $\mathcal{P} = 0$], four quasiholes in Fig. 4.2 (a) [with $\mathcal{P} = +1$], four quasielectrons in Fig. 4.2 (c) [with $\mathcal{P} = +2$], and two quasiholes-two quasielectrons in Fig. 4.2 (e) [with $\mathcal{P} = 0$]. We have $\mathcal{P} = 0$ always for the case of the absence of anyons in the state. We represent the particle densities of the lattice sites by the colorbar and estimate an errorbar of size 10^{-4} arising due to the Monte-Carlo simulations.

We find that the anyons are screened well with a radii of a few lattice constants, and the density profiles vary with the distance from the anyons. We note that the non-zeros values of \mathcal{P} give rise to the edge effects in Fig. 4.1 (a), (c) and in Fig. 4.2 (a), (c). The plots show that these do not hamper the bulk properties and hence the anyons remain unaffected. We speculate that if a quasihole or a quasielectron approaches a lattice site then it increases the probability of that lattice site respectively to be unoccupied or to be occupied.

Intuitively we can think of the edge effects, arising from the charge at infinity, as follows. We are keeping the particle numbers to be fixed as M in both the cases of the presence and of the absence of anyons in the systems. Now when we have the quasiholes then we want to create the deficiency of the particles locally. That is we want to expel the particles from the vicinity of the quasihole positions. Therefore these particles reside around the edge which creates the edge effects. In the opposite manner if we have the quasielectrons then we want to accumulate the particles locally. That is we want to attract the particles at the vicinity of the quasielectron positions. And therefore we draw the particles from the edge which is responsible for the edge effects. Now when we have an equal number of quasiholes and quasielectrons in the system then the particles which are expelled from the vicinity of the quasihole positions, are accumulated in the vicinity of the quasielectron positions and thereby making no edge effects.

4.1.2 Charges of anyons

We note the anyon charges are expected to be

$$\frac{p_k}{q}, \text{ with } p_k = \pm \frac{1}{2}. \quad (4.9)$$

Experimental measurements of the quasihole charges in the continuum are found in Refs. [21, 183, 187, 234, 55]. Thereby it is indispensable to investigate if the anyons fetch similar charges in the lattice models also.

We take the standard charge of a fermionic particle to be -1 and inscribe the excess charge of the k th anyon, elucidated to be the sum of minus the density profile $\rho(z_i)$ over a circular region of radius r around the anyon, as

$$Q_k(w_k) = -\sum_i \rho(z_i), \text{ with } |z_i - w_k| \leq r, \quad (4.10)$$

where $k \in \{1, 2, \dots, Q\}$ and $\rho(z_i)$ is defined in Eq. (4.2). The charge Q of the anyon is defined to be the value that the total excess charge converges to for large r , when the region is far from the edge and also far from any other anyon in the system.

We show the excess charges of the anyons as a function of the radial distances from the anyon positions in Fig. 4.1 and in Fig. 4.2. We display the excess charges corresponding to the choices of two quasiholes in Fig. 4.1 (b), two quasielectrons in Fig. 4.1 (d), one quasihole-one quasielectron in Fig. 4.1 (f), four quasiholes in Fig. 4.2 (b), four quasielectrons in Fig. 4.2 (d), and two quasiholes-two quasielectrons in Fig. 4.2 (f). We note that the anyon charges approach the values $Q \simeq \pm 0.25$ up to an errorbar of size 10^{-4} arising from the Monte-Carlo simulations.

These results also confirm that the charges at infinity, and thereby the edge effects, do not affect the anyon properties. Thereby we claim the anyons to be the Ising anyons and also infer that the quasielectrons behave as similar to the quasiholes. Moreover the density profiles of the quasiholes and the quasielectrons are very similar except for the sign, as evident from the plots of $\sum_k Q_k$ in Fig. 4.1 (f) and in Fig. 4.2 (f).

4.2 Fractional braiding statistics of anyons

In Sec. 4.1 we have found that the anyons are screened well and exhibit proper charges. These license us to compute the braiding properties of the anyons. We employ Monte-Carlo simulations and take $n_j \in \{0, 1\}$, $\eta = 1$, and $q = 2$ in the anyonic lattice Moore-Read states, as defined in Sec. 3.3 in Eqs. (3.59), (3.62).

While braiding, we adiabatically circulate one anyon at position w_k around another anyon at position w_j , where $j \in \{1, \dots, Q\}$, $k \in \{1, \dots, Q\}$ and $j \neq k$, along a closed path Γ . Therefore the normalized state picks up a unitary phase matrix and is transformed as [31, 77]

$$|\Psi_\alpha\rangle \longrightarrow \gamma_A \gamma_M \gamma_B |\Psi_\alpha\rangle, \quad (4.11)$$

where we have three contributions in the story as follows.

We have the Aharonov-Bohm phase γ_A which arises when a charged particle circulates in a background magnetic field, the monodromy matrix γ_M which comes from the analytic continuation of the states and the Berry matrix

$$\gamma_B = e^{i\theta_B} \quad (4.12)$$

with the elements

$$[\theta_B]_{\alpha\beta} = i \sum_{k=1}^Q \oint_{\Gamma} \left(\langle \Psi_{\alpha} | \frac{\partial \Psi_{\beta}}{\partial w_k} \rangle dw_k + \langle \Psi_{\alpha} | \frac{\partial \Psi_{\beta}}{\partial \bar{w}_k} \rangle d\bar{w}_k \right), \quad (4.13)$$

where

$$\alpha, \beta \in \{I, \psi\} \quad (4.14)$$

for our case with two and with four anyons in the states.

Now Bonderson *et al.* in Ref. [31] has shown that, in the continuum as long as the quasipoles are sufficiently separated from one another, if the conformal blocks of the states possess matrix elements which are independent of the quasipole positions, and also if the matrix is diagonal in the basis spanned by the conformal blocks then the Berry matrix becomes trivial. And the quasipole braiding statistics can be read off directly from the monodromy matrix alone. This simply means that the overlap matrix of the degenerate states should satisfy the above conditions to get the Berry matrix proportional to the identity matrix with an Abelian phase factor called the Aharonov-Bohm phase which comes due to the circulation of the quasipole in the background magnetic field.

When a particle of charge q' circulates in a magnetic field B through a closed loop of area A , then the particle picks up a phase factor

$$e^{-2\pi i q' BA/hc}, \quad (4.15)$$

which is known as the Aharonov-Bohm phase, where h is the Planck's constant and c is the speed of light in free space.

We investigate the aforesaid conditions for the case of the anyons in the lattice systems. We evaluate the braiding statistics for both the quasipoles and the quasielectrons. We inscribe the Berry matrix elements from Eq. (4.13) to circulate the k th anyon as

$$[\theta_B]_{\alpha\beta} = i \sum_{k=1}^Q \oint_{\Gamma} \langle \Psi_{\alpha} | \frac{\partial \Psi_{\beta}}{\partial w_k} \rangle dw_k + \text{c.c.}, \quad (4.16)$$

where c.c. denotes the complex conjugate of the first term and we use

$$|\Psi_{\alpha}\rangle = \frac{1}{C_{\alpha}} \sum_n \Psi_{\alpha}|n\rangle \text{ and } |\Psi_{\beta}\rangle = \frac{1}{C_{\beta}} \sum_{n'} \Psi_{\beta}|n'\rangle, \text{ with } \langle n|n'\rangle = \delta_{nn'}. \quad (4.17)$$

Therefore we write

$$\begin{aligned}
\langle \Psi_\alpha | \frac{\partial \Psi_\beta}{\partial w_k} \rangle &= \sum_n \frac{\bar{\Psi}_\alpha}{C_\alpha} \frac{\partial}{\partial w_k} \left(\frac{\Psi_\beta}{C_\beta} \right) \\
&= \frac{\partial}{\partial w_k} \left(\sum_n \frac{\bar{\Psi}_\alpha \Psi_\beta}{C_\alpha C_\beta} \right) - \sum_n \frac{\Psi_\beta}{C_\beta} \frac{\partial}{\partial w_k} \frac{\bar{\Psi}_\alpha}{C_\alpha} \\
&= \frac{\partial}{\partial w_k} \left(\frac{1}{C_\alpha C_\beta} \sum_n \bar{\Psi}_\alpha \Psi_\beta \right) - \frac{1}{C_\alpha C_\beta} \sum_n \Psi_\beta \frac{\partial \bar{\Psi}_\alpha}{\partial w_k} - \frac{1}{C_\beta} \sum_n \bar{\Psi}_\alpha \Psi_\beta \frac{\partial}{\partial w_k} \left(\frac{1}{C_\alpha} \right).
\end{aligned} \tag{4.18}$$

We have chosen the states to be normalized. Now if we can show that the states are orthogonal, that is if we can show

$$\langle \Psi_\alpha | \Psi_\beta \rangle = \delta_{\alpha\beta} \tag{4.19}$$

then we can write Eq. (4.18) as

$$\begin{aligned}
\langle \Psi_\alpha | \frac{\partial \Psi_\beta}{\partial w_k} \rangle &= \frac{\partial}{\partial w_k} \delta_{\alpha\beta} - \frac{1}{C_\alpha C_\beta} \sum_n \Psi_\beta \frac{\partial \bar{\Psi}_\alpha}{\partial w_k} - C_\alpha \delta_{\alpha\beta} \frac{\partial}{\partial w_k} \left(\frac{1}{C_\alpha} \right) \\
&= -C_\alpha \delta_{\alpha\beta} \frac{\partial}{\partial w_k} \left(\frac{1}{C_\alpha} \right),
\end{aligned} \tag{4.20}$$

since $\bar{\Psi}_\alpha$ depends only on \bar{w}_k and therefore $\bar{\Psi}_\alpha$ is independent of w_k .

Hence we can write the Berry matrix elements from Eq. (4.16) as

$$\begin{aligned}
[\theta_B]_{\alpha\beta} &= -i \oint_\Gamma C_\alpha \delta_{\alpha\beta} \frac{\partial}{\partial w_k} \left(\frac{1}{C_\alpha} \right) dw_k + c.c. \\
&= i \delta_{\alpha\beta} \oint_\Gamma \frac{1}{C_\alpha} \left(\frac{\partial C_\alpha}{\partial w_k} \right) dw_k + c.c. \\
&= i \delta_{\alpha\beta} \oint_\Gamma I dw_k + c.c.,
\end{aligned} \tag{4.21}$$

where we have

$$I = \frac{1}{C_\alpha} \left(\frac{\partial C_\alpha}{\partial w_k} \right) = \frac{\partial \ln(C_\alpha)}{\partial w_k}. \tag{4.22}$$

Now if we can show that C_α , and hence $\ln(C_\alpha)$, is periodic in w_k then we have γ_B is equal to the identity matrix, that is we have

$$[\gamma_B]_{\alpha\beta} = \delta_{\alpha\beta}. \tag{4.23}$$

Under this circumstance, the braiding statistics of the anyons can be evaluated directly from the γ_M alone. Also the braiding statistics will be the same as the braiding statistics in the continuum if we can show

$$C_\alpha = C_\beta. \quad (4.24)$$

Therefore we collect the sufficient conditions in the lattices in correspondence to the sufficient conditions in the continuum [31] as follows.

Conditions in the continuum	Conditions in the lattice
(i). We require to show that the degenerate states $ \Psi_\alpha\rangle$ and $ \Psi_\beta\rangle$ are orthogonal.	(i). We have to show that $ \sum_{n_i} \Psi_\alpha^* \Psi_\beta = C \delta_{\alpha\beta}$ up to exponentially small finite size effects and C is a constant.
(ii). We require that the norm of the states are independent of the quasi-hole positions.	(ii). We have to show that C_α is periodic when we move one anyon through a closed loop.
(iii). We require that the degenerate states $ \Psi_\alpha\rangle$ and $ \Psi_\beta\rangle$ have the same norm.	(iii). We have to show that $C_\alpha = C_\beta$ up to exponentially small finite size effects. However this condition is already included in the condition as written in (i) in this column.

We extensively study the braiding properties of two anyons and of four anyons in the systems as follows.

4.2.1 Two anyons scenario

We incorporate either two quasiholes or two quasielectrons or one quasihole-one quasi-electron in the state. We compute the Berry matrix, the monodromy matrix and the Aharonov Bohm phase as follows.

(a). Berry matrix

We have only one state in this case as Eq. (3.59). Hence only the condition (ii) is to be satisfied. And the Berry matrix becomes the Berry phase in this case. We place the anyons in the bulk of the system and keep them isolated from one another. We circulate one anyon, say the k th one where $k \in \{1, 2\}$, around one lattice site through a closed path while keeping the other anyon fixed in its initial position. We choose the path to be along the midway in the lattice plaquette and expect the same outcome to hold if we circulate the anyon through any other closed path as well. We show the path in Fig. 4.3 (a) where proper choices of the anyon charges correspond to the anyon configurations as depicted in Fig. 4.1 (a), (c), (e).

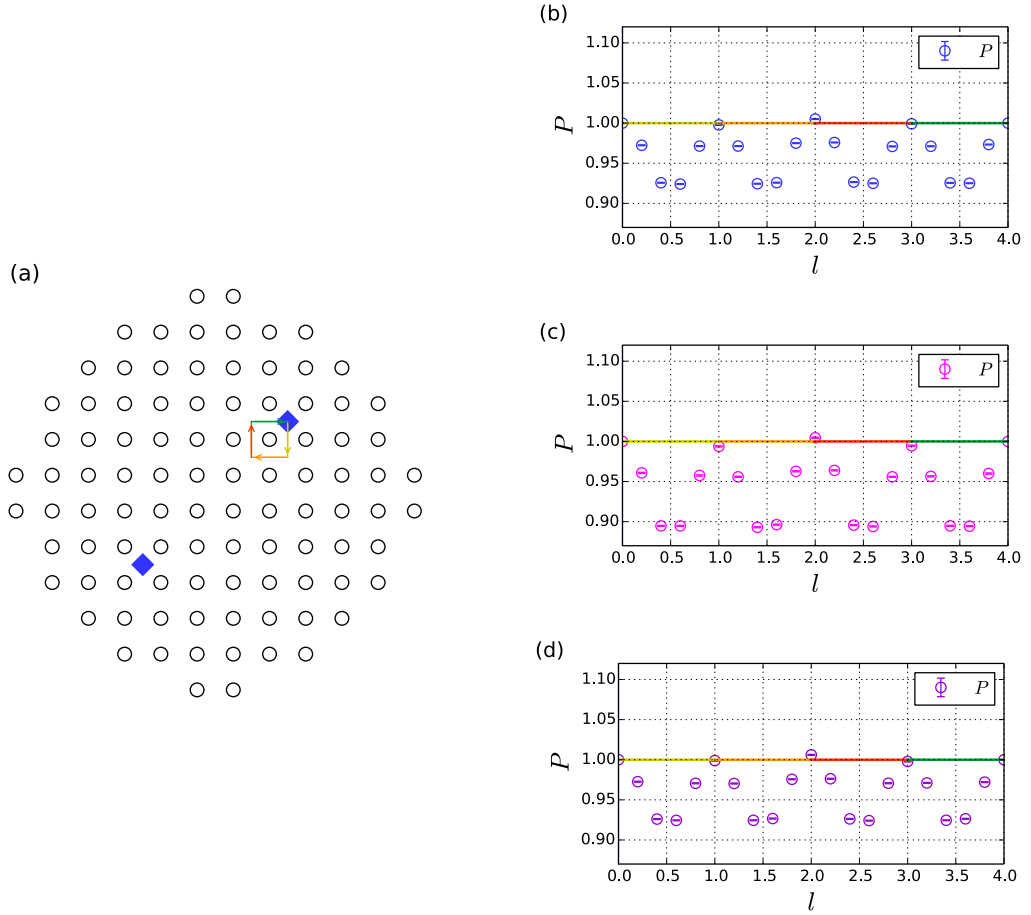


Figure 4.3.: In (a): We picture the lattice sites and the anyons by the black circles and the blue diamonds, respectively. Proper choices of the charges of the anyons lead to the configurations as shown in Fig. 4.1 (a), (c), (e). We place the anyons in the bulk and keep the anyons sufficiently separated from one another. We circulate one anyon around one lattice site through a closed loop along the path midway in the lattice plaquette, while keeping the other anyon position fixed in its initial position. We take the lattice size to be $N = 96$. In (b), (c), (d): We plot the quantity P from Eq. (4.25) as a function of the different moves, that is the position l , of the moving anyon for the cases of two quasiholes, two quasielectrons, and one quasihole-one quasielectron in (b), (c), and (d) respectively. For all the cases, we find that the quantity P varies with the period of the lattice up to some finite size effects arising from the Monte-Carlo simulations.

We study the variation of the square of the norm C^2 of the state with respect to the moving anyon positions. Therefore we define the following quantity to investigate as

$$P = \frac{C_0^2}{C_l^2}, \quad (4.25)$$

where C_l and C_0 denote the normalization constants of the anyonic state when the moving anyon is at position l and is at its initial position $l = 0$, respectively. Therefore the quantity

P denotes the inverse ratio between the overlaps at the l th and at the $l = 0$ th positions of the anyon.

We display the above-mentioned quantity P as a function of the different moves l of the circulating anyon in Figs. 4.3 (b), (c), (d) for the cases of the two quasiholes, two quasielectrons, and one quasihole-one quasielectron in the state respectively. We find the periodic variations of the quantity P with different positions of the circulating anyon up to some finite size effects appearing due to the Monte-Carlo simulations. Hence we write the Berry phase $\gamma_B = 1$.

(b). Monodromy matrix

The counter-clockwise exchange of the two anyons at positions w_k and w_j gives rise to the monodromy matrix which is just a phase factor here. This analytic continuation can be obtained straightforwardly from the anyonic state in Eq. (3.59) at face value. We find the statistical phase to be

$$\gamma_M = e^{i\pi \left[\frac{p_j p_k}{q} - \frac{1}{8} \right]}. \quad (4.26)$$

(c). Aharonov-Bohm phase

Counterclockwise circulation of the anyon at position w_k around a lattice site gives rise to the phase from Eq. (3.59) as

$$\gamma_A = e^{-2\pi i p_k / q}. \quad (4.27)$$

This is interpreted as the Aharonov-Bohm phase of a particle with charge p_k/q , which is circulating around a closed loop and is enclosing a background magnetic flux of unity.

Investigations of the braiding properties above show that the exchange of two anyons gives rise to the phase factors only. It might seem that the anyons are of Abelian in nature. However we see in the next section that when we have four anyons in the system then the ground state is degenerate and the non-Abelian nature of the anyons are revealed, as expected for the Ising anyons in the Moore-Read fractional quantum Hall state.

4.2.2 Four anyons scenario

We incorporate either four quasiholes or four quasielectrons or two quasiholes-two quasielectrons in the states. We compute the Berry matrix, the monodromy matrix and the Aharonov Bohm phase as follows.

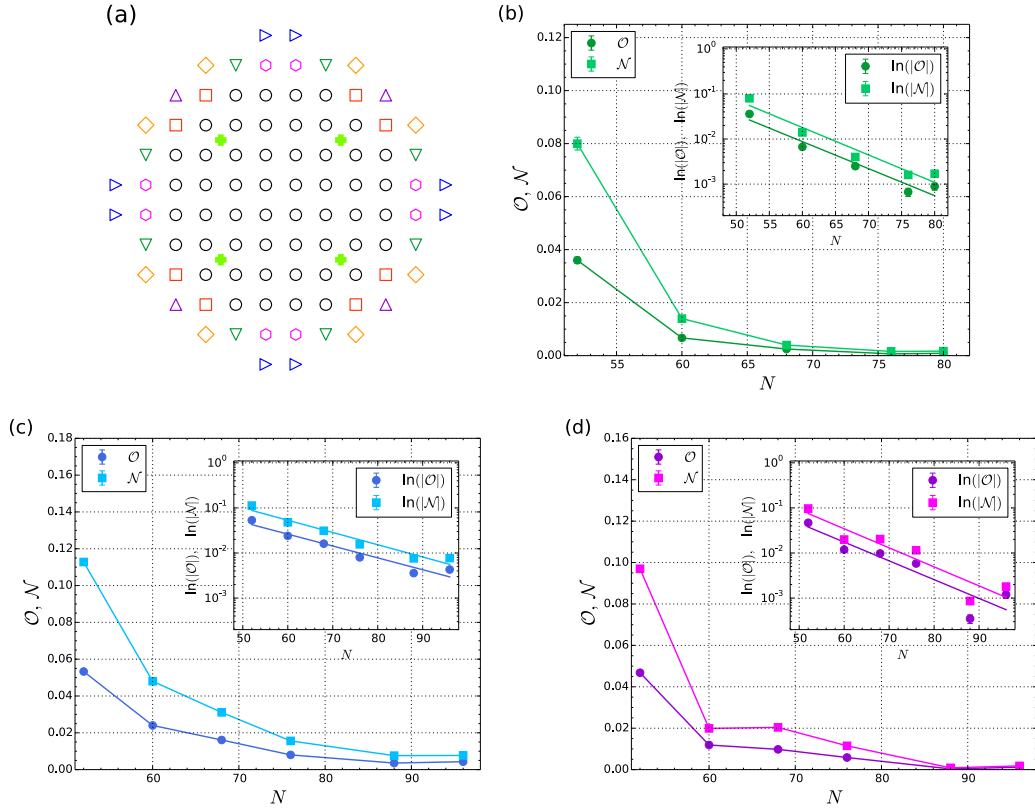


Figure 4.4.: In (a): We keep the anyons, as pictured by the light green pluses, fixed in the bulk and place them sufficiently separated from one another. We increase the lattice size N by adding more sites. We denote different lattice sizes with different symbols as $N = 52$, as pictured by the black circles, as $N = 60$, as pictured by the red squares added, as $N = 68$, as pictured by the pink hexagons added, as $N = 76$, as pictured by the dark green down pointing triangles added, as $N = 80$, as pictured by the violet up pointing triangles added, as $N = 88$, as pictured by the orange diamonds added, and as $N = 96$, as pictured by the blue right pointing triangles added. Proper choices of the anyon charges lead to the configurations as shown in Fig. 4.2 (a), (c), (e). In (b), (c), (d): We plot the quantities \mathcal{O} , by circles, and \mathcal{N} , by squares, as defined in Eq. (4.29) as a function of the lattice size N for the cases of the four quasipoles, four quasielectrons, and two quasipoles-two quasielectrons in the system in (b), (c), (d) respectively. We note that the quantities \mathcal{O} and \mathcal{N} in all the plots follow exponential decays. In the insets we show the data in the semi-log scale where the linear fits confirm the exponential decay of the quantities. These imply that the states Ψ_I and Ψ_ψ are orthogonal and have the same norm in the thermodynamic limit $N \rightarrow \infty$, where the errorbars, arising from the Monte-Carlo simulations, are small.

(a). Berry matrix

We have two degenerate states, namely Ψ_I and Ψ_ψ , in this case. Hence the Berry matrix elements are given by Eq. (4.13) where we have

$$\alpha, \beta \in \{I, \psi\}. \quad (4.28)$$

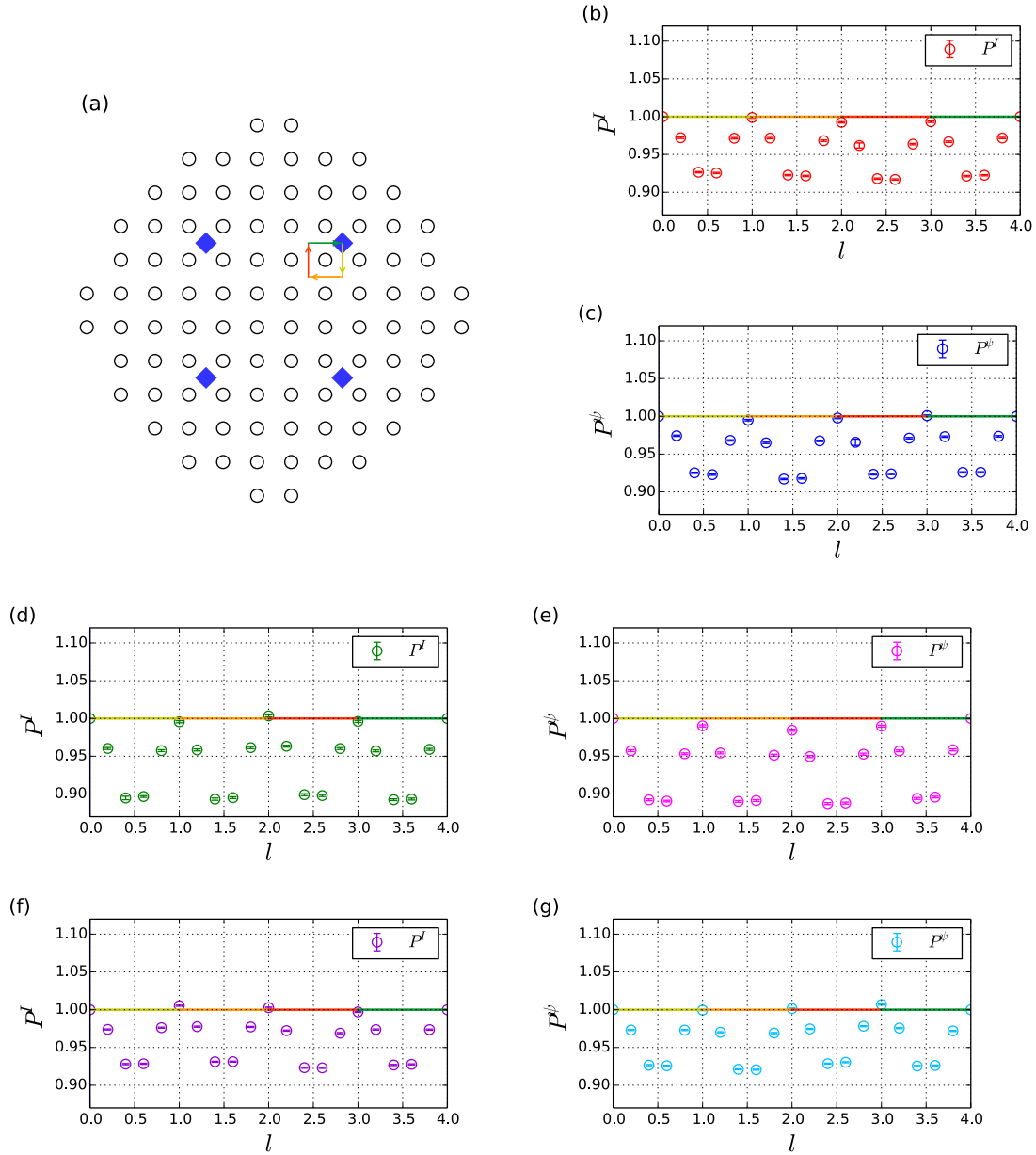


Figure 4.5.: In (a): We picture the lattice sites and the anyons by the black circles and the blue diamonds, respectively for the lattice size of $N = 96$. We note that the proper choices of the charges of the anyons lead to the configurations as shown in Fig. 4.2 (a), (c), (e). We place the anyons in the bulk and keep them sufficiently separated from one another. We circulate one anyon around one lattice site through a closed path along the midway in the lattice plaquette while keeping the other anyon positions fixed in their initial positions. In (b), (c), (d), (e), (f), (g): We plot the quantities P^J and P^Ψ from Eq. (4.31) as a function of the different moves l of the moving anyon for the cases of four quasipoles, four quasihole, and two quasipoles-two quasihole in (b)-(c), (d)-(e), (f)-(g) respectively. For all the cases, we note that the quantities P^J and P^Ψ vary with the period of the lattice up to some finite size effects arising from the Monte-Carlo simulations.

In order to investigate conditions (i) and (iii) we inspect two quantities, namely the overlap \mathcal{O} of the two states and the ratio \mathcal{N} of the respective norms of the two states, as a function of the systems size N . Henceforth we define

$$\mathcal{O} = \frac{\left| \sum_{n_i} \Psi_I^* \Psi_\Psi \right|}{\sqrt{\sum_{n_i} |\Psi_I|^2 \sum_{n_i} |\Psi_\Psi|^2}} \text{ and } \mathcal{N} = 1 - \frac{\sum_{n_i} |\Psi_I|^2}{\sum_{n_i} |\Psi_\Psi|^2}. \quad (4.29)$$

We place the anyons in the bulk and keep them sufficiently separated from one another. We increase the lattice size by putting more lattice sites in the system as displayed in Fig. 4.4 (a) where proper choices of the anyon charges lead to the anyon configurations as in Figs. 4.2 (a), (c), (e).

We plot \mathcal{O} and \mathcal{N} as a function of the system size N in Figs. 4.4 (b), (c), (d) for the cases of four quasiholes, four quasielectrons, and two quasiholes-two quasielectrons in the states respectively. We find that each of the quantities \mathcal{O} and \mathcal{N} exhibits an exponential decay as a function of the lattice size. The insets show the data in the semi-log scale. A linear fit in the inset for each case dictates the decay as $e^{-\lambda N}$, where λ is the decay coefficient. For the case of four quasiholes, the decay coefficient is $\lambda = 0.0599$ for \mathcal{O} and is $\lambda = 0.0608$ for \mathcal{N} . For the case of four quasielectrons, the decay coefficient is $\lambda = 0.0263$ for \mathcal{O} and is $\lambda = 0.0271$ for \mathcal{N} . For the case of two quasiholes-two quasielectrons, the decay coefficient is $\lambda = 0.0416$ for \mathcal{O} and is $\lambda = 0.0422$ for \mathcal{N} .

Therefore in the thermodynamic limit $N \rightarrow \infty$, the two states are expected to be orthogonal with the same norm up to some finite size effects arising due to the Monte-Carlo simulations. This provides the license to inscribe

$$\left| \sum_{n_i} \Psi_\alpha^* \Psi_\beta \right| = \mathcal{C} \delta_{\alpha\beta} + \mathcal{O}\left(e^{-\lambda N}\right), \quad (4.30)$$

where \mathcal{C} is a constant and $\mathcal{O}\left(e^{-\lambda N}\right)$ is a contribution which exponentially decays with the system size and in the thermodynamic limit, this factor vanishes. Henceforth, the overlap matrix becomes the identity matrix.

Now to check the condition (ii) we use the same formalism as we have done in the case of the two anyons. We place the anyons in the bulk by isolating them from one another. We circulate one anyon, say the k th one with $k \in \{1, 2, 3, 4\}$, around a lattice site through a closed loop by keeping the other anyons fixed to their initial positions. We choose the path to be along the midway in the lattice plaquette and expect the same outcome to hold if we circulate the anyon through any other closed path as well. We show the path in Fig. 4.5 (a) where proper choices of the anyon charges lead to the anyon configurations as depicted in Fig. 4.2 (a), (c), (e).

We note that since the overlap matrix is diagonal for sufficiently large N , therefore it is enough to investigate the diagonal elements only, that is it is sufficient to study the case for $\alpha = \beta$. We define the following quantity to inspect as

$$P^\alpha = \frac{C_{\alpha 0}^2}{C_{\alpha l}^2} \text{ with } \alpha \in \{I, \psi\}, \quad (4.31)$$

where $C_{\alpha l}$ and $C_{\alpha 0}$ denote the normalization constants when the circulating anyon is at the l th position and at its initial position $l = 0$, respectively.

In Figs. 4.5 (b)-(c), (d)-(e), (f)-(g) we show the quantities P^I and P^ψ as a function of the different moves l , respectively for the cases of four quasiholes, four quasielectrons and two quasiholes-two quasielectrons in the systems. We find that the quantities P^I and P^ψ vary with the period of the lattice up to some numerical uncertainties arising from the Monte-Carlo simulations and from the finite size effects. Therefore we inscribe the Berry matrix contribution as

$$\gamma_B = \hat{I}, \quad (4.32)$$

where \hat{I} is the identity matrix.

(b). Monodromy matrix

We investigate the analytic continuation of the states in Eqs. (3.62) at face value and thereby compute the monodromy matrix γ_M . We choose the j th and k th anyons, where $j, k \in \{1, 2, 3, 4\}$ symbolizes the anyons, to be exchanged in the counter-clockwise fashion while keeping the other anyons fixed at their positions. The states Ψ_I and Ψ_ψ are transformed under this exchange $w_j \rightleftharpoons w_k$ as follows.

We have for $w_1 \rightleftharpoons w_2$ or equivalently for $w_3 \rightleftharpoons w_4$,

$$\Psi_I \mapsto e^{i\pi \left[\frac{p_j p_k}{q} - \frac{1}{8} \right]} \Psi_I \text{ and } \Psi_\psi \mapsto e^{i\pi \left[\frac{p_j p_k}{q} - \frac{1}{8} \right]} i \Psi_\psi \quad (4.33)$$

where $j = 1(3)$, $k = 2(4)$,

and we have for $w_2 \rightleftharpoons w_3$ or equivalently for $w_1 \rightleftharpoons w_4$,

$$\Psi_I \mapsto e^{i\pi \left[\frac{p_j p_k}{q} + \frac{1}{8} \right]} \left(\frac{\Psi_I - i \Psi_\psi}{\sqrt{2}} \right) \text{ and } \Psi_\psi \mapsto e^{i\pi \left[\frac{p_j p_k}{q} + \frac{1}{8} \right]} \left(\frac{-i \Psi_I + \Psi_\psi}{\sqrt{2}} \right) \quad (4.34)$$

where $j = 2(1)$, $k = 3(4)$,

and we have for $w_1 \rightleftharpoons w_3$ or equivalently for $w_2 \rightleftharpoons w_4$,

$$\Psi_I \mapsto e^{i\pi \left[\frac{p_j p_k}{q} + \frac{1}{8} \right]} \left(\frac{\Psi_I + \Psi_\psi}{\sqrt{2}} \right) \text{ and } \Psi_\psi \mapsto e^{i\pi \left[\frac{p_j p_k}{q} + \frac{1}{8} \right]} \left(\frac{-\Psi_I + \Psi_\psi}{\sqrt{2}} \right) \quad (4.35)$$

where $j = 1(2)$, $k = 3(4)$,

where we use the \rightleftharpoons symbol to denote the exchange of two anyons in the counter-clockwise direction.

Now the Eqs. (4.33) - (4.35) provide the monodromy matrices, under the analytic continuation operation which transmute the states

$$\left[\Psi_I, \Psi_\psi \right]^T \mapsto \gamma_M^{j \rightleftharpoons k} \left[\Psi_I, \Psi_\psi \right]^T, \quad (4.36)$$

as follows

$$\begin{aligned} \gamma_M^{1 \rightleftharpoons 2 / 3 \rightleftharpoons 4} &= e^{i\pi \left[\frac{p_j p_k}{q} - \frac{1}{8} \right]} \begin{bmatrix} 1 & 0 \\ 0 & i \end{bmatrix} \\ \gamma_M^{2 \rightleftharpoons 3 / 1 \rightleftharpoons 4} &= e^{i\pi \left[\frac{p_j p_k}{q} + \frac{1}{8} \right]} \frac{1}{\sqrt{2}} \begin{bmatrix} 1 & -i \\ -i & 1 \end{bmatrix} \\ \gamma_M^{1 \rightleftharpoons 3 / 2 \rightleftharpoons 4} &= e^{i\pi \left[\frac{p_j p_k}{q} + \frac{1}{8} \right]} \frac{1}{\sqrt{2}} \begin{bmatrix} 1 & -1 \\ 1 & 1 \end{bmatrix}. \end{aligned} \quad (4.37)$$

(c). Aharonov-Bohm phase

When we circulate an anyon at position w_k around a lattice site then we get a phase from Eq. (3.62) as

$$\gamma_A = e^{-2\pi i p_k / q}. \quad (4.38)$$

This is called as the Aharonov-Bohm phase of a particle with charge p_k/q , which is circulating around a closed loop and is enclosing a background magnetic flux of unity.

We find that the monodromy matrices, in Eq. (4.26) for two anyons and in Eq. (4.37) for four anyons, and hence the braiding statistics of the anyons are the same as found in the continuum for the quasiholes. The monodromy matrices in Eq. (4.37) do not commute with each other and thereby these matrices serve as the members of the non-Abelian braid group. This comprises the building blocks of the non-Abelian statistics of the Moore-Read Ising anyons in the system.

4.3 Parent Hamiltonians

Till now we have analyzed the properties of the anyons in the analytical lattice Moore-Read states. Naturally it is relevant to investigate if the states are the ground states of some Hamiltonians. Therefore we derive the parent Hamiltonians for the states containing an even number Q of anyons and for $n_j \in \{0, 1\}$, $q \geq 2$. We commence by constructing the Hamiltonians for the states hosting quasiholes and for $\eta = 1$. Afterwards we generalize the Hamiltonians for the case of $\eta \leq 1$ and for the states containing quasiholes. And afterwards we construct the Hamiltonians for the case when we have quasielectrons in the system in addition to the quasiholes and for $\eta \leq 1$.

One advantage of these Hamiltonians is that the anyons can be braided by changing the coupling strengths in the Hamiltonians since the Hamiltonians are functions of the anyon positions. Also one can go from the lattice limit to the continuum limit by changing the coupling strengths which are functions of η . The Hamiltonians contain few-body interactions and are long-range.

4.3.1 Parent Hamiltonians for the states containing quasiholes

We exploit the null fields construction [169, 64] of the underlying conformal field theory and derive the Hamiltonians for $\eta = 1$ first and thereby generalizing the results for the case of $\eta < 1$.

(a). Parent Hamiltonians for $\eta = 1$

We know that the states are constructed from the conformal field correlators as

$$\Psi(\{z_j\}, \{w_k\}) = \langle \prod_{j=1}^N V_{n_j}(z_j) \prod_{k=1}^Q W_{p_k}(w_k) \rangle, \quad (4.39)$$

which we utilize to derive the parent Hamiltonians by using the null fields of the considered conformal field theory. Null field, say $\chi(v)$ at position v , has the property that the correlator vanishes when we insert the null field in the correlator of the primary fields. That is we have

$$\langle \prod_{j=1}^N V_{n_j}(z_j) \chi(v) \prod_{k=1}^Q W_{p_k}(w_k) \rangle = 0. \quad (4.40)$$

The task is to rewrite Eq. (4.40) as

$$\Lambda |\Psi\rangle = 0, \quad (4.41)$$

where Λ is the annihilation operator for the state $|\Psi\rangle$ and thereby parent Hamiltonian becomes

$$H = \Lambda^\dagger \Lambda. \quad (4.42)$$

Explicit derivations of the null fields in this case, by following Ref. [69], are done in the Appendix-B. And we derive the following q number of operators, in the Appendix-C, which serve as the annihilation operators for the states as

$$\Lambda^0 = \sum_i d_i, \quad \Lambda_i^p = \sum_{j(\neq i)} \frac{1}{(z_i - z_j)^p} d_j n_i,$$

$$\Lambda_i^{q-1} = \sum_{j(\neq i)} \left[\frac{d_j n_i}{(z_i - z_j)^q} + \sum_{h(\neq i)} \frac{[q n_j - 1] d_h n_i}{(z_i - z_h)^{q-1} (z_i - z_j)} \right] + \sum_j \sum_{h(\neq i)} \frac{p_j d_h n_i}{(z_i - z_h)^{q-1} (z_i - z_j)}$$
(4.43)

and thereby we have

$$\Lambda_i^a |\Psi_\alpha^{\eta=1, \text{qh}}\rangle = 0 \text{ with } a \in \{0, 1, \dots, q-1\},$$
(4.44)

where 'qh' stands for the quasiholes. Here d_j is the hardcore bosonic or fermionic annihilation operators respectively for q odd or q even, and is acting on the j th lattice site. The particle number operator acting at the j th lattice site is defined as

$$n_j = d_j^\dagger d_j.$$
(4.45)

We write these operators in the matrix form with respect to the basis $(|0\rangle, |1\rangle)$ acting on the j th lattice site as

$$d_j = \mathcal{S} \begin{bmatrix} 0 & 1 \\ 0 & 0 \end{bmatrix}, \quad d_j^\dagger = \mathcal{S} \begin{bmatrix} 0 & 0 \\ 1 & 0 \end{bmatrix}, \quad n_j = \begin{bmatrix} 0 & 0 \\ 0 & 1 \end{bmatrix}, \text{ with } \mathcal{S} = (-1)^{(q+1)\sum_{k=1}^{j-1} n_k}$$

as the sign factor. We inscribe the following Hermitian operators as the parent Hamiltonians for the states as

$$H = \sum_{i=1}^N \sum_{a=0}^{q-1} \Lambda_i^{a\dagger} \Lambda_i^a.$$
(4.46)

We note that the Hamiltonians are positive semi-definite because their eigenvalues are all positive including zero.

(b). Parent Hamiltonians for $\eta < 1$

We utilize the annihilation operators in Eq. (4.43) to derive the parent Hamiltonians for the case of $\eta < 1$. We note that the states with $\eta < 1$, which we denote here as $|\Psi_\alpha^{\eta, \text{qh}}\rangle$, have the particle number

$$M = \frac{(\eta N - \sum_{k=1}^Q p_k)}{q}.$$
(4.47)

And the states with $\eta = 1$ and a charge \mathcal{P}/q at infinity contain

$$M = \frac{\left(N - \mathcal{P} - \sum_{k=1}^Q p_k\right)}{q} \quad (4.48)$$

number of particles. Therefore the particle numbers in both the states will be equal if we take

$$\mathcal{P} = N(1 - \eta). \quad (4.49)$$

In the Appendix-C we find that the operators in Eq. (4.43), which annihilate the states $|\Psi_\alpha^{\eta=1, \text{qh}}\rangle$, are also the annihilation operators for the states with the charge at infinity provided the following condition is fulfilled as

$$\mathcal{P} > \left(-2q - \sum_{k=1}^Q p_k + Q\right). \quad (4.50)$$

Now with the choice

$$\mathcal{P} = N(1 - \eta), \quad (4.51)$$

we obtain the restriction on the η values as

$$\eta < 1 + \frac{1}{N} \left(2q + \sum_{k=1}^Q p_k - Q\right). \quad (4.52)$$

Hence in the thermodynamic limit $N \rightarrow \infty$ the parent Hamiltonians, as provided below, are valid for $\eta \leq 1$.

To obtain the Hamiltonian, we note that the state $|\Psi_\alpha^{\eta, \text{qh}}\rangle$ differs from the state $|\Psi_\alpha^{\eta=1, \text{qh}}\rangle$ by the factor

$$\prod_{j \neq l} (z_l - z_j)^{(\eta-1)n_l} \quad (4.53)$$

and thereby we write the following term as

$$\Theta = \prod_l \left(\prod_{j(\neq l)} (z_l - z_j)^{(\eta-1)} \right)^{n_l} = \prod_l \gamma_l^{n_l} \text{ with } \gamma_l = \prod_{j \neq l} (z_l - z_j)^{(\eta-1)}. \quad (4.54)$$

Hence we have

$$\Theta |\Psi_\alpha^{\eta, \text{qh}}\rangle = |\Psi_\alpha^{\eta=1, \text{qh}}\rangle. \quad (4.55)$$

Now from Eq. (4.44) as we have

$$\Lambda_i^a |\Psi_\alpha^{\eta=1, \text{qh}}\rangle = 0, \quad (4.56)$$

and therefore we write

$$\Theta^{-1} \Lambda_i^a \Theta |\Psi_\alpha^{\eta, \text{qh}}\rangle = 0 \text{ with } a \in \{0, 1, \dots, q-1\}. \quad (4.57)$$

We note that

$$\Theta^{-1} d_i \Theta = \prod_l \gamma_l^{-n_l} d_i \prod_m \gamma_m^{n_m} = \gamma_i^{-n_i} d_i \gamma_i^{n_i} = \gamma_i d_i \quad (4.58)$$

and therefore we write the following q operators

$$\Lambda_i^{\prime a} = \Theta^{-1} \Lambda_i^a \Theta \quad (4.59)$$

which annihilate the state $|\Psi_\alpha^{\eta, \text{qh}}\rangle$. That is we have

$$\Lambda_i^{\prime a} |\Psi_\alpha^{\eta, \text{qh}}\rangle = 0 \text{ with } a \in \{0, 1, \dots, q-1\}. \quad (4.60)$$

We derive the explicit form of the $\Lambda_i^{\prime a}$ operators as

$$\begin{aligned} \Lambda_i^{\prime 0} &= \sum_i \gamma_i d_i, \quad \Lambda_i^{\prime p} = \sum_{j(\neq i)} \frac{1}{(z_i - z_j)^p} \gamma_j d_j n_i, \\ \Lambda_i^{\prime q-1} &= \sum_{j(\neq i)} \left[\frac{\gamma_j d_j n_i}{(z_i - z_j)^q} + \sum_{h(\neq i)} \frac{[q n_j - 1] \gamma_h d_h n_i}{(z_i - z_h)^{q-1} (z_i - z_j)} \right] + \sum_j \sum_{h(\neq i)} \frac{p_j \gamma_h d_h n_i}{(z_i - z_h)^{q-1} (z_i - w_j)}. \end{aligned} \quad (4.61)$$

Therefore we obtain the parent Hamiltonians for $\eta \leq 1$ as

$$H = \sum_{i=1}^N \sum_{a=0}^{q-1} \Lambda_i^{\prime a \dagger} \Lambda_i^{\prime a}. \quad (4.62)$$

4.3.2 Parent Hamiltonians for the states containing quasielectrons

We exploit here the annihilation operators in Eq. (4.61) for the states $|\Psi_\alpha^{\eta, \text{qh}}\rangle$, containing quasiholes only, to derive the parent Hamiltonians for the states containing at least one quasielectron, which we denote as $|\Psi_\alpha^{\eta, \text{qe}}\rangle$, with 'qe' standing for the quasielectrons.

We have the particle number for the states $|\Psi_\alpha^{\eta, \text{qh}}\rangle$ as

$$M^{\text{qh}} = \frac{(\eta_{\text{qh}}N - \sum_k p_k^{\text{qh}})}{q} \quad (4.63)$$

and for the states $|\Psi_\alpha^{\eta, \text{qe}}\rangle$ as

$$M = \frac{(\eta N - \sum_k p_k)}{q}. \quad (4.64)$$

Here we take the number of lattice sites N to be the same and η_{qh} is for the state with quasiholes only and p_k^{qh} is the charge of the k th quasihole. Now to achieve the same number of particles for both the states, that is to have

$$M^{\text{qh}} = M, \quad (4.65)$$

we find the following condition to be satisfied as

$$\eta = \eta_{\text{qh}} - \frac{1}{N} \left(\sum_k p_k^{\text{qh}} - \sum_k p_k \right), \quad (4.66)$$

with the restriction on η_{qh} values as given in Eq. (4.52). Hence in the thermodynamic limit $N \rightarrow \infty$ we have here $\eta \leq 1$.

Now, to derive the Hamiltonian, we note that

$$T|\Psi_\alpha^{\eta, \text{qe}}\rangle = |\Psi_\alpha^{\eta, \text{qh}}\rangle \quad (4.67)$$

where we have

$$T = \prod_i \beta_i^{n_i} \theta_i^{n_i} \text{ with } \beta_i = \prod_{j \neq i} (z_i - z_j)^{(\eta - \eta_{\text{qh}})} \text{ and } \theta_i = \prod_j (w_j - z_i)^{(p_j^{\text{qh}} - p_j)}. \quad (4.68)$$

We set here $\eta_{\text{qh}} = 1$ and recall the annihilation operators for the states $|\Psi_\alpha^{\eta=1, \text{qh}}\rangle$ from Eq. (4.43) as

$$\Lambda_i^a |\Psi_\alpha^{\eta=1, \text{qh}}\rangle = 0, \quad a \in \{0, 1, \dots, q-1\}. \quad (4.69)$$

We rewrite this as

$$T^{-1} \Lambda_i^a T |\Psi_\alpha^{\eta, \text{qe}}\rangle = 0. \quad (4.70)$$

Therefore we define the annihilation operators for the state $|\Psi_\alpha^{\eta, \text{qe}}\rangle$ as

$$\Lambda_i^{\prime\prime a} = T^{-1} \Lambda_i^a T \text{ such that } \Lambda_i^{\prime\prime a} |\Psi_\alpha^{\eta, \text{qe}}\rangle = 0, \quad a \in \{0, 1, \dots, q-1\}. \quad (4.71)$$

We utilize the expressions of Λ_i^q in Eq. (4.43) and derive the following q number of annihilation operators as

$$\begin{aligned}\Lambda_i''^0 &= \sum_i \beta_i \theta_i d_i, \quad \Lambda_i''^p = \sum_{j(\neq i)} \frac{\beta_j \theta_j d_j n_i}{(z_i - z_j)^p}, \\ \Lambda_i''^{q-1} &= \sum_{j(\neq i)} \left[\frac{\beta_j \theta_j d_j n_i}{(z_i - z_j)^q} + \sum_{h(\neq i)} \frac{[qn_j - 1] \beta_h \theta_h d_h n_i}{(z_i - z_h)^{q-1} (z_i - z_j)} \right] + \sum_j \sum_{h(\neq i)} \frac{p_j \beta_h \theta_h d_h n_i}{(z_i - z_h)^{q-1} (z_i - w_j)}\end{aligned}\quad (4.72)$$

Therefore we obtain the parent Hamiltonians for $\eta \leq 1$ as

$$H = \sum_{i=1}^N \sum_{a=0}^{q-1} \Lambda_i''^{a\dagger} \Lambda_i''^a. \quad (4.73)$$

We have tested numerically that the parent Hamiltonians, as given in this section, have unique ground state when we have two anyons and have two degenerate ground states when we have four anyons in the system. These also signify the non-Abelian nature of the anyons. The parent Hamiltonians, we have derived, are non-local and contain up to five-body interaction terms. These may be a starting point to find simpler Hamiltonians with practically the same ground state physics.

4.4 Anyons in the Kapit-Mueller model

Kapit and Mueller proposed a lattice model [119, 120] which realizes the fractional quantum Hall physics at appropriate filling factors. The model shows an exact equivalence between a realistic lattice system and the lowest Landau level of the fractional quantum Hall effect. That is the lattice model is defined with the same ground state structure as the ground state of the continuum and thereby the model becomes a good starting point for the numerical studies of the fractional quantum Hall problems. It is interesting that the fractional quantum Hall ground states physics exist in the lattice systems which have no direct continuum analog. The model Hamiltonian is relatively simple and is computationally tractable. It consists of the hopping terms and of the on-site hardcore interactions.

So far we have found the shapes and the charges of the anyons with the analytical lattice Moore-Read states. One may speculate that if these anyonic properties are very specific to the analytical states or not. Therefore we compare the anyons in the Kapit-Mueller model to the anyons in the analytical states. We take the filling factor $q = 1$ for which the ground state of the model is known to be in the same topological phase as that of the bosonic Moore-Read state.

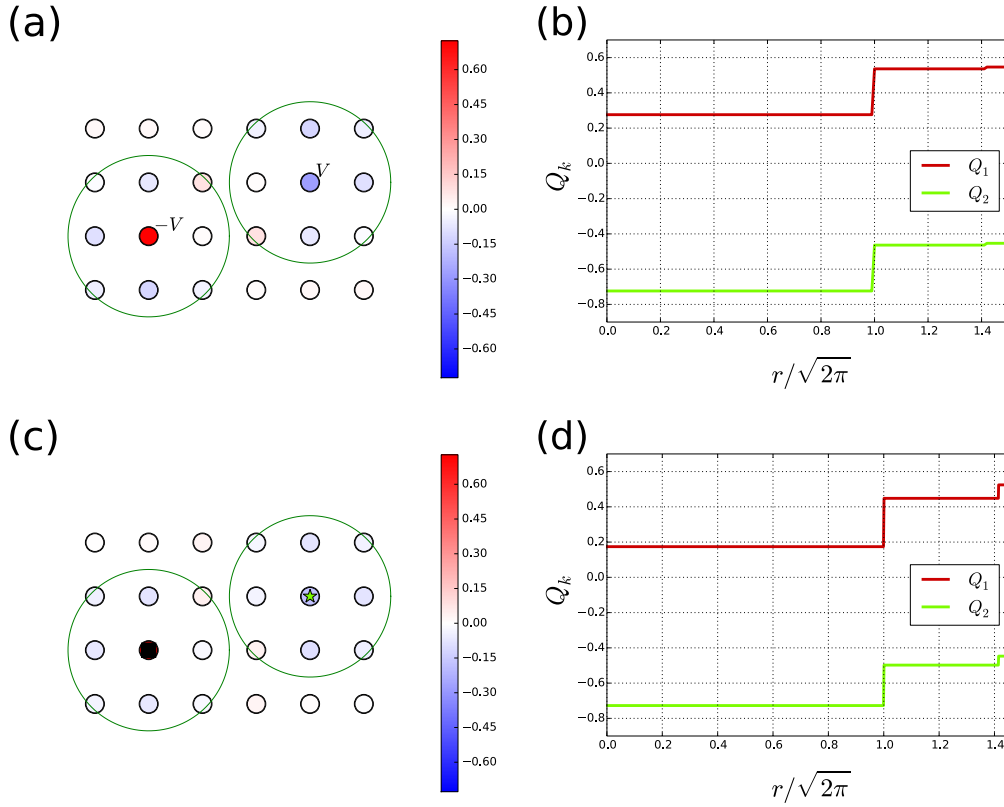


Figure 4.6.: In (a), (c): We mark the $N = 24$ lattice sites by the black circles and symbolize the quasihole, and the quasielectron, by the green star, and by the black square respectively. We place the potential $+V$ and the potential $-V$ on two different lattice sites to trap one quasihole and one quasielectron respectively. The density profile $\rho(z_i)$, defined as the particle density difference between the states in the presence and in the absence of the anyons in the systems, is plotted with colorbar for the anyons in the Kapit-Mueller model (4.74) in (a) by using Eq. (7.7) and for the anyons in the Moore-Read state (3.59) in (c) by using Eq. (4.2). In (b), (d): We plot the excess charge distributions Q_k , as defined in (4.10), as a function of the radial distances from the anyon positions in (b) for the Kapit-Mueller model and in (d) for the lattice Moore-Read state. We mark the regions, within which we compute the excess charges, by the green circles in (a) and in (c). We find that the quasiholes and the quasielectrons are trapped with the charges $\simeq 0.5$ and $\simeq -0.5$, respectively. We note that the excess charge distributions in (b) and in (d) are similar.

4.4.1 The Kapit-Mueller Hamiltonian

We write the Hamiltonian [119, 120] on a two-dimensional square lattice with open boundary conditions as

$$H_0 = - \sum_{j,k} J_{jk} e^{i\phi_{jk}} c_j^\dagger c_k + \text{H.c.} \quad (4.74)$$

The creation and the annihilation operators of the hard-core bosons at the k th lattice site at position z_k are denoted by c_k^\dagger and c_k respectively. We take unit lattice spacing and we define

$$\xi_{jk} = z_j - z_k \text{ and } a = \text{Re}(\xi_{jk}), b = \text{Im}(\xi_{jk}). \quad (4.75)$$

Due to the uniform background magnetic field B we have the Peierls phase factor as

$$i\phi_{jk} = -\frac{\pi\phi}{2} \left(z_j \xi_{jk}^* - z_j^* \xi_{jk} \right), \quad (4.76)$$

where ϕ is the density of flux quanta $\phi_0 = h/e$, where h is the Planck's constant and e is the electric charge, through each lattice plaquette. This flux is only defined modulo 1 and having a flux quanta through each lattice plaquette is gauge invariant to no flux at all. Therefore we need $0 \leq \phi \leq 1$ and we define $\phi = p/m$ as the ratio of two relatively prime integers.

We note that if we take $J_{jk} = -J$, with $J > 0$, and only the nearest neighbor couplings in Eq. (4.74) then in the non-interacting case, that is in the single particle picture, the Hamiltonian H_0 becomes the Hofstadter model. The Peierls phase factor in Eq. (4.76) is written in the symmetric gauge choice of

$$\vec{A} = \frac{B}{2} (x\hat{y} - y\hat{x}) \quad (4.77)$$

but one can choose any other gauge as well.

We have the Gaussian hopping in Eq. (4.74) as

$$J_{jk} = G(\xi_{jk}) \exp\left(-\frac{\pi}{2}(1-\phi)|\xi_{jk}|^2\right) \text{ with } G(\xi_{jk}) = (-1)^{1+a+b+ab}. \quad (4.78)$$

This particular choice of the hopping couplings gives rise to the robust fractional quantum Hall states.

One promising experimental realization of the model is with ultra-cold atoms in optical lattices. This allows to investigate larger magnetic fluxes than is achievable with the real magnetic fields. Though the long range hopping are difficult to arrange but as J_{jk} exhibits a Gaussian fall, therefore only the nearest and next-nearest neighbor couplings are sufficient when ϕ is small.

4.4.2 Creation of anyons in the ground state

We modify the Hamiltonian H_0 , as in Eq. (4.74), to trap the anyons in the ground state. We add a potential term H_V to the Kapit-Mueller Hamiltonian to trap the quasiholes and the quasielectrons. We provide energy penalties to the lattice sites to be occupied for the quasiholes and to be unoccupied for the quasielectrons respectively.

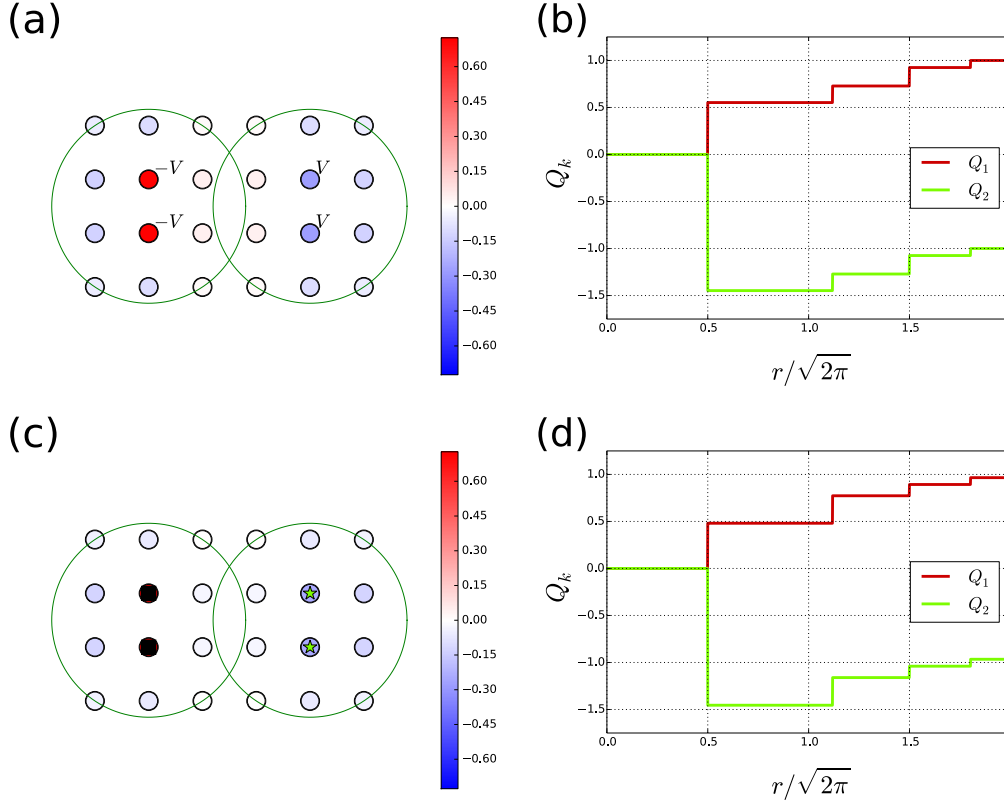


Figure 4.7.: In (a), (c): We mark the $N = 24$ lattice sites by the black circles and symbolize the quasiholes, and the quasielectrons, by the green stars, and by the black squares respectively. We place two potentials each of $+V$ and two potentials each of $-V$ on four different lattice sites to trap two quasiholes and two quasielectrons respectively. The density profile $\rho(z_i)$, defined as the particle density difference between the states in the presence and in the absence of the anyons in the system, is plotted with colorbar for the anyons in the Kapit-Mueller model (4.74) in (a) by using Eq. (7.7) and for the anyons in the Moore-Read state (3.62) in (c) by using Eq. (4.2). In (b), (d): We plot the excess charge distributions Q_k , as defined in (4.10), as a function of the radial distances from the anyon positions in (b) for the Kapit-Mueller model and in (d) for the lattice Moore-Read state. We mark the regions, within which we compute the excess charges, by the green circles in (a) and in (c). We find that the quasiholes and the quasielectrons are trapped with the charges $\simeq 0.5$ and $\simeq -0.5$, respectively. We note that the excess charge distributions in (b) and in (d) are similar.

We define the following operators as

$$H_V = Vn_a - Vn_b \text{ and } H_V = Vn_a + Vn_b - Vn_c - Vn_d, \quad (4.79)$$

where

$$n_k = c_k^\dagger c_k \quad (4.80)$$

is the number operator at the k th lattice site and V is the strength of the potential at the k th lattice site, which is sufficiently larger than the hopping strengths. The first operator in Eq. (4.79) traps one quasihole-one quasielectron and the second operator traps two quasiholes-two quasielectrons.

4.4.3 Density profiles and charges of anyons

We define the density profiles of the anyons as

$$\rho(z_i) = [\langle n(z_i) \rangle_{H_0+H_V} - \langle n(z_i) \rangle_{H_0}], \quad (4.81)$$

where

$$\langle n(z_i) \rangle_{H_0+H_V} \text{ and } \langle n(z_i) \rangle_{H_0} \quad (4.82)$$

are the particle densities at the i th lattice site in the presence and in the absence of the anyons in the systems respectively. The excess charges and the charges of the anyons are computed by using Eq. (4.10).

We take the lattice size to be $N = 24$ and the particle number as $M = 4$. Therefore we have $\phi = 1/6$ and the relation

$$\frac{M}{\phi N} = \frac{1}{q} = 1, \text{ for } q = 1 \quad (4.83)$$

is satisfied.

We show the density profiles of anyons, by using Eq. (7.7), in Fig. 4.6 (a) and in Fig. 4.7 (a) for one quasihole-one quasielectron and for two quasiholes-two quasielectrons cases respectively. In Fig. 4.6 (b) and in Fig. 4.7 (b) we show the excess charge distributions of the trapped anyons as a function of the radial distances from the anyon positions. We find that the anyons are screened well. And each quasihole exhibits the charge $\simeq 0.5$, and each quasielectron exhibits the charge $\simeq -0.5$.

In principle we can trap more anyons by adding more trapping potentials to H_V in Eq. (4.79). However we need larger lattice sizes to make sufficient spaces for the anyons. And we may not be able to achieve those systems sizes by the exact diagonalizations studies.

We compare our analytical bosonic Moore-Read states, from Eqs. (3.51), (3.62), (3.62), on the same lattice. We take $N = 24$, $M = 4$, $q = 1$ and hence we have $\eta = 1/6$ which satisfy the condition

$$\frac{M}{\eta N} = \frac{1}{q} = 1. \quad (4.84)$$

We note the equivalence $\eta \equiv \phi$. We place the anyons on the lattice sites.

We show the anyon density profiles, by using Eq. (4.2), in Fig. 4.6 (c) and in Fig. 4.7 (c) for one quasihole-one quasielectron and for two quasiholes-two quasielectrons cases respectively. We display the excess charge distributions, by using Eq. (4.10), of the trapped anyons as a function of the radial distances from the anyon positions in Fig. 4.6 (d) and in Fig. 4.7 (d). Each of the quasiholes and each of the quasielectrons exhibits the charge $p_k/q \simeq 0.5$, for $p_k = 1/2$, and the charge $p_k/q \simeq -0.5$, for $p_k = -1/2$, respectively.

We have well-screened anyons in the system. We note from Fig. 4.6 (b), (d) and from Fig. 4.7 (b), (d) that the density profiles and the excess charge distributions of the anyons are very similar. These display similarities between the topological properties of the ground state of the Kapit-Mueller model and the topological properties of the analytical lattice Moore-Read states. We point out that the anyon density profiles and excess charge distributions are similar but not exactly the same. The reason is that the analytical lattice Moore-Read states containing anyons are not the exact ground states of the Kapit-Mueller Hamiltonian with the trapping potential, that is of the Hamiltonian $H_0 + H_V$, but they share the same topological properties. Hence our analytical states are relevant to the Kapit-Mueller model.

4.5 Conclusions

In this chapter we have researched the properties of the non-Abelian Ising anyons in the lattice Moore-Read states, at the Landau level filling factor $5/2$, by using Monte-Carlo simulations. We have shown that the quasielectrons can be created and can be investigated in a similar way that of the quasiholes. Therefore we have simpler wavefunctions for the quasielectrons, both from the analytical and from the numerical viewpoint, than the continuum.

We have investigated the cases of two quasiholes, two quasielectrons, one quasihole-one quasielectron, four quasiholes, four quasielectrons and two quasiholes-two quasielectrons in the systems. By inspecting the density profiles and charges of the anyons we have shown that the anyons are screened well and have radii up to a few lattice constants. We find that a quasihole exhibits a charge $\simeq 0.25$ and a quasielectron carries a charge $\simeq -0.25$. This agrees with the findings for the Ising quasihole charge in the continuum. We probe the topological properties of the systems by computing the fractional braiding statistics of the anyons. We find that the anyons are non-Abelian and the braiding statistics are the same as expected from the continuum. We have used the null fields construction of the underlying conformal field theory and have derived the parent Hamiltonians for which the analytical states are the exact ground states. We have found the degenerate ground states for the case of the four anyons in the system which also signify the non-Abelian nature of the anyons. The parent Hamiltonians are long-rang and contain few-body interactions which may be a starting point to search for the local Hamiltonians with practically the same ground state physics.

We have investigated a simpler lattice model, which is known as the Kapit-Mueller model, and have created the quasielectrons in the same way as that of the quasiholes.

By using exact diagonalizations we have found that the anyons in this model are well-screened and have right charges. We have shown that the excess charge distributions and the shapes of the anyons are similar to those in the analytical lattice Moore-Read states. Therefore our analytical states are suitable to this experimentally relevant model.

Anyons and Fractional Quantum Hall Physics in Quasicrystals and in Fractal Lattices

” *It is the glory of geometry that from so few principles, fetched from without, it is able to accomplish so much.*

— Sir Isaac Newton

Interplay between the long-range order and the non-periodic structure in quasicrystals gives rise to a wealth of intriguing phenomena [150, 152, 8, 41, 134, 135, 133, 139, 206, 114, 65, 270, 99, 231, 66], such as the existence of topological properties from higher dimensions, and the presence of non-trivial structure on all length scales. Properties of a system often depends strongly on the dimension of the system because of the restrictions on the particle movements along the different directions. Fractal structures open up the possibilities to research non-integer dimensions, such as between 0 and 2, which constitute an intermediate regime to expect interesting physics [67, 266, 233, 254, 35, 136, 102]. The questions about the topological phases are being investigated recently [2, 179], for example the construction of the non-interacting Chern insulator models on the fractal lattices.

In this chapter we investigate the strongly interacting topologically ordered phases namely the fractional quantum Hall physics and the anyons in quasicrystals and in fractal spaces. We construct the lattice fractional quantum Hall models containing anyons and provide the analytical states and the corresponding parent Hamiltonians. We show that the anyons are well-screened, possess right charges, and have the right braiding properties. We find that the fractional quantum Hall physics and the anyons exist in quasicrystals and in fractal lattices with all the Hausdorff dimensions $1 \leq \text{dimension} \leq 2$. Our findings suggest that the local structures of the fractal lattices become important than the corresponding Hausdorff dimensions in determining the topological properties of the fractal systems.

To study chiral topological orders one of the possibilities is to construct the fractional Chern insulator models. Such constructions require the systems to exhibit translational symmetry, since fractionally filled flat-bands are to be constructed and many-body Chern numbers are to be computed. Now an important common point of the structures of the quasicrystals and of the fractal lattices is that these lack translational symmetry. Therefore

it is worth to note that the construction of the fractional Chern insulator models are not possible to realize such physics in these systems. We take the first step to use our construction of lattice models to obtain anyons and the fractional quantum Hall physics on such lattices to directly probe the chiral topological orders.

We show two types of quasicrystals in Sec. 5.1. In Sec. 5.2 we describe how to generate fractal lattices and how to compute fractal dimensions with a particular example as the Sierpinski gasket. We show in Sec. 5.3 that both type of quasicrystals host well-screened anyons and we display the existence of well-screened anyons in fractal dimension $\simeq 1.585$ on the Sierpinski gasket geometry. In one-dimensional linear system the absence of anyons is known since the model is known to be critical. However, interestingly, we find that anyons can exist in one dimension in fractal space. In particular we show that the anyons and the fractional quantum Hall physics can be obtained in all dimensions $1 \leq \text{dimension} \leq 2$ and even we show that anyons can be present in dimension less than one such as in dimension $\ln(4)/\ln(5) \simeq 0.86$. Our investigations reveal that the lattice points distributions are more important in hosting the anyons and in displaying the fractional quantum Hall physics rather than the Hausdorff dimensions of the fractal spaces. We derive the braiding statistics of the anyons in Sec. 5.4 and show that the analytical states are topological in quasicrystals and in fractal spaces. We construct parent Hamiltonians of our lattice models in Sec. 5.5, for which the analytical states are the exact ground states, and Sec. 5.6 draws the conclusions. This chapter is based on parts of the following Refs. [57, 180]:

[1] : **Sourav Manna***, Biplab Pal*, Wei Wang* and Anne E. B. Nielsen, "Anyons and fractional quantum Hall effect in fractal dimensions", *Physical Review Research* **2**, 023401 (2020) [* authors equally contributed to this work]

[2] : Callum Duncan, **Sourav Manna** and Anne E. B. Nielsen, "Topological models in rotationally symmetric quasicrystals", *Physical Review B* **101**, 115413 (2020) [*Editors' Suggestion*]

5.1 Quasicrystals

Quasicrystals are the quasi-periodic structures in two-dimensions which are long-range ordered but are not periodic [239, 32, 107, 14, 240, 33, 226, 195, 196, 185]. A quasicrystalline geometry continuously fills in all available space, but it lacks translational symmetry, that means a shifted copy of the quasicrystal will never match exactly with its original. Quasicrystals possess long-range order but are non-periodic. Their long-range order gives rise to the sharp diffraction peaks [239], as found in the crystals. They contain a small set of local environments which reappear again and again, but in a non-periodic fashion. Because of this fact, the Bloch's theorem no longer holds. A two-dimensional crystal can exhibit only two-fold, three-fold, four-fold, and six-fold rotational symmetries while a two-dimensional quasicrystal can have five-fold, eight-fold, and ten-fold rotational symmetries, which are noncrystallographic. Hence a crystal has translational symmetry whereas a quasicrystal does not have translational symmetry. Therefore it follows that

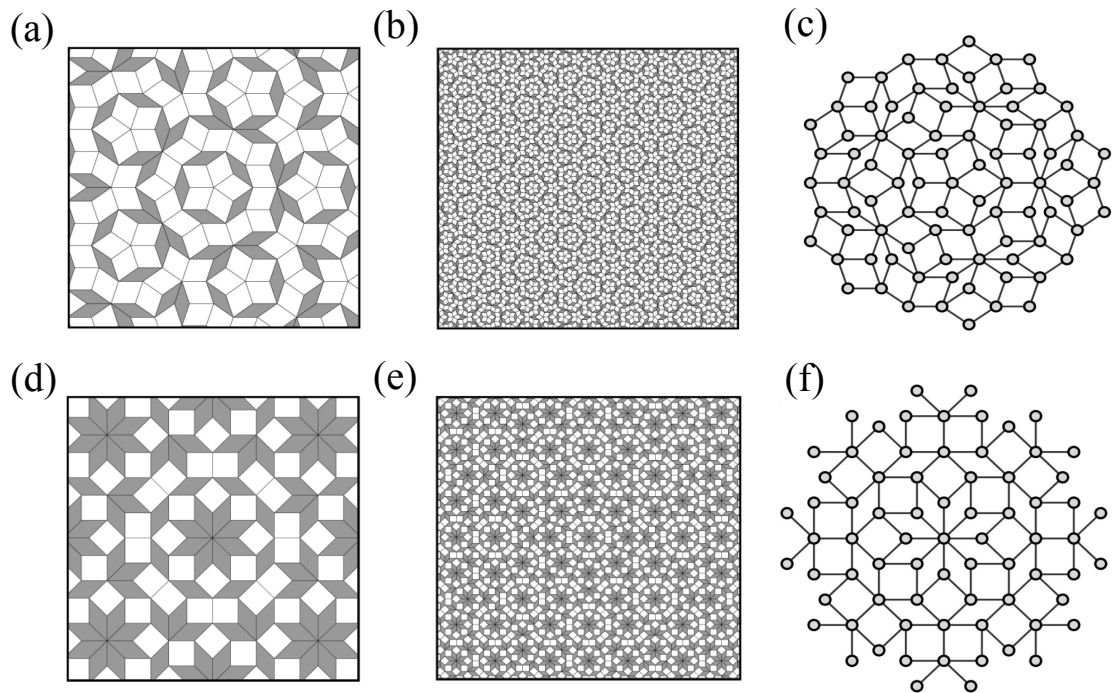


Figure 5.1.: In the upper panel we show the examples of the rhombus Penrose tiling, as the five-fold rotationally symmetric quasicrystal, as obtained from the Robinson triangle decomposition method. In (a), a zoomed portion of the Penrose tiling is showing the two types of rhombuses by the grey colored shading and by the white colored shading. In (b), a larger portion of the Penrose tiling is showing the self-similar structure. In (c), we show the couplings, that is the connections along the rhombuses, of the Penrose tiling by using solid lines with 86 lattice sites, which are pictured as the grey colored circles and are sitting at the vertices of the tiling. In the lower panel we show the examples of the rhombus Ammann-Beenker tiling, as the eight-fold rotationally symmetric quasicrystal, as obtained from the cut-and-project method. In (d), a zoomed portion of the Ammann-Beenker tiling is showing the two types of rhombuses by the grey colored shading and by the white colored shading. In (e), a larger portion of the Ammann-Beenker tiling is showing the self-similar structure. In (f), we show the couplings, that is the connections along the rhombuses, of the Ammann-Beenker tiling by using solid lines with 73 lattice sites, which are pictured as the grey colored circles and are sitting at the vertices of the tiling.

the long-range order in quasicrystals cannot originate from a periodic arrangement of the unit cells rather it requires a different origin.

Quasicrystalline orders arise from the incommensurate projection of the higher dimensional periodic structures or from the continuous tiling of space having discrete unit cells, and hence enables the investigation of physics of higher dimensions, in particular in the context of topology. Quasicrystals become important in condensed matter physics over the recent years, for example the study of the twisted bilayer graphene system. Recently the experimental demonstration [239] of an eight-fold rotationally symmetric optical

lattice, realizing a two-dimensional quasicrystalline potential with ultra-cold atoms, opens up the door to experimentally study the properties of quasicrystal structures.

5.1.1 Examples as the Penrose tiling and the Ammann-Beenker tiling

An approach to construct the quasicrystals was discovered by Penrose [181], where a set of tiles and the associated matching rules that ensure the aperiodic long-range order, when tiling a plane, were described. The resulting quasicrystal was five-fold rotationally symmetric and it is known as the Penrose tiling as we show in Fig. 5.1 (a), (b), (c), where we use the Robinson triangle decomposition method which gives the Penrose tiling with rhombuses. Here all the tiles have the same side length.

Also a closely related eight-fold rotationally symmetric quasicrystal was described which has octagonal tiling and which is known as the Ammann-Beenker tiling [5, 20] as we show in Fig. 5.1 (d), (e), (f), where we utilize the cut-and-project method. Here all the tiles have the same side length. In addition to their peculiar rotational symmetries, these tilings have the remarkable feature of being self-similar at large scales.

5.2 Fractal lattices and fractional dimensions

The theory of vector spaces provides the oldest and the most natural definition of dimensions, that is, an object has dimension k if it is visible from k orthogonal directions. But an object, such as a sea-coast or a snow-flake, is too irregular to be properly described by the traditional dimensional analysis. Therefore a more general definition of the dimension was provided by Felix Hausdorff which takes into account the irregularity of the object that is measured, and the dimension is called the Hausdorff dimension or the fractal dimension. This gives the feeling for the most fitted scale to measure the object. The roughness of such objects makes these objects hard to analyze and the mathematician Benoit Mandelbrot, coined a new chapter of mathematics, which is called the fractal geometry [189, 68, 203, 123, 244]. The name appears from the Latin word "fractus" which means broken. Mathematically a fractal is a subset of an Euclidean space which exhibits fractional dimension. In the words of Mandelbrot, "Clouds are not spheres, mountains are not cones, coastlines are not circles, and bark is not smooth, nor does lightning travel in a straight line."

We illustrate the traditional notions of geometry, which define the scaling and dimension, in Fig. 5.2. The measurement of the length of a line using one stick, and then the measurement of the same length using two sticks with $1/2$ of the previous stick length, and again the measurement of the same length using three sticks with $1/3$ of the first stick length, and so on, correspond to one dimension. This holds in two dimensions as measuring the area of a square with one box, and measuring the same area with four boxes each having side length as $1/2$ of the previous one, and again measuring the same

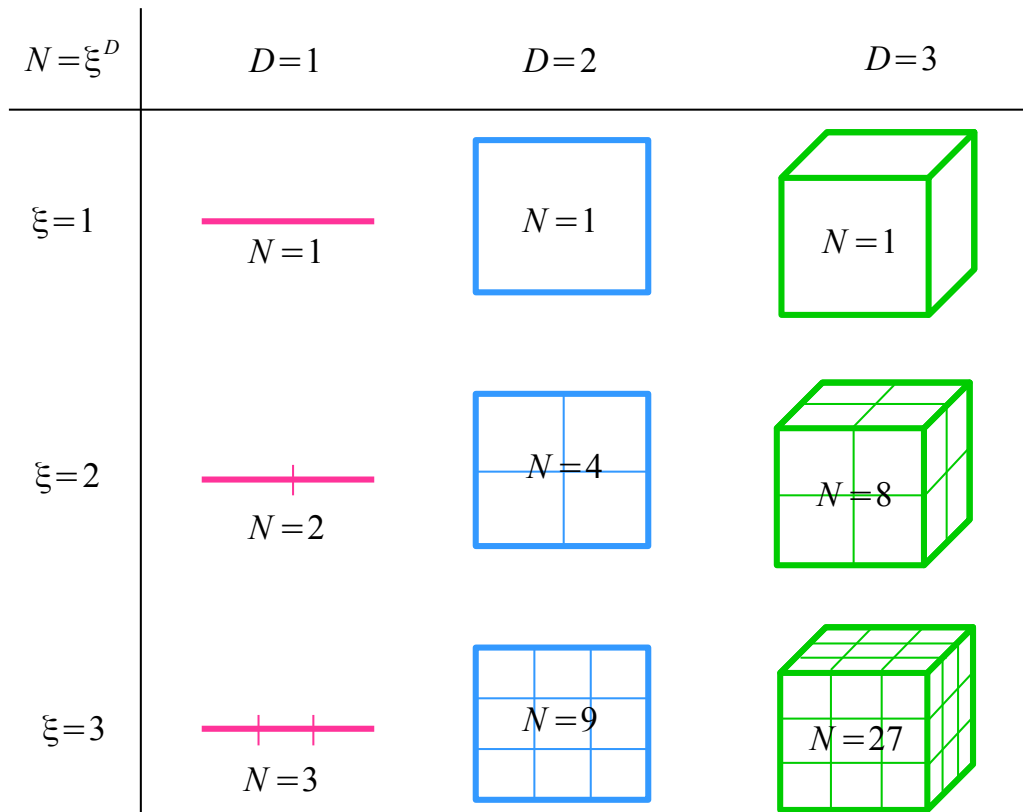


Figure 5.2.: We show the traditional concepts of geometry to define dimension and scaling in one dimension as displayed by the pink lines, in two dimensions as displayed by the indigo squares, and in three dimensions as displayed by the light-green cubes (redrawn from Wikipedia).

area with eight boxes each having side length as $1/3$ of the first one, and so on. Similarly we have three-dimensional case also.

Mathematically we define this scaling as

$$N = \xi^{-D} \text{ or } D = -\frac{\ln N}{\ln \xi}, \quad (5.1)$$

where N is the total number of units as for example the total number of sticks for one dimension, the total number of squares for two dimensions etc. which cover the whole space, ξ is the scaling factor as for example $1/2$, $1/3$ etc. and D stands for the dimension.

The same rule of scaling as we show in Eq. (5.1) holds for the fractal geometry and D is termed as the fractal dimension or the Hausdorff dimension which corresponds to a ratio providing an index of complexity by comparing how details of a fractal pattern changes with the measurement scale. It also gives a measurement of the space filling capacity that shows how a fractal pattern scales differently from the space where it is embedded in. Therefore D can be a fraction in the fractal space. This property is solely based on the

scaling and on the self-similarity, which means that the fractals exhibit similar patterns at increasingly small length scales.

5.2.1 Example as the Sierpinski gasket of dimension $\simeq 1.585$

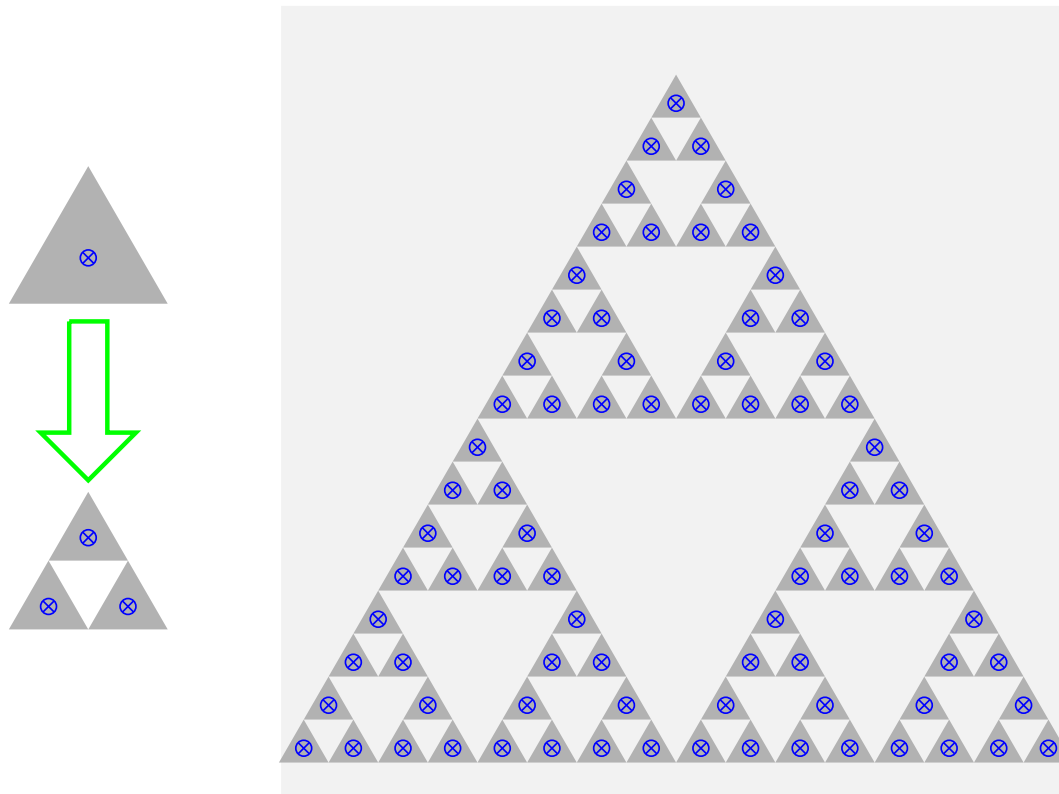


Figure 5.3.: A Sierpinski gasket fractal model, as shown by the dark grey regions, exhibits the Hausdorff dimension $\ln(3)/\ln(2) \simeq 1.585$ and is embedded in the two-dimensional plane, as shown by the light grey color in the background. On the left figures we show the operation to create the different generations. The blue crossed-circles display the positions of the lattice sites on the fractal structures.

A fractal structure is constructed by using the generations repeatedly and a full fractal structure is defined in the infinite generation. The Sierpinski gasket [34] is one of the famous examples of the fractal geometries. The 0th generation of it is an equilateral triangle to start with and then the $(n + 1)$ th generation is obtained from the n th generation by applying the operation as we show in Fig. 5.3, in the left side, to all the triangles in the gasket. At any stage of the generations we have the Hausdorff dimension

$$D = \frac{\ln(3)}{\ln(2)} \simeq 1.585. \quad (5.2)$$

The full fractal can be obtained in the limit of infinite generation.

The generation of a fractal remains finite since in any physical system, there is a limit to how small the smallest length scale of a fractal lattice can be and a limit to how large the total fractal lattice can be. Therefore the investigations of fractals at a length scale, which is large compared to the smallest fractal structure and small compared to the total size of the fractals, would be independent of the fractal generations as finite or as infinite and the system would be effectively in a space with the fractal dimension.

Here we consider a lattice model on the fractal, where there is one lattice site at the center of each of the smallest triangles. In the limit of large enough generation, it does not make a significant difference, whether we treat each triangle as a triangle or a single point, since the triangles are much smaller than the length scales of interest.

5.3 Anyon density profiles and charges

In this section we take the lattice Laughlin states in the presence and in the absence of anyons in the systems as defined in Eqs. (3.39), (3.46) in the quasicrystals and in the fractal lattices. We show that the state has the right topological properties to qualify for being a Laughlin type state. We claim this by investigating anyon density profiles and charges and by showing that the anyons are well-screened and possess correct charge and right braiding properties as those of the Laughlin anyons. We employ Monte-Carlo simulations and take $n_j \in \{0, 1\}$, $Q = 2$ anyons, $p_k = 1$ for the quasiholes, $p_k = -1$ for the quasielectrons, and consider $q = 3$ while studying anyons in the quasicrystals and consider $q = 2$ while studying anyons in the fractal lattices. We mention that we investigate both the quasiholes and the quasielectrons in quasicrystals and investigate only the quasiholes in the fractal lattices. We keep the total number of particles M and the total flux ηN fixed while going from one generation to the next generation for the case of the fractal lattices.

We define the particle density difference at the j th lattice as

$$\rho(z_j) = \langle n(z_j) \rangle_{Q \neq 0} - \langle n(z_j) \rangle_{Q=0}, \quad (5.3)$$

where $n(z_i)$ is the particle occupation number at the j th lattice site. We have

$$\langle n(z_j) \rangle_{Q \neq 0} \text{ and } \langle n(z_j) \rangle_{Q=0} \quad (5.4)$$

as the particle densities of the j th lattice site in the presence and in the absence of anyons in the states respectively. Therefore the quantity $\rho(z_j)$ gives the expectation value of the particle numbers on the j th lattice site in the presence of the anyons, relative to the same quantity in the absence of the anyons. We keep the magnetic flux ηN same in the two cases by suitably choosing the particle number M in the system.

We define the excess charge of the k th anyon, by taking the standard particle charge to be -1 , as

$$Q_k(r) = - \sum_{i=1}^N \rho(z_i) \Theta(r - |z_i - w_k|), \quad (5.5)$$

where $\Theta(\dots)$ is the Heaviside step function which we define as

$$\begin{aligned}\Theta(r - |z_i - w_k|) &= 1, \text{ if } |r - |z_i - w_k|| \leq 0, \text{ and} \\ &= 0, \text{ otherwise.}\end{aligned}\tag{5.6}$$

Therefore the excess charge is minus the sum of $\rho(z_i)$ within a circular region of radius r . For properly screened and well-separated anyons, we note that $Q_k(r)$ is constant, when r is much larger than the size of the anyon, but small enough that the circular region is far from all the other anyons in the system and far from the edge. This constant is called the charge of the anyon and should be equal to p_k/q . Below we research anyons in the quasicrystals and in a number of fractal geometries.

5.3.1 Anyons in quasicrystals

We use Eqs. (5.3) and (5.5) respectively to investigate the density profiles and the excess charge distributions of anyons. We display the outcomes in Fig. 5.4 and in Fig. 5.5. We choose the anyon flavors as two quasiholes, two quasielectrons, one quasihole-one quasielectron and plot the density profiles with colorbars in Fig. 5.4 (a), (c), (e) respectively for the five-fold rotationally symmetric Penrose tiling, where we take the number of lattice sites $N = 381$, and in Fig. 5.5 (a), (c), (e) respectively for the eight-fold rotationally symmetric Ammann-Beenker tiling, where we take the number of lattice sites $N = 273$.

We find that the anyons are well-screened with radii of a few lattice constants. The excess charge distributions Q_k are plotted as a function of the radial distances $r/\sqrt{2\pi}$, from the anyon positions, corresponding to the above mentioned anyon configurations in Fig. 5.4 (b), (d), (f) for the Penrose tiling and in Fig. 5.5 (b), (d), (f) for the Ammann-Beenker tiling. We note that the anyon charges approach $\simeq \pm 0.33$ for large r . We find that the sizes of the anyons depend on the local structures of the lattice sites around the anyons. This is reasonable because the screening is affected by the lattice points which are close to the anyons and where we allow particles to be present. But in all the cases we have well-screened anyons with proper charges.

5.3.2 Anyons in the Sierpinski gasket of dimension $\simeq 1.585$

The density of particles sets the relevant length scale of the system, and this corresponds to choose the number of particles such that the typical distance between two particles becomes large compared to the smallest lattice spacing and at the same time becomes small compared to the complete fractal. We use Eqs. (5.3) and (5.3) respectively to investigate the density profiles and to compute the charges of anyons, take the particle number $M = 30$, and show that the anyons are well-screened with expected charge $\simeq 0.5$ in Fig. 5.6.

We note that the two generations, as the 4th generation and the 5th generation, of the Sierpinski gasket have the same typical distance between the particles and therefore the

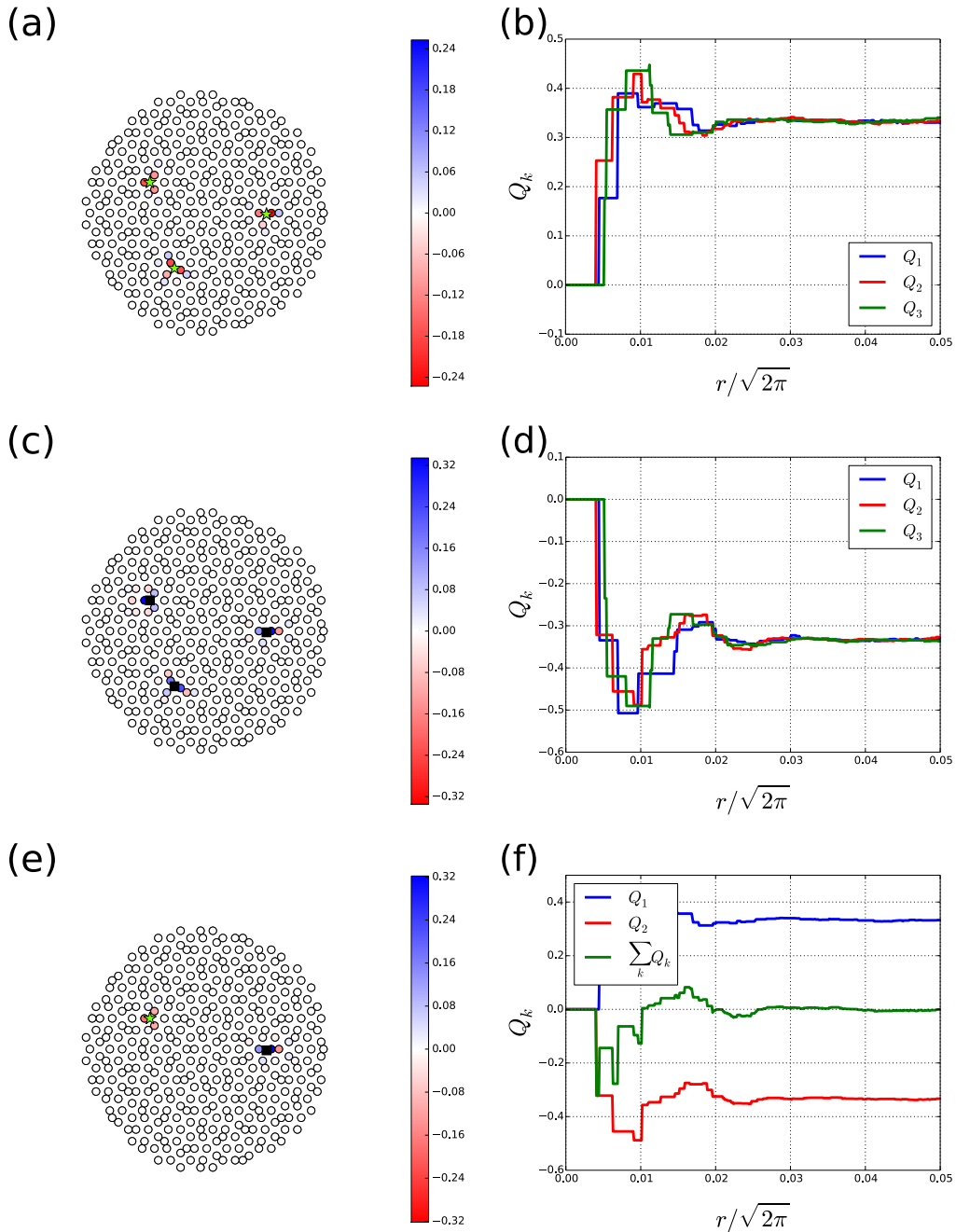


Figure 5.4.: In (a), (c), (e): We denote lattice sites, quasiholes, and quasielectrons by the black circles, the green stars, and the black squares respectively. The density profiles $\rho(z_i)$ from Eq. (5.3), defined as the particle density difference between the states in the presence and in the absence of the anyons in the systems, are plotted with colorbars for the cases of two quasiholes, two quasielectrons, one quasihole-one quasielectron in (a), (c), (e) respectively for the five-fold rotationally symmetric Penrose tiling, where we take the number of lattice sites $N = 381$. We find that the anyons are well-screened with radii of a few lattice constants. In (b), (d), (f): The excess charge distributions Q_k are computed from Eq. (5.5) and are plotted as a function of the radial distances $r/\sqrt{2\pi}$, from the anyon positions, corresponding to the above mentioned anyon configurations. The anyon charges approach $\simeq \pm 0.33$ for large r with an errorbar of size 10^{-4} arising due to the Monte-Carlo simulations.

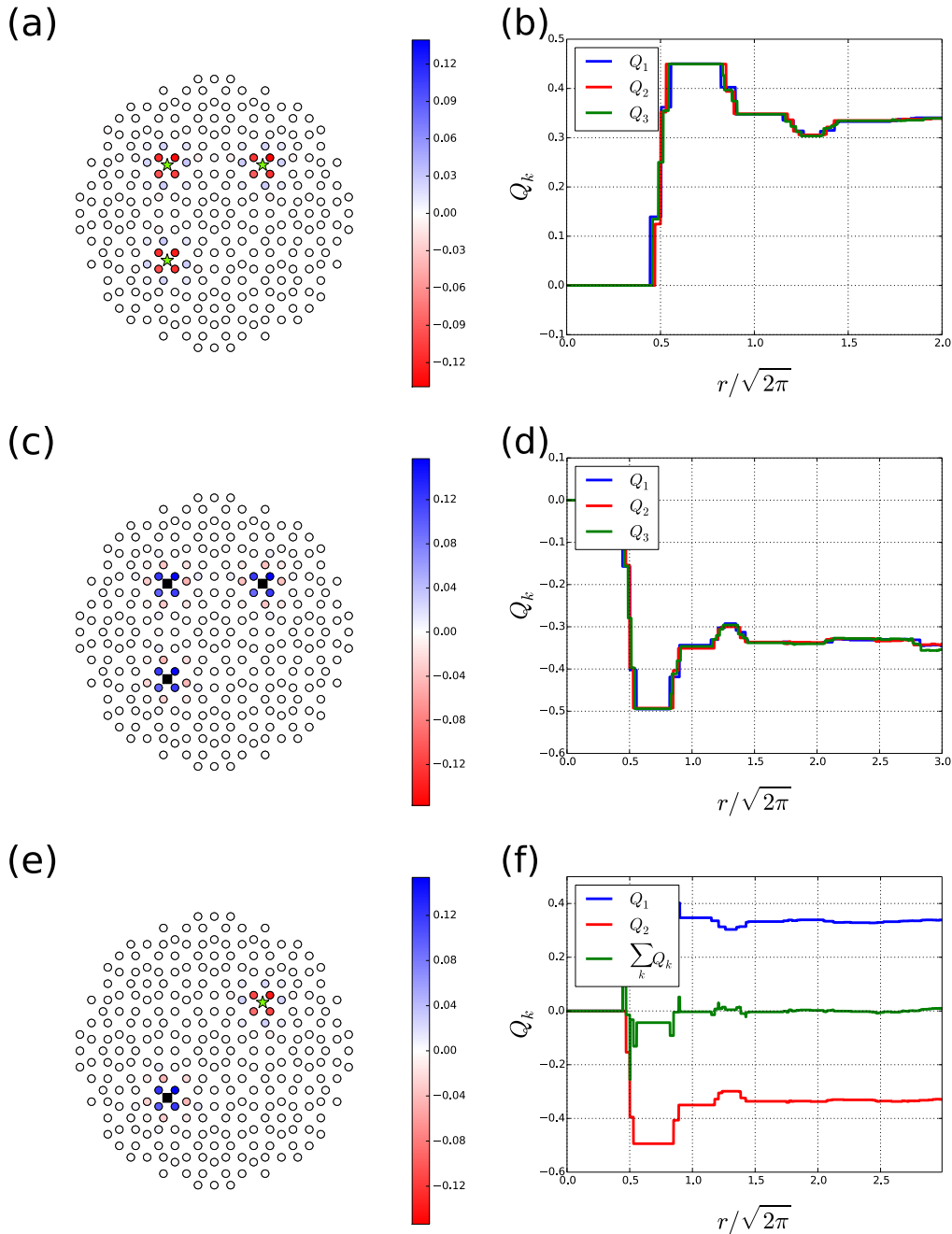


Figure 5.5.: In (a), (c), (e): We denote lattice sites, quasiholes, and quasielectrons by the black circles, the green stars, and the black squares respectively. The density profiles $\rho(z_i)$ from Eq. (5.3), defined as the particle density difference between the states in the presence and in the absence of the anyons in the systems, are plotted with colorbars for the cases of two quasiholes, two quasielectrons, one quasihole-one quasielectron in (a), (c), (e) respectively for the eight-fold rotationally symmetric Ammann-Beenker tiling, where we take the number of lattice sites $N = 273$. We find that the anyons are well-screened with radii of a few lattice constants. In (b), (d), (f): The excess charge distributions Q_k are computed from Eq. (5.5) and are plotted as a function of the radial distances $r/\sqrt{2\pi}$, from the anyon positions, corresponding to the above mentioned anyon configurations. The anyon charges approach $\simeq \pm 0.33$ for large r with an errorbar of size 10^{-4} arising due to the Monte-Carlo simulations.

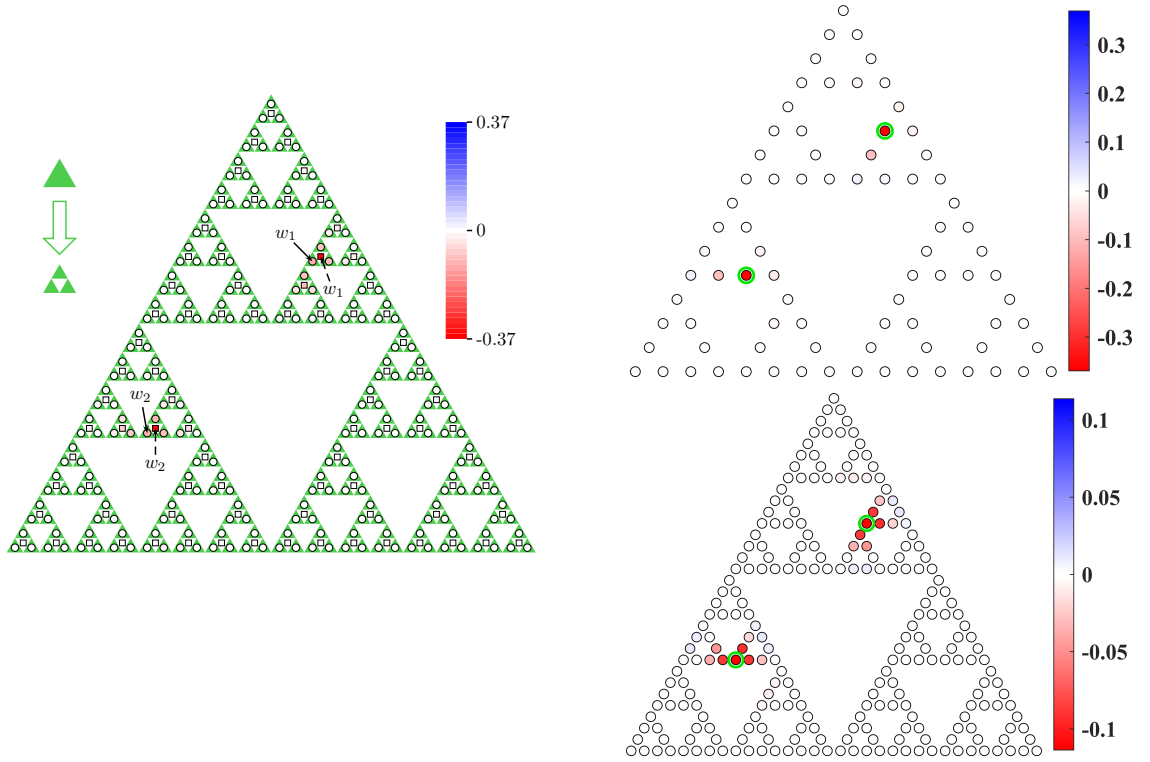


Figure 5.6.: In the left figure the green triangles form a Sierpinski gasket. The operation needed to go from one generation to the next is shown there also. The considered lattice model has one lattice site on each triangle. Generation five and generation four are shown with circles and with squares respectively. The solid and the dashed arrows mark the coordinates w_1 and w_2 for two anyons respectively. We separately show the anyons in the Sierpinski gasket at the 4th generation, as given in the upper right figure, and at the 5th generation, as given in the lower right figure. We picture the lattice sites as the black circles, and we place two anyons on the lattice sites as marked by the green ring. In all the figures we show the density profiles ρ_j of the anyons from Eq. (5.3) with colorbar. The error-bars arising for the Monte-Carlo simulations are small and of the order 10^{-4} . We find that the anyons are well-screened. We keep the particle number and the total flux fixed while going from one generation to the next generation. We note that the particle densities are spread over more lattice sites but the total size of the anyons remain the same.

size of the anyons do not change significantly while going from one generation to the next generation. Also the anyons are small compared to the full fractal and hence the anyon shapes would not be hampered if we replace the finite generation fractal with an infinite generation fractal. When we increase the generation by one, each lattice site splits into three, but if the generation is already high, there will still be at most one particle on the three sites, since the wavefunction is very small if particles are close. The sites therefore effectively act as a single site, and this leads to convergence. It is already visible in the Fig. 5.6 that the size of the anyon is practically the same for generation 4 and 5, and the generation is hence large enough to capture the physics of the infinite generation limit.

We find that the sizes of the anyons depend on the local structures of the lattice sites around the anyons. This is reasonable because the screening is affected by the lattice points which are close to the anyons and where we allow particles to be present. But in all the cases we have well-screened anyons with proper charges.

We point out the reason of not considering quasielectrons in fractal lattices as follows. We note that the fractal lattices are defined in the infinite generations. While going from one generation to the next generation, we keep the particle number and the total flux fixed. In each next generation we have larger number of lattice sites and thereby smaller amount of flux through each lattice site. Therefore in infinite generation, the number of lattice sites becomes infinite while the amount of flux through each lattice site becomes vanishingly small. This situation corresponds to the scenario of approaching the continuum limit where the quasihole converges to a particular shape, as we show here in Fig. 5.6, but the quasielectron approaches a singularity and hence does not converge to a particular shape.

5.3.3 Anyons in other fractal dimensions $0 < \text{dimension} \leq 2$

We have shown that the anyons and the fractional quantum Hall physics can exist in fractional dimension $D \simeq 1.585$. Now we demonstrate that the effects can be seen in any fractal dimension $0 < \text{dimension} \leq 2$. We take the particle number $M = 40$ for all the computations here. We construct a family of fractals to obtain different dimensions as follows.

We start from a square, and we divide it into $L \times L$ squares of equal sizes. We proceed from one generation to the next generation by keeping U number of squares in a particular pattern, and then by repeating the process. Therefore the fractal dimension becomes

$$D = \frac{\ln(U)}{\ln(L)}. \quad (5.7)$$

The particular pattern for a fixed U can be taken as will, and this pattern corresponds to only the structure of the distribution of the lattice sites for a fixed D . We take $L = 4$ and generate fractal lattices of different dimensions by suitably choosing U . We show that the anyons are well-screened and possess the charge $\simeq 0.5$ for all dimensions ranging from 2 to 1 in Figs. 5.7, 5.8, 5.9.

In Fig. 5.10 (a) we place the model on a one dimensional line, and we find that the anyons are not screened. This is expected since this particular model is known to be critical [227]. However, interestingly, in Fig. 5.10 (b) we find that the well-screened anyons and the fractional quantum Hall physics exist in one dimension if we choose the fractal lattice as shown in the last inset in Fig. 5.9. Similarly we take $L = 5$ and $U = 4$, such that the fractal dimension becomes

$$D = \ln(4)/\ln(5) \simeq 0.86, \quad (5.8)$$

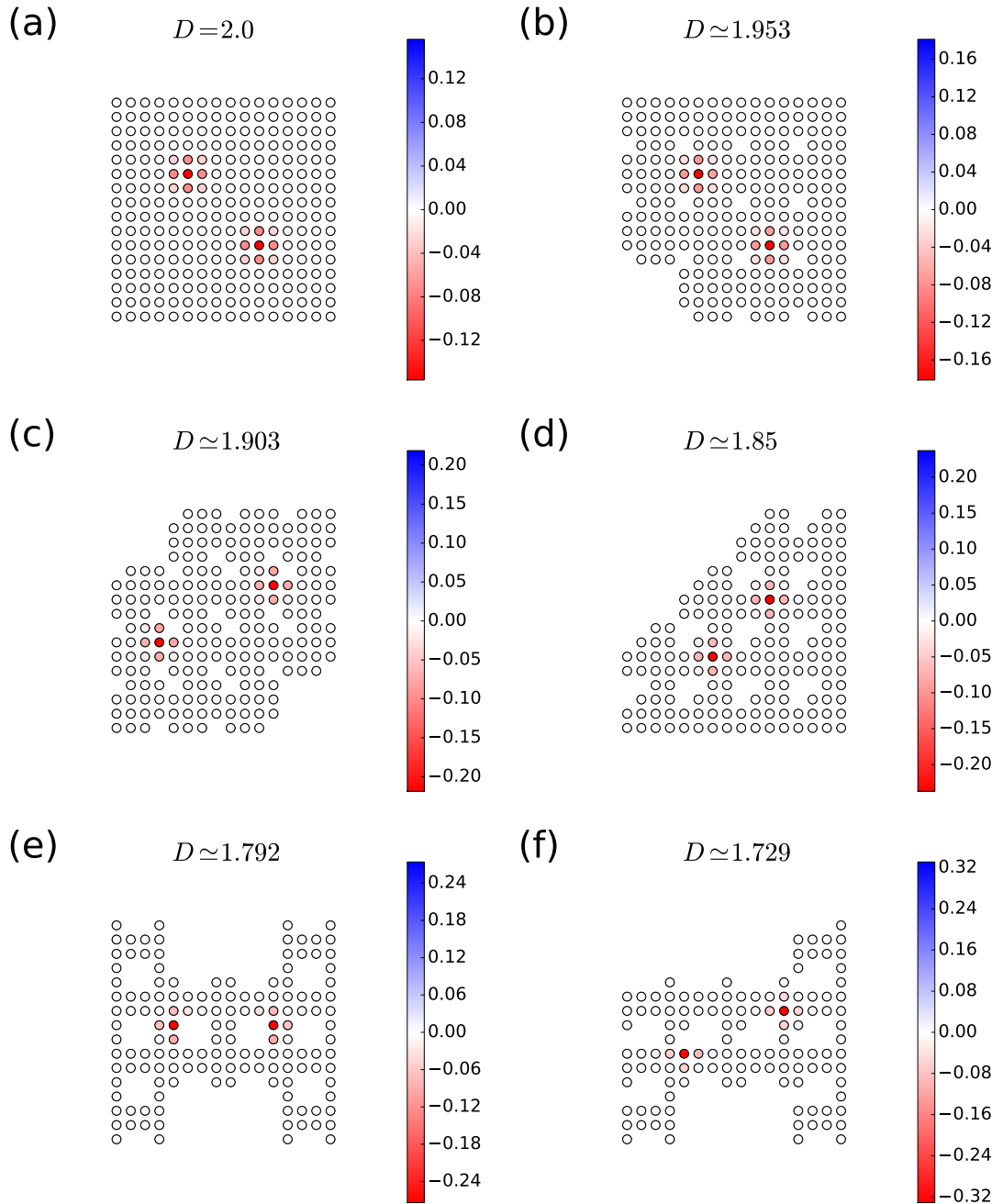


Figure 5.7.: We show anyons on the fractal lattices of different dimensions D . We plot the density profiles ρ_j of the anyons from Eq. (5.3) with colorbar. We generate the fractals by using Eq. (5.7) and by starting from the 0th generations as shown in Fig. 5.9 in the insets. We take the number of lattice sites as 16^2 in (a), as 15^2 in (b), as 14^2 in (c), as 13^2 in (d), as 12^2 in (e), and as 11^2 in (f). We find that the anyons are well-screened in all the cases and the errorbars, coming from the Monte-Carlo simulations, are of the order 10^{-4} . We note the shapes of the anyons depend on the local structure of the fractal lattices.

and we investigate anyons in this model in Fig. 5.10 (c). This shows that well-screened anyons and the fractional quantum Hall physics can be obtained even in dimension less than one.

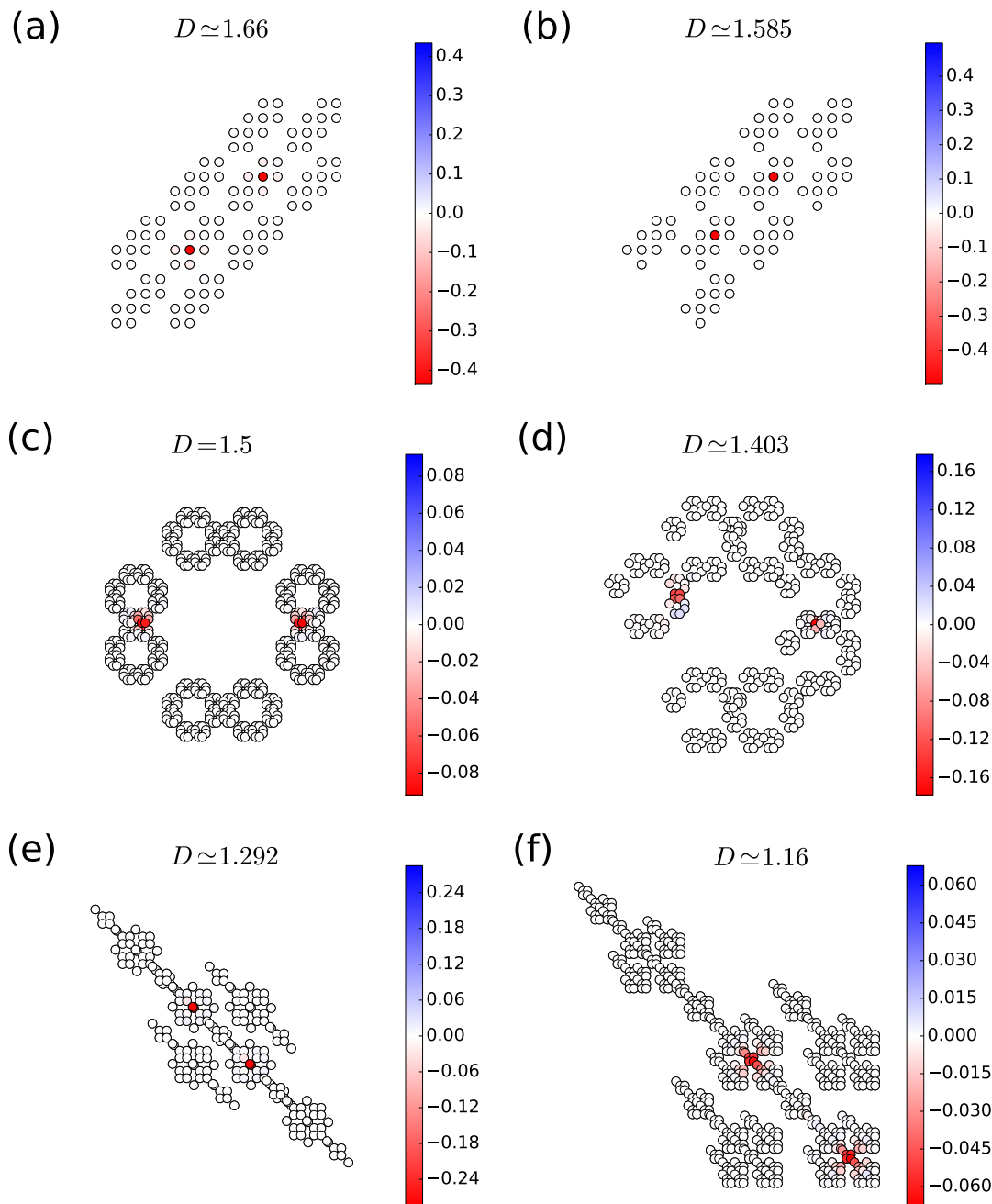


Figure 5.8.: We show anyons on the fractal lattices of different dimensions D . We plot the density profiles ρ_j of the anyons from Eq. (5.3) with colorbar. We generate the fractals by using Eq. (5.7) and by starting from the 0th generations as shown in Fig. 5.9 in the insets. We take the number of lattice sites as 10^2 in (a), as 9^2 in (b), as 8^3 in (c), as 7^3 in (d), as 6^3 in (e), and as 5^4 in (f). We find that the anyons are well-screened in all the cases and the errorbars, coming from the Monte-Carlo simulations, are of the order 10^{-4} . We note the shapes of the anyons depend on the local structure of the fractal lattices.

Our results suggest that the lattice points distributions are more important in having the anyons and the fractional quantum Hall physics rather than the Hausdorff dimensions of the fractal spaces.

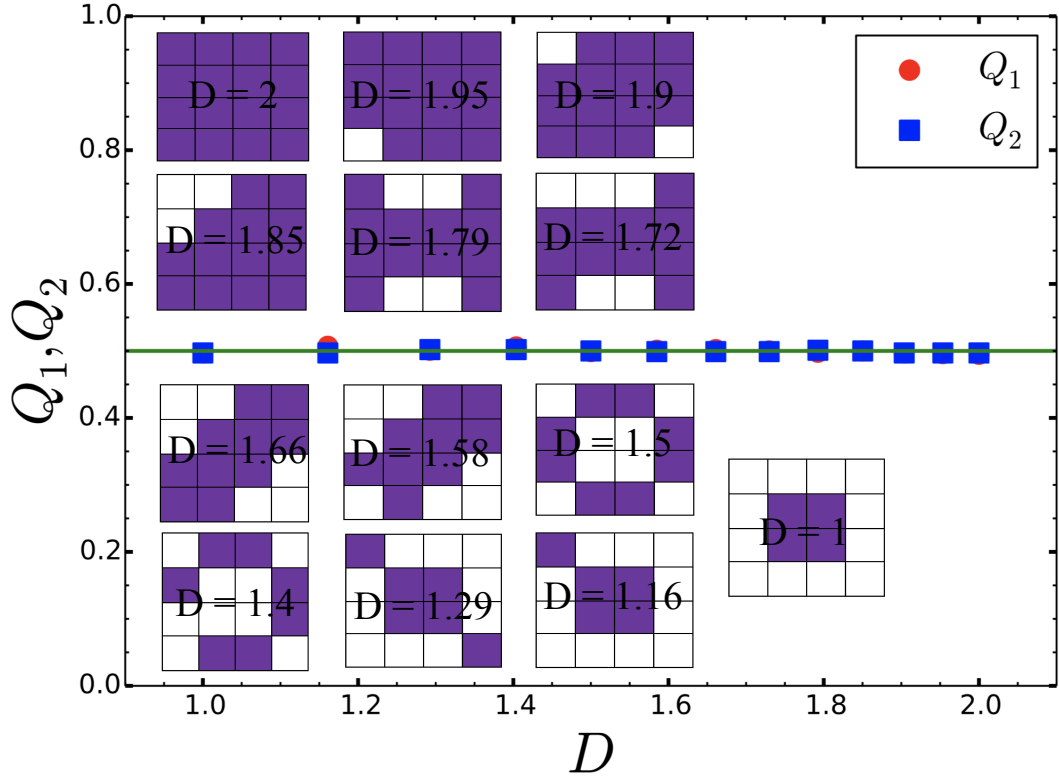


Figure 5.9.: In the insets we divide a square into 16 squares, and keep only the squares in the violet color, and then repeat the process. Thereby we generate the fractals of different dimensions D by using Eq. (5.7). We restrict to the generation 4 for $D < 1.2$, to the generation 3 for $1.2 < D < 1.55$, and to the generation 2 for $D > 1.55$. In the main plot we show the charges of the two anyons as a function of D , where we take the same radius r of the local regions around the anyons. The anyon charges Q_1 and Q_2 are found to be $\simeq 0.5$, as we mark by the green line, for all the fractal dimensions. We find small enough errorbars of the order 10^{-4} arising from the Monte-Carlo simulations. The results show that the anyons and the fractional quantum Hall physics can exist in all the dimensions ranging from 2 to 1.

5.4 Braiding statistics of anyons

Well-screened anyons are the license to obtain fractional braiding statistics. We braid the anyons by moving them in a continuous path. In a two-dimensional plane we do this by placing the anyon at any point. In the fractal lattices we note that even when an anyon is between the lattice sites, the anyon is still only present on the fractal lattice since we allow the particles to reside on the lattice sites only.

We adiabatically circulate one anyon, say the k th anyon, around another anyon, say the j th anyon, along a closed path, say Γ . Therefore the state transforms as

$$|\Psi\rangle \rightarrow \gamma_B |\Psi\rangle, \quad (5.9)$$

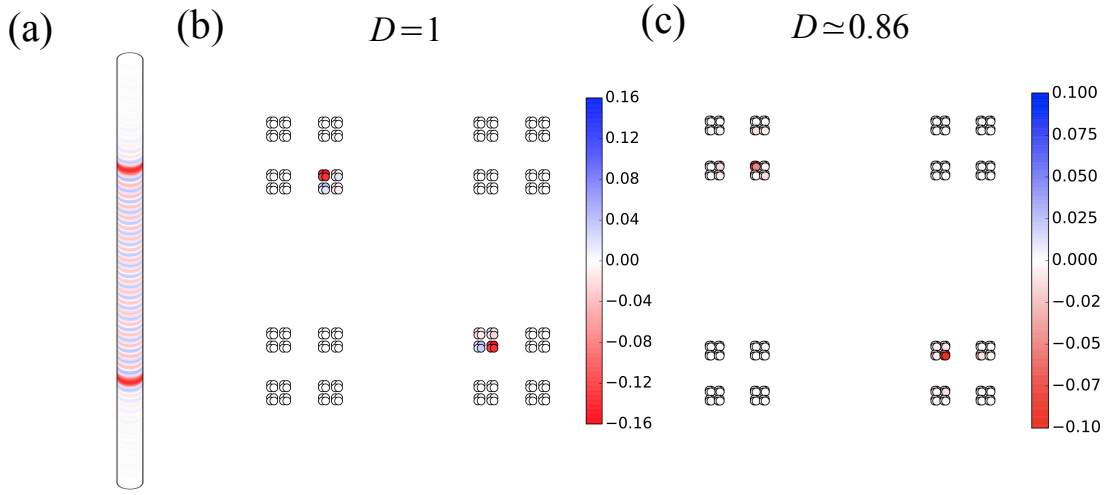


Figure 5.10.: In (a) we place our model on a one-dimensional line. We find that the anyons are not screened. That is no matter how far we put the anyons from one another, they always overlap. In (b) we find, however, that it is possible to have the well-screened anyons and the fractional quantum Hall physics in one dimension if we instead choose to keep 4 squares as shown in the last inset of Fig. 5.9. In (c) we show well-screened anyons in fractal dimension $D \simeq 0.86$. In all the cases we take 4^4 number of lattice sites and plot the anyon density profiles ρ_j from Eq. (5.3) with colorbars. We estimate small errorbars of the order 10^{-4} arising from the Monte-Carlo simulations.

where the Berry phase

$$\gamma_B = e^{i\theta_B} \quad (5.10)$$

is defined as

$$\theta_B = i \oint_{\Gamma} \langle \Psi | \frac{\partial \Psi}{\partial w_k} \rangle dw_k + c.c., \quad (5.11)$$

where c.c. denotes the complex conjugate of the first term. We exploit Eq. (3.46) to write θ_B in Eq. (5.11) as

$$\theta_B = i \frac{p_k}{2} \oint_{\Gamma} \sum_i \frac{\langle n_i \rangle}{w_k - z_i} dw_k + c.c. \quad (5.12)$$

To find the statistics of the anyons the quantity of interest becomes

$$\delta \theta_B = \theta_B^{\text{inside}} - \theta_B^{\text{outside}}, \quad (5.13)$$

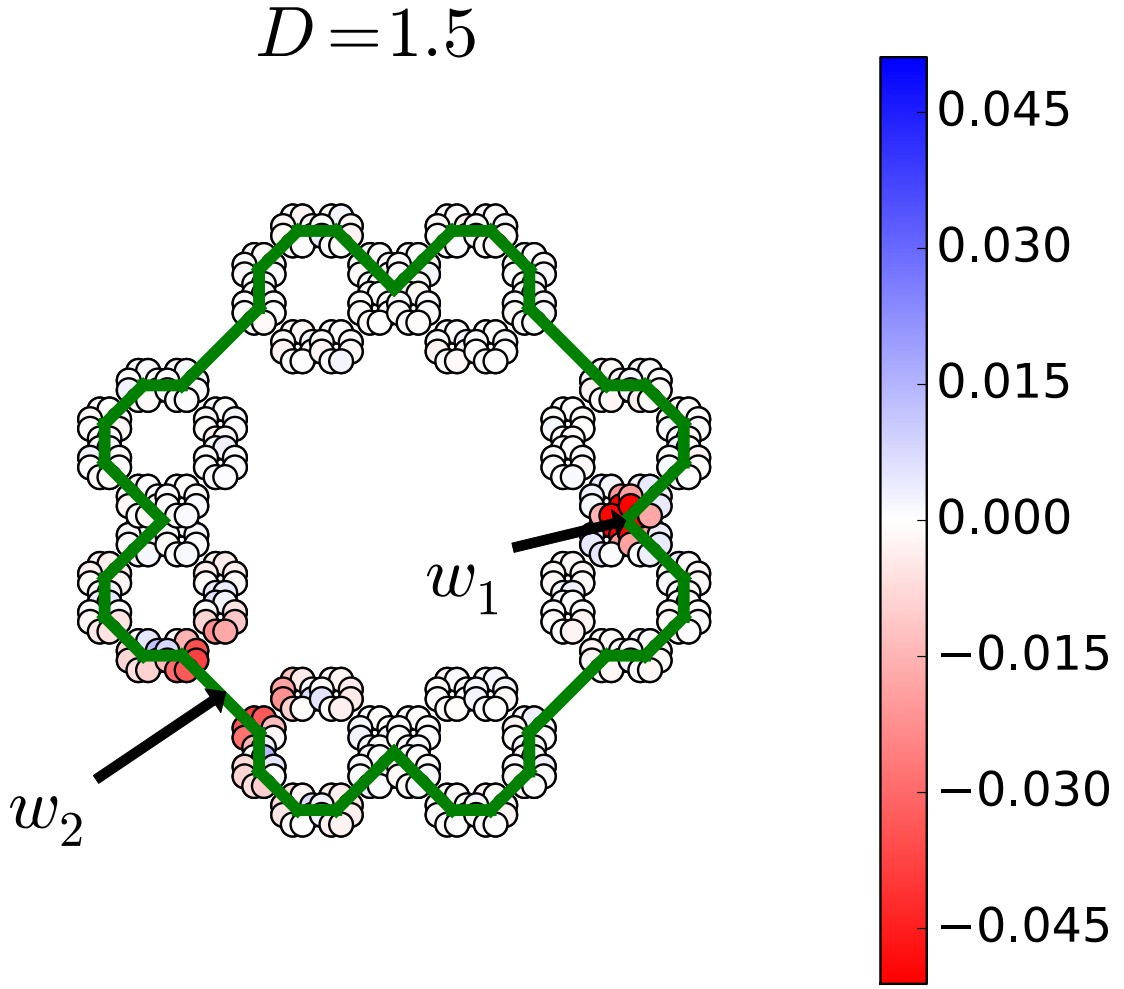


Figure 5.11.: Anyons on fractal of dimension $D = 1.5$. The color of each lattice site gives $\rho(z_j)$ and the positions w_1 and w_2 of the anyons are marked by the arrows. The green line shows the braiding path chosen. The anyons remain screened while placed in different positions along the braiding path. Here, $q = 2$, $M = 40$, and the number of lattice sites is 8^3 .

where θ_B^{inside} and $\theta_B^{\text{outside}}$ are the Berry phases respectively when the j th anyon is inside and is outside the closed path Γ . Therefore we write

$$\delta\theta_B = i\frac{p_k}{2} \oint_{\Gamma} \sum_i \frac{\langle n_i \rangle^{\text{inside}} - \langle n_i \rangle^{\text{outside}}}{w_k - z_i} dw_k + c.c. \quad (5.14)$$

Now the particle densities are only modified locally around the anyon positions and hence the factor

$$\langle n_i \rangle^{\text{inside}} - \langle n_i \rangle^{\text{outside}} \quad (5.15)$$

in Eq. (5.14) is non-zero only around the j th anyon. Therefore we write

$$\begin{aligned}\delta\theta_B &= -2\pi p_k \sum_{i \in \Gamma} \langle n_i \rangle^{\text{inside}} - \langle n_i \rangle^{\text{outside}}, \\ &= 2\pi p_k p_j / q,\end{aligned}\quad (5.16)$$

which is the expected braiding statistics for the two Abelian anyons of charges p_k/q and p_j/q in the lattice Laughlin state.

We explicitly compute the braiding statistics for fractal lattices. We take one choice of the fractal lattice and one choice of the braiding path as shown in Fig. 5.11. We compute the integrals in Eq. (5.14) and find the numerical value $\delta\theta_B/2 = 0.5\pi$ for the exchange statistics, which agrees with the expected value $\pi/2$. Thereby we conclude that the Laughlin type states in the quasicrystals and in the fractal lattices have the desired topological properties.

5.5 Parent Hamiltonians

Till now, we have constructed the analytical states, in the presence and in the absence of the anyons, and have demonstrated that the anyons and the fractional quantum Hall physics exist in the quasicrystals and in the fractal lattices having fractional dimensions. We now use the underlying conformal field theory construction as shown in Chapter-4 in Sec. 4.3 to obtain the parent Hamiltonian for our analytical lattice states by employing the following null field, which can be demonstrated to be the null field by following the method as shown in Appendix-B, as

$$\chi(v) = \oint_v \frac{dz}{2\pi i} \frac{1}{z-v} \left[G^+(z) V_0(v) - qJ(z) V_1(v) \right], \quad (5.17)$$

where we have the following operators as

$$G^+(z) =: e^{i\sqrt{q}\phi(z)} :, V_{n_j}(v) = (-1)^{(j-1)n_j} : e^{i(qn_j-1)\phi(v)/\sqrt{q}} :, J(z) = \frac{i}{\sqrt{q}} \partial_z \phi(z). \quad (5.18)$$

We exploit the method as shown in Appendix-C and construct the following parent Hamiltonian, provided the condition

$$\eta \leq 1 + q/N + \sum_k p_k/N \quad (5.19)$$

is satisfied, as

$$\begin{aligned}H &= \sum_i \sum_{k(\neq i)} \sum_{j(\neq i)} \frac{1}{\bar{z}_i - \bar{z}_k} \frac{1}{z_i - z_j} \left[\bar{T}_k^{-1} T_j^{-1} b_k^\dagger b_j - \bar{T}_k^{-1} T_i^{-1} b_k^\dagger b_i (qn_j - 1) \right. \\ &\quad \left. - \bar{T}_i^{-1} T_j^{-1} (qn_k - 1) b_i^\dagger b_j + |T_i|^{-2} n_i (qn_k - 1) (qn_j - 1) \right]. \quad (5.20)\end{aligned}$$

We have here b_j as the hardcore bosonic or fermionic annihilation operator on the j th lattice site, when q is even or q is odd respectively, and we write

$$n_j = b_j^\dagger b_j \quad (5.21)$$

as the number operator at the j th lattice site, and

$$T_k = e^{i\phi_k} e^{-i\pi(k-1)} \prod_i (w_i - z_k)^{p_i} \prod_j (z_j - z_k)^{1-\eta}. \quad (5.22)$$

Numerically we find that the ground state of H is unique, when we have M number of particles in the system. Braiding is done by varying w_k , which amounts to varying the strengths of the terms in the Hamiltonian.

5.6 Conclusions

In this chapter we have constructed a new type of the fractional quantum Hall models on the quasicrystals and on the fractal lattices. We have shown that the anyons and the fractional quantum Hall physics can exist in the quasicrystals and in the fractal lattices in all dimensions $1 \leq \text{dimension} \leq 2$. We have also shown one example with anyons existing in fractal lattices having dimension less than one. Our investigations have shown that the lattice points distributions are more important in hosting the anyons and in realizing the fractional quantum Hall physics rather than the Hausdorff dimensions of the fractal spaces.

These outcomes are the beginning to explore further studies such as the transport properties and the entanglement properties which strongly depends on the dimensions of the spaces. Besides our constructions provide some hints to build up the fractional Chern insulator type model Hamiltonians, on the quasicrystals and on the fractal lattices, having interactions and complex hoppings resembling the magnetic field. Such kind of models motivate to realize the fractional quantum Hall physics with the ultra-cold atoms in optical lattices.

Also our work strongly motivates the development of additional methods to test for the topology in the geometries, having fractional dimensions and having open surfaces. The outcomes show that we can use our construction to obtain the anyons and the fractional quantum Hall physics on the lattices, to directly probe the topological order, where one can not easily construct a topological flat band, due to the lack of translational symmetry, which invalidates the computation of the many-body Chern number.

Anyonic Quasiparticles of Hardcore Anyons

“ *Not only is the Universe stranger than we think, it is stranger than we can think.* ”

— **Werner Heisenberg**

One of the most well known systems that can deliver anyons [10], having unusual properties such as bespoke fractional charge and exotic braiding statistics, is the fractional quantum Hall system. The lattice versions of the fractional quantum Hall systems are of particular interest due to their potential to be experimentally realized in the field of the ultra-cold atoms in optical lattices. Much work has been done to investigate and classify different types of anyons that can appear in the fermionic or in the bosonic fractional quantum Hall systems.

In this chapter we show that the anyons themselves can give rise to their own anyonic quasiparticles. And the emergent anyons can have different charge and different statistics as compared to the same quantities of the original anyons in the systems. We consider the model systems as the family of the lattice Laughlin states on a plane [169]. The family is described by the Landau level filling factor $1/q$. If q is odd then the family is for the fermions and if q is even then the family is for the bosons. These families are known to support the anyonic quasiparticles. Now we consider the case of q as non-integer and thereby the family is for the anyons. We allow maximum one particle in each lattice site and hence consider a system of the hardcore anyons. Our constructions give rise to different types of the fractional quantum Hall models. We show that the positively charged and the negatively charged anyonic quasiparticles, so called the quasiholes and the quasielectrons respectively, can be created in the systems. We investigate the density profiles, charges and braiding properties of the emergent anyons.

In Sec. 6.1 we introduce the lattice systems of the hardcore anyons, containing the anyonic quasiparticles. We study the density profiles and charges of the emergent anyons in Sec. 6.2 which show that the anyonic quasiparticles are well-screened and possess right charges. In Sec. 6.3 we compute braiding statistics of the anyonic quasiparticles and show that it is different from the statistics of the elementary anyons which constitute the system. We draw the conclusions in Sec. 6.4. This chapter is based on parts of the following Ref. [256]:

[1] : Julia Wildeboer, Aniket Patra, **Sourav Manna** and Anne E. B. Nielsen, "Anyonic quasiparticles of hardcore anyons", *Physical Review B* **102**, 125117 (2020)

6.1 Model of the hardcore anyons

We recall the lattice Laughlin state at the Landau level filling fraction $1/q$ without anyonic quasiparticles on a two-dimensional complex plane from Eq. (3.39) in Chapter-3 in Sec. 3.3 as

$$\Psi(\{z_j\}) = \delta_n \prod_{i<j} (z_i - z_j)^{qn_i n_j} \prod_{i \neq j} (z_i - z_j)^{-\eta n_i}, \quad (6.1)$$

where the condition $\delta_n = 1$ fixes the particle number to

$$M = \frac{\eta N}{q} \quad (6.2)$$

and otherwise $\delta_n = 0$.

We take $n_i \in \{0, 1\}$ as the particle occupation number at the j th lattice site at position z_j . We recast the state as

$$\Psi(\{z_j\}) = \delta_n \prod_{i<j} (Z_i - Z_j)^q \prod_{\{i,j|Z_i \neq z_j\}} (Z_i - z_j)^{-\eta}, \quad (6.3)$$

where $Z_j \in \{z_1, z_2, \dots, z_N\}$ is the position of the j th particle. From this expression, we observe that the state acquires a phase factor $e^{2\pi i q}$ if one particle is circulated in the counter-clockwise fashion around another particle. Therefore, the state describes the fermions if q is odd, describes the hardcore bosons if q is even, and describes the hardcore anyons if q is non-integer.

6.2 Anyon density profiles and charges

We define the particle density of the i th lattice site for any state $|\Phi\rangle$ as

$$\langle n(z_i) \rangle = \langle \Phi | n(z_i) | \Phi \rangle. \quad (6.4)$$

Therefore we write the anyon density profiles as

$$\rho(z_i) = \langle n(z_i) \rangle_{Q \neq 0} - \langle n(z_i) \rangle_{Q=0}, \quad (6.5)$$

where $n(z_i)$ is the particle occupation number at the i th lattice site. We define

$$\langle n(z_i) \rangle_{Q \neq 0} \text{ and } \langle n(z_i) \rangle_{Q=0} \quad (6.6)$$

respectively as the particle density at the i th lattice site in the presence of Q anyons in the systems and at the i th lattice site without any anyon inserted in the systems.

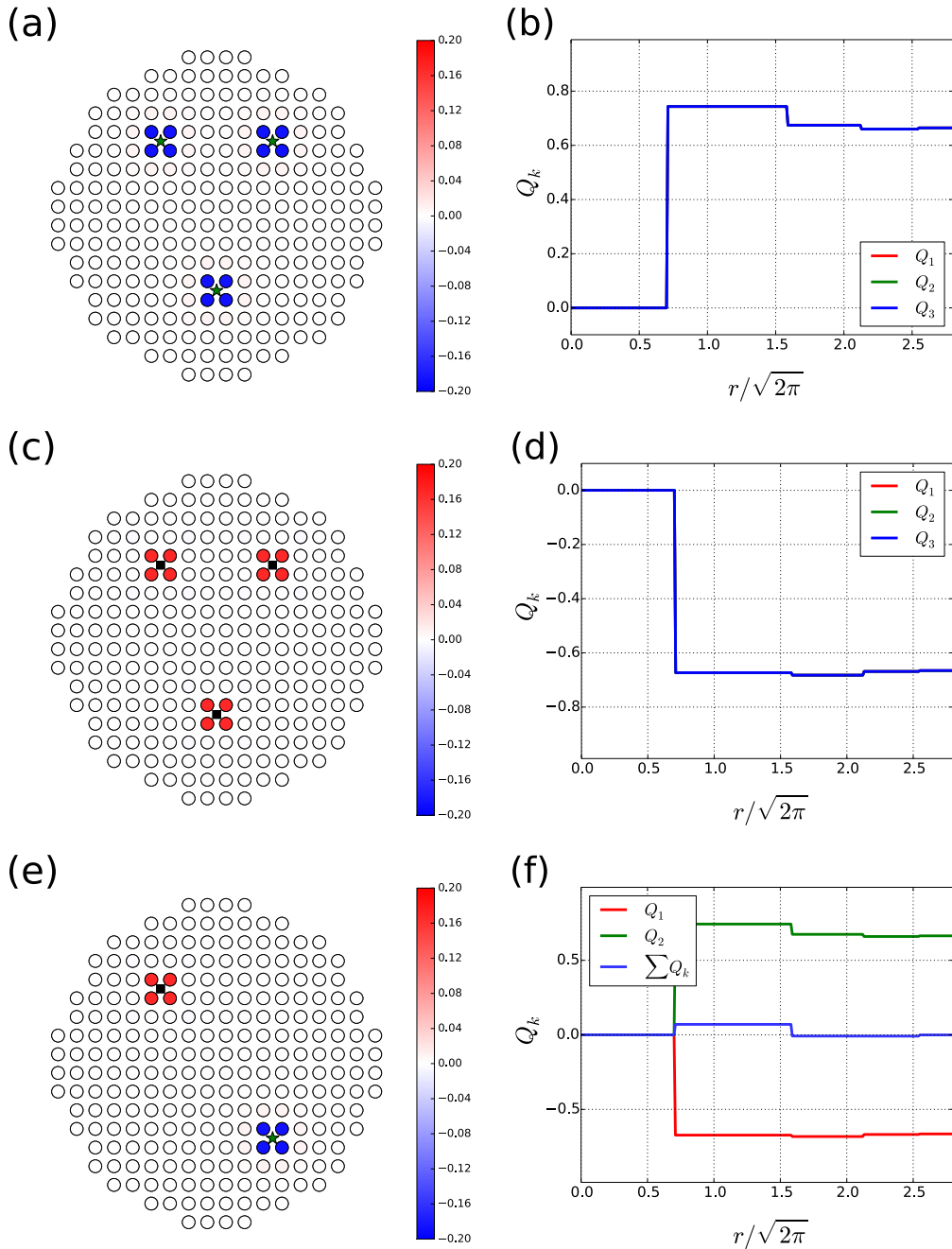


Figure 6.1.: In (a), (c), (e): The black circles, the green stars, and the black squares represent the lattice sites, the quasiholes, and the quasielectrons respectively. The number of lattice sites is fixed to $N = 240$ and we take $\eta = 1$. The density profiles $\rho(z_i)$ from Eq. (6.5), defined as the difference in the expectation value of the number of particles on the i th lattice site in the presence and in the absence of the anyons in the systems, are plotted with colorbars for the cases of three quasiholes, three quasielectrons, one quasihole-one quasielectron for $q = 3/2$ in (a), (c), (e) respectively. We show that the anyons are well-screened with a radii of a few lattice constants. In (b), (d), (f): The excess charge distributions from Eq. (6.7) are computed by summing over the density distribution of the anyons over the lattice sites in a small region around each anyon and are plotted as a function of the radial distances $r/\sqrt{2\pi}$ from the anyon positions corresponding to the above mentioned anyon configurations. We note that the anyon charges approach the values $\simeq \pm 2/3$. Also, the density profiles are very similar for the quasiholes and the quasielectrons except for the sign as evident from the plot of $\sum Q_k$ in (f).

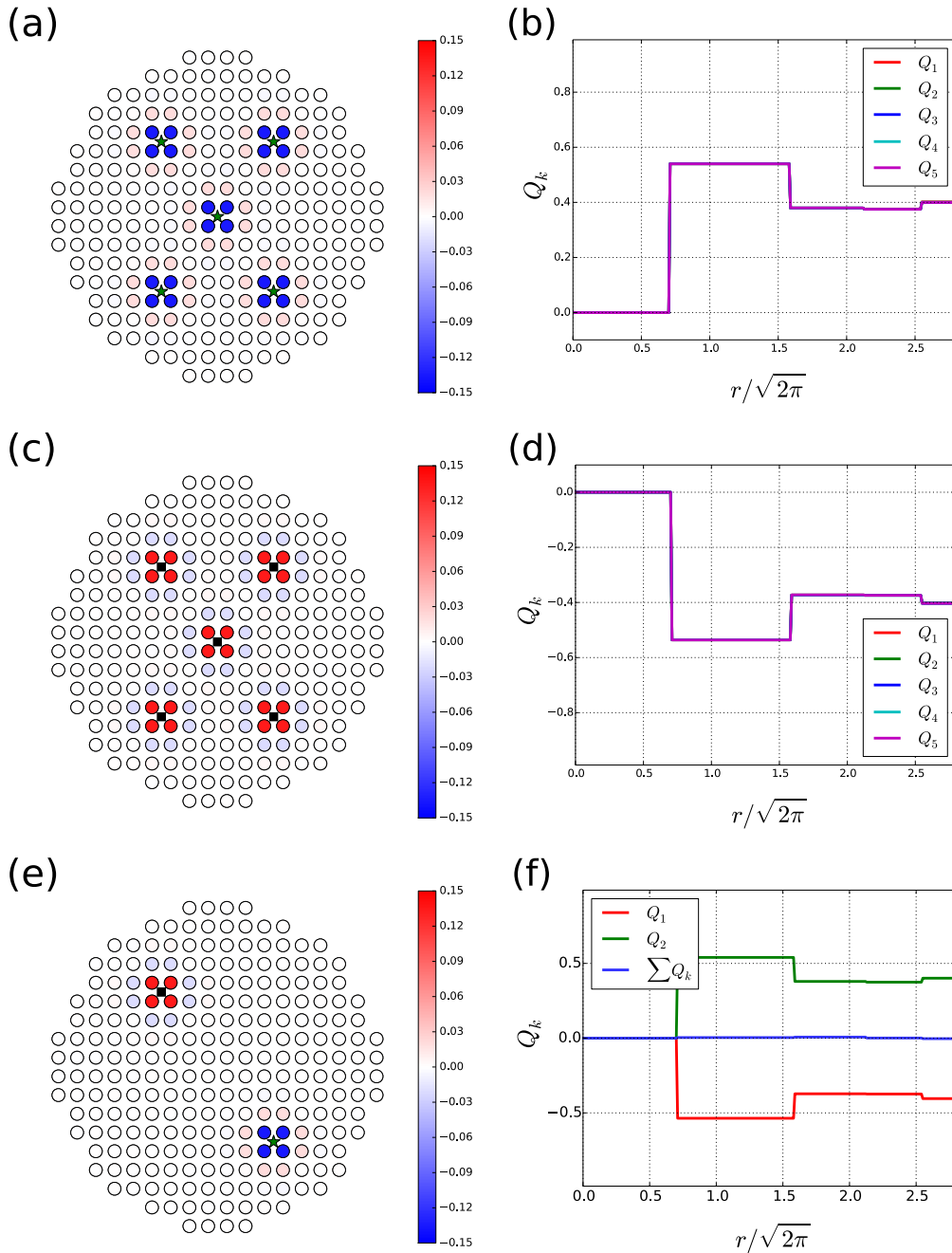


Figure 6.2.: In (a), (c), (e): The black circles, the green stars, and the black squares represent the lattice sites, the quasipoles, and the quasielectrons respectively. The number of lattice sites is fixed to $N = 240$ and we take $\eta = 1$. The density profiles $\rho(z_i)$ from Eq. (6.5), defined as the difference in the expectation value of the number of particles on the i th lattice site in the presence and in the absence of the anyons in the systems, are plotted with colorbars for the cases of five quasipoles, five quasielectrons, one quasipole-one quasielectron for $q = 5/2$ in (a), (c), (e) respectively. We show that the anyons are well-screened with a radii of a few lattice constants. In (b), (d), (f): The excess charge distributions from Eq. (6.7) are computed by summing over the density distribution of the anyons over the lattice sites in a small region around each anyon and are plotted as a function of the radial distances $r/\sqrt{2\pi}$ from the anyon positions corresponding to the above mentioned anyon configurations. We note that the anyon charges approach the values $\simeq \pm 2/5$. Also, the density profiles are very similar for the quasipoles and the quasielectrons except for the sign as evident from the plot of $\sum Q_k$ in (f).

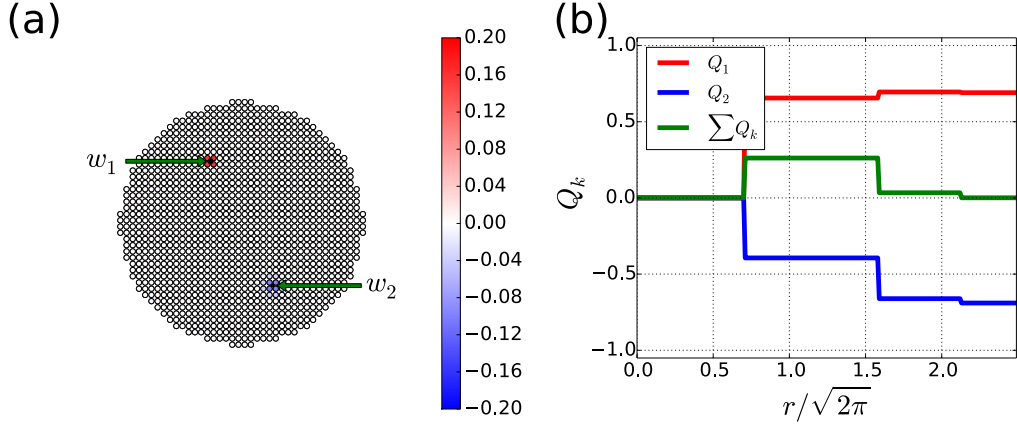


Figure 6.3.: (a) The particle density difference $\rho(z_i)$ and (b) the excess particle numbers Q_k , as well as $\sum Q_k$, as a function of the radial distance from the anyon positions for $q = 3/2$, $\eta = 30/151$, and $N = 1208$. In (a), the circles represent the lattice sites. The square at w_1 and the star at w_2 denote a quasielectron and a quasihole, respectively. The system has $\eta N/q = 160$ particles. The plots show that the anyons are screened.

We take the standard particle charge as -1 and write the excess charge of the k th anyon, described as the sum of minus the density profile $\rho(z_i)$ over a circular region of radius r around the anyon, as

$$Q_k(w_k) = -\sum_i \rho(z_i) \text{ with } |z_i - w_k| \leq r, \quad (6.7)$$

where $k \in \{1, 2, \dots, Q\}$ and $\rho(z_i)$ is defined in Eq. (6.5). The charge Q of the anyon is the value that the excess charge converges to for large r when the region is far from the edge and far from other anyons in the system.

We recall the lattice Laughlin state with anyons from Eq. (3.46) in Chapter-3 in Sec. 3.3 where the anyon charge is given as p_k/q with $p_k = \pm 1$. We take the specific choices for q as $q = 3/2$ and $q = 5/2$. We present the results in Fig. 6.1 and in Fig. 6.2. We show the anyon density profiles in Fig. 6.1 (a), (c), (e) for the systems with three quasiholes, three quasielectrons, one quasihole-one quasielectron for $q = 3/2$ respectively and in Fig. 6.2 (a), (c), (e) for the systems with five quasiholes, five quasielectrons, one quasihole-one quasielectron for $q = 5/2$ respectively.

We find that the anyons are well-screened with a radii of a few lattice constants. The excess charge distributions of the anyons are plotted as a function of the radial distances from the anyon positions as shown in Fig. 6.1 (b), (d), (f) for $q = 3/2$, where we note the anyon charges to approach the values $\simeq \pm 2/3$, and in Fig. 6.2 (b), (d), (f) for $q = 5/2$, where we note the anyon charges to approach the values $\simeq \pm 2/5$. Also, the density profiles are very similar for the quasiholes and the quasielectrons except for the sign as evident from the plot of $\sum Q_k$, defined as the sum of quasihole and quasielectron excess charge distributions, in Fig. 6.1 (f) and in Fig. 6.2 (f).

In Fig. 6.3, we show the particle density difference for the combination of quasihole and quasielectron, when we are much closer to the continuum limit. We take $q = 3/2$,

$\eta = 30/151$, and $N = 1208$. Also in this case we observe screening. This property is retained for even smaller values of η . Proceeding this way, one can obtain a consistent continuum limit for the quasihole. However, such a limit generally does not exist for the quasielectron.

6.3 Braiding statistics of anyons

We determine the result of braiding the anyon coordinate w_k around the anyon coordinate w_j in the counter-clockwise manner. The Berry phase $e^{i\theta_k}$ acquired by the state when w_k is circulated along the closed path c is

$$\begin{aligned}\theta_k &= i \oint_c \langle \Psi | \frac{\partial \Psi}{\partial w_k} \rangle dw_k + \text{c.c.} \\ &= i \frac{p_k}{2} \oint_c \sum_i \frac{\langle \Psi | n_i | \Psi \rangle}{w_k - z_i} dw_k + \text{c.c.},\end{aligned}\quad (6.8)$$

where c.c. denotes the complex conjugate of the first term.

We are interested in the statistical phase of the anyons and therefore in the quantity

$$\Delta\theta_k = \theta_{k,\text{in}} - \theta_{k,\text{out}},\quad (6.9)$$

where $\theta_{k,\text{in}}$ and $\theta_{k,\text{out}}$ are the Berry phases when w_j is well-inside and is well-outside the closed path c respectively. We have

$$\Delta\theta_k = i \frac{p_k}{2} \oint_c \sum_i \frac{\langle n_i \rangle_{\text{in}} - \langle n_i \rangle_{\text{out}}}{w_k - z_i} dw_k + \text{c.c.}\quad (6.10)$$

Since the anyons are well-screened, therefore the particle densities are only modified around the vicinity of the anyon positions. Hence we can take

$$\langle n_i \rangle_{\text{in}} - \langle n_i \rangle_{\text{out}}\quad (6.11)$$

outside the integral, which leads to

$$\Delta\theta_k = -2\pi p_k \sum_{i \text{ inside } c} (\langle n_i \rangle_{\text{in}} - \langle n_i \rangle_{\text{out}}).\quad (6.12)$$

The sum is precisely minus the charge of the anyon at position w_j , and thereby it follows that

$$\Delta\theta_k = 2\pi p_k p_j / q.\quad (6.13)$$

This is the same result as the Berry phase for the lattice Laughlin states, except that q is now a non-integer.

6.4 Conclusions

In this chapter we have found that the systems of hardcore anyons can support the formation of the anyonic quasiparticles, and the charge and braiding properties of the emergent anyons can differ from the same properties of the original anyons, which constitute the systems.

We have shown that the lattice Laughlin states with non-integer q provide the models of hardcore anyons, where the above mentioned phenomena occur. We have found that braiding one of the original anyons around another anyon gives a phase factor $e^{2\pi i q}$ on the state, while braiding one of the emergent anyons of charge p_k/q around another emergent anyon of charge p_j/q , where p_k and p_j are integers, gives a phase factor $e^{2\pi i p_k p_j / q}$ on the state if there is screening of the anyonic quasiparticles in the systems. We have shown numerically that the anyonic quasiparticles are well-screened for $q = 3/2$ and for $q = 5/2$.

The work motivates several further investigations. In particular, it would be interesting to see which types of anyons can be hosted by the systems of non-Abelian anyons. It would also be interesting to look for the possible physical implementations and to investigate which types of quantum gates can be constructed by using such systems. Another interesting future investigation could involve the question if the entanglement properties can be extracted from the hardcore anyonic states and if the parent Hamiltonians exist for which the analytical states with hardcore anyons are the exact ground states.

Quasiparticles Detect Topological Quantum Phase Transitions

” *We appear to live in the best of all possible worlds, where the computable functions make life predictable enough to be survivable, while the noncomputable functions make life (and mathematical truth) unpredictable enough to remain interesting, no matter how far computers continue to advance.*

— **Gottfried Wilhelm von Leibniz**

Phases and phase transitions provide an important framework to probe the physics of strongly correlated quantum many-body systems. Describing physical systems in terms of phases allows us to eye on key properties without going into the full set of microscopic details. Quantum phase transitions take place at zero temperature and are driven by the quantum fluctuations, which are rooted in the Heisenberg uncertainty principle. These phase transitions occur when a control parameter, such as the pressure or the magnetic field strength [198, 209], is varied and imply the non-analytic behavior of the ground state energy as a function of the control parameter. Quantum phase transition can be characterized by a local order parameter, which arises from the broken symmetry of the system, in the conventionally ordered phases. And often the choice of the order parameter is obvious, for example the total magnetization can be used in the ferromagnetic-paramagnetic phase transitions. The Landau-Ginzburg theory of the quantum fluctuations of order parameter was developed to describe such symmetry breaking phase transitions. However the notion of detecting phase transitions by using the local order parameters breaks down for the case of the topologically ordered systems [251]. Different topologically ordered phases can exhibit the same symmetry and therefore such phases can not be distinguished by using the symmetry breaking analysis. These phases of matter are characterized by the long-range entanglement and go beyond the painting of the Landau-Ginzburg theory, and thereby become particularly challenging to investigate. These incompressible phases can not be described by the local order parameters, rather they are characterized by the global order parameters instead. Therefore different kinds of probes are required to distinguish the topologically ordered phases and thereby to detect the topological quantum phase transitions. Strongly correlated quantum many-body systems complicate the scenario further, since the needed numerical computations are generally demanding. For example the density matrix renormalization group calculations

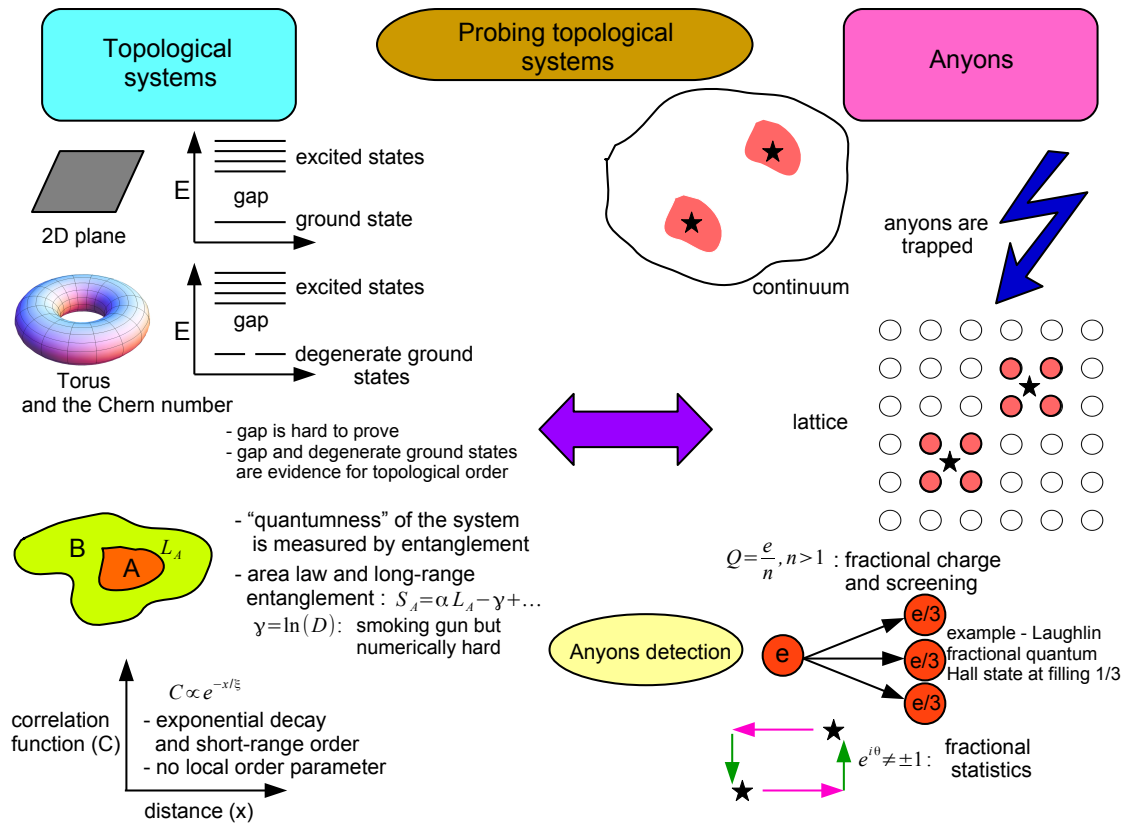


Figure 7.1.: Topologically ordered systems have an energy gap above the ground state, and have the ground state degeneracy that depends on the non-trivial topology of the surface, such as the torus, on which the system is defined. The entanglement entropy S_A of a subsystem A typically follows an area law $S_A = \alpha L_A - \gamma + \dots$, where \dots represents the sub-leading terms which vanish in the thermodynamic limit, α is a non-universal constant, L_A is the boundary length of A , and γ is called the topological entanglement entropy which defines the long-range entanglement of the system. Another probe for the topological order is the many-body Chern number on the torus. Topologically ordered systems have short-range order and therefore the correlation function decays exponentially. Topologically ordered systems can host the anyonic quasiparticles, which have non-trivial fractional braiding properties and fractional charges. The theme of the present chapter is that one can detect the topological quantum phase transitions by creating the quasiparticles in the systems and by investigating their properties.

are usually restricted for the one-dimensional systems or for the quasi two-dimensional systems, such as the thin cylinders or the ladders [76]. Many systems, that may harbor topologically ordered phases, are afflicted with the so called "sign problem" and thereby excluding the investigations by the large-scale quantum Monte-Carlo simulations [257].

Some probes have been developed to probe the topological quantum phase transitions. Examples include the ground state degeneracy [250], the topological entanglement entropy [112, 128, 143], the many-body Chern number [210, 217, 176, 137], the spectral flow [167, 193, 98], and the entanglement spectrum [193, 219, 94, 212, 268, 144]. We show

an overview of the different probes in Fig. 7.1. However these probes are generally expensive to compute, often rely on the particular choices of the boundary conditions, and typically do not provide the complete information. Therefore there is a strong demand in developing new probes to detect the topological quantum phase transitions.

In this chapter we demonstrate that the quasiparticles are a powerful tool in detecting the topological quantum phase transitions. We know that the topologically ordered systems can host anyons, which are neither fermions nor bosons. This can be revealed from the fractional braiding statistics of the anyons. Additionally the anyons have fractional charges. Therefore a direct way to show that a system is topologically ordered, is to generate the anyons in the system and to demonstrate their properties. Both anyonic braiding properties and fractional charge have been confirmed in numerical studies [11, 31, 262, 156, 153]. Here, we propose to use quasiparticles to detect phase transitions that happen when a parameter in the Hamiltonian is varied. We commence by modifying the Hamiltonian to trap the quasiparticles at well-defined positions in the ground state. In the simplest case we can do this by adding a potential. Then we study the quasiparticle properties as a function of the parameter. When the two phases do not support the same set of quasiparticles, a change is seen at the phase transition point. The procedure works for all types of topological orders, and hence for all types of anyons. And the method does not require a particular choice of the boundary conditions.

We test the method on five concrete examples. In Sec. 7.1 we consider a lattice Moore-Read fractional quantum Hall state on a square lattice and in Sec. 7.2 on a fractal lattice, which undergoes a topological quantum phase transition as a function of the lattice filling factor. We show that the anyon charges detect the topological quantum phase transition. In Sec. 7.3, we investigate an interacting Hofstadter model in the absence and in Sec. 7.4 in the presence of disorder. The model in the absence of disorder has a Laughlin type ground state which also undergoes a topological quantum phase transition as a function of the lattice filling factor. We modify the Hamiltonian and create the anyons in the ground state. We find that the anyon charges detect the topological quantum phase transition. In Sec. 7.5, we study the Kitaev's toric code model, which undergoes a topological quantum phase transition when a sufficiently strong magnetic field is added. We create the anyons in the ground state and show that the anyons dictate the topological quantum phase transition. Among these models, we have included two, for which the phase transition point is already known, since this allows us to compare with other methods and check the reliability of the anyon approach. For all the five rather different examples, we find that it is sufficient to compute a relatively simple property, such as the charge of the anyons, to determine the phase transition point. This means that the method is numerically cheap.

For the Moore-Read model on a square lattice, as for example, a large speed up is found compared to previous computations of the topological entanglement entropy, and this enables us to determine the transition point much more accurately. For the interacting Hofstadter model, we only need two exact diagonalizations for each data point, which is much less than what is needed to compute the many-body Chern number. Finally, for the model on the fractal, we do not know of other methods that could be used for detecting the phase transition.

We conclude the chapter in Sec. 7.6. This chapter is based on parts of the following Ref. [155]:

[1] : **Sourav Manna**, N. S. Srivatsa, Julia Wildeboer and Anne E. B. Nielsen, "Quasiparticles as detector of quantum phase transitions", [submitted to Physical Review Research (Rapid Com.)], arXiv:1909.02046 (2019)

7.1 Detection of a topological quantum phase transition in a Moore-Read state on a square lattice

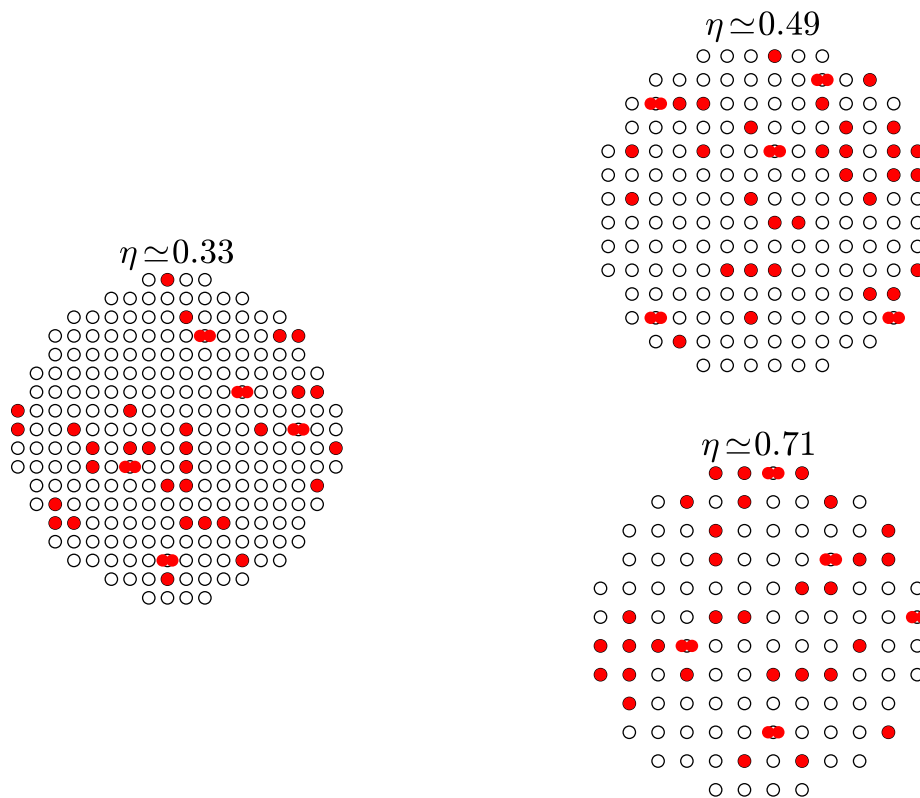


Figure 7.2.: For the computations in this section, we use square lattices with a roughly circular edge. The lattice sites are shown as black circles, and the particles are shown as red disks. There can be either 0, 1, or 2 particles on each site. The total number of particles M , the number of lattice sites N , the flux per lattice site η , and the number of flux units per particle q fulfil the relation $q = \eta N / M$. The phase transition is encountered as a function of η for fixed ηN and fixed M . In other words, we increase η by reducing the number of lattice sites as shown, while keeping the number of particles M and the total magnetic flux ηN fixed. We here take $q = 2$ and $M = 40$.

We introduced the family of the lattice Moore-Read states on a two-dimensional complex plane in Chapter-3 in Sec. 3.3. In this section we investigate a particular member of that family. The properties of the state can be investigated by using the Monte-Carlo

simulations. Earlier studies in Ref. [69] revealed, by computations of the topological entanglement entropy γ , that this state undergoes a topological quantum phase transition as a function of the lattice filling factor η . The transition point was found to be between a lattice filling factor of $1/8$ and $1/2$. Here we show that the topological quantum phase transition point can be obtained based on the computations of the quasiparticle charges in the system. Numerically our computation is significantly cheaper than the γ computation, which involves the calculations of the entanglement properties. These are done by using the replica trick, which needs to consider two copies of the system. And therefore the simulated system carries twice as many particles and twice as many lattice sites as the physical system. On the other hand no doubling is needed to compute the quasiparticle charges. In fact, for many systems, it is only possible to compute the topological entanglement entropy for a range of system sizes that are too small to allow for an extrapolation to the thermodynamic limit. For the system considered here, the simplifications mean that we can obtain results for many more lattice fillings and thereby determine the phase transition point more accurately than in Ref. [69].

For the computations in this section we would like to vary the lattice filling factor $M/N = \eta/q$, without changing the number of flux units per particle. This can be done by varying η and N , while keeping the total flux ηN and the number of particles M fixed as illustrated in Fig. 7.2.

7.1.1 Topological properties

It was shown in Ref. [69] that the particular member of the lattice Moore-Read family at the Landau level filling factor $5/2$, as defined by $q = 2$ and $n_j \in \{0, 1, 2\}$, undergoes a topological quantum phase transition while changing η . In the topological phase, the finite value of the topological entanglement entropy γ is related to the total quantum dimension \mathcal{D} of the anyons in the system as [278]

$$\gamma = \ln \mathcal{D}, \text{ where } \mathcal{D} = \sqrt{\sum_i d_i^2}, \quad (7.1)$$

and d_i is the quantum dimension of the i th anyon. For the Moore-Read family of states we have

$$\mathcal{D} = \sqrt{4q}. \quad (7.2)$$

It was shown in Ref. [69] that for $\eta = 1/4$ the value of γ is close to $\frac{1}{2} \ln(8)$, which indicates that the system is in the topological phase which is the same as the continuum Moore-Read state, and for $\eta = 1$ the value of $\gamma \simeq 0$ which defines the non-topological phase. This shows that there is a phase transition in the interval $\eta \in \{1/4, 1\}$ and η serves as a parameter that drives the system back and forth between a topological and a non-topological phase. The analytical forms of the states in the absence of the anyons, in the presence of the Abelian type anyons, and in the presence of the two non-Abelian type anyons in the systems are given in Eqs. (3.51), (3.59) and (3.68) respectively. Following the procedure as shown in Chapter-4 in Sec. 4.2 and in Chapter-5 in Sec. 5.4 we find that

both types of anyons have the right braiding statistics in the topological phase. We have done this computation for one value of $\eta = 1/3$. We show below that the anyon charges are sufficient to detect the topological quantum phase transition.

7.1.2 Excess charges and the topological quantum phase transition detection

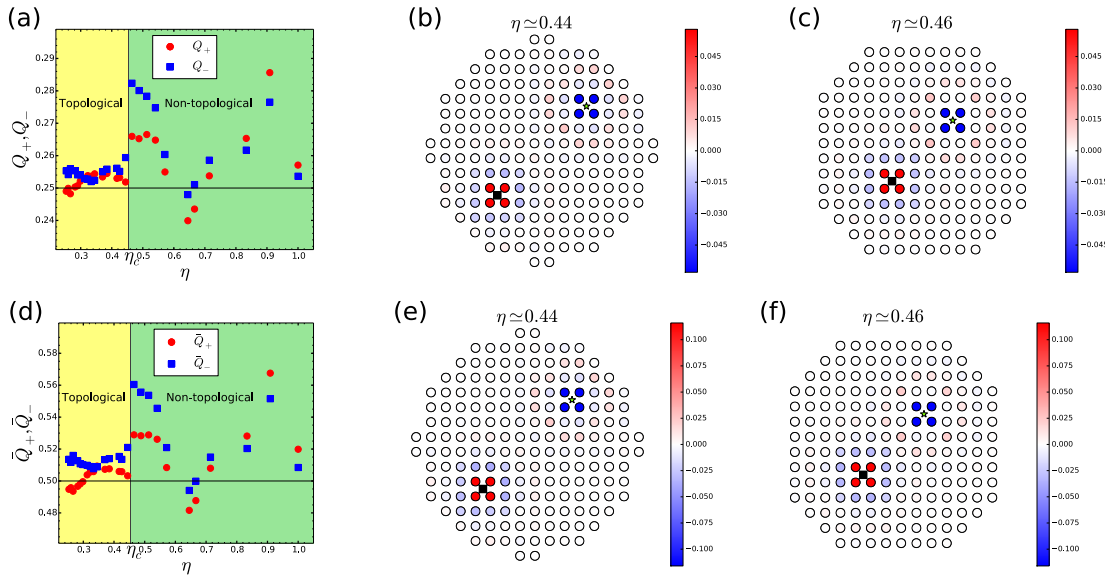


Figure 7.3.: In (a) we plot the absolute value of the excess charge Q_+ , as denoted by the red circles, around w_1 which is the position of one non-Abelian quasiparticle and the absolute value of the excess charge Q_- , as denoted by the blue squares, around w_2 which is the position of another non-Abelian quasiparticle for the Moore-Read state as a function of the flux per site η . In the topological phase, w_1 and w_2 are the centers of the anyons, and Q_+ and Q_- are close to the absolute value of the charge of the anyons, which is marked by the horizontal line at $1/4$. In the non-topological phase, Q_+ and Q_- may take any value. The plot shows a jump away from the horizontal line when going from $\eta \simeq 0.44$ to $\eta \simeq 0.46$, so the data predict that the phase transition point η_c is in the interval $\eta_c \in [0.44, 0.46]$. We shade the topological region $\eta < \eta_c$ with yellow color and the non-topological region $\eta > \eta_c$ with green color. To test the robustness of the method, we do a similar computation for the Moore-Read state hosting Abelian quasiparticles in (d), and this leads to the same transition point and in this case the absolute value of the anyon charge is $1/2$. In (b), (c), (e), and (f), the coloring shows the density profiles below, where $\eta \simeq 0.44$, and above, where $\eta \simeq 0.46$, the transition point. The lattice sites are shown as the black circles, the point w_1 is marked by a green star, and the point w_2 is marked by a black square. The plots in (b) and (c) are for the Moore-Read state hosting non-Abelian quasiparticles, and the plots in (e) and (f) are for the Moore-Read state hosting Abelian quasiparticles. The errorbars arising from the Monte-Carlo simulations are of order 10^{-4} .

When the system is in the topological phase, the density of particles is constant in the bulk. By density of particles, we mean $\langle n(z_i) \rangle = \langle \Phi | n_i | \Phi \rangle$, where $|\Phi\rangle$ is the state of the system. If anyons are present in the system, the density will differ from the bulk value in a small region around each anyon. The number of particles missing on average in this region compared to the bulk value is equal to the charge of the anyon, that is $\pm 1/2$ for the Abelian anyons and $\pm 1/4$ for the non-Abelian anyons. In the non-topological phase, a more complicated density pattern can arise, and in general there is no rule for how much charge there should be within a given region. This suggests that we may be able to see the phase transition by computing how many particles are missing on average within a circular region of radius R around each w_k , where R is large compared to the size of an anyon at position w_k , but small enough that other anyons are not inside the circle and small compared to the smallest distance to the edge. The expectation is that the number of particles missing is a constant within the topological phase and varies with η in the non-topological phase.

The number of particles missing is given by the excess charge

$$Q_k = - \sum_{i=1}^N \rho(z_i) \theta(R - |z_i - w_k|), \quad (7.3)$$

where the Heaviside step function $\theta(\dots)$ ensures that only the region inside the circle contributes to Q_k and the density profile

$$\rho(z_i) = \langle n(z_i) \rangle_{Q \neq 0} - \langle n(z_i) \rangle_{Q=0} \quad (7.4)$$

is the difference in particle density between the state with $Q \neq 0$ and the state with $Q = 0$, where Q is the number of anyons in the system. Below, we shall consider the case, where the sum of the anyon charges is zero, i.e. $\sum_k p_k = 0$. For this case, $\rho(z_i)$ is zero in the topological phase, not only in the bulk but also on the edge, if no anyons are in the vicinity. It is therefore acceptable that the circular region contains part of the edge.

We compute Q_k with $Q = 2$ and $p_1 = -p_2 = 1$ for both the non-Abelian and Abelian anyons in the states. In other words, if the system is in the topological phase, there are two anyons of opposite charge in the system. We choose $R = |w_1 - w_2|/2$. We define the quantities $Q_+ = |Q_1|$ and $Q_- = |Q_2|$ for the state with non-Abelian anyons. If the system is in the topological phase, then Q_+ and Q_- are the absolute values of the charge of the positively and negatively charged anyon respectively. That is we have $Q_+ = Q_- = 1/4$ up to finite size effects. Likewise, we define $\bar{Q}_+ = |Q_1|$ and $\bar{Q}_- = |Q_2|$ for the state with Abelian anyons. If the system is in the topological phase, then $\bar{Q}_+ = \bar{Q}_- = 1/2$ up to finite size effects. We fix the number of particles to be $M = 40$ and vary the number of lattice sites from $N = 316$ to $N = 80$ to achieve different η values ranging from $\eta \simeq 1/4$ to $\eta = 1$. We keep ηN fixed throughout this interpolation.

We present the results in Fig. 7.3. From Fig. 7.3 (a), we observe that the excess charges Q_+ and Q_- are close to $1/4$ for $\eta < \eta_c$ and fluctuate for $\eta > \eta_c$, where $\eta_c \in [0.44, 0.46]$. The excess charges are hence able to detect the phase transition. In Fig. 7.3 (b) and 7.3 (c), we show the density profiles (7.4) for the state with non-Abelian anyons near the phase transition point for $\eta \simeq 0.44$, which is in the topological phase, and for $\eta \simeq 0.46$,

which is in the non-topological phase, respectively. It is seen that there is less screening for $\eta \simeq 0.46$ than for $\eta \simeq 0.44$.

As a test of the robustness of the approach, we also use the Abelian anyons in the state to detect the phase transition. The results are given in the bottom part of Fig. 7.3. We observe that the prediction for the phase transition is, indeed, the same as before. We have also checked that the fact that there is large jump in the excess charges from $\eta \simeq 0.44$ to $\eta \simeq 0.46$ is insensitive to the precise choice of the distance $|w_1 - w_2|$.

7.2 Detection of a topological quantum phase transition in a Moore-Read state on a fractal lattice

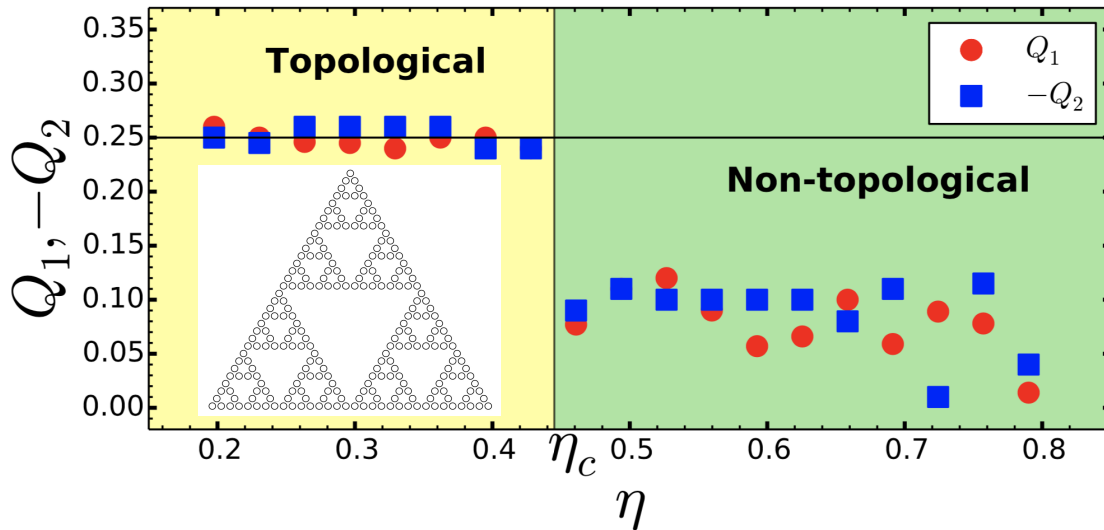


Figure 7.4.: Excess charges Q_1 and Q_2 for the Moore-Read state $|\Psi_a\rangle$ on a Sierpinski gasket fractal lattice (inset) as a function of the flux per site η . In the topological phase, Q_1 and $-Q_2$ are close to the charge of the positive anyon (horizontal line at $1/4$). In the nontopological phase, Q_1 and Q_2 may take any value. The jump away from $1/4$ predicts the transition point $\eta_c \in [0.43, 0.46]$. The Monte Carlo errors are of order 10^{-4} .

We next consider the Moore-Read model on a Sierpinski gasket fractal lattice. The fractal lattice is not periodic, and we can therefore not apply methods, such as ground state degeneracy, spectral flow, or many-body Chern number computations to detect a possible phase transition. Methods based on entanglement computations do also not apply, since we do not have a thorough understanding of entanglement properties of topological many-body states on fractal lattices. Quasiparticle properties, on the contrary, can detect a transition, as we will now show.

Lattice Laughlin fractional quantum Hall models were recently constructed on fractals [180], and we here consider a similar construction for the Moore-Read state. Specifically, we define the state $|\Psi_a\rangle$ on a lattice constructed from the Sierpiński gasket with $N = 243$ triangles by placing one lattice site on the center of each triangle. In Fig. 7.4, we vary the particle number $M \in [24, 96]$ to have different $\eta \in [0.19, 0.79]$ values and plot the excess charges as a function of η . The excess charges are $Q_1 \approx -Q_2 \approx 1/4$ for $\eta < \eta_c$ and fluctuate for $\eta > \eta_c$, which reveals a phase transition at the transition point $\eta_c \in [0.43, 0.46]$.

7.3 Detection of a topological quantum phase transition in an interacting Hofstadter model

We study a Hofstadter model for hardcore bosons on a square lattice. This model is a Bose-Hubbard type model under a uniform background magnetic field on a square lattice in the limit of hardcore interactions. Earlier studies in Refs. [79, 210] have shown that this model exhibits a topological quantum phase transition, when the filling factor of the lattice is varied, while the number of magnetic flux units per particle is kept fixed. This was concluded based on computations of the many-body Chern number. The system sizes that can be reached with exact diagonalization are too small to allow for a computation of the topological entanglement entropy. We show that one can detect the topological quantum phase transition from the charges of the anyons. We perform the computations for open boundary conditions using exact diagonalization. In our case, two diagonalizations per value of the lattice filling factor are sufficient to determine the phase transition point. This is significantly faster than the Chern number computation, where a large number of diagonalizations are carried out for each data point, because the eigenstates are needed for a grid of angles in two dimensions corresponding to different twisted boundary conditions.

7.3.1 Interacting Hofstadter model

Our starting point is the Hofstadter model, which describes particles hopping on a two-dimensional square lattice in the presence of a magnetic field pointing in the direction perpendicular to the plane. Hopping is allowed between nearest neighbor sites, and the magnetic field is taken into account through the Peierls substitution, i.e. by making the hopping amplitudes complex. More precisely, the phases of the hopping amplitudes are chosen in such a way that, whenever a particle hops around a closed loop, the wavefunction acquires a phase, which is equal to the Aharonov-Bohm phase for a charged particle encircling the same amount of magnetic flux.

We make this model interacting, by considering bosons that interact through a hardcore interaction. In other words, we assume that it is not possible to have more than one boson

on each site. For a lattice with $N = L_x \times L_y$ sites, the resulting Hamiltonian takes the form

$$H_0 = - \sum_{x=1}^{L_x-1} \sum_{y=1}^{L_y} \left(c_{x+1,y}^\dagger c_{x,y} e^{-i\pi\alpha y} + \text{H.c.} \right) - \sum_{x=1}^{L_x} \sum_{y=1}^{L_y-1} \left(c_{x,y+1}^\dagger c_{x,y} e^{i\pi\alpha x} + \text{H.c.} \right), \quad (7.5)$$

where $c_{x,y}$ is the hardcore boson annihilation operator acting on the lattice site at the position (x,y) with $x \in \{1, \dots, L_x\}$ and $y \in \{1, \dots, L_y\}$. If a particle hops around a plaquette, the phase acquired is $2\pi\alpha$. The number α is hence the magnetic flux through each plaquette of the lattice measured in units of h/e , where h is Planck's constant, and e is the elementary charge. We here consider the case, where the number of flux units per particle is two, i.e. $N\alpha/M = 2$.

The phase transition is encountered, when we vary α , keeping $N\alpha/M = 2$. Equivalently, we can say that we vary the lattice filling factor M/N , while keeping $N\alpha/M = 2$. It was found in [79, 210] that the Laughlin fractional quantum Hall state provides a reasonable description of the ground state of the model for $\alpha \lesssim 0.3$. Computations of the Chern number showed that the model remains topological for even higher values of α . It was found that the model is still topological for $\alpha = 0.375$, but non-topological for $\alpha = 0.400$. The phase transition must hence happen in this interval.

7.3.2 Creation of anyons in the ground state

We now test the ability of the anyons in the model to detect the phase transition. The starting point is to modify the Hamiltonian, so that anyons are trapped in the ground state, if the system is in the topological phase. It is already known that this can be done by adding a local potential with a strength that is sufficiently large compared to the hopping amplitude. Specifically, we shall here choose the potential

$$H_V = V n_{x_1, y_1} - V n_{x_2, y_2}, \quad (x_1, y_1) \neq (x_2, y_2), \quad (7.6)$$

where $V \gg 1$, $n_{x,y} = c_{x,y}^\dagger c_{x,y}$ is the number operator, and (x_1, y_1) and (x_2, y_2) are two of the lattice sites. This potential traps one positively charged anyon at the site (x_1, y_1) and one negatively charged anyon at the site (x_2, y_2) . The physical picture behind this is that the positive potential at the site (x_1, y_1) gives rise to an energy penalty if this site is occupied, and hence the system tends to reduce the density of particles at this site, corresponding to a positively charged anyon. At the site (x_2, y_2) , the potential will instead favor an increase in particle density, corresponding to a negatively charged anyon.

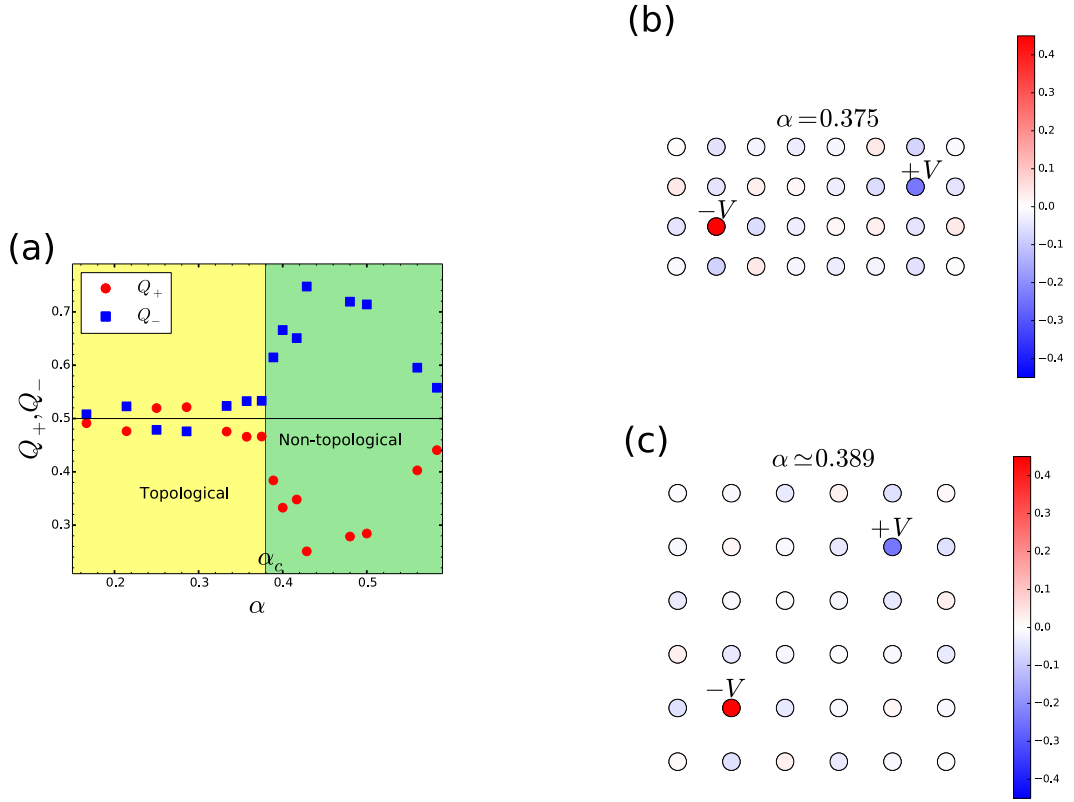


Figure 7.5.: In (a) we plot the absolute values of the excess charges Q_+ , as denoted by the red circles, and Q_- , as denoted by the blue squares, as a function of the magnetic flux per plaquette α . The expected absolute value of the excess charges in the topological phase is $1/2$, as marked by the solid black line. Q_+ and Q_- display a transition when going from $\alpha = 0.375$ to $\alpha \simeq 0.389$, so the data predict that the phase transition point α_c is in the interval $\alpha_c \in [0.375, 0.389]$. We shade the topological region $\alpha < \alpha_c$ with yellow color and the non-topological region $\alpha > \alpha_c$ with green color. In (b) and (c), the coloring shows the density profiles from Eq. (7.7) below, where $\alpha = 0.375$, and above, where $\alpha \simeq 0.389$, the transition point. The lattice sites are shown as the black circles, and $\pm V$ marks the lattice sites, where the trapping potentials are applied.

7.3.3 Excess charges and the topological quantum phase transition detection

Similar to the case above, we use the excess charge in a region around the sites (x_1, y_1) and (x_2, y_2) to detect the phase transition. We define the density profile as

$$\rho(x + iy) = \langle n_{x,y} \rangle_{H_0 + H_V} - \langle n_{x,y} \rangle_{H_0}, \quad (7.7)$$

where $\langle n_{x,y} \rangle_{H_0 + H_V}$ is the particle density, when the trapping potential is present, and $\langle n_{x,y} \rangle_{H_0}$ is the particle density, when the trapping potential is absent. The excess charge is then defined as in Eq. (7.3) with $w_1 = x_1 + iy_1$ and $w_2 = x_2 + iy_2$. We use the symbol Q_+

to denote the absolute value of the excess charge around the site (x_1, y_1) , and the symbol Q_- to denote the absolute value of the excess charge around the site (x_2, y_2) . For all the numerical computations in this section, we choose R such that the circular region includes all sites up to the second nearest neighbor sites. The absolute value of the excess charge should be close to $1/2$ in the topological region, while it can take any value and may vary with α in the non-topological region.

M	N	$L_x \times L_y$	α	$\dim(\mathcal{H})$	Q_+	Q_-
2	24	6×4	0.17	276	0.491	0.507
3	28	7×4	0.21	3276	0.476	0.522
3	24	6×4	0.25	2024	0.519	0.478
4	28	7×4	0.28	20475	0.521	0.475
4	24	6×4	0.33	10626	0.475	0.520
5	28	7×4	0.35	98280	0.465	0.532
6	32	8×4	0.37	906192	0.466	0.533
7	36	6×6	0.39	8347680	0.380	0.610
5	25	5×5	0.4	53130	0.332	0.666
5	24	6×4	0.42	42504	0.348	0.650
6	28	7×4	0.43	376740	0.250	0.747
6	25	5×5	0.48	177100	0.278	0.719
7	28	7×4	0.5	1184040	0.284	0.714
7	25	5×5	0.56	480700	0.402	0.595
7	24	6×4	0.58	346104	0.440	0.557

Table 7.1.: We show here the different choices we make for the number of particles M , the shapes and sizes $N = L_x \times L_y$ of the lattices, and the fluxes per plaquette $\alpha = 2M/N$. The quantity $\dim(\mathcal{H})$ is the dimension of the corresponding Hilbert spaces. We display the data for the absolute values of the excess charges Q_+ and Q_- . There is a significant change in Q_+ and Q_- , when going from $\alpha = 0.375$ to $\alpha \simeq 0.389$.

We take values of M and N , as listed in Tab. 7.1, which are numerically accessible for exact diagonalization, and for each choice $\alpha = 2M/N$. This gives us different values in the interval $\alpha \in [0.1, 0.6]$. We present the results in Fig. 7.5, where we plot Q_+ and Q_- as a function of α in (a) and show examples of the density profiles just above and below the transition point in (b) and (c). It is seen that Q_+ and Q_- are quite close to $1/2$ for α values up to 0.375. From $\alpha = 0.375$ to $\alpha \simeq 0.389$, on the other hand, there is a quite large change in Q_+ and Q_- , and for higher values of α , the values of Q_+ and Q_- deviate much more from $1/2$ than for low α . The data hence predict that the phase transition value α_c lies in the interval $\alpha_c \in [0.375, 0.389]$. This is consistent with the result $\alpha_c \in [0.375, 0.400]$ found in Refs. [79, 210].

7.4 Detection of a topological quantum phase transition in a disordered interacting Hofstadter model

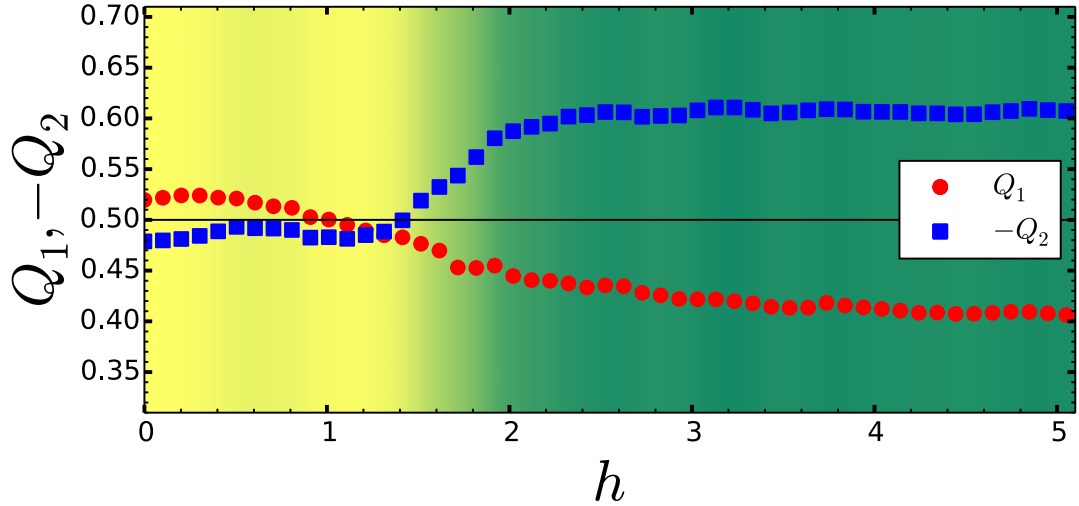


Figure 7.6.: Excess charges Q_1 and Q_2 as a function of the disorder strength h for the interacting Hofstadter model with $M = 3$, $N = 24$, and $\alpha = 0.25$. In the topological phase, $Q_1 \approx -Q_2 \approx 1/2$ (horizontal line), and the observed change away from this value predicts the transition point $h_c \simeq 1.5$. We average over 2000 statistically independent disorder realizations for each h to ensure convergence of the data.

We consider the Hamiltonian

$$H_0 + \sum_{x=1}^{L_x} \sum_{y=1}^{L_y} h_{x,y} n_{x,y}, \quad (7.8)$$

last term in (7.8) is the disordered potential, and $h_{x,y} \in [-h, h]$ is drawn from a uniform distribution of width $2h$, where h is the disorder strength.

We choose a point, which is deep in the topological phase for $h = 0$, namely $M = 3$, $N = 24$, and $\alpha = 0.25$, and plot the excess charges as a function of the disorder strength h in Fig. 7.6. We observe that Q_1 and $-Q_2$ are close to $1/2$ up to $h \simeq 1.5$, while the excess charges deviate more from $1/2$ for $h > 1.5$. The data hence predict the phase transition to happen at $h_c \simeq 1.5$.

7.5 Detection of a topological quantum phase transition in the Kitaev's toric code model

We study Kitaev's toric code [126, 125] on a square lattice with periodic boundary conditions, which is known to exhibit a \mathbb{Z}_2 topologically ordered phase. Adding a sufficiently strong, uniform magnetic field drives the system into a polarized phase [237, 238, 58, 269, 75]. Here we show that anyons inserted into the system are able to detect this phase transition. Our computations rely on exact diagonalization for a system with 18 spins and are hence relatively cheap to do numerically. We find that the anyons are significantly better at predicting the phase transition point than the energy gap closing for the same system size.

7.5.1 The Kitaev's toric code model

Here we consider the Kitaev's toric code model [126, 125] constructed on a $N_x \times N_y$ square lattice. There is a Pauli spin operator on each edge as illustrated in Fig. 7.7 (a). Therefore the total number of the spins is

$$N = 2N_x N_y \quad (7.9)$$

and hence the Hilbert space dimension is 2^N . We write the Hamiltonian as

$$H_{\text{TC}} = - \sum_p B_p - \sum_s A_s, \quad (7.10)$$

where the sums are over all the plaquettes p and over all the stars s of the lattice. The plaquette operator B_p acts on the four spins on the bonds which surround the plaquette p , and the star operator A_s acts on the four spins on the bonds which surround the star s , as shown in Fig. 7.7 (a). We write the operators as

$$B_p = \prod_{i \in p} \sigma_i^z \text{ and } A_s = \prod_{i \in s} \sigma_i^x, \quad (7.11)$$

where $\{\sigma_i^x, \sigma_i^y, \sigma_i^z\}$ is the set of the Pauli matrices acting on the i th edge. There are $N/2$ of the B_p operators and there are $N/2$ of the A_s operators. The A_s and the B_p operators commute with each other. Hence we write

$$[B_p, B_{p'}] = 0, [A_s, A_{s'}] = 0, [B_p, A_s] = 0 \quad (7.12)$$

for all p, p', s, s' . We note that when B_p and A_s do not share any edge then they commute and when they do share edges then, due to the underlying geometric structure, they must share two edges. Therefore the commutation relation between each shared σ_i^x and σ_i^z gives rise to a negative sign. Owing to the two shared edges the net sign is accumulated as positive and the two operators commute. This makes the Hamiltonian H_{TC} exactly solvable, and the ground states are those states for which each eigenvalue of the B_p operator is equal to 1 and each eigenvalue of the A_s operator is equal to 1. The

ground state space is four-fold degenerate on the torus, that is with the periodic boundary conditions. This can be noted as follows. On the torus we have the following conditions

$$\prod_s A_s = 1 \text{ and } \prod_p B_p = 1, \quad (7.13)$$

since in the first product every σ_i^x spin operator appears twice and in the second product every σ_i^z spin operator appears twice. Hence for a lattice of $N/2$ sites, there are $N/2 - 1$ independent choices of the star eigenvalues and are $N/2 - 1$ independent choices of the plaquette eigenvalues, because of the constraints as given in Eq. (7.13). Consequently there are $2^{2(N/2-1)}$ independent specifications of the star eigenvalues and of the plaquette eigenvalues. However, the total Hilbert space dimension is 2^N . Therefore we count the degeneracy as

$$\frac{2^N}{2^{2(N/2-1)}} = 4, \quad (7.14)$$

that is for every specification of the star and of the plaquette eigenvalues, there are four independent states. The model exhibits a \mathbb{Z}_2 topological order with the Abelian anyonic excitations.

7.5.2 Creation of anyons in the ground state

In the toric code, the states containing anyons can be created by applying certain string operators to the ground state. The string operator either changes the eigenvalues of the two A_s operators to -1 or the eigenvalues of the two B_p operators to -1 . In the former case, two electric excitations e_s are created, and in the latter case two magnetic excitations m_p are created. The state acquires a minus sign if one m_p is moved around one e_s or if one e_s is moved around one m_p , and therefore the excitations are Abelian anyons. More precisely the excitations are mutual semions, as the counter-clockwise exchange of the e_s and m_p gives rise to the phase factor $e^{i\pi/2}$ on the state.

In our case, we instead modify the toric code Hamiltonian, such that anyons are created in the ground states. The idea is to add suitable operators to the Hamiltonian H_{TC} such that the signs of the two of the B_p or the signs of the two of the A_s operators are inverted. The motivation behind this way of creating anyons is as follows. While the toric code model is under perturbations, like under an added magnetic field, then the model is no longer exactly solvable and the method of creating anyons by using string operators, as in the original toric code model, is not valid. But our method of creating anyons in the ground state, by providing energy penalties, is still valid. In particular, the ground states of the Hamiltonian

$$H_{\text{TC}} + H_m, \quad (7.15)$$

where

$$H_m = 2 \prod_{i \in p_1} \sigma_i^z + 2 \prod_{i \in p_2} \sigma_i^z, \quad (7.16)$$

has one m_p on each of the plaquettes p_1 and p_2 . Similarly, the ground states of the Hamiltonian

$$H_{\text{TC}} + H_e, \quad (7.17)$$

where

$$H_e = 2 \prod_{i \in s_1} \sigma_i^x + 2 \prod_{i \in s_2} \sigma_i^x, \quad (7.18)$$

has one e_s on each of the stars s_1 and s_2 .

7.5.3 Detection of the topological quantum phase transition

We aspire to drive the system through a phase transition. We do this by turning on a uniform magnetic field in the z -direction or in the y -direction, which amounts to adding the term

$$H_\lambda^k = \lambda \sum_i \sigma_i^k, \text{ where } k \in \{z, y\}, \quad (7.19)$$

to the Hamiltonian. Here $\lambda > 0$ is proportional to the strength of the field. Owing to the term H_λ^k , which does not commute with H_{TC} in Eq. (7.10), the model

$$H_{\text{TC}} + H_\lambda^k \quad (7.20)$$

is not exactly solvable. For sufficiently large λ , the term H_λ^k will drive the system into a polarized phase, as it is energetically favorable to polarize all the spins.

Previous investigations, based on perturbative, analytical calculations and tensor network studies [237, 238, 58], have shown that the model

$$H_{\text{TC}} + H_\lambda^z \quad (7.21)$$

has a second order phase transition at the field strength $\lambda_c \simeq 0.33$, while the model

$$H_{\text{TC}} + H_\lambda^y \quad (7.22)$$

has a first order phase transition at the field strength $\lambda_c = 1$. One can also determine the phase transition point from exact diagonalization using an order parameter for the magnetic phase. Specifically, we plot the magnetization per spin M_s^k and the magnetic susceptibility χ_s^k per spin,

$$M_s^k = \frac{1}{N} \langle \sum_i \sigma_i^k \rangle \text{ and } \chi_s^k = -\frac{\partial M_s^k}{\partial \lambda}, \quad (7.23)$$

for the ground state of

$$H_{\text{TC}} + H_\lambda^k \quad (7.24)$$

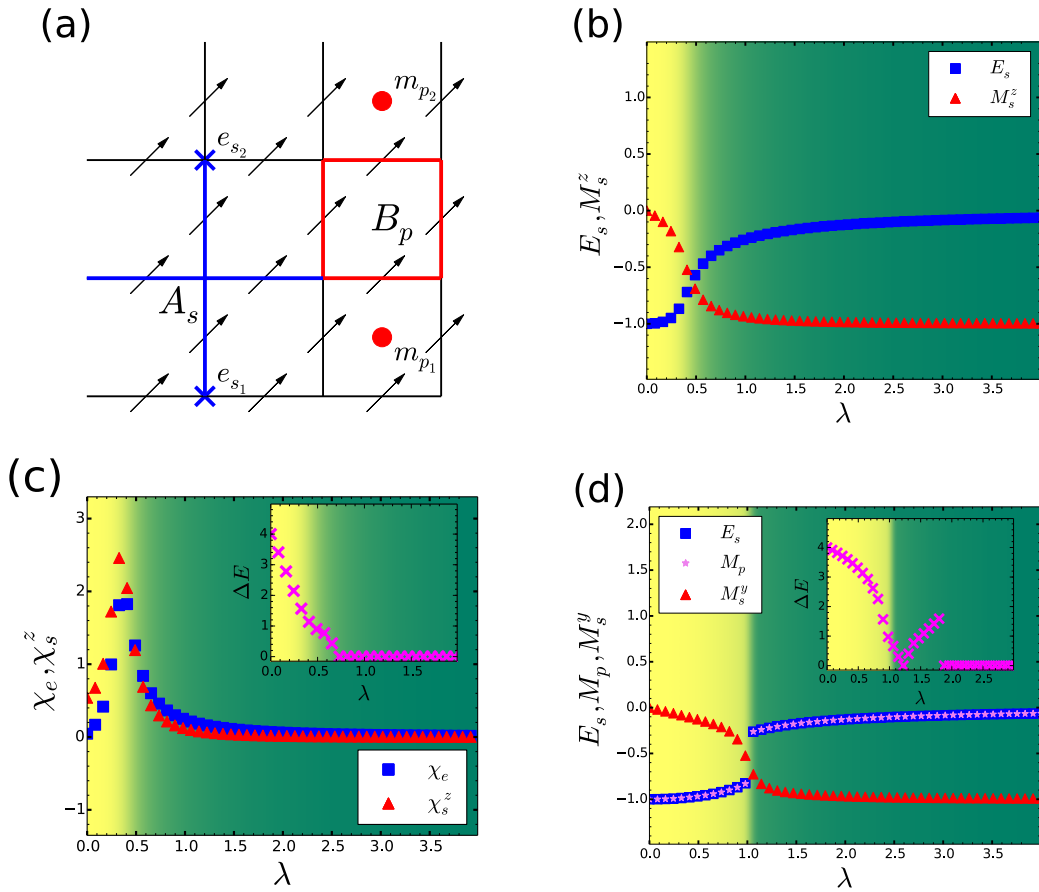


Figure 7.7.: In (a) we show the toric code model with $N = 18$ spins, as pictured by the arrows, on the square lattice and on the torus. The spins reside on the middle of each edge. We denote the plaquette operator by B_p , as shown by the red square, and the star operator by A_s , as shown by the blue star, respectively. We show that two types of anyons can be created, namely the m_p , as symbolized by the red circles, in the plaquettes p_1 and p_2 and the e_s , as symbolized by the blue crosses, in the stars s_1 and s_2 by using Eq. (7.16) and Eq. (7.18), respectively. In (b) and (c) we consider the case of a magnetic field in the z direction. In (b) we plot the quantity E_s , as shown by the blue squares, from Eq. (7.25) as the measure of the anyons and the quantity M_s^z , as shown by the red triangles, from Eq. (7.23) as the magnetization of the system as a function of the external magnetic field strength λ . We note that E_s gradually tends to zero from the value -1 , at $\lambda = 0$, and that M_s^z gradually approaches the value -1 from zero, at $\lambda = 0$. In (c) we show the quantity χ_e , as shown by the blue squares, and the quantity χ_s^z , as shown by the red triangles, from Eq. (7.25) as a function of λ . We note that the peak in χ_e and in χ_s^z are consistent with $\lambda_c \simeq 0.33$. In (d) we consider the case of a magnetic field in the y direction and we plot the quantity E_s , as shown by the blue squares, the quantity M_p , as shown by the pink stars, from Eq. (7.25) as the measures of the anyons and the quantity M_s^y , as shown by the red triangles, from Eq. (7.23) as the magnetization per spin of the system as a function λ . We notice that both E_s and M_p gradually tends to zero from the value -1 , at $\lambda = 0$, and that M_s^y gradually approaches the value -1 from zero, at $\lambda = 0$. We note that the transition is at around $\lambda_c \simeq 1.0$. The insets in (c) and (d) show the energy gap ΔE , as denoted by the magenta crosses, between the fourth and the fifth energy eigenstate as a function of λ . We choose these states since the ground state of the toric code is fourfold degenerate. All in (b), (c), and (d) we show the color gradient from the yellow, which is for small λ and hence signifies the topological phase, to the green, which is for large λ and hence signifies the non-topological phase, as plotted according to the value of E_s .

in Fig. 7.7. The results are consistent with a transition around 0.33 when $k = z$, as shown in Fig. 7.7 (b), (c) and a transition around 1 when $k = y$, as shown in Fig. 7.7 (c).

We now show that the transition can be detected by studying the anyons. Similarly to the examples in the previous sections, we do not need to compute the braiding properties to find the transition point. Instead we compute the quantities

$$M_p = \langle \prod_{i \in p} \sigma_i^z \rangle, E_s = \langle \prod_{i \in s} \sigma_i^x \rangle, \chi_e = \frac{\partial E_s}{\partial \lambda} \quad (7.25)$$

to detect the anyons in the system, where

$$s \in \{s_1, s_2\} \text{ and } p \in \{p_1, p_2\}. \quad (7.26)$$

We note that $E_s = -1$ and $M_p = -1$ signify the presence of the anyons in those stars and plaquettes respectively. In the fully polarized phase, on the other hand, both E_s and M_p vanish when $k = y$ and E_s vanishes and M_p acquires a value $+1$ when $k = z$. Below we study these two cases.

(a). Case when $k = z$

We use exact diagonalization to compute E_s and χ_e for the ground states of the Hamiltonian

$$H_{\text{TC}} + H_e + H_\lambda^z \quad (7.27)$$

as a function of λ , as shown in Fig. 7.7 (a) and (b), respectively. We note that E_s changes from -1 in the topological phase to 0 in the polarized phase as expected. The phase transition point is consistent with $\lambda_c \simeq 0.33$. Both the prediction for the phase transition point and the width of the transition region, which is due to finite size effects, are comparable to the same quantities obtained from the magnetic order parameter. The energy gap, as shown in Fig. 7.7 (b), closes only at $\lambda \simeq 0.7$, which is quite far from $\lambda_c \simeq 0.33$. The anyons hence reproduce the transition point found in Ref. [58] more accurately than the energy gap closing for the same system size.

We could also have chosen to study M_p . This expectation value is, however, not a good choice to detect the topological quantum phase transition for the following reason. The operator

$$B_p = \prod_{i \in p} \sigma_i^z \quad (7.28)$$

is itself one of the plaquette operators, and it commutes with all terms in the Hamiltonian

$$H_{\text{TC}} + H_m + H_\lambda^z. \quad (7.29)$$

This means that all eigenstates of the Hamiltonian are also eigenstates of B_p , and half of these eigenstates have B_p eigenvalue $+1$ and the other half have eigenvalue -1 . The value of M_p is hence always either $+1$ or -1 , and it only measures whether the ground state has B_p eigenvalue $+1$ or -1 . We find that the first transition to a ground state with B_p eigenvalue $+1$ happens around $\lambda \simeq 2.08$, but this does not exclude gap closings at smaller λ values. On the contrary, H_e does not commute with H_λ^z , and the above problems are hence not encountered for E_s .

We point out that we have also investigated the case when $k = x$. In this case the roles of the quantities E_s and M_p are interchanged. That is in this case M_p is sensitive to the phase transition and capture the same phase transition point consistent with $\lambda_c \simeq 0.33$, whereas E_s is insensitive and shows the the first transition from a ground state with A_s eigenvalue -1 to a ground state with A_s eigenvalue $+1$ around $\lambda \simeq 2.08$. This scenario is expected since the Kitaev's toric code model remains the same if we interchange the roles of the Pauli spin operators in defining the plaquettes and the stars.

(b). Case when $k = y$

We use exact diagonalization to compute E_s and M_p for the ground states of the Hamiltonian

$$H_{\text{TC}} + H_e + H_\lambda^y \quad (7.30)$$

as a function of λ , as shown in Fig. 7.7 (c). We note that both E_s and M_p change from -1 in the topological phase to 0 in the polarized phase as expected. The phase transition point is around $\lambda_c \simeq 1.0$. In this case, the transition is sharper than for the magnetic order parameter. The anyons also better reproduce the transition point $\lambda_c = 1.0$ found in Ref. [58] than the energy gap closing, which happens around $\lambda \simeq 1.2$ for the same system size. We notice that, since H_λ^y does not commute either with H_e or with H_m , both the quantities E_s and M_p are sensitive to the phase transition and capture the same phase transition point.

7.6 Conclusions

In this chapter we have benchmarked the quasiparticles as the topological quantum phase transitions detector. Topologically ordered systems can host the anyonic quasiparticles with particular braiding properties and particular fractional charges. The anyons can be trapped in the ground state of the system by adding the suitable trapping operators to the Hamiltonian. As long as the quasiparticles are anyonic, we know that the system is topologically ordered. We now change a parameter in the Hamiltonian, which could drive the system into a non-topological phase or into another topological phase with a different set of anyons. When looking at a type of anyons that is only supported on one side of the transition, the anyons must undergo a change, when the phase transition is crossed. The main idea of this chapter is to use this change to detect the topological quantum phase transitions. We have tested this approach for the five different cases as follows. We

have taken models on a square lattice and on a fractal lattice with an analytical lattice Moore-Read fractional quantum Hall state as the ground state and thereby having the chiral topological order. The model exhibits a phase transition as a function of the lattice filling factor. We have created the anyonic quasiparticles in the model and have shown that the quasiparticle charges detect the phase transition. We have investigated an interacting Hofstadter model, which is a fractional Chern insulator model, having the ground state as the Laughlin type fractional quantum Hall state and thereby having the chiral topological order. The model encounters a phase transition as a function of the lattice filling factor. We have studied this model both in the presence and in the absence of disorder. We have modified the Hamiltonian to trap the anyonic quasiparticles in the ground state and have demonstrated that the quasiparticle charges detect the phase transition. We have researched the stability of the topological phase of the Kitaev's toric code model, having the \mathbb{Z}_2 topological order, under the applications of the external magnetic fields in different directions. We have modified the Hamiltonians to trap the anyonic quasiparticles in the ground state and in all cases, we have found that the quasiparticles can accurately detect the quantum phase transition.

If we are able to do the robust braiding in a system with results corresponding to a particular topological order, then we know that the system allows these braiding properties. The studied examples show, however, that the phase transition point can often be detected by computing a simpler property, such as the charge of the anyons. This makes the computations numerically cheap.

There is currently a high demand for finding appropriate methods to detect topological quantum phase transitions, both for numerical investigations and for experimental implementations. The approach suggested here is particularly direct, since, to fully exploit the interesting properties of topologically ordered systems, one needs to be able to create anyons in the systems, move the anyons around in controlled ways, and measure their properties. In the interacting Hofstadter model, the anyons can be created by adding a local potential, and the charge of the anyons used to detect the phase transition can be measured by measuring the expectation value of the number of particles on each site. Both of these can be done in experiments with ultracold atoms in optical lattices [249, 188]. For the toric code model, the anyons are harder to create. It is interesting to note, however, that the operators needed to create the anyons are of the same type as the operators already appearing in the Hamiltonian, so if one finds a way to implement the Hamiltonian experimentally, one can also create the anyons.

The ideas presented in this work can be applied to any type of topological system with anyonic quasiparticles. In the future, it would be interesting to test the ideas for other types of systems. One could, as for example, study what quasiparticles tell us about transitions between different non-topological phases. It would also be interesting to apply similar ideas to gapless phases.

Spin-1/2 Chain and Ladder Models with Two-Body Interactions and Analytical Ground States

“*What I cannot create, I do not understand.*”

— **Richard P. Feynman**

Models that can be solved partially or fully by using analytical tools play a crucial role to illuminate the physics of strongly correlated quantum many-body systems. They overcome, in particular cases, the bottleneck that the resources needed to do numerical computations generally grow exponentially with system size, they provide insight into mechanisms lying behind many-body phenomena, and they can be used to test numerical approximation schemes.

A number of different exactly solvable models have been found in one-dimensional systems. These models can be grouped into a few categories [56, 78]. One member is the Heisenberg spin model [168] and other related models in one-dimension [161, 264] with their exact solutions by Bethe’s ansatz [82]. Another member is the Tomonaga-Luttinger liquids [83, 151, 222], solved by the bosonization techniques. These models reveal the non Fermi-liquid properties of one-dimensional fermionic systems. Another family are models related to the Calogero-Sutherland model [215] with long range interactions. The Calogero-Sutherland model is defined in the continuum, and a lattice spin version of the model was found by Haldane and Shastry [80, 205]. In addition, tensor networks provide an efficient tool to find models with known ground states and short range interactions [1, 61, 62].

Important works have also been done in the context of exactly solvable ladder models, as for example in Refs. [248, 146, 51, 54, 223, 18, 59, 235]. An exactly solvable spin ladder with biquadratic interactions has been obtained via the Bethe’s ansatz in Ref. [248]. In Ref. [54], a spin ladder model with interactions between spins on neighboring rungs, and in [235], behavior of the two leg frustrated quantum spin-1/2 ladder containing Heisenberg intra-rung and Ising inter-rung interactions has been studied. A three leg spin ladder with isotropic Heisenberg interactions and additional many-body terms in the context of magnetization is discussed in Ref. [51], and recently entanglement entropy has

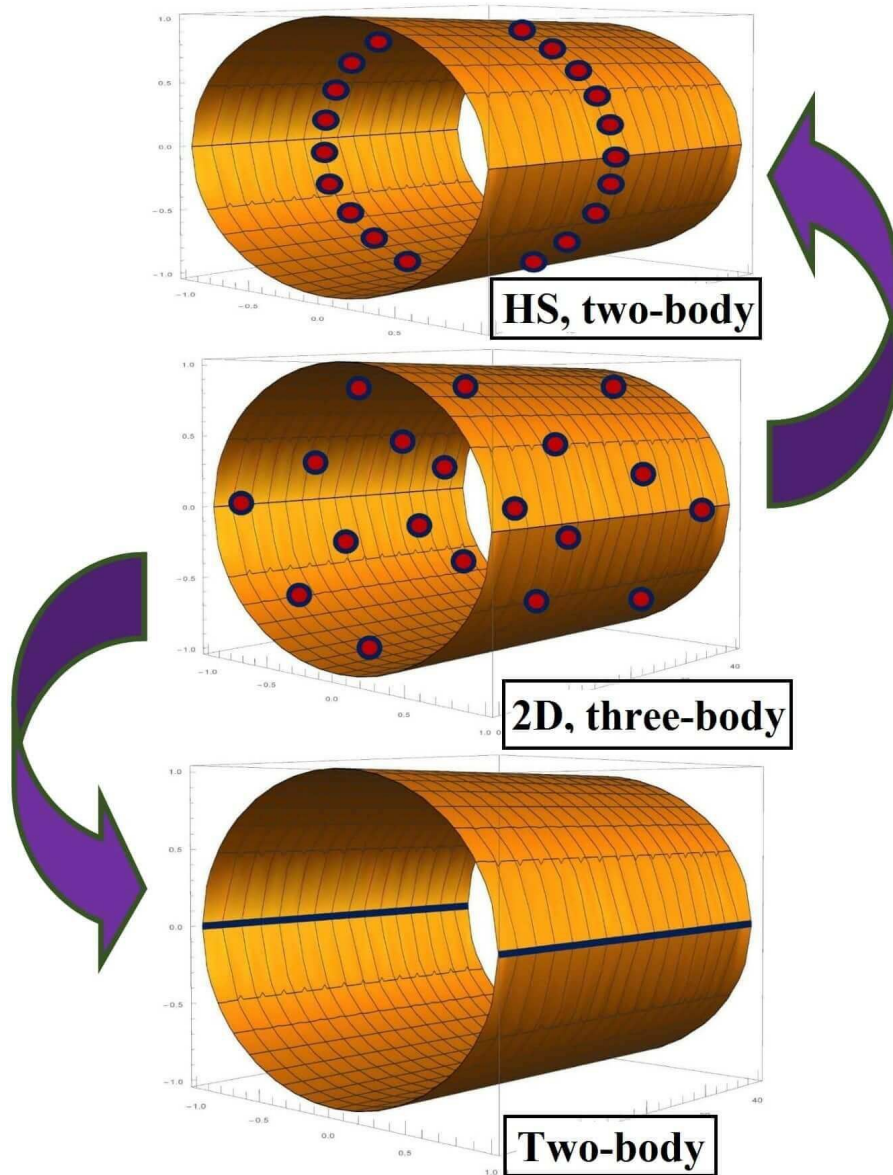


Figure 8.1.: We consider a model, in which the lattice points or the spins are placed on the surface of a cylinder. The middle cylinder depicts the two-dimensional generalization of the one-dimensional Haldane-Shastry model, which can be defined for spins on an arbitrary lattice. In general, it has two- and three-body interactions. The one-dimensional Haldane-Shastry model, as shown on the upper most cylinder, is a special case with only two-body interactions. In this chapter, we show that if the positions of the spins are restricted to the blue lines, as shown on the lower most cylinder, we also get a model with only two-body interactions.

been investigated for an exactly solvable two leg spin ladder which contains three body interactions in Ref. [59].

In this chapter, we construct the family of spin-1/2 chain and ladder models with $SU(2)$ invariant Hamiltonians having two-body interactions and analytical ground states that are related to the one-dimensional Haldane-Shastry model [211]. In the original

one-dimensional Haldane-Shastry model, N equidistant spin-1/2 particles are arranged on a one-dimensional circle and interact antiferromagnetically through an exchange interaction. The interaction strength is inversely proportional to the square of the chord distance between two spins on the circle. The Hamiltonian of the one-dimensional Haldane-Shastry model

$$H_{\text{HS}} = \sum_{i \neq j}^N \left[\frac{N}{\pi} \sin \left(\frac{i-j}{N} \pi \right) \right]^{-2} \mathbf{S}_i \cdot \mathbf{S}_j \quad (8.1)$$

is exactly solvable up to all of its ground and excited states. An interesting feature of this model is that it contains elementary excitations named spinons, which are spin-1/2 particles obeying semion statistics. The possibility of having a one-dimensional hyperbolic version of the Haldane-Shastry model with infinitely many spins has been investigated by Inozemtsev [103].

A generalization of the one-dimensional Haldane-Shastry model, which is valid for arbitrary lattices on a cylinder surface, has been found recently [171] and is illustrated in Fig. 8.1. The model has two- and three-body interactions, and the ground state, but not the excited states, is known analytically. In two-dimensions, the ground state is closely related to the Kalmeyer-Laughlin state [116] which is the spin version of the bosonic Laughlin state at half filling. It is known that if one restricts the positions of the spins to a circle around the cylinder, one gets a two-body model. If, in addition, the spins are uniformly distributed on the circle, as visualized on the upper most cylinder in Fig. 8.1, the model reduces to the one-dimensional Haldane-Shastry model [172]. A different choice of the spin positions gives a one-dimensional Haldane-Shastry model with open boundary conditions [228].

Here, we show that there is also a different way to obtain a family of two-body models, and we investigate the properties of some members of this family. More specifically, the two-body models are obtained, when the spin positions are restricted to be on the two blue lines depicted on the lower most cylinder in Fig. 8.1. In particular, this allows us to construct a family of one-dimensional models and of ladder models with only two-body interactions and analytical ground states. It is interesting to ask, whether the properties of these models are similar to those of the original one-dimensional Haldane-Shastry model or not. Our investigations show that the properties of the models depend on how large the circumference of the cylinder is compared to the other length scales in the system. If this ratio is large, the models have properties close to those of the one-dimensional Haldane-Shastry model, and if the ratio is small, the wavefunction reduces to a product of singlets. In between, we find an interesting behavior, where the correlations and entropy display critical properties over short distances and exponential decay of correlations and area law entropy for large distances. As the parameter controlling the ratio varies, the length scale separating the two behaviors changes.

The chapter is organized as follows. In Sec. 8.1, we briefly recall the two-dimensional Haldane-Shastry model for spins on an arbitrary lattice on the cylinder. In Sec. 8.2, we discuss the one-dimensional Haldane-Shastry model on the circle. In Sec. 8.3, we show that the two-dimensional Haldane-Shastry model reduces to a two-body model for particular choices of the lattice. Special cases include spin chain models, which

we analyze in Sec. 8.4, and ladder models, which we analyze in Sec. 8.5. Section 8.6 concludes the chapter. This chapter is based on the following Ref. [154]:

[1] : **Sourav Manna** and **Anne E. B. Nielsen**, "Chain and ladder models with two-body interactions and analytical ground states", *Physical Review B* **97**, 195143 (2018)

8.1 The two-dimensional Haldane-Shastry model

We first briefly recall the two-dimensional Haldane-Shastry model [171] on the cylinder. The position of the j th spin on the cylinder is specified by the complex number W_j . $\text{Re}(W_j)$ is the position in the direction along the cylinder axis, and $\text{Im}(W_j)$ is the position in the perpendicular direction around the cylinder. We take the circumference of the cylinder to be 2π , and therefore $\text{Im}(W_j)$ is periodic with period 2π . We also define a corresponding set of points z_j in the complex plane through the mapping

$$z_j = e^{W_j}. \quad (8.2)$$

We shall assume throughout that all spins are at different positions, that is $z_j \neq z_k$ whenever $j \neq k$.

The local Hilbert space on site number j is spanned by the states $|s_j\rangle$ with $s_j \in \{-1, 1\}$. In the following, we choose the number of spins N to be even and consider the many-body state

$$|\psi\rangle = \sum_{s_1, s_2, \dots, s_N} \psi_{s_1, s_2, \dots, s_N}(z_1, z_2, \dots, z_N) |s_1, s_2, \dots, s_N\rangle \quad (8.3)$$

with

$$\psi_{s_1, s_2, \dots, s_N}(z_1, z_2, \dots, z_N) = \delta_{\mathbf{s}} \prod_{p=1}^N \chi_{p, s_p} \prod_{j < k}^N (z_j - z_k)^{\frac{1}{2}(s_j s_k - 1)}, \quad (8.4)$$

which is the spin version of the bosonic Kalmeyer-Laughlin state at half filling. Here, $\delta_{\mathbf{s}} = 1$ for $\sum_{j=1}^N s_j = 0$ and $\delta_{\mathbf{s}} = 0$ otherwise, and the phase factors are

$$\chi_{p, s_p} = \exp[i\pi(p-1)(s_p+1)/2], \quad (8.5)$$

since this ensures that (8.4) is a spin singlet [171]. The state (8.4) is invariant under relabelling of the indices [13], and we can hence choose the numbering of the spins after convenience.

We define a set of positive semi-definite and Hermitian operators

$$H_i = \frac{1}{2} \sum_{j(\neq i)} |w_{ij}|^2 - \frac{2i}{3} \sum_{j \neq k(\neq i)} \bar{w}_{ij} w_{ik} \mathbf{S}_i \cdot (\mathbf{S}_j \times \mathbf{S}_k) + \frac{2}{3} \sum_{j(\neq i)} |w_{ij}|^2 \mathbf{S}_i \cdot \mathbf{S}_j + \frac{2}{3} \sum_{j \neq k(\neq i)} \bar{w}_{ij} w_{ik} \mathbf{S}_j \cdot \mathbf{S}_k \quad (8.6)$$

acting on the N spins. Here,

$$w_{ij} = \frac{g(z_i)}{(z_i - z_j)} + h(z_i), \quad (8.7)$$

where g and h are arbitrary functions of z_i , \bar{w}_{ij} is the complex conjugate of w_{ij} , and $\mathbf{S}_i = (S_i^x, S_i^y, S_i^z)$ is the spin operator acting on the spin positioned at z_i . We have $|s_i\rangle$ as the eigenstates of S_i^z with eigenvalues $s_i/2$. We use the notation $\sum_{p \neq q}$ as the sum over p and q and $\sum_{p(\neq q)}$ as the sum over p only. Likewise, $\sum_{p \neq q(\neq r)}$ means the sum over p and q with $p \neq q$, $p \neq r$, and $q \neq r$.

It can be shown [171] that all the H_i , and also $\sum_i \mathbf{S}_i$, annihilate the state (8.4). Any linear combination of the H_i and $\sum_{i,j} \mathbf{S}_i \cdot \mathbf{S}_j$ with non-negative coefficients is hence a parent Hamiltonian for (8.4). In this chapter, we will use

$$H = \frac{1}{4} \sum_i H_i \quad (8.8)$$

as our Hamiltonian, unless specified otherwise.

8.2 The one-dimensional Haldane-Shastry model

The standard one-dimensional Haldane-Shastry model (8.1) is obtained as a special case of the two-dimensional Haldane-Shastry model by choosing the Hamiltonian as [172]

$$H_{\text{HS}} = \frac{\pi^2}{2N^2} \sum_i H_i + \frac{\pi^2(N+1)}{3N^2} \sum_{i,j} \mathbf{S}_i \cdot \mathbf{S}_j - \frac{\pi^2(N^2+5)}{12N} \quad (8.9)$$

and by putting

$$z_j = \exp(2\pi i j/N) \text{ and } w_{ij} = \frac{2z_i}{(z_i - z_j)} - 1. \quad (8.10)$$

We note that the three-body term in H_i vanishes in this case, since $\bar{w}_{ij} = -w_{ij}$. The ground state is again given by (8.4) with $z_j = \exp(2\pi i j/N)$. The standard one-dimensional Haldane-Shastry model is a critical model belonging to the $SU(2)_1$ Wess-Zumino-Witten universality class [53]. For later comparison, we will now discuss a few important properties of this model.

We first consider the spin-spin interaction strength b_{ij}^{HS} , which is defined such that

$$H_{\text{HS}} = \sum_{i \neq j} b_{ij}^{\text{HS}} \mathbf{S}_i \cdot \mathbf{S}_j + C_{\text{HS}}, \quad (8.11)$$

where C_{HS} is a constant. Hence

$$b_{ij}^{\text{HS}} = \left[\frac{N}{\pi} \sin \left(\frac{i-j}{N} \pi \right) \right]^{-2} = d_{ij}^{-2}. \quad (8.12)$$

Here, d_{ij} is the chord distance between the spins i and j , when the spins are put on a circle with circumference N . The spin-spin interaction hence decays as the inverse of the square of the chord distance between the spins. For spins that are nearby each other, that is for $|i - j| \ll N$, the chord distance is approximately the same as the distance along the circle, and the expression simplifies to

$$b_{ij}^{\text{HS}} \approx (i - j)^{-2} \text{ with } |i - j| \ll N. \quad (8.13)$$

We next consider the spin-spin correlation function

$$\langle S_j^z S_k^z \rangle = \frac{\sum_{s_1, \dots, s_N} s_j s_k |\Psi_{s_1, \dots, s_N}(z_1, \dots, z_N)|^2}{4 \sum_{s_1, \dots, s_N} |\Psi_{s_1, \dots, s_N}(z_1, \dots, z_N)|^2}, \quad (8.14)$$

which is the expectation value of a product of two spin operators S_j^z acting on different lattice sites. In the standard one-dimensional Haldane-Shastry model, the spin-spin correlation function can be computed analytically [172]. The analytical expression for the correlation function simplifies to

$$\langle S_{j+k}^z S_j^z \rangle \approx \frac{\pi(-1)^k}{8N \sin(\pi k/N)} - \frac{1}{4N^2 \sin^2(\pi k/N)} \quad (8.15)$$

in the limit $k \gg 1$ and $N \gg 1$ with k/N fixed. It follows that the correlation function shows critical behavior with the power law decay

$$(-1)^k / (8k) \text{ for } 1 \ll k \ll N. \quad (8.16)$$

This is consistent with Haldane's conjecture [23].

Finally, we consider the Renyi entropy of order two, which is defined as follows. We divide the system into two parts A and B . In our case, A is the first x spins, and B is the remaining $N - x$ spins. The Renyi entanglement entropy gives the entanglement of one part with the other part. Now, we construct the density matrix $\rho = |\Psi\rangle\langle\Psi|$ for the whole system and evaluate the reduced density matrix of part A as $\rho_A = \text{Tr}_B(\rho)$. Here, $\text{Tr}_B(\rho)$ is the trace of ρ over the spins in part B . The Renyi entanglement entropy of order two is then given by

$$S_x = -\ln[\text{Tr}(\rho_A^2)]. \quad (8.17)$$

The reason for considering this entanglement entropy is that it can be computed efficiently using a Metropolis Monte-Carlo algorithm and the replica trick [44, 89].

The leading order behavior of the Renyi entropy of order α in a one-dimensional critical system is generally given by [46, 96, 236, 37, 132, 36]

$$S_x^{(\alpha)} \approx \frac{c}{6\eta} \left(1 + \frac{1}{\alpha}\right) \ln[\eta N \sin(\pi x/N) / \pi] + \text{constant}, \quad (8.18)$$

where α is the order of the Renyi entropy, c is the central charge of the underlying conformal field theory, and $\eta = 1$ or $\eta = 2$ is for periodic or open boundary conditions

respectively. The expected leading order behavior for the standard one-dimensional Haldane-Shastry model is hence

$$S_x \approx \frac{c}{4} \ln \left[\frac{N}{\pi} \sin \left(\frac{\pi x}{N} \right) \right] + \text{constant}, \quad (8.19)$$

which agrees with numerics [44] for $c = 1$. The numerical results for the Haldane-Shastry model also show an oscillation with period 2, which is present in the subleading terms.

8.3 Two-body chain and ladder models

We now demonstrate that the Hamiltonian (8.8) also reduces to a two-body Hamiltonian in other particular cases. Specifically, if we take all w_{ij} to be real, the three-body terms in (8.6) vanish, and the Hamiltonian simplifies to

$$H = \frac{1}{4} \sum_i H_i = \sum_{i \neq j} b_{ij} \mathbf{S}_i \cdot \mathbf{S}_j + C, \quad (8.20)$$

where C is a constant and

$$b_{ij} = \frac{1}{6} w_{ij}^2 + \frac{1}{6} \sum_{k(\neq i \neq j)} w_{ki} w_{kj} \quad (i \neq j) \quad (8.21)$$

expresses the strength of the interaction between the spins at positions i and j . We note that $b_{ij} = b_{ji}$.

Since

$$w_{ij} = \frac{g(z_i)}{(z_i - z_j)} + h(z_i), \quad (8.22)$$

where g and h are arbitrary functions of z_i , we can achieve that w_{ij} are real by choosing all z_i real and taking g and h to be real functions. Requiring z_i to be real corresponds to restricting $\text{Im}(W_i)$ to be an integer times π . In other words, all the lattice points should be on the blue lines on the lower most cylinder in Fig. 8.1.

Lattice points on the blue lines can be expressed in the form

$$z_j = \sigma_j e^{\Lambda f(j)}, \quad (8.23)$$

where $\sigma_j \in \{-1, +1\}$, Λ is a positive number, and $f(j) \in \mathbb{R}$ is a real valued function of j . If we take all σ_j to be $+1$, we get a one-dimensional chain model, and if we take some σ_j to be $+1$ and some to be -1 , we get a ladder model. Note that these models have open boundary conditions by construction. In the following, we shall refer to the spins with positive and negative σ_j as the spins on the front and back of the cylinder respectively. The circumference of the cylinder is fixed to 2π , and changing Λ corresponds to a scale transformation in the direction parallel to the cylinder axis. If Λ is very small or large, the circumference of the cylinder will be large or small respectively compared to the other length scales in the system.

8.3.1 Symmetries

The wavefunction (8.4) can be written as a conformal block times a normalization constant, and it is therefore invariant under all global conformal transformations, that is transformations of the type

$$z_j \rightarrow \frac{az_j + b}{cz_j + d}, \quad (8.24)$$

where a , b , c , and d are complex numbers fulfilling $ad - bc = 1$. If we do the same transformation on the Hamiltonian, we still have the same expression for the Hamiltonian, but g and h are, in general, modified. The Hamiltonian is hence not invariant under the full set of conformal transformations, unless $g = h = 0$, but for particular choices of g and h , the Hamiltonian is invariant under a smaller set of transformations [71].

A particularly natural choice of Hamiltonian for the models we are looking at is to take

$$w_{ij} = \frac{2z_i}{(z_i - z_j)} - 1 = \frac{(z_i + z_j)}{(z_i - z_j)}. \quad (8.25)$$

In that case, the Hamiltonian is invariant under the transformations

$$z_j \rightarrow az_j \text{ and } z_j \rightarrow z_j^{-1}, \quad (8.26)$$

where a is a constant number. These two transformations correspond, respectively, to displacing the lattice points along the blue lines in Fig. 8.1 plus a rotation around the cylinder axis if a is complex and to inverting the directions of the blue lines.

8.3.2 Spin-spin correlations and Renyi entropy

As part of our investigations of the properties of the models, we shall below compute the spin-spin correlation function and the Renyi entropy of order two for particular cases. It was found in Ref. [172] that if the spins are put on a circle around the cylinder and

$$w_{ij} = \frac{(z_i + z_j)}{(z_i - z_j)}, \quad (8.27)$$

then the spin-spin correlations fulfil the following set of linear equations

$$w_{ij} \langle S_i^z S_j^z \rangle + \sum_{k(\neq i \neq j)} w_{ik} \langle S_k^z S_j^z \rangle + \frac{1}{4} w_{ij} = 0. \quad (8.28)$$

Following the same steps as in Ref. [172], we find that (8.28) also applies whenever all the

$$w_{ij} = \frac{g(z_i)}{(z_i - z_j)} + h(z_i) \quad (8.29)$$

are real. Since as long as w_{ij} are real, we can choose $g(z_i)$ and $h(z_i)$ after convenience. This allows us to easily compute the spin-spin correlations for quite large systems. We compute the Renyi entropy using Monte Carlo simulations.

8.3.3 Small Λ limit and the decoupling of the legs

When Λ is sufficiently small, the circumference of the cylinder is large compared to all other relevant length scales in the system, and it would be natural if the two legs decouple in that limit. Specifically, we shall assume that

$$\Lambda|f(j) - f(k)| \ll 1 \quad (8.30)$$

for all j and k . In this section, we shall label the N_+ spins with $\sigma_j > 0$ from 1 to N_+ and the N_- spins with $\sigma_j < 0$ from $N_+ + 1$ to $N = N_+ + N_-$.

Let us first look at the Hamiltonian for

$$w_{ij} = \frac{(z_i + z_j)}{(z_i - z_j)}. \quad (8.31)$$

Using Eq. (8.30), we get

$$w_{ij} = \frac{\sigma_i e^{\Lambda f(i)} + \sigma_j e^{\Lambda f(j)}}{\sigma_i e^{\Lambda f(i)} - \sigma_j e^{\Lambda f(j)}} \approx \begin{cases} 2/\{\Lambda[f(i) - f(j)]\} & \text{for } \sigma_i = \sigma_j \\ \Lambda[f(i) - f(j)]/2 & \text{for } \sigma_i = -\sigma_j \end{cases}. \quad (8.32)$$

In other words, w_{ij} is large if the i th and the j th spins sit on the same leg and small if they sit on different legs. Inserting this into Eq. (8.21), we observe that the spin-spin interaction strength between spins sitting on the same leg is larger by a factor of Λ^{-2} compared to the spin-spin interaction strength between spins sitting on different legs. When Eq. (8.30) applies, we can hence neglect the interactions between spins on different legs.

In appendix D, we show that if there is an even number of spins on both of the legs, then the wavefunction (8.4) reduces to

$$\Psi_{s_1, \dots, s_N}(z_1, \dots, z_N) \approx \text{constant} \times \Psi_{s_1, \dots, s_{N_+}}(z_1, \dots, z_{N_+}) \times \Psi_{s_{N_++1}, \dots, s_N}(z_{N_++1}, \dots, z_N), \quad (8.33)$$

when (8.30) applies. In other words, the ladder model reduces to two copies of the chain model with N_+ and N_- spins, respectively. If there is an odd number of spins on each of the legs, the wavefunction is a sum of two terms

$$\begin{aligned} \Psi_{s_1, \dots, s_N}(z_1, \dots, z_N) \approx \text{constant} \times & [\Psi_{s_1, \dots, s_{N_+}}^{(1)}(z_1, \dots, z_{N_+}) \Psi_{s_{N_++1}, \dots, s_N}^{(-1)}(z_{N_++1}, \dots, z_N) \\ & - \Psi_{s_1, \dots, s_{N_+}}^{(-1)}(z_1, \dots, z_{N_+}) \Psi_{s_{N_++1}, \dots, s_N}^{(1)}(z_{N_++1}, \dots, z_N)]. \end{aligned} \quad (8.34)$$

Here, $\psi^{(1)}$ or $\psi^{(-1)}$ is defined as in Eq. (8.4), except that we now take δ_s to be one if the sum of the spin variables s_j is 1 or -1 respectively. Note, however, that since we found above that the Hamiltonian with

$$w_{ij} = \frac{(z_i + z_j)}{(z_i - z_j)} \quad (8.35)$$

does not couple the two legs, each of these terms are individually zero energy eigenstates of the Hamiltonian. The ground state is hence degenerate in that case.

8.3.4 Large Λ limit and the product of singlets

In appendices E and F, we show that the wavefunction (8.4) reduces to a product of $N/2$ singlets in the limit of sufficiently large Λ for almost all choices of the lattice coordinates (8.23). Without loss of generality, we will here label the lattice sites such that

$$f(j+1) \geq f(j) \text{ for all } j \in \{1, 2, \dots, N-1\}. \quad (8.36)$$

Stated more precisely, we find that

$$\Psi_{s_1, s_2, \dots, s_N}(z_1, z_2, \dots, z_N) \propto \Psi_s(s_1, s_2) \otimes \Psi_s(s_3, s_4) \otimes \dots \otimes \Psi_s(s_{N-1}, s_N) \quad (8.37)$$

when

$$\exp\{\Lambda[f(2j+1) - f(2j)]\} \gg 1 \text{ for all } j \in \{1, 2, \dots, N/2 - 1\}. \quad (8.38)$$

Here,

$$\Psi_s(s_{2j-1}, s_{2j}) = (|+1, -1\rangle - |-1, +1\rangle)/\sqrt{2} \quad (8.39)$$

is the singlet wavefunction of the spins s_{2j-1} and s_{2j} . Note that Eq. (8.38) can only be fulfilled provided

$$f(2j+1) > f(2j) \text{ for all } j \in \{1, 2, \dots, N/2 - 1\}. \quad (8.40)$$

The wavefunction hence reduces to a product of singlets for sufficiently large Λ unless there is a j for which lattice site number $2j+1$ and lattice site number $2j$ are placed on opposite sides of the cylinder. The same result applies also in the case, where the σ_k in Eq. (8.23) are general phase factors. Finally, we comment that the pattern of singlets in the state is fixed, because the model has open boundary conditions per construction. It is hence always the first spin that forms a singlet with the second, the third spin that forms a singlet with the fourth, and so on.

8.4 Uniform one-dimensional spin chain

In this section, we study the one-dimensional model obtained by choosing

$$z_j = \exp(2\pi\lambda j/N) \quad (8.41)$$

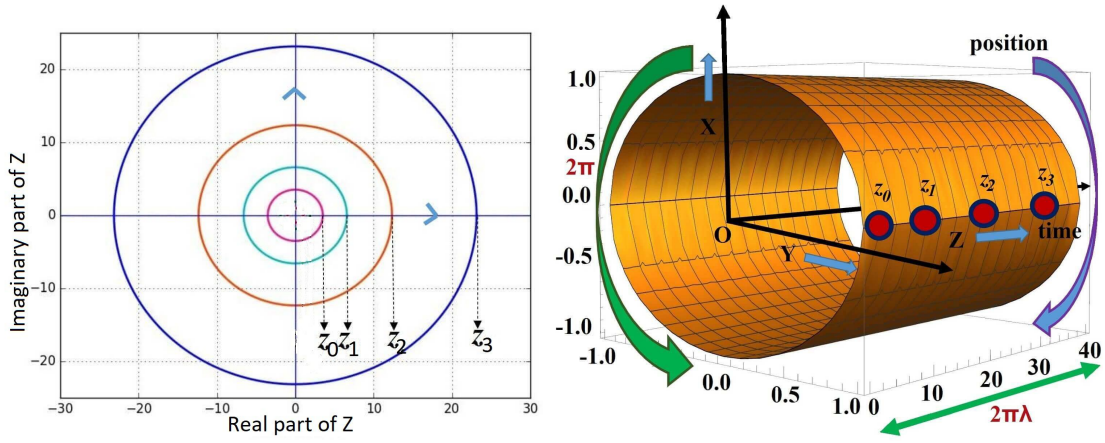


Figure 8.2.: Mapping of the spin positions from the complex plane, as shown in the upper plot, to the cylinder surface, as shown in the lower plot, for the uniform one-dimensional chain. The radii of the consecutive circles in the plane are $z_j = \exp(2\pi\lambda j/N)$.

in more detail. Here, N is the number of sites in the chain, which must be even, and we shall take $j \in \{0, 1, \dots, N-1\}$. The positive number λ controls the ratio between the total length of the chain, which is $2\pi\lambda$, and the circumference of the cylinder, which is 2π . Note that in this case a possible choice of ω_{jk} is

$$w_{jk} = \frac{z_j + z_k}{z_j - z_k} = \frac{1}{\tanh[\pi\lambda(j-k)/N]}. \quad (8.42)$$

Figure 8.2 shows the lattice both in the complex plane and on the cylinder. In the following, we first study the physics of the ground state by computing the spin-spin correlations and the Renyi entropy. We then investigate the spin-spin interaction strengths in the Hamiltonian. Finally, we briefly discuss possibilities to construct models with an odd number of spins.

8.4.1 Spin-spin correlations

The spin-spin correlations are, in general, an important tool to extract information about the physics of a system. The typical situation is that the ground state is either critical with correlations that decay as a power law or noncritical with correlations that decay exponentially. We now take a look at the spin-spin correlations (8.14) for the uniform one-dimensional model by solving Eq. (8.28) numerically. We find that $\langle S_j^z S_k^z \rangle$ is positive for $|j-k|$ even and negative for $|j-k|$ odd. To simplify the plots, we hence only consider the absolute value of the correlations in the following.

Figs. 8.3 and 8.4 show the spin-spin correlations $\langle S_j^z S_k^z \rangle$ for a spin in the bulk of the chain and for a spin on the edge, respectively. For the bulk spin, we fix $j = N/2$ and plot the correlations as a function of k for $k > j$, and for the edge spin, we fix $j = 0$ and plot the correlations as a function of k . These figures show several interesting features, as we now discuss.

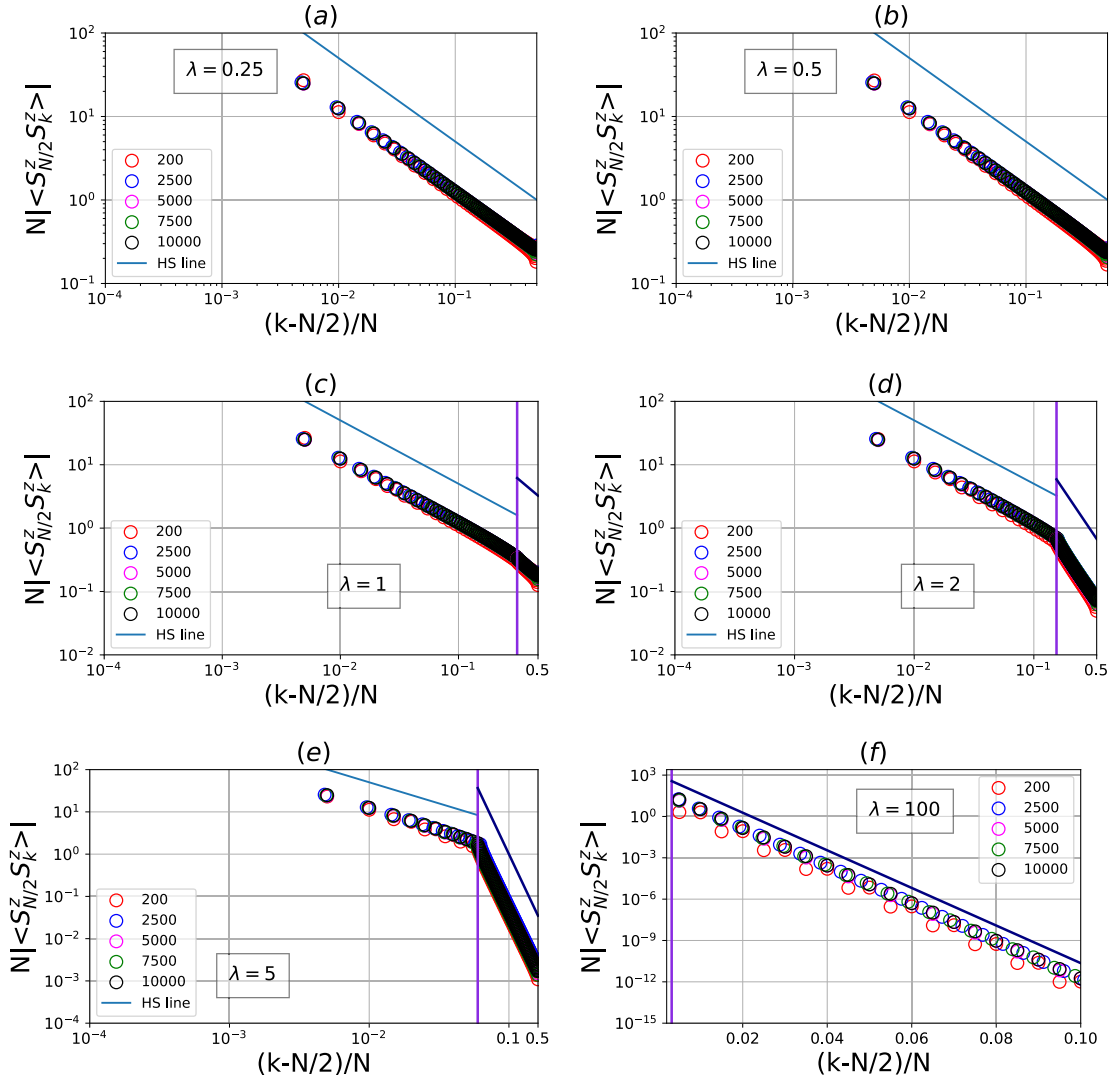


Figure 8.3.: Absolute value of the spin-spin correlation $\langle S_{N/2}^z S_k^z \rangle$ for the uniform one-dimensional chain as a function of $(k - j)/N$ for $j = N/2$, which is the bulk spin, and $k \in \{N/2 + 1, N/2 + 2, \dots, N - 1\}$. For clarity we plot only some of these k values. The different plots are for different values of λ , and there are $N = 200$, as symbolized by red circles, $N = 2500$, as symbolized by blue circles, $N = 5000$, as symbolized by magenta circles, $N = 7500$, as symbolized by green circles, or $N = 10000$, as symbolized by black circles, spins in the chain. Note that in (c-f) the x -axis is in log scale to the left of the vertical line and in linear scale to the right of the vertical line. For $\lambda = 0.25$, the correlations are seen to follow a power law, and for $\lambda = 100$, the correlations decay exponentially. For intermediate values of λ , the correlations decay as a power law for short distances and exponentially for large distances, and the transition is seen to occur approximately at the vertical line, which is positioned at $(k - N/2)/N = 1/(\pi\lambda)$. In the standard one-dimensional Haldane-Shastry model the correlations decay as the inverse of the distance, and in the region, where the x -axis is in log scale, we plot a straight line with slope -1 for comparison. The straight line plotted in the region to the right of the vertical line is proportional to $\exp(-\pi\lambda(k - N/2)/N)$.

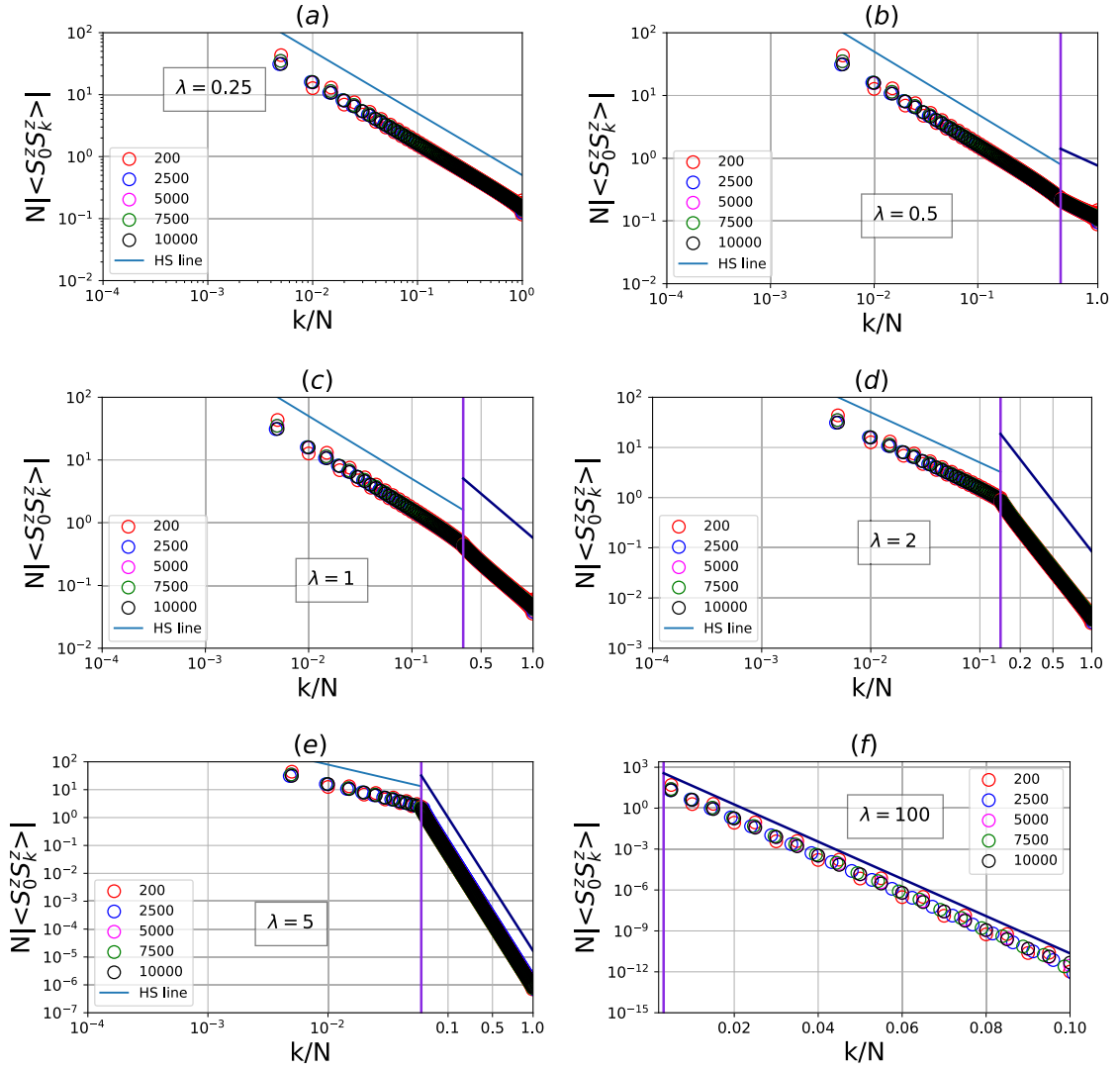


Figure 8.4.: Absolute value of the spin-spin correlation $\langle S_j^z S_k^z \rangle$ for the uniform one-dimensional chain as a function of $(k - j)/N$ for $j = 0$, which is the edge spin, and $k \in \{1, 2, \dots, N - 1\}$. For clarity we plot only some of these k values. The different plots are for different values of λ , and there are $N = 200$, as symbolized by red circles, $N = 2500$, as symbolized by blue circles, $N = 5000$, as symbolized by magenta circles, $N = 7500$, as symbolized by green circles, or $N = 10000$, as symbolized by black circles, spins in the chain. Note that in (c-f) the x -axis is in log scale to the left of the vertical line and in linear scale to the right of the vertical line. For $\lambda = 0.25$, the correlations are seen to follow a power law, and for $\lambda = 100$, the correlations decay exponentially. For intermediate values of λ , the correlations decay as a power law for short distances and exponentially for large distances, and the transition is seen to occur approximately at the vertical line, which is positioned at $k/N = 1/(\pi\lambda)$. In the standard one-dimensional Haldane-Shastry model the correlations decay as the inverse of the distance, and in the region, where the x -axis is in log scale, we plot a straight line with slope -1 for comparison. The straight line plotted in the region to the right of the vertical line is proportional to $\exp(-\pi\lambda k/N)$.

For $\lambda = 0.25$, we observe that the correlations decay as the power law

$$|\langle S_j^z S_k^z \rangle| \propto |j - k|^{-1}. \quad (8.43)$$

Here, $|j - k|$ is proportional to the distance between the spins. This is the same behavior as for the standard one-dimensional Haldane-Shastry model, where the correlations also decay as the inverse of the distance between the spins when $|j - k|$ is large compared to 1 and small compared to N , as we shown in the discussion below Eq. (8.15). In the opposite limit of large λ , we observe that the correlations decay exponentially. In this limit, the model is hence qualitatively different from the standard one-dimensional Haldane-Shastry model. This is expected, since we found in Sec. 8.3.4 that the state reduces to a product of singlets in the large λ limit.

Given the qualitatively different behavior for small and large λ , the natural next question is how the transition from one behavior to the other occurs. The figures show that the transition happens gradually in the sense that for intermediate λ , the correlations decay as a power law for short distances and exponentially for large distances. As λ increases, the range of distances for which there is exponential decay increases. A look at Eq. (8.42) suggests that the point

$$\frac{|j - k|}{N} = \frac{1}{(\pi\lambda)} \quad (8.44)$$

plays a special role, and from the figures we observe that the transition from power law to exponential decay indeed occurs around this point. The power law decay at short distances again follows the behavior

$$|\langle S_j^z S_k^z \rangle| \propto |j - k|^{-1}, \quad (8.45)$$

and at long distances the exponential decay is described by

$$|\langle S_j^z S_k^z \rangle| \propto \frac{1}{N} \exp\left(-\frac{\pi\lambda |j - k|}{N}\right). \quad (8.46)$$

The curves in the figures are practically independent of the number of spins N , when N is large enough, and this shows that the proportionality constants in Eqs. (8.45) and (8.46) are independent of N . The independence of N is also interesting because it shows that the possibility to have power law decay at short distances and exponential decay at long distances remains in the thermodynamic limit.

It is relevant to note that in the above discussion, short and long distances refer to $|j - k|/N$ taking a value close enough to zero and close enough to unity, respectively. The distances in question are hence measured relative to the length of the chain and do not refer to how many spins there are between the two considered spins. When $|j - k|/N$ is kept fixed, the number of spins between the considered spins grows linearly with N , when N increases. We could instead consider the correlations between spins that are $|j - k|$

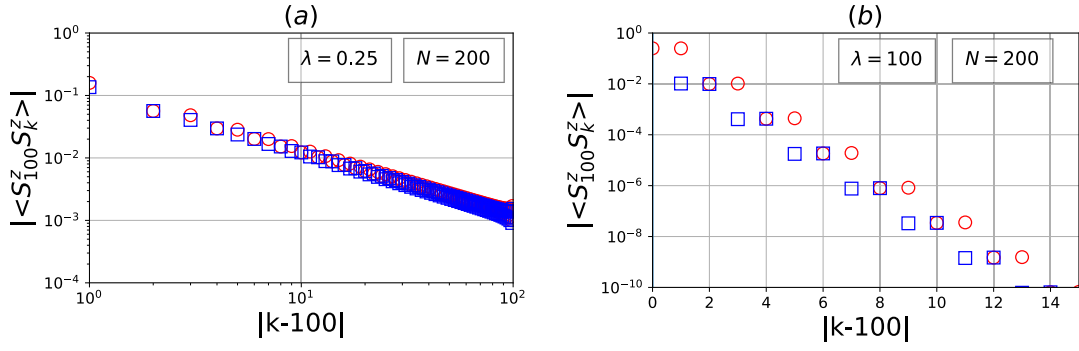


Figure 8.5.: Absolute value of the spin-spin correlation $\langle S_j^z S_k^z \rangle$ for the uniform one-dimensional chain as a function of $|k - j|$ for $j = 100$, which is the bulk spin, and $k \in \{0, 1, \dots, 199\}$. We have plotted both halves of the spin chain. The red circles are for $k - j \geq 0$, and the blue squares are for $k - j < 0$. Note that the spin with $k = 100$ is more strongly correlated with the spin with $k = 101$ than with the spin with $k = 99$.

spins apart with $|j - k|$ of order unity. Since the transition from power law to exponential decay occurs around

$$|j - k| = \frac{N}{(\pi\lambda)}, \quad (8.47)$$

we are always on the left hand side of the transition, when N is large enough. In other words, if we take the thermodynamic limit $N \rightarrow \infty$ with fixed $|j - k|$, the correlations decay as the inverse of the distance as in the one-dimensional Haldane-Shastry model, independent of λ .

We have only plotted the correlations for $k - j > 0$ in Fig. 8.3 for clarity. The conclusions regarding power law and exponential decay are the same for $k - j < 0$. It is interesting to note, however, that there is not a perfect symmetry between the left and the right hand side of the chain, simply because the number of spins in the chain is even. This means that on one side of the bulk spin there is an odd number of spins, and on the other side of the bulk spin there is an even number of spins. We find that the bulk spin is generally more strongly correlated with the first neighbor sitting on the side with an odd number of spins than with the first neighbor sitting on the side with an even number of spins. This effect is particularly strong for large λ , where the bulk spin forms a singlet with the nearest neighbor sitting on the side, where there is an odd number of spins. The effect is illustrated in Fig. 8.5 for both small and large λ . We note that this effect does not occur in the standard HS model, since this model is defined on a circle, where there is symmetry between the left and the right hand side.

We noted in Sec. 8.3.4 that the chain is perfectly dimerized into a product of singlets in the limit $\lambda \rightarrow \infty$. To investigate the behavior for large but finite λ , we plot numerical results for the dimer order parameter in Fig. 8.6 for $\lambda = 100$ and $N = 200$. Since our model is $SU(2)$ invariant, we have

$$\langle S_j^x S_{j+1}^x \rangle = \langle S_j^y S_{j+1}^y \rangle = \langle S_j^z S_{j+1}^z \rangle, \quad (8.48)$$

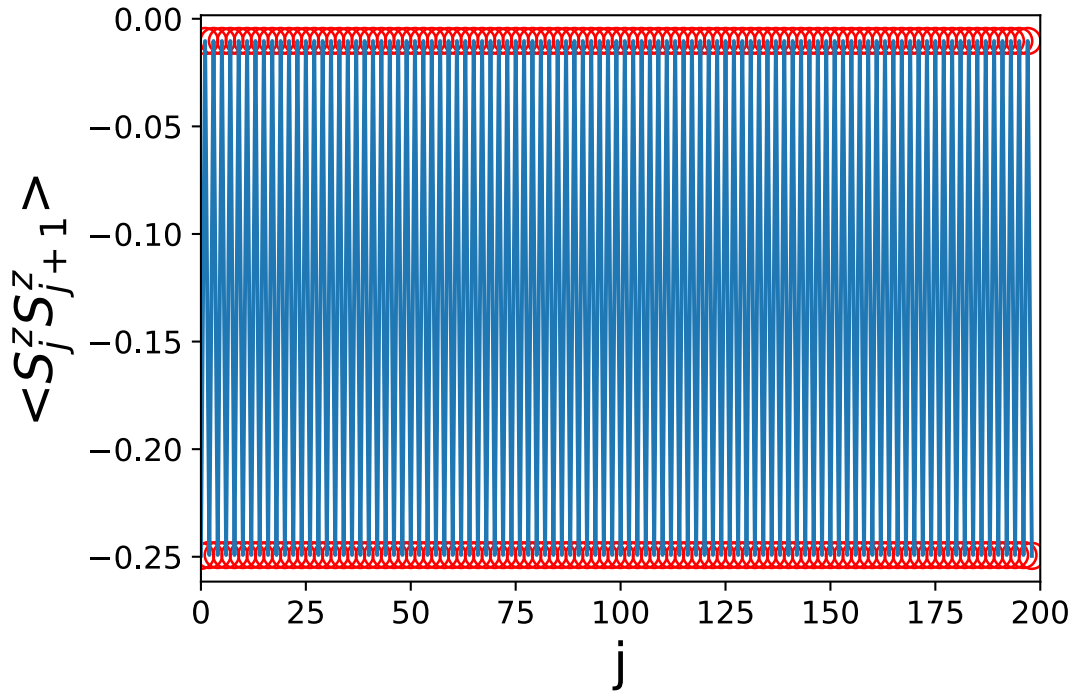


Figure 8.6.: Variation of $\langle S_j^z S_{j+1}^z \rangle$ as a function of j for the one-dimensional spin chain with $\lambda = 100$ and $N = 200$. It is seen that for j even, spin number j is almost perfectly anticorrelated with spin number $j + 1$ and almost not correlated with spin number $j - 1$.

and it is sufficient to focus on $\langle S_j^z S_{j+1}^z \rangle$ only. The figure shows that $\langle S_j^z S_{j+1}^z \rangle$ oscillates as a function of j . For j even, $\langle S_j^z S_{j+1}^z \rangle$ is close to -0.25 , and for j odd, $\langle S_j^z S_{j+1}^z \rangle$ is almost zero. This is the expected behavior for a chain that is close to a product of singlets.

Finally, we note that the Hamiltonian is nonlocal, and we cannot conclude from the behavior of the correlation functions, whether there is an energy gap or not to the first excited state in the thermodynamic limit.

8.4.2 Renyi Entropy of order two

The Renyi entropy is another general tool to extract important information about the behavior of a spin system. As already noted in (8.18), the Renyi entropy grows logarithmically with subsystem size for critical systems. For noncritical systems, the entanglement entropy of the ground state typically follows an area law, which means that the Renyi entropy grows linearly with the boundary area of the selected region. In one-dimension, the boundary area is independent of subsystem size, and the Renyi entropy is hence constant.

In the computations below, we take part A of the system to be the first x spins in the chain and part B to be the remaining spins. Since the chain is symmetric under inversion of the direction of the spin chain, we have that the Renyi entropy of the first x spins is the

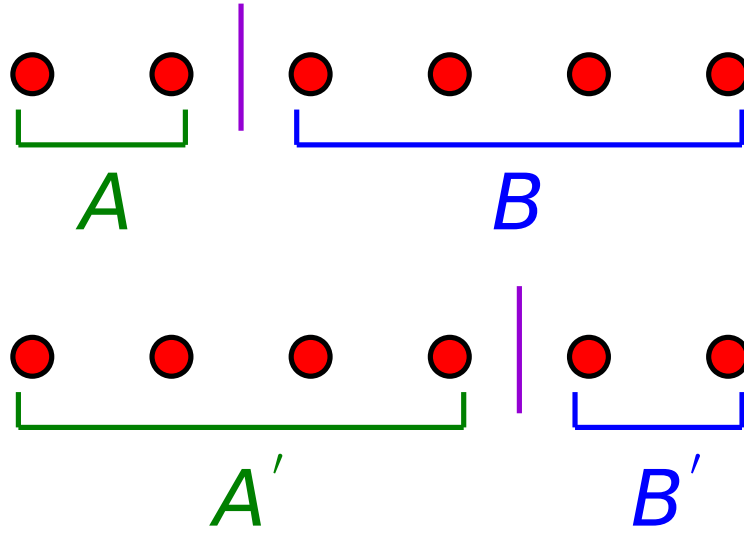


Figure 8.7.: Relation between Renyi entropies for different cuts of a spin chain in a pure quantum state. The upper part of the figure shows a spin chain partitioned into two regions A and B , and the lower part of the figure shows the same spin chain partitioned into two different regions A' and B' . We choose the regions such that A and B' contain x spins each, while A' and B contain $N - x$ spins each. It is always the case that $S_A = S_B$ and $S_{A'} = S_{B'}$, but it is not necessarily the case that S_A and $S_{A'}$ are the same. When the state of the chain has inversion symmetry, however, it is ensured that $S_A = S_{B'}$, and hence that $S_A = S_{A'}$.

same as the Renyi entropy of the first $N - x$ spins. This statement is explained pictorially in Fig. 8.7. We therefore only compute the Renyi entropy for $x \leq N/2$. It is more time consuming to compute the Renyi entropy than the correlations, since we use Monte-Carlo simulations. We shall therefore restrict ourselves to $N = 200$ throughout. The results are shown in Fig. 8.8.

For $\lambda = 100$, we observe that the Renyi entropy is close to zero whenever x is even and close to 0.7 whenever x is odd. This is a consequence of the results in Sec. 8.3.4. When x is even, we do not cut any of the singlets apart, and there are almost no correlations between the two parts. When x is odd, we break one singlet into two when cutting the chain, and the entropy is close to $\ln(2) \approx 0.693$.

For $\lambda = 0.25$, the correlations follow a power law decay, and we hence expect that the Renyi entropy is linear in $\ln(x)$ for $1 \ll x \ll N$, possibly plus some oscillations. From Eq. (8.18), we get the leading order behavior

$$S_x \approx c \frac{\ln(x)}{8} + \text{constant}. \quad (8.49)$$

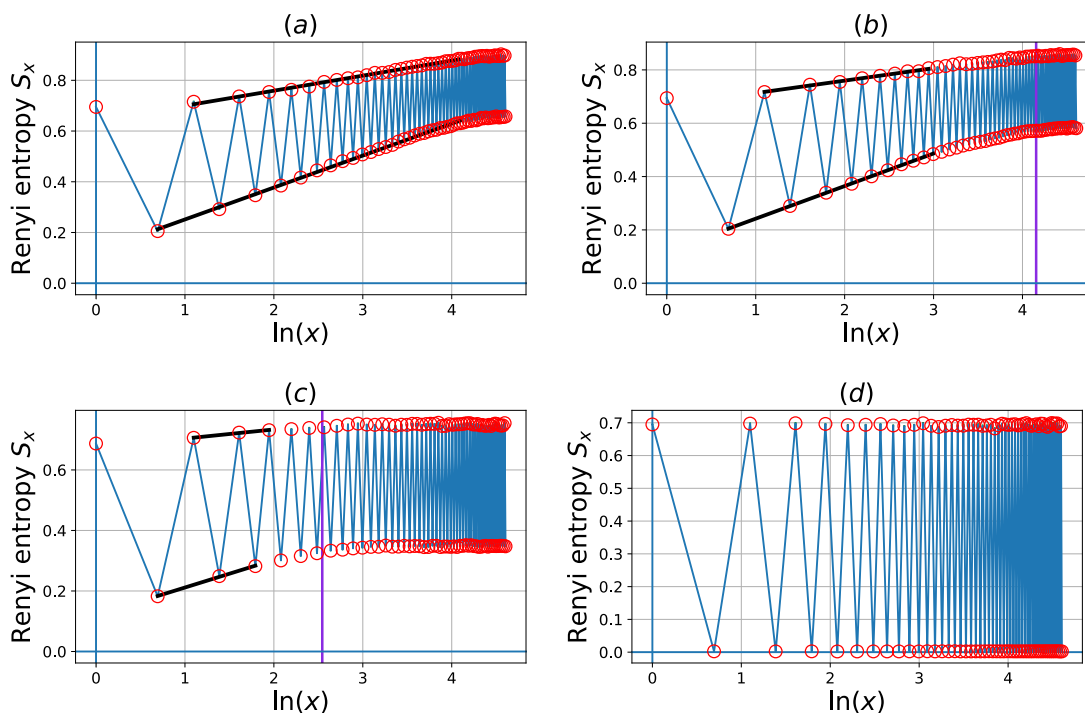


Figure 8.8.: Renyi entanglement entropy S_x of order two for the uniform one-dimensional chain versus $\ln(x)$, when the subsystem consists of the spins $0, 1, \dots, x-1$. There are $N = 200$ spins in the chain, and in (a) $\lambda = 0.25$, in (b) $\lambda = 1$, in (c) $\lambda = 5$, and in (d) $\lambda = 100$. The vertical lines in (b) and (c) are at $x = N/(\pi\lambda)$. In (a) this line is to the right of the plotted region and in (d) it is to the left of the plotted region. In (a-c), we show two linear fits to the upper and the lower set of points, respectively. In (a, b, c), the slopes of the upper lines are (0.059, 0.047, 0.030) respectively, and the slopes of the lower lines are (0.126, 0.122, 0.091) respectively.

For the one-dimensional Haldane-Shastry model, the central charge is $c = 1$, and it is hence relevant to compare the entropy plot to a straight line with slope $1/8$. Figure 8.8(a) shows that the entropy oscillates with period 2. If we look only at the points with x even in the region $1 \ll x \ll N$, the points approximately fall on a straight line with slope 0.126. This fits with the expected value $1/8$ within the uncertainty of choosing the fitting region. If we look at the points with odd x , however, the slope of the line is around 0.059, which does not fit with $1/8$. It may be that this discrepancy is related to the asymmetry observed in Fig. 8.5. For $\lambda = 1$, the slopes of the two fitted lines have changed to 0.122 and 0.047. It is interesting that the slope for x even is again close to $1/8$, while the slope for x odd seems to change with λ . For $\lambda = 5$, both slopes are reduced, but the results are likely inaccurate, since the number of points in the region with linear increase is small.

For intermediate values of λ , we observe a transition from a linear increase with $\ln(x)$ for small x to an area law behavior for large x . The figure shows that the transition occurs approximately at

$$x = \frac{N}{\pi\lambda}. \quad (8.50)$$

This fits with the behavior of the correlations, where we saw a transition from power law decay to exponential decay.

8.4.3 Strengths of the spin-spin interactions

To investigate the Hamiltonian that gives rise to the physics discussed above, we now take a closer look at the spin-spin interaction strengths (8.21) for the choice

$$w_{ij} = \frac{(z_i + z_j)}{(z_i - z_j)}. \quad (8.51)$$

We first investigate some limiting cases analytically, and after that present numerical results for different values of N and λ .

(a). Behavior for small and large λ with N fixed

We first consider the limit, where $2\pi\lambda \ll 1$. In this case

$$w_{ij} = \frac{e^{2\pi i\lambda/N} + e^{2\pi j\lambda/N}}{e^{2\pi i\lambda/N} - e^{2\pi j\lambda/N}} \approx \frac{N}{\pi(i-j)\lambda} \quad (8.52)$$

and hence

$$b_{i,i+d} \approx \frac{N^2}{6\pi^2\lambda^2d^2} \left(1 + \sum_{k(\neq i\neq i+d)} \frac{d^2}{(k-i)(k-i-d)} \right). \quad (8.53)$$

The sum can be simplified by utilizing

$$\frac{d}{(k-i)(k-i-d)} = \frac{1}{k-i-d} - \frac{1}{k-i}. \quad (8.54)$$

For $d > 0$ this leads to

$$b_{i,i+d} \approx \frac{N^2}{6\pi^2\lambda^2d^2} \left[3 - \sum_{k=1}^d \left(\frac{d}{k+i-i_0} - \frac{d}{k-N+i-i_0} \right) \right], \quad (8.55)$$

where i_0 is the lowest possible value of i (i.e., $i = i_0$ for the left most spin in the chain). The result for $d < 0$ is obtained by taking $d \rightarrow -d$ and $i - i_0 \rightarrow N - 1 - (i - i_0)$ in Eq. (8.55). If we consider a spin in the bulk of the chain, the expression for $b_{i,i+d}$ simplifies further to

$$b_{i,i+d} \approx \frac{N^2}{2\pi^2\lambda^2d^2}. \quad (8.56)$$

In this limit, we hence observe that the interaction strength is inversely proportional to the square of the distance between the spins as in the original one-dimensional Haldane-Shastry model. In the one-dimensional Haldane-Shastry model, the spins are sitting on a circle, but as long as $|d| \ll N$, the chord distance is approximately the same as $|d|$, as already noted in Eq. (8.13). For small λ and large N , we hence expect that the uniform

one-dimensional chain model behaves similarly to the one-dimensional Haldane-Shastry model, except for possible edge effects. This is consistent with the observations made in the last two sections.

The result derived above for $2\pi\lambda \ll 1$ is also a good approximation for spins in the bulk under the less strict condition $2\pi\lambda|i-j| \ll N$. Although in this case there are some values of k for which Eq. (8.52) does not provide a good approximation for w_{ki} and w_{kj} , those terms are much smaller than those for which Eq. (8.52) is a good approximation. The error made by nevertheless using Eq. (8.52) for all k is hence small.

Next we consider the limit $2\pi\lambda \gg N$. We have

$$b_{ij} = \frac{1}{6} \frac{(e^{\frac{2\pi\lambda i}{N}} + e^{\frac{2\pi\lambda j}{N}})^2}{(e^{\frac{2\pi\lambda i}{N}} - e^{\frac{2\pi\lambda j}{N}})^2} + \frac{1}{6} \sum_{k(\neq i \neq j)} \frac{(e^{\frac{2\pi\lambda k}{N}} + e^{\frac{2\pi\lambda i}{N}})(e^{\frac{2\pi\lambda k}{N}} + e^{\frac{2\pi\lambda j}{N}})}{(e^{\frac{2\pi\lambda k}{N}} - e^{\frac{2\pi\lambda i}{N}})(e^{\frac{2\pi\lambda k}{N}} - e^{\frac{2\pi\lambda j}{N}})}. \quad (8.57)$$

Now, for $2\pi\lambda \gg N$, we have

$$\frac{e^{\frac{2\pi\lambda k}{N}} + e^{\frac{2\pi\lambda j}{N}}}{e^{\frac{2\pi\lambda k}{N}} - e^{\frac{2\pi\lambda j}{N}}} \approx \text{sign}(k - j), \quad (8.58)$$

and hence

$$b_{ij} \approx \frac{1}{6} (N - 2|j - i| + 1). \quad (8.59)$$

In this case, the interaction strength is decaying linearly, and the range of the interaction is determined by the system size. We would hence expect a behavior of the system that is different from the one-dimensional Haldane-Shastry model. This is consistent with the observation that the ground state is a product of singlets in that limit.

(b). Numerical results

We plot results for $|b_{N/2,j}|$ for different values of λ and N in Fig. 8.9. The limit (8.56) is shown as the red dotted line in the plots. This behavior is followed as long as $|j - N/2|/N$ is small enough, and this suggests that there is a connection between this behavior of the interaction strengths and the power law decay of correlations in the ground state. The limiting behavior (8.59) is approximately followed in panel (f).

An important conclusion from the plots is that the Hamiltonian is, generally, nonlocal. We also see that $|b_{N/2,j}|$ does not follow a simple decay law over the entire range of $|j - N/2|/N$ values, but changes behavior qualitatively depending on the distance between the spins. Motivated by the observations for the spin-spin correlations, one may speculate if there is a change of behavior at

$$\frac{|j - N/2|}{N} = \frac{1}{\pi\lambda}. \quad (8.60)$$

We do, however, not observe sharp transitions at these points in the plots. This may happen since the correlations between spin number $N/2$ and spin number j are not

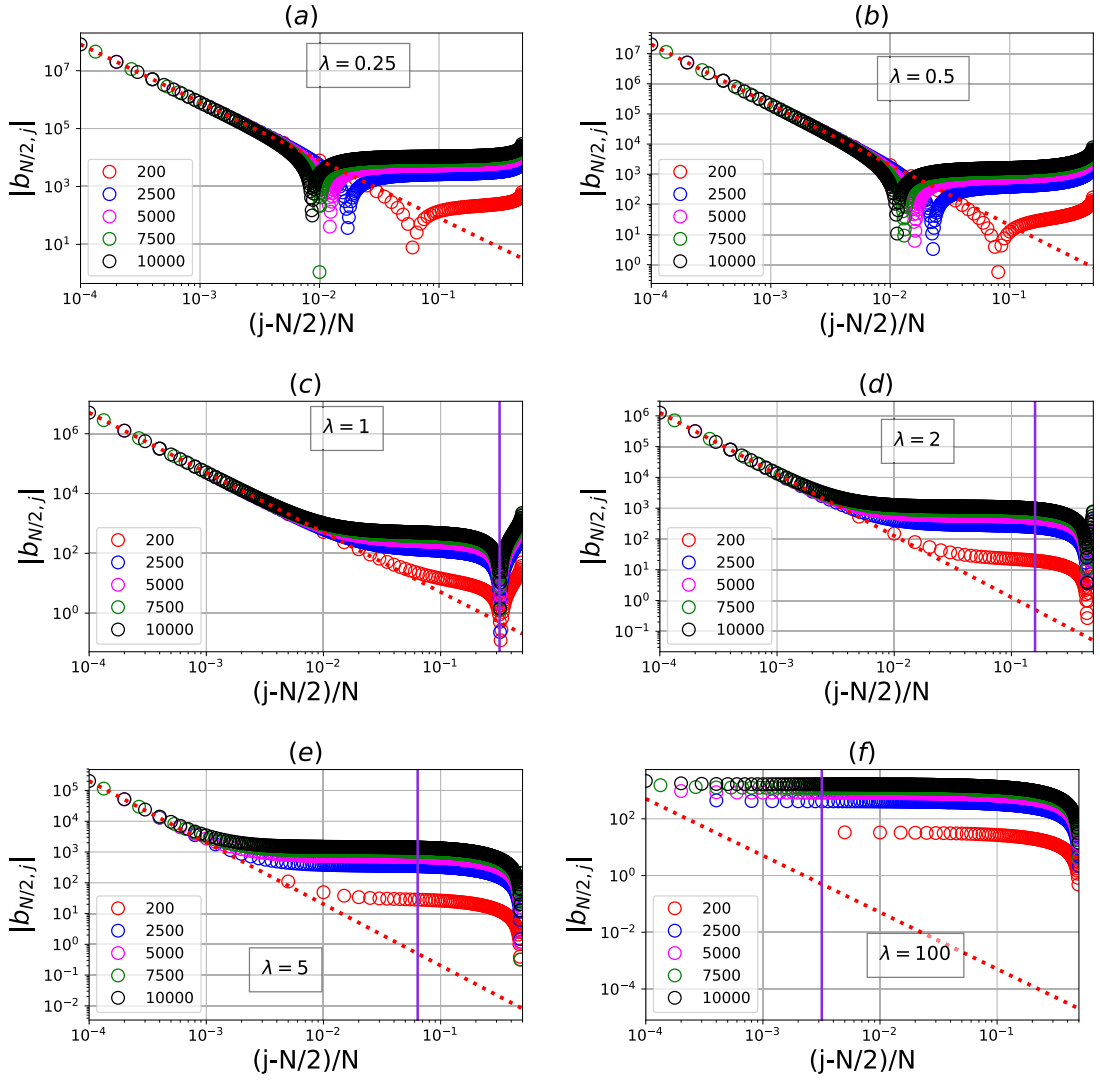


Figure 8.9.: We plot the absolute value of the spin-spin interaction strength b_{kj} , from Eq. (8.21), for the uniform one-dimensional chain as a function of $|j-k|/N$ for $k = N/2$, which is the bulk spin, and $j \in \{N/2 + 1, N/2 + 2, \dots, N - 1\}$. For clarity we plot only some of these j values. The different plots are for different values of λ , and there are $N = 200$, as symbolized by red circles, $N = 2500$, as symbolized by blue circles, $N = 5000$, as symbolized by magenta circles, $N = 7500$, as symbolized by green circles, or $N = 10000$, as symbolized by black circles, spins in the chain. The red dotted line in each plot is the limit (8.56), and the vertical lines in the plots (c-f) are positioned at $(j - N/2)/N = 1/(\pi\lambda)$.

determined by $b_{N/2,j}$ alone, but depend on all the b_{jk} . The fact that $|b_{N/2,j}|$ changes behavior depending on distance in this model suggests that such changes may be a general mechanism to obtain models, where the correlations follow different decay laws depending on the distance between the spins.

Finally, we note that there is a whole family of two-body Hamiltonians having the analytical state as ground state. There are hence many different, possible behaviors of b_{jk} , and the results presented here show only one example.

8.4.4 Spin chains with an odd number of spins

We have only considered spin chains with an even number of spins so far, since the wavefunction (8.4) is zero unless the total number of spins is even. One may speculate, however, if it is possible to decouple one of the spins from all the others by moving it infinitely far away and in this way obtain a model for a spin chain with an odd number of spins. We show here that this is possible for general λ , but the resulting model does not have the natural property to be symmetric under inversion of the direction of the spin chain.

We move the N th spin infinitely far away from the others by taking $z_N \rightarrow \infty$ along the positive real axis in the complex plane. With the definition

$$w_{ij} = \frac{(z_i + z_j)}{(z_i - z_j)}, \quad (8.61)$$

we have $w_{iN} \rightarrow -1$, and with the definition

$$w_{ij} = \frac{1}{(z_i - z_j)}, \quad (8.62)$$

we have $w_{iN} \rightarrow 0$. It follows from Eq. (8.21) that the spin interaction b_{iN} between the i th and the N th spin is zero for all i for the choice

$$w_{ij} = \frac{1}{(z_i - z_j)}, \quad (8.63)$$

but not for the choice

$$w_{ij} = \frac{(z_i + z_j)}{(z_i - z_j)}. \quad (8.64)$$

The N th spin hence decouples from the others in the former case, but not in the latter. It is, however, the latter choice that gives a Hamiltonian that is symmetric under inversion of the direction of the chain.

For small λ , it is possible to have a chain with an odd number of spins and a Hamiltonian that is symmetric. This follows from Eq. (8.21) and

$$w_{ij} = \frac{1}{(z_i - z_j)} \approx \frac{N}{2\pi\lambda(i - j)}. \quad (8.65)$$

Another way to obtain chains with an odd number of spins for small λ is to consider a ladder model with an odd number of spins on each leg as already demonstrated in Sec. 8.3.3.

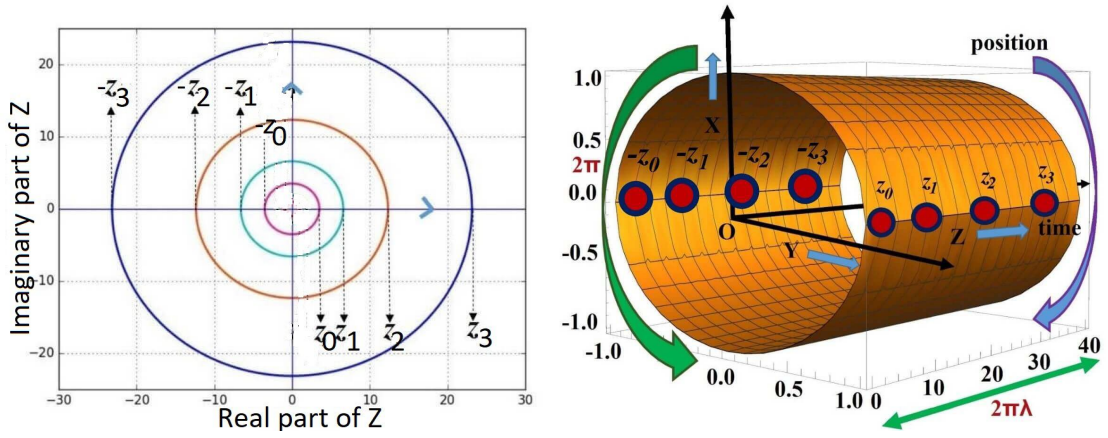


Figure 8.10.: Mapping of the spin positions from the complex plane, as shown in the upper plot, to the cylinder surface, as shown in the lower plot, for the uniform ladder. The radii of the consecutive circles in the plane are $\exp(2\pi\lambda j/N)$.

8.5 Uniform ladder model

In this section, we investigate the uniform ladder model obtained by choosing

$$z_{j\pm} = \pm \exp(2\pi\lambda j/N). \quad (8.66)$$

Here, N is the total number of spins, which must be even, and $j \in \{0, 1, \dots, N/2 - 1\}$. Note that $j+$ and $j-$ refers to spin number j on the front and back of the cylinder respectively. The parameter $\lambda/2$ determines the ratio between the length of the ladder, which is $\pi\lambda$, and the circumference of the cylinder, which is 2π . The mapping from the complex plane to the cylinder is shown in Fig. 8.10. In the complex plane, the spins are along both the positive and the negative part of the real axis, and on the cylinder they are placed on opposite sides.

8.5.1 Strengths of the spin-spin interactions

From Secs. 8.3.3 and 8.3.4, we know that for λ very small, the ladder decouples into two chains, and for λ very large, each spin on one of the legs forms a singlet with the neighboring spin on the other leg. We hence expect that the legs of the ladder are weakly coupled for small λ and strongly coupled for large λ .

To see what the coupling looks like, we plot the spin-spin interaction strength (8.21) for different values of λ in Fig. 8.11. For $\lambda = 1$, we indeed observe that interactions between spins on different legs are much weaker than the strongest interactions between spins on the same leg. For $\lambda = 100$, the interactions with the neighboring spin on the opposite leg are the strongest. For the intermediate case $\lambda = 10$, the interactions are strongest for neighboring spins on the same leg, but there are also considerable interactions between spins on different legs.

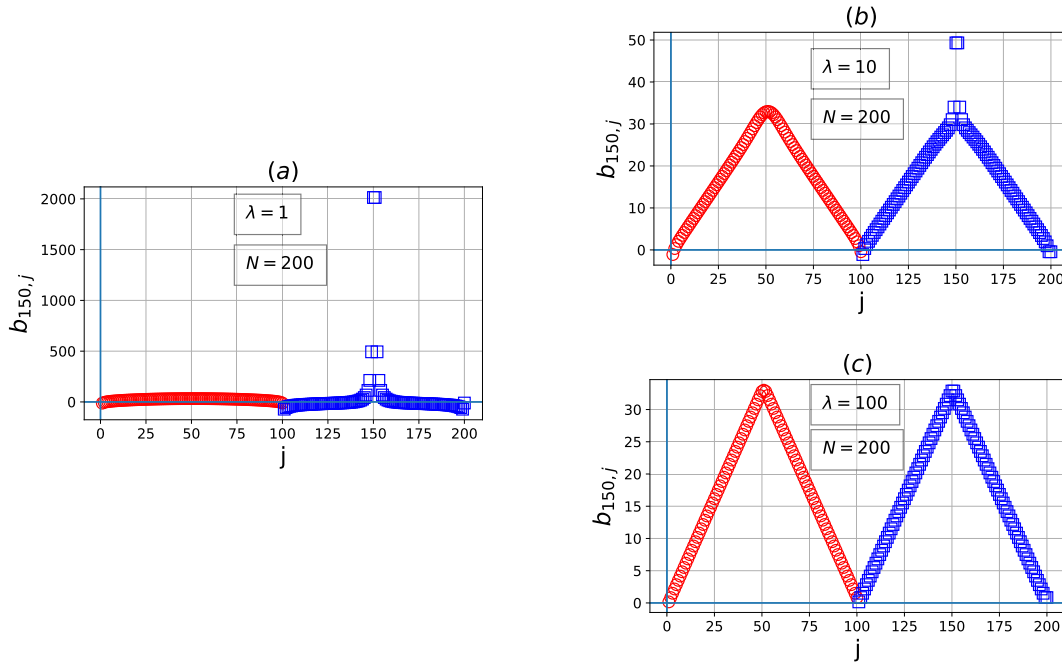


Figure 8.11.: Spin-spin interaction (8.21) between spin number 49– and all other spins for a uniform ladder with $N = 200$ spins. In this plot, we use a numbering such that 1 to 100 are the spins 0+ to 99+ on the front of the cylinder and 101 to 200 are the spins 0– to 99– on the back of the cylinder.

Another important conclusion from the plot is that the spin-spin interactions between spins on the same leg qualitatively display the same behavior as for the chain. We can hence, at least for the middle spin, roughly think of the ladder as two copies of the chain model plus interactions between the two legs. It is also interesting to note that for the larger values of λ , the strength of the spin-spin interaction is approximately the same for spins on the same leg as for spins on opposite legs, except when the distance between the spins is small. Finally, the plots show that the interactions are highly nonlocal for λ large.

8.5.2 Weak coupling

We first consider the case of small λ , where the interactions between the two legs of the ladder are weak. We found in Sec. 8.3.3 that the ladder decouples into two independent spin chain models in the limit of small λ . Here, we take the small, but finite, value $\lambda = 10^{-6}$ and plot the spin-spin correlations and the Renyi entropy in Figs. 8.12 and 8.13, respectively. The plots show results both for the ladder and for two independent spin chains, and we indeed see that these two cases give practically the same values.

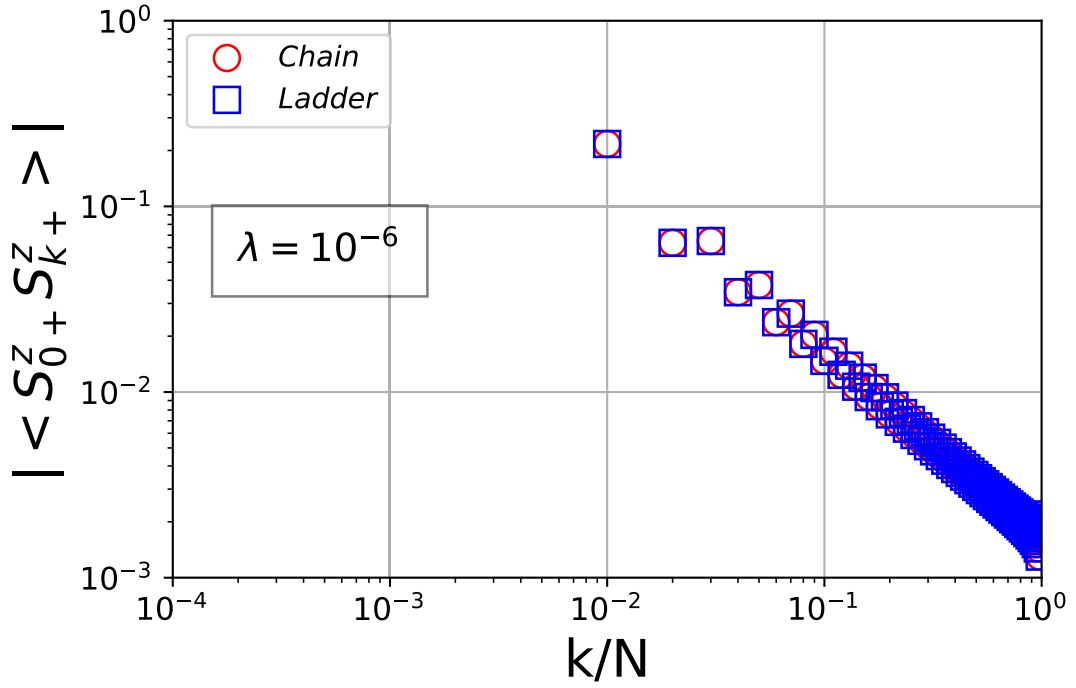


Figure 8.12.: Comparison of the spin-spin correlations for the ladder and the chain. The blue squares show the absolute value of the spin-spin correlation $\langle S_{0+}^z S_{k+}^z \rangle$ between spins on the front of the cylinder for the uniform ladder with $N = 200$ and $\lambda = 10^{-6}$ as a function of $k \in \{1, 2, \dots, 99\}$. The red circles show the same correlations for the chain model obtained by removing all the spins on the back of the cylinder.

8.5.3 Spin-spin correlations

Results for the spin-spin correlations for a bulk spin and different values of λ and N are provided in Fig. 8.14. We find that the sign of the correlations is generally positive or negative if the two spins are separated by an even or odd number of nearest neighbor links respectively. We hence plot only the absolute value of the correlations. For spins on the same leg, it is seen that the correlations follow the same pattern as for the one-dimensional chain. In the region well to the left of the line

$$\frac{(k - N/4)}{N} = \frac{1}{\pi\lambda}, \quad (8.67)$$

the correlations decay as

$$|\langle S_{j+}^z S_{k+}^z \rangle| \propto |j - k|^{-1}, \quad (8.68)$$

and in the region well to the right of the line

$$\frac{(k - N/4)}{N} = \frac{1}{\pi\lambda}, \quad (8.69)$$

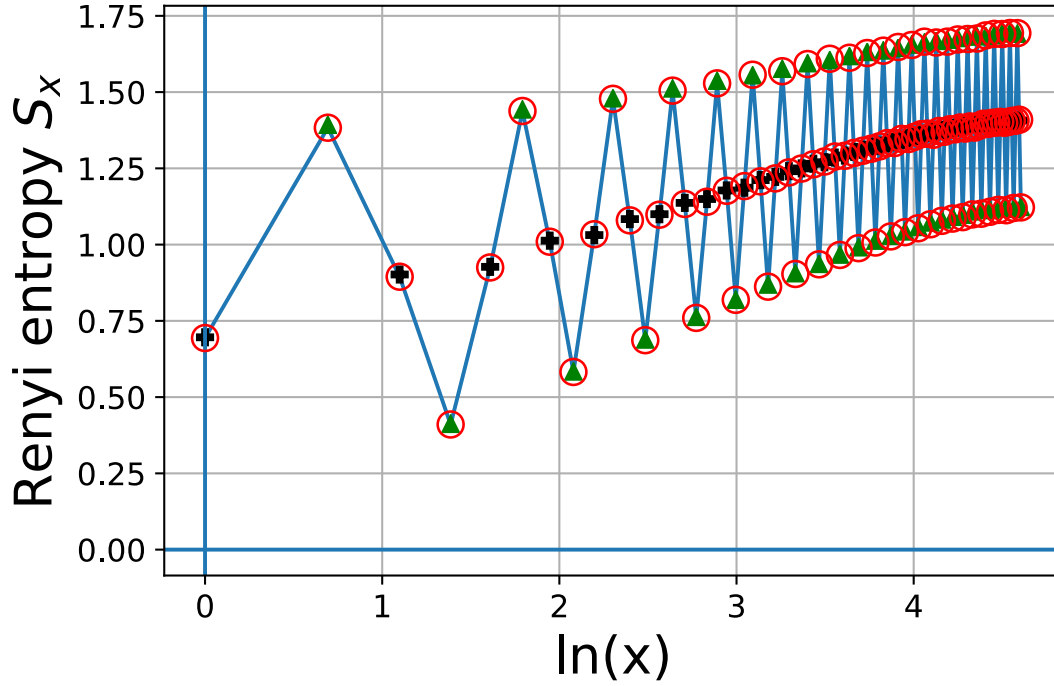


Figure 8.13.: Renyi entropy S_x of order two for the uniform ladder with $N = 200$ and $\lambda = 10^{-6}$. For x even or odd, part A of the system consists of the first $x/2$ or the first $(x+1)/2$ spins on the front leg and the first $x/2$ or the first $(x-1)/2$ spins on the back leg of the ladder respectively. The green triangles and the black pluses show the sum of the entropies for two independent spin chains, when the spin chains are cut at the same positions as the legs of the ladder.

they decay as

$$|\langle S_{j+}^z S_{k+}^z \rangle| \propto \frac{1}{N} \exp\left(-\frac{\pi\lambda |k - N/4|}{N}\right). \quad (8.70)$$

For spins on different legs, we see that the correlations are almost independent of distance in the region well to the left of the line

$$\frac{(k - N/4)}{N} = \frac{1}{\pi\lambda}, \quad (8.71)$$

and well to the right of the line they follow Eq. (8.70) with practically the same proportionality constant as for spins on the same leg. The conclusion is hence that also for the ladder model, we can have a situation, where the nature of the decay changes depending on the distance between the spins.

8.5.4 Renyi Entropy of order two

Results for the Renyi entropy of order two are shown in Fig. 8.15 for $N = 200$ and different values of λ . For $\lambda = 200$, the entropy is close to $\ln(2) \approx 0.693$, whenever the

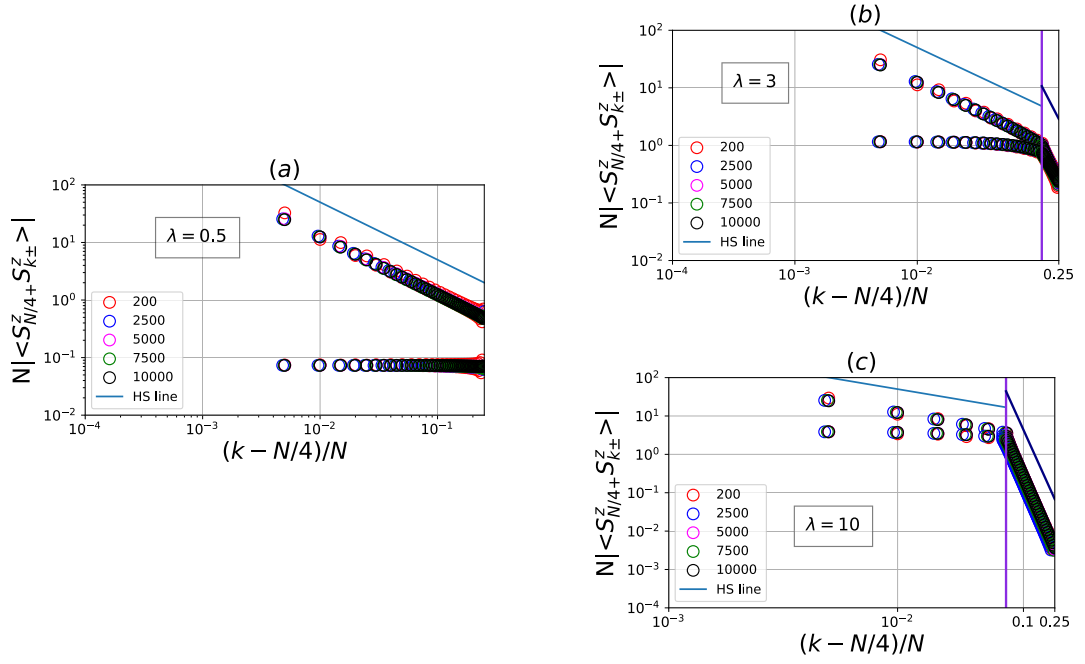


Figure 8.14.: We plot absolute value of the spin-spin correlation $\langle S_{j+}^z S_{k\pm}^z \rangle$ for the uniform ladder as a function of $(k - j)/N$ for $j = N/4$, which is the bulk spin, and $k \in \{N/4 + 1, N/4 + 2, \dots, N/2 - 1\}$. For clarity we plot only some of these k values. In each plot, the upper and lower data points show the correlations of the bulk spin with other spins on the same and opposite leg respectively. The different plots are for different values of λ , and there are $N = 200$, as symbolized by red circles, $N = 2500$, as symbolized by blue circles, $N = 5000$, as symbolized by magenta circles, $N = 7500$, as symbolized by green circles, or $N = 10000$, as symbolized by black circles, spins in the chain. The vertical lines in (b-c) are positioned at $(k - N/4)/N = 1/(\pi\lambda)$. Note that the x -axis is in log scale to the left of these lines and in linear scale to the right of these lines. For $\lambda = 0.5$, the correlations between spins on the same leg are seen to follow a power law decay, while the correlations between spins on opposite legs are much smaller and almost independent of distance. For larger values of λ , we still see a power law decay for short distances, but at longer distances the correlations decay exponentially, both for correlations between spins on the same leg and for correlations between spins on opposite legs. The transition from power law to exponential decay is seen to occur approximately at the vertical lines. In the standard one-dimensional Haldane-Shastry model the correlations decay as the inverse of the distance, and in (a-c) we plot a straight line of slope -1 for comparison in the region where the x -axis is in log scale. The straight lines in the region to the right of the vertical line in the plots (b-c) are proportional to $\exp(-\pi\lambda(k - N/4)/N)$.

partition cuts a singlet apart, and it is close to zero, whenever none of the singlets are cut apart. For $\lambda = 1$, we see that the entropy grows linearly with $\ln(x)$ in the region $1 \ll x \ll N$, except for oscillations. Considering only the points for which x is a multiple of four, which corresponds to both legs being cut after an even number of spins, the fitted slope is 0.23. In the limit of λ going to zero, the two legs of the ladder decouple

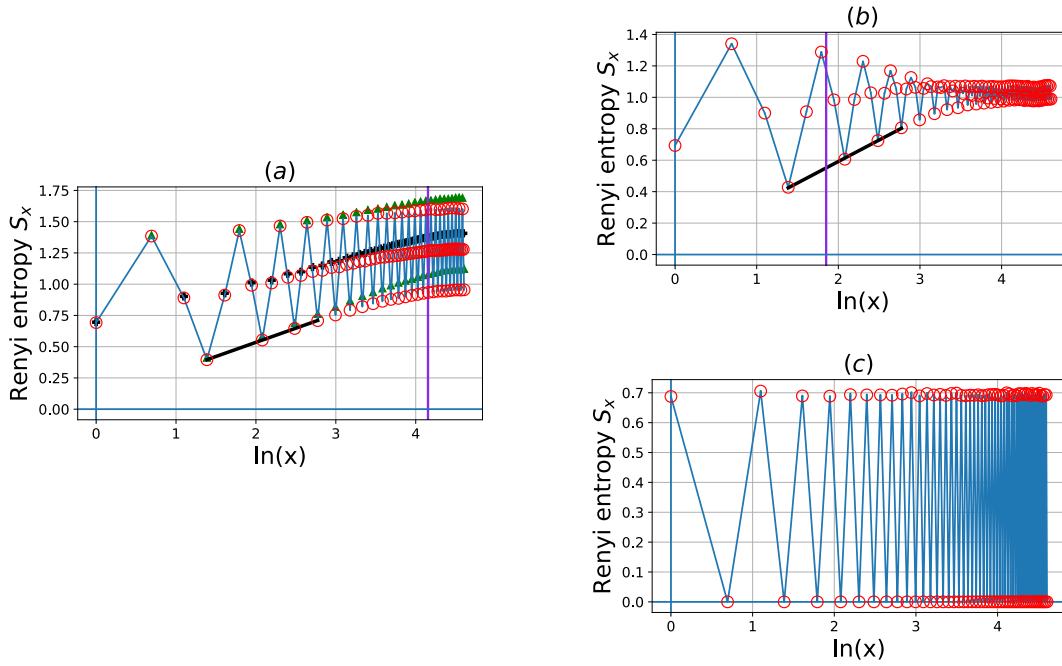


Figure 8.15.: Renyi entropy S_x of order two for the uniform ladder with $N = 200$ and (a) $\lambda = 1$, (b) $\lambda = 10$, and (c) $\lambda = 200$. For x even or odd, part A of the system consists of the first $x/2$ or the first $(x+1)/2$ spins on the front and the first $x/2$ or the first $(x-1)/2$ spins on the back of the cylinder respectively. In (a), we also plot, with green triangles and black pluses, the sum of the entropies for two independent spin chains with the same λ and cut at the same positions as the legs of the ladder. The discrepancies show that the interchain interactions in the ladder model are important for $\lambda = 1$. The straight line fits in (a) and (b) have slope 0.23 and 0.27, respectively. The vertical lines in (a) and (b) are at $x = N/(\pi\lambda)$.

into two independent spin chains, and the entanglement entropy for the ladder is twice the entanglement entropy for a single chain. The relevant slope to compare to is hence $c/4 = 0.25$ rather than $c/8$. It is also seen that the vertical line

$$x = \frac{N}{\pi\lambda} \quad (8.72)$$

is approximately at the transition between linear growth with $\ln(x)$ for small x and area law behavior for large x , after averaging out the oscillations. This is consistent with the results for the correlations in the previous section.

8.6 Conclusions

We have constructed and studied a family of two-body spin models on a cylinder that are related to the one-dimensional Haldane-Shastry model. The usual one-dimensional Haldane-Shastry model corresponds to placing the spins uniformly on a circle around the

cylinder. Here, we have instead placed the spins along one or two lines on the cylinder that are parallel to the cylinder axis. This gives rise to chain and ladder models, respectively. The construction allows us to scale the distance between the spins and hence the length of the chain or ladder independently from the circumference of the cylinder, and we have studied the significance of this extra parameter λ on the physics.

When the length of the chain or ladder is small compared to the circumference of the cylinder for small λ , the properties of the ground state are described by the $SU(2)_1$ Wess-Zumino-Witten universality class. The spin-spin correlations decay as a power law with exponent -1 , and for subsystems consisting of an even number of spins in each of the legs or in the chain, the Renyi entropy of order two grows as the logarithm of the subsystem size with a proportionality constant consistent with a central charge of $c = 1$. There are also some edge effects. A spin in the chain is more strongly correlated with the neighboring spin on the side, where there is an odd number of spins, than with the neighboring spin on the side, where there is an even number of spins. In addition, when the number of spins in the subregion is odd, the proportionality constant in the Renyi entropy is lower than predicted by a critical theory with central charge $c = 1$, and the slope varies with λ . In the small λ limit, the ladder model reduces to a product of two chain models, and the spin-spin interaction strengths for spins in the bulk are inversely proportional to the square of the distance between the spins as in the one-dimensional Haldane-Shastry model. The conclusion is hence that for small λ , the physics of the investigated model is the same as for the one-dimensional Haldane-Shastry model, except for edge effects.

When keeping the number of spins N fixed and taking the limit, where the length of the chain or ladder is large compared to the circumference of the cylinder, for large λ , the wavefunction of the ground state reduces to a product of singlets, and the singlets are formed between neighboring spins. In this limit, the correlations decay exponentially, and the Renyi entropy follows an area law. The model hence enables us to transform between one or two copies of a one-dimensional Haldane-Shastry like model and a product of singlets with a Hamiltonian that contains only two-body interactions. All the way along this path the ground state is known analytically and various properties can be computed for large system sizes using Monte-Carlo simulations or analytical tools.

When changing λ from small to large, we do not observe a sharp transition between the two behaviors described above. Instead the transition occurs gradually, in the sense that the chain shows different behaviors depending on the distances considered. For small distances and small subsystem sizes, the system behaves as in the critical phase. For large distances and large subsystem sizes, the correlations decay exponentially, and the entropy follows an area law. As λ changes, the border between small and large distances moves. The ladder model shows a similar behavior.

The results presented in this chapter are interesting, because they show that it is possible to have a system, where the correlations and the entropy behave in different ways depending on the distances considered. Although the precise pattern of interaction strengths present in the considered models is difficult to realize in experiments, the study suggests that having interaction strengths in the Hamiltonian that change behavior depending on the distance may be a mechanism to obtain a model, where the correlations and the entropy change behavior depending on distance.

The investigated models contain several parameters, since the spin positions can be chosen freely on two lines, and for each choice there is a family of two-body Hamiltonians having the same ground state. Several further investigations could hence be done within the same framework. Apart from being a nontrivial generalization of the one-dimensional Haldane-Shastry model with only two-body interactions, the models presented in this work provide an interesting playground for testing numerical approximation schemes. The models display a variety of physical properties, and they have the unusual feature of combining possibly long-range two-body interactions with an analytically known ground state for which various properties can easily be computed.

Conclusions

“ *Nothing is better than reading and gaining more and more knowledge.* ”

— **Stephen Hawking**

Topologically ordered phases can not be described by the local order parameters, rather these phases are characterized by the global quantities such as the topology of the system. A remarkable property of such short-range ordered and long-range entangled phases is the existence of anyonic quasiparticle excitations which carry fractional charges and exhibit fractional braiding statistics. In this thesis we have studied the anyonic quasiparticles in the topologically ordered lattice systems. The main theme is to construct or modify the lattice models to create the anyons in the ground state and to investigate the anyon properties. A glimpses of the main conclusions of different chapters presented in this thesis are highlighted as follows.

In Chapter-3 we have explicitly constructed the lattice fractional quantum Hall models. Our constructions are based on the fact that the infinite-dimensional matrix product states can be expressed as the correlator of conformal fields of the underlying conformal field theory. We have inserted anyons in our lattice models and have shown that the singularity problem for the quasielectrons, as appear in the continuum, can be avoided in the lattice systems. Therefore we have found simpler states for the quasielectrons in the lattices than in the continuum. We have constructed the lattice Laughlin and the lattice Moore-Read fractional quantum Hall models both in the presence and in the absence of anyons on a two-dimensional plane. We have introduced a parameter in the system to interpolate between the lattice limit and the continuum limit. We have shown that our lattice states resemble the states in the continuum if we take the continuum limit.

We have researched the non-Abelian anyons in the lattice Moore-Read models in Chapter-4. We have investigated the cases of the two quasiholes, two quasielectrons, one quasihole-one quasielectron, four quasiholes, four quasielectrons, and two quasiholes-two quasielectrons in the systems at the Landau level filling factor $5/2$. We have found that the anyons are well-screened with the radii of a few lattice constants and the quasielectrons have very similar density profiles to those of the quasiholes apart from a sign. The charges of the quasiholes and of the quasielectrons approach $\simeq +0.25$ and $\simeq -0.25$ respectively. This agrees with the findings for the quasihole charge in the continuum. We have probed the topological properties of the systems by computing the fractional braiding statistics of the anyons. We have found that the anyons are non-Abelian and the braiding statistics are the same as expected from the continuum. We have used the Monte-Carlo simulations to compute the aforementioned properties. Therefore we have confirmed that the quasielectrons can be created and can be investigated in a similar way

to those of the quasiholes. We have used the conformal field theory approach to construct the parent Hamiltonians for which our analytical states are the exact ground states. By numerically diagonalizing the Hamiltonians we have found degenerate ground states for the case of the four anyons in the system which also signify the non-Abelian nature of the anyons. These Hamiltonians are long-range and contain few-body interactions and allow for the manipulation of the anyons by tuning the coupling strengths of the interactions. Since the bulk correlations, in the topologically ordered phases, decay exponentially therefore these Hamiltonians would be a starting point to obtain the local Hamiltonians, having the same ground state physics, by using the truncation procedure. Experimental realizations of such local Hamiltonians provide the stage to study the topological systems and to use them in topological quantum computations.

By using potentials we have trapped the non-Abelian quasielectrons in a similar way to that of the non-Abelian quasiholes in the ground state of the Kapit-Mueller model Hamiltonian for hardcore bosons which is known to exhibit the bosonic Moore-Read fractional quantum Hall physics. By using exact diagonalizations we have found that the anyons in this model are screened well and possess right charges. The excess charge distribution and the shapes of the anyons are shown to be similar to the corresponding quantities computed in our analytical lattice Moore-Read states. Therefore our analytical states are relevant to this simpler and experiment friendly model.

Anyons and the fractional quantum Hall physics have been explored in the two-dimensional systems. And often they are researched in the crystal structures, that is in the structures which have the translational symmetry. In Chapter-5 we have taken the step to realize these phenomena in the quasicrystalline structures and in the fractional dimensional systems, such as in the fractal lattices. We have constructed new type of fractional quantum Hall models containing anyons on the quasicrystals and on the fractal lattices. We have shown that the well-screened anyons exist in the quasicrystals and in the fractal dimension of $\simeq 1.585$ on the Sierpinski gasket fractal lattice geometry. We have also shown the well-screened anyons to exist in the fractal dimensions between 1 and 2. It is known that the one-dimensional system is critical and therefore the anyons can not exist there. However we have shown that the anyons can exist in one dimension on the particular fractal space geometry. And interestingly our results have revealed that the anyons can be present in the dimension less than one such as in the dimension $\ln(4)/\ln(5) \simeq 0.86$. Therefore we have shown that the anyons and the fractional quantum Hall physics can be obtained in all dimensions $1 \leq \text{dimension} \leq 2$. We have concluded that the lattice points distributions are more important in hosting anyons and in realizing the fractional quantum Hall physics rather than the Hausdorff dimensions of the fractal spaces. We have explicitly shown that the anyons obey the right braiding statistics and we have derived the parent Hamiltonians for which our analytical anyonic lattice states are the exact ground states.

We emphasize on the important common point, for the investigations of the anyons and of the topological order in the quasicrystals and in the fractal lattices, that we can use our construction to obtain the anyons and the fractional quantum Hall physics on lattices where one can not easily construct a topological flat band, for example a fractional Chern insulator model, due to the lack of the translational symmetry.

It is known that the topologically ordered systems of fermions or bosons host the anyonic quasiparticles. In Chapter-6 we have shown that the systems of hardcore anyons can give rise to their own anyonic quasiparticles. We have constructed the lattice Laughlin fractional quantum Hall models of the hardcore anyons and have shown that the anyonic quasiparticles of these systems are well-screened and possess right charges. We have demonstrated that the braiding statistics of the emergent anyonic quasiparticles are different than that of the original hardcore anyons in the systems.

It is well appreciated that the topologically ordered systems can host anyonic quasiparticles with particular braiding properties and with fractional charges. Whenever the quasiparticles are anyonic, we know that the system is topologically ordered. Therefore when a system enters into a non-topological phase or into a phase with different topological order, then the anyon properties change across the transition. We have used these ideas in Chapter-7 and we have benchmark the quasiparticles as the detector of the topological quantum phase transitions. We have examined our method on five examples as follows. We have considered a lattice Moore-Read fractional quantum Hall state on a square lattice and on a fractal lattice, which encounters a topological quantum phase transition while changing the lattice filling factor. We have shown that the anyon charges detect the topological quantum phase transition. We have investigated an interacting Hofstadter fractional Chern insulator model in the absence of disorder with open boundary condition, which has a Laughlin type fractional quantum Hall ground state, and which undergoes a topological quantum phase transition as a function of the lattice filling factor. We have also considered the same model in the presence of disorder. We have modified the Hamiltonian to trap the anyons in the ground state and have found that the anyon charges detect the topological quantum phase transition. We have studied the Kitaev's toric code model on the torus, which undergoes a topological quantum phase transition when a sufficiently strong magnetic field is applied. We have modified the Hamiltonian and have created the anyons in the ground state and have shown that the anyons detect the topological quantum phase transition.

We have found that for all these quite different examples, it is sufficient to compute the anyon charges to determine the phase transition points. Therefore the method is numerically cheaper than the computations of other probes such as the topological entanglement entropy, the many-body Chern number, the spectral flow, and the entanglement spectrum. We have also concluded that our probe works for all types of topological orders and the method is independent of the choice of the boundary conditions.

In Chapter-8 we have considered a family of spin-1/2 models with few-body, $SU(2)$ invariant Hamiltonians and analytical ground states related to the one-dimensional Haldane-Shastry wavefunction. The spins are placed on the surface of a cylinder and we have shown that interesting family of models with two-body exchange interactions is obtained if we place the spins along one or two lines parallel to the cylinder axis, giving rise to chain and ladder models, respectively. We can change the scale along the cylinder axis without changing the radius of the cylinder, which gives us a parameter that controls the ratio between the circumference of the cylinder and all other length scales in the system. We have used Monte-Carlo simulations and analytical investigations to study how this ratio affects the properties of the models. If the ratio is large, we have found that the two legs of the ladder decouple into two chains that are in a critical phase with

Haldane-Shastry-like properties. If the ratio is small, we have found that the wavefunction reduces to a product of singlets. In between, we have found that the behavior of the correlations and the Renyi entropy depends on the distance considered. For small distances we have found that the behavior is critical, and for long distances the correlations decay exponentially and the entropy shows an area law behavior. And the distance up to which there is critical behavior gets larger and larger as the ratio increases.

Future Directions

” *Tea is where we explain to each other what we do not understand.*

— **Robert Oppenheimer**

We have studied quasiparticles in the strongly correlated quantum many-body systems with an emphasis on the topologically ordered phases of matter. Our investigations open up the avenue for further research directions as we outline below.

We have benchmarked the quasiparticles as the detector of the topological quantum phase transitions. It would be interesting to apply our quasiparticle probe in investigating the frustrated quantum magnets, which give birth to the rich phase diagrams and become the potential candidates to realize the quantum spin liquids, such as the spin-1/2 J_1 - J_2 XY models and the spin-1/2 J_1 - J_2 Heisenberg models on different lattices like on the Kagome lattice, on the triangular lattice, on the square lattice, and on the honeycomb lattice. Also it would be worth to use our quasiparticle probe in investigating the quantum phases of the three-dimensional rare-earth pyrochlore magnets. It would be interesting to apply our probe in studying quantum phase transitions between different non-topological phases including gapless phases.

Recently a neural network based machine learning technique, which is known as the "quantum loop topography", has been introduced to study the topologically ordered phases of matter and to draw the phase diagram therein. It would be interesting to merge this technique with our quasiparticle probe approach in determining the phase diagram of various systems.

The Kitaev's honeycomb model under the external magnetic field, in any direction, draws much attentions due to the rich phase diagram and the possibility of having both the gapped topological and the gapless quantum spin liquid phases and the polarized phase in its phase diagram. It would be interesting to apply our quasiparticle probe in detecting the different quantum phases there and thereby in drawing the phase diagram. Also topological nature of the quantum spin liquid phase can be concluded from the cornerstone of its quasiparticle properties. While turning on the magnetic field, the Kitaev's honeycomb model is no longer exactly solvable and the anyons can not be created in the way as that of the model without the magnetic field. Therefore our approach in trapping quasiparticles in the ground state in the presence of the magnetic field, by giving energy penalties, would be quite eye-catching for different purposes.

Local lattice fractional quantum Hall models are of immense interest from their own right since the local models are experiment friendly and thereby the control over anyons becomes easier. We have constructed the anyonic lattice Moore-Read Hamiltonians which

are long-range. It would be important to construct local models, having practically the same ground state physics as the original one, by truncating the long-range Hamiltonians since the bulk correlations decay exponentially. A recent work in Ref. [69] has already shed some light in this direction where the local models for a particular lattice Moore-Read state family, in the absence of the anyons in the system, have been constructed. And therefore that approach suggests the same to be true for the models hosting the anyons.

Braiding statistics for the quasiholes have been explicitly computed in the Kapit-Mueller model in Ref. [119] which is a simpler and a realistic model. We have shown how to create the quasielectrons in that model and therefore it would be interesting to explicitly calculate the fractional braiding statistics of the quasielectrons there. This is important for the topological quantum computations as well.

The Fibonacci anyons are one of the potential candidates for the topological quantum computations and for constructing universal quantum gates. These anyons appear in the Read-Rezayi fractional quantum Hall states at the Landau level filling factor $12/5$. We have created and have investigated the Ising anyons in the lattice Moore-Read fractional quantum Hall models. Therefore it would be important to construct the lattice versions of the Read-Rezayi models containing the Fibonacci anyons and thereby to investigate their properties.

Quasicrystals provide a wealth of the intriguing phenomena in topological orders, such as the legacy of topological properties from higher dimensions, due to the long-range order and the non-periodic structure of the atoms. The fractal lattices provide the stage to understand the intriguing physics of the topological orders in fractional dimensions $1 \leq \text{dimension} \leq 2$. We have shown that the anyons and the fractional quantum Hall physics exist on the quasicrystals and on the fractals by constructing the lattice Laughlin models containing anyons and by investigating the anyon properties. It would be interesting to construct the lattice models carrying non-Abelian anyons on the quasicrystals and on the fractal lattices. Besides our constructions provide some hints to build up the fractional Chern insulator type model Hamiltonians in future on the quasicrystals and on the fractal lattices, having the interactions and the complex hoppings resembling the magnetic field. Also the investigations of the entanglement properties and the transport properties would be important directions to explore. Recently twisted bilayer graphene systems, which are also quasicrystals, are attracting a lot of recognitions. It would be important to proceed with our investigations on such systems.

We have proposed that the systems of hardcore anyons can give rise to their own anyonic quasiparticles. We have shown this to happen in the lattice Laughlin fractional quantum Hall systems. It would be interesting to motivate these ideas further to realize the non-Abelian anyonic quasiparticles from the systems of the hardcore anyons, that is to construct the lattice Moore-Read models of hardcore anyons and to investigate their anyonic quasiparticle properties.

Study of the non-equilibrium dynamics, such as the quench dynamics are important in their own right. Investigations of the stability of different phases including the topologically ordered phases by following a quench are the active areas of research. We have created and have researched the anyonic quasiparticles in various topologically ordered systems. Therefore it would be interesting to investigate the fate of the anyons by

following different types of quench protocols. These studies would reveal the long-time non-equilibrium behavior of the anyons. It would be important to determine the stability of the topologically ordered phases, by following a quench, by using their quasiparticle properties such as the quasiparticle charges. Also these ideas could be extended in studying the non-equilibrium dynamics of different other types of systems, such as the frustrated quantum magnets, by looking at their quasiparticle properties.

A recent work in Ref. [267] shows the emergence of the fractional quantum Hall physics in a non-Hermitian fractional Chern insulator model, which they claim to be a relevant model with the ultra-cold atoms in optical lattice experiments. They draw the conclusions by computing the ground state degeneracy and the many-body Chern number on the torus. It would be an interesting direction to create the anyons and to investigate the anyon properties such as the charge and the braiding statistics on this model. These investigations would motivate the study of anyons in open quantum systems, which interact with the environment and thereby are essentially non-Hermitian, in accordance with the experiments.

The investigated chain and ladder models contain several parameters, since the spin positions can be chosen freely on two lines, and for each choice there is a family of two-body Hamiltonians having the same ground state. Therefore several further investigations could be done within the same framework, which may give rise to interesting spin models.

Numerical Techniques

” *Monte Carlo originated as a form of emergency first aid, in answer to the question: What do we do until the mathematician arrives?*

— **George Dyson**

Exact solutions of the quantum many-body systems are very rare beyond one dimension, where there exist several important cases. In two dimensions there are also some examples but usually the analytical calculations rely on the assumptions or on the approximations those can not be justified rigorously. Therefore the numerical studies of model systems are essential. Besides providing the insight to the physics of the systems, the unbiased numerical results are important for testing the theories and the analytical calculations. Moreover, the numerical simulations set the playground for the explorations and for the discoveries in both the theoretical and the experimental directions.

Two classes of the computational methods are used in this thesis as the numerical exact diagonalization and the Metropolis Monte-Carlo simulation which are discussed as follows. In Sec. A.1 we discuss the exact diagonalization [199] and in Sec. A.2 we narrate the Metropolis-Hastings Monte-Carlo algorithm [253, 90].

A.1 Exact diagonalization

By exactly diagonalizing the Hamiltonian, a complete understanding of a system can be obtained. Any static or dynamic quantity can be computed with the available eigenstates and the energies. Given a Hamiltonian in hand, the first step of an exact diagonalization is to choose a basis in which the Hamiltonian and the other operators will be expressed. The choice of the basis is not unique. Different choices of the basis will lead to the different matrix forms of the Hamiltonian and the other operators, which are related by the unitary transformations, but the physical quantities like the energies, correlation functions, entanglement properties, magnetizations etc. remain the same.

We consider a system of N lattice sites. Any quantum many-body state $|\Psi\rangle$ with the local Hilbert space dimension p can be defined in terms of the p^N coefficients as

$$|\Psi\rangle = \frac{1}{C} \sum_{n_1, \dots, n_N} \Psi(n_1, \dots, n_N) |n_1, \dots, n_N\rangle, \quad (\text{A.1})$$

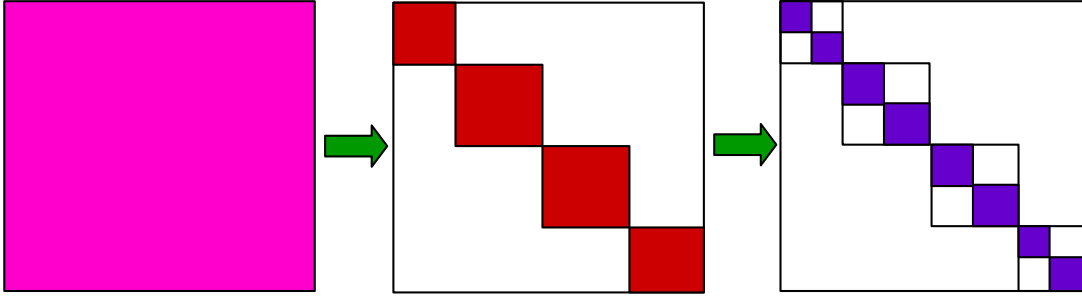


Figure A.1.: We show the pictorial illustration of the block diagonalization. In the original basis, the system Hamiltonian has no structure as we show in the left figure with the pink shaded area. By constructing the basis states as labeled by a conserved quantum number, the Hamiltonian matrix breaks up into the blocks, as we show in the middle figure with the red shaded area, those can be diagonalized independent of each other. By applying another symmetry, that is by using another conserved quantity of the system, the previously constructed blocks can be further reduced into smaller blocks, as we show in the right figure with the violet shaded area, as labeled by the different quantum numbers. We note that all the matrix elements which are outside the shaded blocks are zero.

where

$$|n_1, \dots, n_N\rangle = |n_1\rangle \otimes \dots \otimes |n_N\rangle \quad (\text{A.2})$$

is the basis state and $n_j \in \{0, 1, \dots, p-1\}$ denotes the occupancy, or the degrees of freedom, of the j th lattice site. Therefore the system Hamiltonian or any operator, written in this many-body Hilbert space, consists of the $p^N \times p^N$ coefficients. For example a system of N lattice sites having the local Hilbert space spanned by the basis states $|n_i\rangle \in \{0, 1\}$, for example the spin-1/2 system, has $p = 2$ and correspondingly the total Hilbert space dimension is 2^N .

In a straight forward manner this system can be treated numerically by constructing the Hamiltonian and the other operators of dimension $p^N \times p^N$ and by constructing the state $|\Psi\rangle$ with the p^N number of $\Psi(n_1, \dots, n_N)$ coefficients and thereby computing their properties. The word "exact" justifies its presence, in the name of this technique, as the Hamiltonian is represented fully without any dimension truncation. After the construction of the Hamiltonian, the energy spectra and the eigenstates are computed by using the standard diagonalization algorithms like the Lanczos diagonalization algorithm.

However because of the exponential growth of the Hilbert space dimension as p^N with the number of the particles in the system, this procedure is limited to the small system sizes. Therefore symmetries, that is the system properties which commute with the Hamiltonian, should be used whenever applicable to first reduce the Hamiltonian to a block-diagonal form. We illustrate such a scheme in Figure A.1. In this process the basis states are ordered properly or combined with the help of the available symmetries. Hence the Hamiltonian is decomposed into the different sectors. The different sectors or the blocks correspond to the states with the different conserved quantum numbers, which are related to the symmetries. Examples of such symmetries and the conservation

include the particle number conservation, or the magnetization conservation in case of the spin systems, or the crystal momentum conservation by following the lattice translational symmetry etc. The obtained blocks can be diagonalized independently and hence one can work with the Hilbert spaces of much smaller dimensions than that of the total Hilbert space of the full system. Therefore one can target a larger system size at a much reduced computational cost. For example with a system of N lattice sites having $|n_i\rangle \in \{0, 1\}$ and conserving the particle number to M , gives rise to the sizes of the blocks as

$$\frac{N!}{M!(N-M)!} \ll 2^N, \text{ where } M \in \{1, \dots, N\}. \quad (\text{A.3})$$

Despite the exponential dependence on N , the exact diagonalization tool is very useful in studying the quantum many-body systems. And the access to the different quantum numbers is indispensable for classifying the excitations. Furthermore being the method to obtain the exact results, the exact diagonalization is used to test the other variational methods and the other approximation techniques. In this thesis we have used this tool on the quantum many-body Hamiltonians to compute the properties of the systems.

A.1.1 Creation of the blocks with fixed number of particles

Our first task is to find the Hilbert space of each block, which conserves the particle number, of the Hamiltonian and to find an appropriate way to label the states. We will first reduce the Hilbert space to only contain states with M particles, that is, to states for which $\sum_j n_j = M$. We would like to set up a map, called a *lin* table, which takes a basis state with $\sum_j n_j = M$ as input and produces the number of this state in the reduced basis as output. Numerically we do this in the following way.

First we divide the lattice into two parts, the left part consisting of the sites $1, 2, \dots, K_1$, and the right part consisting of the sites $K_1 + 1, K_1 + 2, \dots, N$. We note that $K_1 + K_2 = N$. We then consider all possible configurations of the left part and all possible configurations of the right part. The left part has 2^{K_1} different configurations, and the right part has 2^{K_2} different configurations. The $2^{K_1} \times 1$ vector, named as *spsum1* is the number of particles for each possible configuration of the left part, and the $2^{K_2} \times 1$ vector, named as *spsum2*, is the number of particles for each possible configuration of the right part. Instead of running through all 2^N configurations of the N spins, which is too time consuming, we make a for loop, which loops over possible numbers of particles in the left part of the chain. We then know that we need to match these left hand configurations with right hand configurations such that the total number of particles is M .

The vector, named as *aux1*, contains all left hand configurations with exactly mm particles, and the vector, named as *aux2*, contains all the right hand configurations with $M - mm$ particles. By combining these left hand and right hand configurations, we get $l_1 \times l_2$ valid basis states, where l_1 is the length of *aux1* and l_2 is the length of *aux2*. For the lowest possible value of mm , we label the states from 1 to $l_1 \times l_2$. We do this by storing two lists of numbers as *lin1* and *lin2*. For the states in *aux1* we store numbers that jump by l_2 and for the states in *aux2* we store numbers from 1 to l_2 . Hence, when we add up

the numbers in $lin1$ and $lin2$, we get numbers running from 1 to $l_1 \times l_2$. For higher values of mm , we do the same, except that we add the number of states we already had in $lin1$.

When we have constructed $lin1$ and $lin2$, we can get the number N_M of a given state in the reduced basis in the following way

$$N_M = lin1 \left(\sum_{j=1}^{K_1} n_j \times 2^{K_1-j} + 1 \right) + lin2 \left(\sum_{j=K_1+1}^N n_j \times 2^{N-j} + 1 \right). \quad (\text{A.4})$$

(a). Example

Let us take $N = 5$ and $M = 2$ as an example. In this case, $K_1 = 2$ and $K_2 = 3$. The possible left part configurations are 00, 01, 10, and 11, and the possible right hand configurations are 000, 001, 010, 011, 100, 101, 110, and 111. We first find that 00 can be combined with 011, 101, and 110. Therefore $lin1(1)$ is set to zero, $lin2(4)$ to 1, $lin2(6)$ to 2 and $lin2(7)$ to 3. Then we find that 01 and 10 can be combined with 001, 010, and 100. Since we already found 3 states in the previous step, we put $lin1(2)$ equal to 3. We then set $lin2(2)$ to 1, $lin2(3)$ to 2, and $lin2(5)$ to 3. Then $lin1(3)$ should be 6. We now have 9 states in the basis. Finally, we find that 11 can be combined with 000. We hence put $lin1(4)$ equal to 9 and $lin2(1)$ equal to 1.

The resulting lin tables are: $lin1 = [0; 3; 6; 9]$ and $lin2 = [1; 1; 2; 1; 3; 2; 3; 0]$. With the lin tables in place we can take a given configuration and find the corresponding state in the new basis. If, for instance, we consider the configuration $|10100\rangle$, we have $N_2 = lin1(3) + lin2(5) = 9$. Hence this state is number 9 in the reduced basis. Altogether the reduced basis consists of the states as follows

basis state	$lin1$	$lin2$	N_M
$ 00011\rangle$	0	1	1
$ 00101\rangle$	0	2	2
$ 00110\rangle$	0	3	3
$ 01001\rangle$	3	1	4
$ 01010\rangle$	3	2	5
$ 01100\rangle$	3	3	6
$ 10001\rangle$	6	1	7
$ 10010\rangle$	6	2	8
$ 10100\rangle$	6	3	9
$ 11000\rangle$	9	1	10

Now we apply the Hamiltonian to these reduced basis states to construct the block with the desired particle numbers. Then the diagonalizations of the blocks of the Hamiltonian can be done by using the standard algorithms like the Lanczos algorithm.

A.2 The Metropolis-Hastings Monte-Carlo technique

As we have discussed, the exact diagonalization technique is limited to small system sizes due to the exponential explosion of the Hilbert space dimensions. Therefore we have used the Metropolis-Hastings Monte-Carlo simulations to acquire larger system sizes. In this thesis we have used this algorithm to obtain the properties of the analytical states.

The Metropolis-Hastings algorithm is a Markov chain Monte-Carlo method to obtain a sequence of the random samples from a probability distribution. This algorithm generates a sequence of sample values such that more the sample values are produced, better is the approximation of the distribution of values to the desired distribution $P(x)$. These sample values are produced iteratively and the current sample value determines the distribution of the next sample. Hence the sequence of the samples becomes the Markov chain. To be specific, at each step of the iterations the algorithm chooses a candidate for the next sample value depending on the current sample value only. Then the candidate is either accepted or rejected for the next iteration step based on some probability.

A.2.1 Algorithm

A Markov process is defined by the transition probability $P(x'|x)$ which gives the probability of the transition from a given state x to another state x' . The Metropolis-Hastings algorithm starts with the condition of the detailed balance which requires that each transition $x \rightarrow x'$ is reversible, that is for each pair of the states x and x' , the probability of being in the state x and the probability of transitioning to the state x' must be equal to the probability of being in the state x' and the probability of transitioning to the state x . This means we have

$$P(x'|x)P(x) = P(x|x')P(x'). \quad (\text{A.5})$$

Now the transition is separated in the two steps as by proposing a distribution and by following a acceptance-rejection procedure. The proposal distribution $Q(x'|x)$ is an arbitrary probability density which propose a candidate state x' given another state x . For the Metropolis algorithm, Q must be symmetric that is

$$Q(x'|x) = Q(x|x'). \quad (\text{A.6})$$

A suitable choice will be the Gaussian distribution centered at x . The acceptance ratio $A(x'|x)$ is the probability to accept the state x' . The transition probability is written as

$$P(x'|x) = Q(x'|x)A(x'|x). \quad (\text{A.7})$$

Therefore from Eq. A.5 we write

$$\frac{A(x'|x)}{A(x|x')} = \frac{P(x')}{P(x)} \frac{Q(x|x')}{Q(x'|x)}. \quad (\text{A.8})$$

Now the Metropolis choice of the acceptance ratio, which satisfies the above condition in Eq. (A.8), becomes

$$A(x'|x) = \min\left(1, \frac{P(x') Q(x|x')}{P(x) Q(x'|x)}\right). \quad (\text{A.9})$$

Therefore the Metropolis-Hastings algorithm is sketched as follows:

(1) Initialize :

- (i) Pick up any initial state x_0 .
- (ii) Initiate the iteration $t = 0$.

(2) Iterate :

- (i) Randomly generate the candidate state x' according to $Q(x'|x)$.
- (ii) Compute the acceptance probability $A(x'|x) = \min\left(1, \frac{P(x') Q(x|x')}{P(x) Q(x'|x)}\right)$.
- (iii) **Accept or reject :**
 - (a) generate a random number $r \in \{0, 1\}$.
 - (b) if $A(x'|x) \geq r$, accept the new state and set $x_{t+1} = x'$.
 - (c) if $A(x'|x) < r$, reject the new state and proceed with the old state $x_{t+1} = x_t$.
- (iv) **Increment :** Set the iteration step as $t = t + 1$.

The algorithm is run for a certain number of iterations first, without measuring the observable value, such that $Q \approx P$. This is called the warm up steps. Normally the warm up steps time scales with the system size as $\propto (\text{system size})^2$. Then the algorithm is run to collect the data.

A.2.2 Error estimation

To estimate the accuracy of the obtained data, we accumulate the data values from the N_t statistically independent trajectories as $\mathcal{P}^{(k)}$, where $k \in \{1, \dots, N_t\}$, by running the simulation N_t times. Then we calculate the mean and the error bar of the data by reaching the Gaussian distribution of the values and thereby exploiting the central limit theorem. The true value is then expected to lie within the error bar around the mean value and hence we write

$$\mathcal{P}_{\text{true}} = \mathcal{P}_{\text{mean}} \pm \Delta\mathcal{P}, \quad (\text{A.10})$$

where

$$\mathcal{P}_{\text{mean}} = \frac{1}{N_t} \sum_{k=1}^{N_t} \mathcal{P}^{(k)} \quad \text{and} \quad \Delta\mathcal{P} = \sqrt{\frac{1}{N_t(N_t - 1)} \sum_{k=1}^{N_t} (\mathcal{P}_{\text{mean}} - \mathcal{P}^{(k)})^2}. \quad (\text{A.11})$$

We point out that by considering more trajectories, we approximate the Gaussian distribution curve more accurately. That is more the trajectories, more the data points on the Gaussian distribution curve. We also point out that more the number of the Monte-Carlo steps while collecting the data, narrower is the Gaussian distribution curve width which means lesser is the standard deviation and thereby smaller is the errorbar. Normally the error $\Delta\mathcal{P}$ scales with the Monte-Carlo steps as $\Delta\mathcal{P} \propto 1/\sqrt{\text{Monte-Carlo steps}}$.

A.2.3 Example

We present here an example of determining the overlap of the two analytical states. We have used this example in the computations in Chapter-4. We write the overlap of

$$|\Psi_\alpha\rangle = \frac{1}{C_\alpha} \sum_i \Psi_\alpha |n_i\rangle \text{ and } |\Psi_\beta\rangle = \frac{1}{C_\beta} \sum_i \Psi_\beta |n_i\rangle \quad (\text{A.12})$$

as

$$O = \langle \Psi_\alpha | \Psi_\beta \rangle = \frac{\sum_{n_i} \Psi_\alpha^* \Psi_\beta}{\sqrt{\sum_{n_i} |\Psi_\alpha|^2 \sum_{n_i} |\Psi_\beta|^2}}, \quad (\text{A.13})$$

where we have

$$C_\alpha^2 = \sum_{n_i} |\Psi_\alpha|^2 \text{ and } C_\beta^2 = \sum_{n_i} |\Psi_\beta|^2. \quad (\text{A.14})$$

We write Eq. A.13 as

$$\frac{\sum_{n_i} \Psi_\alpha^* \Psi_\beta}{\sqrt{\sum_{n_i} |\Psi_\alpha|^2 \sum_{n_i} |\Psi_\beta|^2}} = \frac{\Lambda_{\alpha\beta}}{\sqrt{\Omega_{\alpha\beta} \Omega_{\beta\alpha}}}, \quad (\text{A.15})$$

where we have

$$\Lambda_{\alpha\beta} = \frac{\sum_{n_i} |\Psi_\alpha \Psi_\beta| \frac{\Psi_\alpha^* \Psi_\beta}{|\Psi_\alpha \Psi_\beta|}}{\sum_{n_i} |\Psi_\alpha \Psi_\beta|}, \quad \Omega_{\alpha\beta} = \frac{\sum_{n_i} |\Psi_\alpha \Psi_\beta| \frac{|\Psi_\alpha|}{|\Psi_\beta|}}{\sum_{n_i} |\Psi_\alpha \Psi_\beta|}, \quad \Omega_{\beta\alpha} = \frac{\sum_{n_i} |\Psi_\alpha \Psi_\beta| \frac{|\Psi_\beta|}{|\Psi_\alpha|}}{\sum_{n_i} |\Psi_\alpha \Psi_\beta|}. \quad (\text{A.16})$$

Now, the quantities

$$\frac{\Psi_\alpha^* \Psi_\beta}{|\Psi_\alpha \Psi_\beta|}, \quad \frac{|\Psi_\alpha|}{|\Psi_\beta|} \text{ and } \frac{|\Psi_\beta|}{|\Psi_\alpha|} \quad (\text{A.17})$$

can be obtained by using the Metropolis-Hastings Monte-Carlo sampling over the distribution with weight $|\Psi_\alpha \Psi_\beta|$. We have O as the complex number and hence we write the mean value over the trajectories as $O_{\text{mean}} = a + ib$. Therefore the magnitude of the mean value becomes $|O_{\text{mean}}| = \sqrt{a^2 + b^2}$. We compute the error $\Delta|O_{\text{mean}}|$ as follows.

(a). Error estimation

We have $O_{\text{mean}} = a + ib$ and $|O_{\text{mean}}| = \sqrt{a^2 + b^2}$, which lead to the following equations as

$$\Delta O_{\text{mean}} = \Delta a + i\Delta b \text{ and } \Delta|O_{\text{mean}}| = \sqrt{\left(\frac{a}{|O_{\text{mean}}|}\Delta a\right)^2 + \left(\frac{b}{|O_{\text{mean}}|}\Delta b\right)^2}. \quad (\text{A.18})$$

Now we evaluate ΔO_{mean} as follows. We write from Eq. (A.13)

$$\begin{aligned} \Delta O = & \left[\left(\frac{\partial O}{\partial [\sum_{n_i} |\Psi_\alpha|^2]} \right)^2 (\Delta [\sum_{n_i} |\Psi_\alpha|^2])^2 + \left(\frac{\partial O}{\partial [\sum_{n_i} |\Psi_\beta|^2]} \right)^2 (\Delta [\sum_{n_i} |\Psi_\beta|^2])^2 \right. \\ & \left. + \left(\frac{\partial O}{\partial [\sum_{n_i} \Psi_\alpha^* \Psi_\beta]} \right)^2 (\Delta [\sum_{n_i} \Psi_\alpha^* \Psi_\beta])^2 \right]^{\frac{1}{2}}. \end{aligned} \quad (\text{A.19})$$

Hence we write

$$\begin{aligned} \Delta O_{\text{mean}} = & \left[\left(\frac{[\sum_{n_i} \Psi_\alpha^* \Psi_\beta]_{\text{mean}}}{2\sqrt{[\sum_{n_i} |\Psi_\beta|^2]_{\text{mean}} [\sum_{n_i} |\Psi_\alpha|^2]_{\text{mean}}^{\frac{3}{2}}}} \right)^2 (\Delta [\sum_{n_i} |\Psi_\alpha|^2])^2 \right. \\ & + \left(\frac{[\sum_{n_i} \Psi_\alpha^* \Psi_\beta]_{\text{mean}}}{2\sqrt{[\sum_{n_i} |\Psi_\alpha|^2]_{\text{mean}} [\sum_{n_i} |\Psi_\beta|^2]_{\text{mean}}^{\frac{3}{2}}}} \right)^2 (\Delta [\sum_{n_i} |\Psi_\beta|^2])^2 \\ & \left. + \left(\frac{1}{[\sum_{n_i} |\Psi_\alpha|^2]_{\text{mean}} [\sum_{n_i} |\Psi_\beta|^2]_{\text{mean}}} \right)^2 (\Delta [\sum_{n_i} \Psi_\alpha^* \Psi_\beta])^2 \right]^{\frac{1}{2}}. \end{aligned} \quad (\text{A.20})$$

We compute the quantities in the right hand side of Eq. (A.20) by using Eq. (A.11) and estimate the error $\Delta|O_{\text{mean}}|$.

Null Fields of the Underlying Conformal Field Theory

” *The two most important days in your life are the day you are born and the day you find out why.*

— Mark Twain

In this Appendix, by following Ref. [69], we derive the null fields of the considered conformal field theory [64] as mentioned in Chapter-4 in Sec. 4.3. We define the following operators from the central charge $c = 1$ massless bosonic conformal field theory with the compactification radius \sqrt{q} as

$$G^\pm(z) = : \psi(z) e^{\pm i\sqrt{q}\phi(z)} : \text{ and } J(z) = \frac{i}{\sqrt{q}} \partial_z \phi(z), \quad (\text{B.1})$$

where $G^\pm(z)$ and $J(z)$ are the two chiral currents and the $U(1)$ conformal current respectively.

We introduce the following $q + 1$ number of fields as

$$\begin{aligned} \chi^p(v) &= \oint_v \frac{dz}{2\pi i} \frac{1}{(z-v)^p} G^+(z) \mathcal{V}_1(v) \text{ with } p \in \{0, 1, \dots, q-3, q-2\}, \\ \chi^{q-1}(v) &= \oint_v \frac{dz}{2\pi i} \left[\frac{1}{(z-v)^{q-1}} G^+(z) \mathcal{V}_1(v) - \frac{1}{(z-v)} \mathcal{V}_2(v) \right], \\ \chi^q(v) &= \oint_v \frac{dz}{2\pi i} \frac{1}{z-v} \left[\frac{1}{(z-v)^{q-1}} G^+(z) \mathcal{V}_1(v) \right] - \oint_v \frac{dz}{2\pi i} \frac{1}{z-v} qJ(z) \mathcal{V}_2(v), \end{aligned} \quad (\text{B.2})$$

where we define

$$V_{n_j}(v) = \chi_{n_j}(v) \mathcal{V}_{n_j}(v) \quad (\text{B.3})$$

from Eq. (3.48) with $\eta = 1$ which are used in Chapter-4.

We explicitly derive that the fields in Eq. (B.2) are null fields. Here we allow an occupancy of $n_j \in \{0, 1, 2\}$ rather than just of $n_j \in \{0, 1\}$. We collect the following expressions, which we utilize onwards, as

$$\begin{aligned}
& : e^{i\alpha\phi(z)} :: e^{i\beta\phi(v)} : = (z-v)^{\alpha\beta} : e^{i\alpha\phi(z)+i\beta\phi(v)} :, \\
\psi_i(z)\psi_j(v) &= \delta_{ij} \left[\frac{1}{z-v} + (z-v)A(v) + \dots \right], \\
e^{i\phi(z)} &\simeq e^{i[\phi(v)+(z-v)\partial_v\phi(v)]} = e^{i\phi(v)} e^{i(z-v)\partial_v\phi(v)} \simeq e^{i\phi(v)} [1 + i(z-v)\partial_v\phi(v)], \\
\partial_z\phi(z) &= \partial_v\phi(v) + (z-v)\partial_v^2\phi(v) + \dots,
\end{aligned} \tag{B.4}$$

where the notation \dots stands for the terms that are proportional to $(z-v)^k$ with $k \geq 2$. We note that we do not require here the particular form of $A(v)$ since the non-zero contributions of the integrals in the null fields come from the terms having the simple poles. The following proofs are applicable for all $q \geq 2$.

B.1 Null field $\chi^q(v)$

We have

$$\begin{aligned}
\chi^q(v) &= \oint_v \frac{dz}{2\pi i} \frac{1}{z-v} \left[\frac{1}{(z-v)^{q-1}} G^+(z) \mathcal{V}_1(v) \right] - \oint_v \frac{dz}{2\pi i} \frac{1}{z-v} qJ(z) \mathcal{V}_2(v) \\
&= \mathcal{I}_1^q(v) - \mathcal{I}_2^q(v),
\end{aligned} \tag{B.5}$$

where \oint_v is the integration contour which is circling around v and conventionally we take the counter-clockwise direction as the positive direction.

Now we evaluate the terms, having the non-zero contributions, in Eq. (B.5) as

$$\begin{aligned}
\mathcal{I}_1^q(v) &= \oint_v \frac{dz}{2\pi i} \frac{1}{z-v} \left[\frac{1}{(z-v)^{q-1}} G^+(z) \mathcal{V}_1(v) \right] \\
&= \oint_v \frac{dz}{2\pi i} \frac{1}{z-v} \left[\frac{1}{(z-v)^{q-1}} \psi(z)\psi(v) e^{+i\sqrt{q}\phi(z)} e^{i(q-1)\phi(v)/\sqrt{q}} \right] \\
&= \oint_v \frac{dz}{2\pi i} \frac{1}{z-v} \left[\frac{(z-v)^{q-1}}{(z-v)^{q-1}} \psi(z)\psi(v) e^{i\sqrt{q}\phi(z)+i(q-1)\phi(v)/\sqrt{q}} \right] \\
&= \oint_v \frac{dz}{2\pi i} \frac{1}{z-v} \left[\left(\frac{1}{z-v} + (z-v)A(v) + \dots \right) e^{i\sqrt{q}\phi(z)+i(q-1)\phi(v)/\sqrt{q}} \right] \\
&= \oint_v \frac{dz}{2\pi i} \left[\frac{1}{(z-v)^2} e^{i\sqrt{q}\phi(z)+i(q-1)\phi(v)/\sqrt{q}} \right] \\
&= \oint_v \frac{dz}{2\pi i} \frac{1}{z-v} \left[i\sqrt{q}\partial_v\phi(v) e^{i(2q-1)\phi(v)/\sqrt{q}} \right]
\end{aligned} \tag{B.6}$$

and

$$\begin{aligned}
\mathcal{I}_2^q(v) &= \oint_v \frac{dz}{2\pi i} \frac{1}{z-v} [qJ(z)V_2(v)] \\
&= \oint_v \frac{dz}{2\pi i} \frac{1}{z-v} \left[\sqrt{qi} \partial_v \phi(z) e^{i(2q-1)\phi(v)/\sqrt{q}} \right] \\
&= \oint_v \frac{dz}{2\pi i} \frac{1}{z-v} \left[\sqrt{qi} \partial_v \phi(v) e^{i(2q-1)\phi(v)/\sqrt{q}} \right].
\end{aligned} \tag{B.7}$$

We note that

$$\mathcal{I}_1^q(v) = \mathcal{I}_2^q(v) \tag{B.8}$$

and thereby we find that $\chi^q(v)$ is a null field.

B.2 Null field $\chi^{q-1}(v)$

We have

$$\begin{aligned}
\chi^{q-1}(v) &= \oint_v \frac{dz}{2\pi i} \frac{1}{(z-v)^{q-1}} G^+(z) \mathcal{V}_1(v) - \oint_v \frac{dz}{2\pi i} \frac{1}{z-v} \mathcal{V}_2(v) \\
&= \mathcal{I}_1^{q-1}(v) - \mathcal{I}_2^{q-1}(v).
\end{aligned} \tag{B.9}$$

Now we proceed in the same way as before and we get

$$\begin{aligned}
\mathcal{I}_1^{q-1}(v) &= \oint_v \frac{dz}{2\pi i} \frac{1}{(z-v)^{q-1}} G^+(z) \mathcal{V}_1(v) \\
&= \oint_v \frac{dz}{2\pi i} \left[\frac{1}{(z-v)^{q-1}} \psi(z) \psi(v) e^{+i\sqrt{q}\phi(z)} e^{i(q-1)\phi(v)/\sqrt{q}} \right] \\
&= \oint_v \frac{dz}{2\pi i} \left[\frac{(z-v)^{q-1}}{(z-v)^{q-1}} \psi(z) \psi(v) e^{i\sqrt{q}\phi(z)+i(q-1)\phi(v)/\sqrt{q}} \right] \\
&= \oint_v \frac{dz}{2\pi i} \left[\left(\frac{1}{z-v} + (z-v)A(v) + \dots \right) e^{i\sqrt{q}\phi(z)+i(q-1)\phi(v)/\sqrt{q}} \right] \\
&= \oint_v \frac{dz}{2\pi i} \left[\frac{1}{(z-v)} e^{i\sqrt{q}\phi(v)+i(q-1)\phi(v)/\sqrt{q}} \right] \\
&= \oint_v \frac{dz}{2\pi i} \left[\frac{1}{(z-v)} e^{i(2q-1)\phi(v)/\sqrt{q}} \right]
\end{aligned} \tag{B.10}$$

and

$$\begin{aligned}
\mathcal{I}_2^{q-1}(v) &= \oint_v \frac{dz}{2\pi i} \frac{1}{z-v} \mathcal{V}_2(v) \\
&= \oint_v \frac{dz}{2\pi i} \left[\frac{1}{(z-v)} e^{i(2q-1)\phi(v)/\sqrt{q}} \right]
\end{aligned} \tag{B.11}$$

We note that

$$\mathcal{I}_1^{q-1}(v) = \mathcal{I}_2^{q-1}(v) \quad (\text{B.12})$$

and hence we find that $\chi^{q-1}(v)$ is a null field.

B.3 Null fields $\chi^p(v)$, $p \in \{0, 1, \dots, q-2\}$

We proceed in the same way as before and we write

$$\begin{aligned} \chi^p(v) &= \oint_v \frac{dz}{2\pi i} \frac{1}{(z-v)^p} G^+(z) V_1(v) \\ &= \oint_v \frac{dz}{2\pi i} \left[\frac{1}{(z-v)^p} \psi(z) \psi(v) e^{+i\sqrt{q}\phi(z)} e^{i(q-1)\phi(v)/\sqrt{q}} \right] \\ &= \oint_v \frac{dz}{2\pi i} \left[\frac{(z-v)^{q-1}}{(z-v)^p} \psi(z) \psi(v) e^{i\sqrt{q}\phi(z)+i(q-1)\phi(v)/\sqrt{q}} \right] \\ &= \oint_v \frac{dz}{2\pi i} \frac{(z-v)^{q-1}}{(z-v)^p} \left[\left(\frac{1}{z-v} + (z-v)A(v) + \dots \right) e^{i\sqrt{q}\phi(z)+i(q-1)\phi(v)/\sqrt{q}} \right] \\ &= \oint_v \frac{dz}{2\pi i} \frac{(z-v)^{q-1}}{(z-v)^p} \left[\left(\frac{1}{z-v} + (z-v)A(v) + \dots \right) e^{i(2q-1)\phi(v)/\sqrt{q}} [1 + i\sqrt{q}(z-v)\partial_v\phi(v) + \dots] \right] \\ &= 0 \end{aligned} \quad (\text{B.13})$$

We find that no term in the above integral exhibits a simple pole to provide the non-zero contribution, since $p \in \{0, 1, \dots, q-2\}$, and thereby we ensure that $\chi^p(v)$ are null fields.

Operators Annihilating the Lattice Moore-Read States with Quasiholes

” *A physicist is just an atom’s way of looking at itself.*

— Niels Bohr

We first derive the annihilation operators for the lattice Moore-Read states when $q \geq 2$, $\eta = 1$ with occupancy $n_j \in \{0, 1, 2\}$ and containing an even number of quasiholes. Next we use these results to derive the annihilation operators, which we provide in Chapter-4 in Sec. 4.3 in Eq. (4.43), for the same systems but now with occupancy $n_j \in \{0, 1\}$. Finally we derive the condition on η as mentioned in Chapter-4 in Sec. 4.3 in Eq. (4.52).

The starting point is to insert the null fields from Eq. (B.2) to the vacuum expectation value of the primary chiral conformal fields, as given in Eqs. (3.48) and (3.53). This procedure leads to the decoupling equations as [69]

$$\langle 0 | \prod_{k=1}^Q W(w_k) \prod_{j=1}^{i-1} V_{n_j}(z_j) \chi^a(z_i) \prod_{j=i+1}^N V_{n_j}(z_j) | 0 \rangle = 0 \text{ with } a \in \{0, 1, \dots, q\} \quad (\text{C.1})$$

and the next step is to rewrite those equations in the form of

$$\Lambda_i^a | \Psi_\alpha^{\eta=1, \text{qh}} \rangle = 0, \quad (\text{C.2})$$

where Λ_i^a are the operators which annihilate the wavefunctions.

C.1 $\eta = 1$ and occupancy $n_j \in \{0, 1, 2\}$

We note that the correlator vanishes if the field at i th lattice site is replaced by the null field. We derive the decoupling equations by deforming the integration contour over the complex plane, by moving the operators $G^+(z)$ and $J(z)$ in the null fields at different

positions, and by using the operator product expansions together with the commutation relations as follows

$$\begin{aligned}
G^+(z)V_{n_j}(z_j) &\sim (-1)^{(j-1)} \left[\frac{\delta_{n_j,0} \delta_{n'_j,1}}{z-z_j} \right] V_{n'_j}(z_j), \\
G^+(z)W(w_j) &\sim 0, \\
V_{n_j}(z_j)G^+(z) &= (-1)^{(q+1)n_j-1} G^+(z)V_{n_j}(z_j), \\
J(z)V_{n_j}(z_j) &\sim \frac{1}{q} \frac{(qn_j-1)}{z-z_j} V_{n_j}(z_j), \\
J(z)W(w_j) &\sim \frac{1}{q} \frac{p_j}{z-w_j} W_{p_j}(w_j), \\
:e^{i\alpha\phi(z)}::e^{i\beta\phi(z_j)}: &= (z-z_j)^{\alpha\beta} :e^{i\alpha\phi(z)+i\beta\phi(z_j)}:, \\
:e^{i\alpha\phi(z)}::e^{i\beta\phi(z_j)}: &= (-1)^{\alpha\beta} :e^{i\beta\phi(z_j)}::e^{i\alpha\phi(z)}:, \\
\psi_i(z)\psi_j(z_j) &= \delta_{ij}(-1)^{n_j} \psi_i(z_j)\psi_j(z),
\end{aligned} \tag{C.3}$$

where the symbol \sim means that we have considered the operator product expansions up to the terms which provide the non zero contributions in our results.

The total number of particles at the j th lattice site is

$$n_j = n_j^{(1)} + 2n_j^{(2)}, \tag{C.4}$$

where

$$n_j^{(1)} = d_j^\dagger d_j \text{ and } n_j^{(2)} = d_j'^\dagger d_j' \tag{C.5}$$

define individual number of particles for the two levels

$$|0\rangle \leftrightarrow |1\rangle \text{ and } |1\rangle \leftrightarrow |2\rangle, \tag{C.6}$$

respectively. Those creation, annihilation and number operators act on the states of the three level system. And thereby lead to the following equations with the proper sign factors, which maintain that q even or q odd defines fermions or bosons respectively, as

$$d_j |n_j\rangle = (-1)^{(q+1)\sum_{k=1}^{j-1} n_k} \begin{cases} 0 & n_j = 0 \\ |0\rangle & n_j = 1 \\ 0 & n_j = 2 \end{cases} \quad (\text{C.7})$$

$$d_j^\dagger |n_j\rangle = (-1)^{(q+1)\sum_{k=1}^{j-1} n_k} \begin{cases} |1\rangle & n_j = 0 \\ 0 & n_j = 1 \\ 0 & n_j = 2 \end{cases} \quad (\text{C.8})$$

$$d'_j |n_j\rangle = (-1)^{(q+1)\sum_{k=1}^{j-1} n_k} \begin{cases} 0 & n_j = 0 \\ 0 & n_j = 1 \\ |1\rangle & n_j = 2 \end{cases} \quad (\text{C.9})$$

$$d_j'^\dagger |n_j\rangle = (-1)^{(q+1)\sum_{k=1}^{j-1} n_k} \begin{cases} 0 & n_j = 0 \\ |2\rangle & n_j = 1 \\ 0 & n_j = 2 \end{cases}. \quad (\text{C.10})$$

We write the above mentioned operators, acting on the j th lattice site, in the matrix form with respect to the basis $(|0\rangle, |1\rangle, |2\rangle)$ as

$$d_j = \mathcal{S} \begin{bmatrix} 0 & 1 & 0 \\ 0 & 0 & 0 \\ 0 & 0 & 0 \end{bmatrix}, \quad d_j^\dagger = \mathcal{S} \begin{bmatrix} 0 & 0 & 0 \\ 1 & 0 & 0 \\ 0 & 0 & 0 \end{bmatrix}, \quad d'_j = \mathcal{S} \begin{bmatrix} 0 & 0 & 0 \\ 0 & 0 & 1 \\ 0 & 0 & 0 \end{bmatrix}, \quad (\text{C.11})$$

$$d_j'^\dagger = \mathcal{S} \begin{bmatrix} 0 & 0 & 0 \\ 0 & 0 & 0 \\ 0 & 1 & 0 \end{bmatrix}, \quad n_j^{(1)} = \begin{bmatrix} 0 & 0 & 0 \\ 0 & 1 & 0 \\ 0 & 0 & 0 \end{bmatrix}, \quad n_j^{(2)} = \begin{bmatrix} 0 & 0 & 0 \\ 0 & 0 & 0 \\ 0 & 0 & 1 \end{bmatrix}, \quad (\text{C.12})$$

where

$$\mathcal{S} = (-1)^{(q+1)\sum_{k=1}^{j-1} n_k} \quad (\text{C.13})$$

is the sign factor as already defined before.

We evaluate here the annihilation operator corresponding to the null field $\chi^q(v)$ form Eq. (B.2) in details. Therefore we write

$$\begin{aligned} 0 &= \langle W(w_1) \dots W(w_Q) V_{n_1}(z_1) \dots V_{n_{i-1}}(z_{i-1}) \chi^q(z_i) V_{n_{i+1}}(z_{i+1}) \dots V_{n_N}(z_N) \rangle \\ &= \oint_{z_i} \frac{dz}{2\pi i} \frac{1}{(z - z_i)^q} \langle W(w_1) \dots W(w_Q) V_{n_1}(z_1) \dots G^+(z) \mathcal{V}_1(z_i) \dots V_{n_N}(z_N) \rangle \\ &\quad - q \oint_{z_i} \frac{dz}{2\pi i} \frac{1}{z - z_i} \langle W(w_1) \dots W(w_Q) V_{n_1}(z_1) \dots J(z) \mathcal{V}_2(z_i) \dots V_{n_N}(z_N) \rangle \\ &= I_1^q + I_2^q. \end{aligned} \quad (\text{C.14})$$

Now the term I_1^q evaluates to

$$\begin{aligned}
I_1^q &= \oint_{z_i} \frac{dz}{2\pi i} \frac{1}{(z-z_i)^q} \langle W(w_1) \dots W(w_Q) V_{n_1}(z_1) \dots G^+(z) \mathcal{V}_1(z_i) \dots V_{n_N}(z_N) \rangle \\
&= - \sum_{j=1(\neq i)}^N \oint_{z_j} \frac{dz}{2\pi i} \frac{1}{(z-z_i)^q} \langle W(w_1) \dots W(w_Q) V_{n_1}(z_1) \dots G^+(z) \mathcal{V}_1(z_i) \dots V_{n_N}(z_N) \rangle \\
&= -(-1)^{i-1} \sum_{j=1}^{i-1} \oint_{z_j} \frac{dz}{2\pi i} \frac{(-1)^{(q+1)\sum_{k=j}^{i-1} n_k}}{(z-z_i)^q} \frac{\delta_{n_j,0} \delta_{n'_j,1}}{z-z_j} \\
&\quad \times \langle W(w_1) \dots W(w_Q) V_{n_1}(z_1) \dots V_{n'_j}(z_j) \dots \mathcal{V}_1(z_i) \dots V_{n_N}(z_N) \rangle \\
&\quad - (-1)^{i-1} \sum_{j=i+1}^N \oint_{z_j} \frac{dz}{2\pi i} \frac{(-1)^{(q+1)} (-1)^{(q+1)\sum_{k=i+1}^{j-1} n_k}}{(z-z_i)^q} \frac{\delta_{n_j,0} \delta_{n'_j,1}}{z-z_j} \\
&\quad \times \langle W(w_1) \dots W(w_Q) V_{n_1}(z_1) \dots \mathcal{V}_1(z_i) \dots V_{n'_j}(z_j) \dots V_{n_N}(z_N) \rangle \\
&= -(-1)^{i-1} \sum_{j=1}^{i-1} \frac{(-1)^{(q+1)\sum_{k=j}^{i-1} n_k}}{(z_j-z_i)^q} \delta_{n_j,0} \delta_{n'_j,1} \\
&\quad \times \langle W(w_1) \dots W(w_Q) V_{n_1}(z_1) \dots V_{n'_j}(z_j) \dots \mathcal{V}_1(z_i) \dots V_{n_N}(z_N) \rangle \\
&\quad - (-1)^{i-1} \sum_{j=i+1}^N \frac{(-1)^{(q+1)} (-1)^{(q+1)\sum_{k=i+1}^{j-1} n_k}}{(z_j-z_i)^q} \delta_{n_j,0} \delta_{n'_j,1} \\
&\quad \times \langle W(w_1) \dots W(w_Q) V_{n_1}(z_1) \dots \mathcal{V}_1(z_i) \dots V_{n'_j}(z_j) \dots V_{n_N}(z_N) \rangle \\
&= -(-1)^{i-1} \sum_{j=1}^{i-1} \sum_{n'_j} \frac{(-1)^{(q+1)\sum_{k=j}^{i-1} n_k}}{(z_j-z_i)^q} \delta_{n_j,0} \delta_{n'_j,1} \\
&\quad \times \langle W(w_1) \dots W(w_Q) V_{n_1}(z_1) \dots V_{n'_j}(z_j) \dots \mathcal{V}_1(z_i) \dots V_{n_N}(z_N) \rangle \\
&\quad - (-1)^{i-1} \sum_{j=i+1}^N \sum_{n'_j} \frac{(-1)^{(q+1)} (-1)^{(q+1)\sum_{k=i+1}^{j-1} n_k}}{(z_j-z_i)^q} \delta_{n_j,0} \delta_{n'_j,1} \\
&\quad \times \langle W(w_1) \dots W(w_Q) V_{n_1}(z_1) \dots \mathcal{V}_1(z_i) \dots V_{n'_j}(z_j) \dots V_{n_N}(z_N) \rangle \\
&= - \sum_{j=1}^{i-1} \frac{(-1)^{(q+1)\sum_{k=j+1}^{i-1} n_k}}{(z_j-z_i)^q} \delta_{n_j,0} \Psi_\alpha^{\eta=1, \text{qh}}(n_1, \dots, 1, \dots, 1, \dots, n_N) \\
&\quad - \sum_{j=i+1}^N \frac{(-1)^{(q+1)} (-1)^{(q+1)\sum_{k=i+1}^{j-1} n_k}}{(z_j-z_i)^q} \delta_{n_j,0} \Psi_\alpha^{\eta=1, \text{qh}}(n_1, \dots, 1, \dots, 1, \dots, n_N) \\
&= - \sum_{j=1}^{i-1} \frac{(-1)^{(q+1)} (-1)^{(q+1)\sum_{k=j+1}^{i-1} n_k}}{(z_i-z_j)^q} \delta_{n_j,0} \Psi_\alpha^{\eta=1, \text{qh}}(n_1, \dots, 1, \dots, 1, \dots, n_N) \\
&\quad - \sum_{j=i+1}^N \frac{(-1)^{(q+1)\sum_{k=i+1}^{j-1} n_k}}{(z_i-z_j)^q} \delta_{n_j,0} \Psi_\alpha^{\eta=1, \text{qh}}(n_1, \dots, 1, \dots, 1, \dots, n_N).
\end{aligned} \tag{C.15}$$

Now we multiply Eq. (C.15) by

$$|n_1, \dots, n_{i-1}, 2, n_{i+1}, \dots, n_N\rangle \quad (\text{C.16})$$

and sum over all n_k , $k \neq i$ and thereby end up with

$$\sum_{j=1(\neq i)}^N \frac{1}{(z_i - z_j)^q} d_j d_i^{\prime\dagger} |\Psi_\alpha^{\eta=1, \text{qh}}\rangle. \quad (\text{C.17})$$

We evaluate the term I_2^q as

$$\begin{aligned} I_2^q &= -q \oint_{z_i} \frac{dz}{2\pi i} \frac{1}{z - z_i} \langle W(w_1) \dots W(w_Q) V_{n_1}(z_1) \dots J(z) \mathcal{V}_2(z_i) \dots V_{n_N}(z_N) \rangle \\ &= q \sum_{j=1(\neq i)}^N \oint_{z_j} \frac{dz}{2\pi i} \frac{1}{z - z_i} \langle W(w_1) \dots W(w_Q) V_{n_1}(z_1) \dots J(z) \mathcal{V}_2(z_i) \dots V_{n_N}(z_N) \rangle \\ &\quad + q \sum_{j=1}^Q \oint_{w_j} \frac{dz}{2\pi i} \frac{1}{z - z_i} \langle W(w_1) \dots W(w_Q) V_{n_1}(z_1) \dots J(z) \mathcal{V}_2(z_i) \dots V_{n_N}(z_N) \rangle \\ &= \sum_{j=1(\neq i)}^N \oint_{z_j} \frac{dz}{2\pi i} \frac{1}{z - z_i} \frac{(qn_j - 1)}{z - z_j} \\ &\quad \times \langle W(w_1) \dots W(w_Q) V_{n_1}(z_1) \dots V_{n_j}(z_j) \dots \mathcal{V}_2(z_i) \dots V_{n_N}(z_N) \rangle \\ &\quad + \sum_{j=1}^Q \oint_{w_j} \frac{dz}{2\pi i} \frac{1}{z - z_i} \frac{p_j}{z - w_j} \langle W(w_1) \dots W(w_Q) V_{n_1}(z_1) \dots \mathcal{V}_2(z_i) \dots V_{n_N}(z_N) \rangle \\ &= \sum_{j=1(\neq i)}^N \frac{(qn_j - 1)}{z_j - z_i} \langle W(w_1) \dots W(w_Q) V_{n_1}(z_1) \dots V_{n_j}(z_j) \dots \mathcal{V}_2(z_i) \dots V_{n_N}(z_N) \rangle \\ &\quad + \sum_{j=1}^Q \frac{p_j}{w_j - z_i} \langle W(w_1) \dots W(w_Q) V_{n_1}(z_1) \dots \mathcal{V}_2(z_i) \dots V_{n_N}(z_N) \rangle \end{aligned} \quad (\text{C.18})$$

We multiply Eq. (C.18) by

$$|n_1, \dots, n_{i-1}, 2, n_{i+1}, \dots, n_N\rangle = \sum_{n'_i} n_i^{(2)} |n_1, \dots, n'_i, \dots, n_N\rangle, \quad (\text{C.19})$$

and sum over all n_k , $k \neq i$ to get

$$- \sum_{j=1(\neq i)}^N \frac{qn_j - 1}{z_i - z_j} n_i^{(2)} |\Psi_\alpha^{\eta=1, \text{qh}}\rangle - \sum_{j=1}^Q \frac{p_j}{z_i - w_j} n_i^{(2)} |\Psi_\alpha^{\eta=1, \text{qh}}\rangle. \quad (\text{C.20})$$

Now we add Eq. (C.17) and Eq. (C.20) and thereby we obtain

$$\lambda_i^q |\Psi_\alpha^{\eta=1, \text{qh}}\rangle = 0, \quad (\text{C.21})$$

where we have

$$\lambda_i^q = \sum_{j=1(\neq i)}^N \frac{d_j d_i'^{\dagger}}{(z_i - z_j)^q} - \sum_{j=1(\neq i)}^N \frac{q n_j - 1}{z_i - z_j} n_i^{(2)} - \sum_{j=1}^Q \frac{p_j}{z_i - w_j} n_i^{(2)} \quad (\text{C.22})$$

We proceed in the same way as before and, by using the other null fields in Eq (B.2), we end up with the following annihilation operators for the states as

$$\begin{aligned} \lambda_i^0 &= \sum_i d_i, \quad \lambda_i^p = \sum_{j(\neq i)} \frac{1}{(z_i - z_j)^p} d_j d_i'^{\dagger}, \\ \lambda_i^{q-1} &= \sum_{j(\neq i)} \frac{1}{(z_i - z_j)^{q-1}} d_j d_i'^{\dagger} + n_i^{(2)}. \end{aligned} \quad (\text{C.23})$$

C.2 $\eta = 1$ and occupancy $n_j \in \{0, 1\}$

We derive here the operators annihilating the states for the occupancy $n_j \in \{0, 1\}$ by using the operators as derived in Eqs. (C.22) and (C.23). We start by dividing the total Hilbert space $\mathcal{H}_1 + \mathcal{H}_2$ into the two subspaces \mathcal{H}_1 and \mathcal{H}_2 . Here \mathcal{H}_1 is the space which consists of all the states with no doubly occupied lattice sites, and \mathcal{H}_2 is the space consisting of all the states with at least one doubly occupied lattice site. Therefore the operators for the occupancy $n_j \in \{0, 1\}$ lie in \mathcal{H}_1 and the operators for the occupancy $n_j \in \{0, 1, 2\}$ reside in $\mathcal{H}_1 + \mathcal{H}_2$. We project the operators in $\mathcal{H}_1 + \mathcal{H}_2$ space to \mathcal{H}_1 space in order to obtain the desired operators.

We commence by multiplying the operators

$$\lambda_i^a, \quad a \in \{0, 1, \dots, q\}, \quad (\text{C.24})$$

as derived in Eqs. (C.22) and (C.23), by d_i' from the left. Since we have

$$d_i' d_i'^{\dagger} = n_i^{(1)}, \quad (\text{C.25})$$

which acts on the \mathcal{H}_1 only, therefore the operators

$$d_i' \lambda_i^a, \quad a \in \{0, 1, \dots, q-2\} \quad (\text{C.26})$$

annihilate the states for the occupancy $n_j^{(1)} \in \{0, 1\}$. We note that $d_i' \lambda_i^{q-1}$ annihilates the wavefunctions for the occupancy $n_j \in \{0, 1, 2\}$ and hence we can write

$$\left[d_i' + \sum_{j(\neq i)} \frac{1}{(z_i - z_j)^{q-1}} d_j n_i^{(1)} \right] |\Psi_\alpha^{\eta=1, \text{qh}}\rangle = 0. \quad (\text{C.27})$$

This allows us to replace the d'_i operator in $d'_i \lambda_i^q$ by

$$- \sum_{h(\neq i)} \frac{1}{(z_i - z_h)^{q-1}} d_h n_i^{(1)}. \quad (\text{C.28})$$

Therefore we obtain the following annihilation operators, after making the projection, as

$$\begin{aligned} \Lambda^0 &= \sum_i d_i, \quad \Lambda_i^p = \sum_{j(\neq i)} \frac{1}{(z_i - z_j)^p} d_j n_i^{(1)}, \\ \Lambda_i^{q-1} &= \left[\sum_{j(\neq i)} \frac{d_j n_i^{(1)}}{(z_i - z_j)^q} + \sum_{h(\neq i)} \frac{[q n_j^{(1)} - 1] d_h n_i^{(1)}}{(z_i - z_h)^{q-1} (z_i - z_j)} \right] + \sum_j \sum_{h(\neq i)} \frac{p_j d_h n_i^{(1)}}{(z_i - z_h)^{q-1} (z_i - w_j)} \end{aligned} \quad (\text{C.29})$$

These operators annihilate the states with occupancy $n_j^{(1)} \in \{0, 1\}$. We denote $n_j^{(1)}$ as n_j in Chapter-4 in Sec. 4.3.

C.3 Condition on η

We first derive the condition on the charge \mathcal{P}/q at infinity. Then we use the relation

$$\mathcal{P} = N(1 - \eta) \quad (\text{C.30})$$

to obtain the condition on η . The starting point is that if we insert a null field then the correlator in Eq. (4.6) becomes zero as

$$\left\langle \prod_{k=1}^Q W(w_k) \Xi_{\mathcal{P}}(\xi \rightarrow \infty) \prod_{j=1}^{i-1} V_{n_j}(z_j) \chi^a(z_i) \prod_{j=i+1}^N V_{n_j}(z_j) \right\rangle = 0, \text{ where } a \in \{0, 1, \dots, q\}. \quad (\text{C.31})$$

We derive the above correlator for different parts of all the null fields as given in Eq. (B.2). Now for the following term we have

$$\begin{aligned} & - \oint_v \frac{dz}{2\pi i} \frac{1}{z-v} q J(z) \mathcal{V}_2(v) \\ & = -q \oint_{z_i} \frac{dz}{2\pi i} \frac{1}{z-z_i} \langle W(w_1) \dots W(w_Q) \Xi_{\mathcal{P}}(\xi) V_{n_1}(z_1) \dots J(z) \mathcal{V}_2(z_i) \dots V_{n_N}(z_N) \rangle \end{aligned} \quad (\text{C.32})$$

We proceed in the same way as before and multiply the term in Eq. (C.32) by

$$|n_1, \dots, n_{i-1}, 2, n_{i+1}, \dots, n_N\rangle = \sum_{n'_i} n_i^{(2)} |n_1, \dots, n'_i, \dots, n_N\rangle, \quad (\text{C.33})$$

and sum over all n_k , $k \neq i$. We thereby obtain the term as

$$\left[- \sum_{j=1(\neq i)}^N \frac{qn_j - 1}{z_i - z_j} n_i^{(2)} - \sum_{j=1}^Q \frac{p_j}{z_i - w_j} n_i^{(2)} - \frac{\mathcal{P}}{z_i - \xi} n_i^{(2)} \right] |\Psi_\alpha^{\eta=1, \text{qh}}\rangle, \quad (\text{C.34})$$

where we note that the last term in Eq. (C.34) vanishes in the limit $\xi \rightarrow \infty$.

Similarly for the following term we have

$$\begin{aligned} & - \oint_v \frac{dz}{2\pi i} \frac{1}{z-v} \mathcal{V}_2(v) \\ & = - \oint_{z_i} \frac{dz}{2\pi i} \frac{1}{z-z_i} \langle W(w_1) \dots W(w_Q) \Xi_{\mathcal{P}}(\xi) V_{n_1}(z_1) \dots \mathcal{V}_2(z_i) \dots V_{n_N}(z_N) \rangle \end{aligned} \quad (\text{C.35})$$

and proceeding as before we get

$$n_i^{(2)} |\Psi_\alpha^{\eta=1, \text{qh}}\rangle. \quad (\text{C.36})$$

Now we consider the following term as

$$\oint_v \frac{dz}{2\pi i} \frac{1}{(z-v)^a} G^+(z) \mathcal{V}_1(v), \text{ where } a \in \{0, 1, \dots, q\}. \quad (\text{C.37})$$

and thereby we have

$$\oint_{z_i} \frac{dz}{2\pi i} \frac{1}{(z-z_i)^a} \langle W(w_1) \dots W(w_Q) \Xi_{\mathcal{P}}(\xi) V_{n_1}(z_1) \dots G^+(z) \mathcal{V}_1(z_i) \dots V_{n_N}(z_N) \rangle \quad (\text{C.38})$$

which after the contour deformation becomes

$$\begin{aligned} & - \sum_{j=1(\neq i)}^N \oint_{z_j} \frac{dz}{2\pi i} \frac{1}{(z-z_j)^q} \langle W(w_1) \dots W(w_Q) \Xi_{\mathcal{P}}(\xi) V_{n_1}(z_1) \dots G^+(z) \mathcal{V}_1(z_i) \dots V_{n_N}(z_N) \rangle \\ & - \oint_\xi \frac{dz}{2\pi i} \frac{1}{(z-z_i)^q} \langle W(w_1) \dots W(w_Q) \Xi_{\mathcal{P}}(\xi) V_{n_1}(z_1) \dots G^+(z) \mathcal{V}_1(z_i) \dots V_{n_N}(z_N) \rangle. \end{aligned} \quad (\text{C.39})$$

Now we proceed as before and multiply the first term in Eq. (C.39) by

$$|n_1, \dots, n_{i-1}, 2, n_{i+1}, \dots, n_N\rangle \quad (\text{C.40})$$

and sum over all n_k , $k \neq i$ and thereby we find

$$\sum_{j=1(\neq i)}^N \frac{1}{(z_i - z_j)^q} d_j d_i'^{\dagger} |\Psi_\alpha^{\eta=1, \text{qh}}\rangle. \quad (\text{C.41})$$

Let us evaluate the second term in Eq (C.39) as

$$\begin{aligned}
& - (-1)^{i-1+p} \sum_{n_i} \delta_{n_i=1} \oint_{\xi} \frac{dz}{2\pi i} \frac{(-1)^{-(i-1)n_i}}{(z-z_i)^a} (-1)^{(q+1)\sum_{k=1}^{i-1} n_k} \\
& \quad \times \langle W(w_1) \dots W(w_Q) \Xi_{\mathcal{P}}(\xi) V_{n_1}(z_1) \dots G^+(z) \mathcal{V}_1(z_i) \dots V_{n_N}(z_N) \rangle.
\end{aligned} \tag{C.42}$$

Now we compute the contour integral and write Eq. (C.42) as

$$\begin{aligned}
& - (-1)^{i-1+p} \delta_{\mathcal{P}<0} \sum_{n_i} \delta_{n_i=1} \lim_{z \rightarrow \xi} \frac{1}{(-\mathcal{P}-1)!} \frac{d^{-\mathcal{P}-1}}{dz^{-\mathcal{P}-1}} \frac{(-1)^{-(i-1)n_i}}{(z-z_i)^a} (-1)^{(q+1)\sum_{k=1}^{i-1} n_k} \\
& \delta_n \text{Pf}(A) \prod_{i,j} (w_i - z_j)^{-\frac{1}{2}} \prod_j (z - z_j)^{(qn_j-1)} \prod_j (-1)^{(j-1)n_j} \prod_j (\xi - z_j)^{(qn_j-1)\frac{\mathcal{P}}{q}} \\
& \prod_j (-1)^{(j-1)n_j} \prod_{j<k} (z_j - z_k)^{(qn_j-1)(qn_k-1)/q} \prod_{j<k} (w_j - w_k)^{\frac{p_j p_k}{q}} \prod_{j,k} (w_j - z_k)^{(qn_k-1)p_j/q},
\end{aligned} \tag{C.43}$$

where we have $\delta_n = 1$ if the total number of particles is

$$M = (N - \mathcal{P} - \sum_k p_k - q)/q \tag{C.44}$$

and we have $\delta_n = 0$ otherwise.

Now Eq. (C.43) = 0 gives rise to the restriction on the choice of \mathcal{P} and hence on the choice of η . This also keeps the derived annihilation operators in Eq. (C.29) unchanged. Now we note that the expression in Eq (C.43) is zero if $\mathcal{P} > 0$ due to the factor $\delta_{\mathcal{P}<0}$. We inspect the derivative and the exponent of the polynomial to find that Eq. (C.43) is also zero when

$$\mathcal{P} > -q - a - \sum_k p_k + Q. \tag{C.45}$$

Since we have $a \in \{0, 1, \dots, q\}$, then we can safely use the maximum value of a in that expression to write

$$\mathcal{P} > -2q - \sum_k p_k + Q. \tag{C.46}$$

Now we use the following relation

$$\mathcal{P} = N(1 - \eta) \tag{C.47}$$

to get the condition on η as

$$\eta < 1 + \frac{1}{N} \left(2q + \sum_{k=1}^Q p_k - Q \right). \tag{C.48}$$

In the thermodynamic limit $N \rightarrow \infty$, this condition becomes $\eta < 1$.

Wavefunction in the Limit of Small Λ

” *In physics, you don't have to go around making trouble for yourself - nature does it for you.*

— Frank Wilczek

In this section, we derive an expression for the wavefunction when (8.30) applies. As mentioned in the main text, we number the spins with $\sigma_j > 0$ from 1 to N_+ and the spins with $\sigma_j < 0$ from $N_+ + 1$ to $N = N_+ + N_-$. First we note that

$$z_j - z_k = \sigma_j e^{\Lambda f(j)} - \sigma_k e^{\Lambda f(k)} = e^{\Lambda[f(j)+f(k)]/2} \times \{ \sigma_j e^{\Lambda[f(j)-f(k)]/2} - \sigma_k e^{-\Lambda[f(j)-f(k)]/2} \}$$

$$\approx \begin{cases} \Lambda[f(j) - f(k)] \sigma_j e^{\Lambda[f(j)+f(k)]/2} & \text{for } \sigma_j = \sigma_k \\ 2\sigma_j e^{\Lambda[f(j)+f(k)]/2} & \text{for } \sigma_j = -\sigma_k \end{cases} .$$
(D.1)

The factor

$$\prod_{j < k} \{ 2e^{\Lambda[f(j)+f(k)]/2} \}^{(s_j s_k - 1)/2} = e^{\sum_{j < k} \{ \Lambda[f(j)+f(k)]/2 + \ln(2) \} (s_j s_k - 1)/2}$$

$$= e^{\sum_{j, k} \{ \Lambda[f(j)+f(k)]/2 + \ln(2) \} (s_j s_k - 1)/4} \quad (D.2)$$

$$= e^{\sum_j [-N\Lambda f(j) - N\ln(2)]/4}$$

does not depend on s_j , so it will be absorbed in the normalization of the wavefunction and can be ignored. We are hence left with

$$\Psi_{s_1, \dots, s_N}(z_1, \dots, z_N) \approx \text{constant} \times \delta_{\mathbf{s}} \prod_{p=1}^N \chi_{p, s_p} \prod_{j < k} \sigma_j^{\frac{1}{2}(s_j s_k - 1)}$$

$$\times \prod_{\{j < k | \sigma_j = \sigma_k\}} \{ \Lambda[f(j) - f(k)]/2 \}^{\frac{1}{2}(s_j s_k - 1)} .$$
(D.3)

Let us introduce the notation

$$s_+ \equiv \sum_{\{j | \sigma_j = +1\}} s_j \quad \text{and} \quad s_- \equiv \sum_{\{j | \sigma_j = -1\}} s_j .$$
(D.4)

We then have

$$\begin{aligned} \prod_{j < k} \sigma_j^{\frac{1}{2}(s_j s_k - 1)} &= (-1)^{\sum_{\{j < k | \sigma_j = -1\}} (s_j s_k - 1)/2} = (-1)^{\sum_{\{j < k | \sigma_j = \sigma_k = -1\}} (s_j s_k - 1)/2} \\ &= (-1)^{\sum_{\{j, k | \sigma_j = \sigma_k = -1\}} (s_j s_k - 1)/4} = (-1)^{(s_+^2 - N_+^2)/4}, \end{aligned} \quad (\text{D.5})$$

where we have used that the spins with $\sigma_j < 0$ have higher indices than those with $\sigma_j > 0$. We also have

$$\begin{aligned} \prod_{p=1}^N \chi_{p, s_p} &= \prod_{p=1}^{N_+} \chi_{p, s_p} \prod_{p=1}^{N_-} e^{i\pi(N_+ + p - 1)(1 + s_{N_+ + p})/2} \\ &= \prod_{p=1}^{N_-} (-1)^{N_+(1 + s_{N_+ + p})/2} \prod_{p=1}^{N_+} \chi_{p, s_p} \prod_{p=1}^{N_-} \chi_{p, s_{N_+ + p}} \\ &= (-1)^{N_+(N_- + s_-)/2} \prod_{p=1}^{N_+} \chi_{p, s_p} \prod_{p=1}^{N_-} \chi_{p, s_{N_+ + p}}. \end{aligned} \quad (\text{D.6})$$

Now we note that

$$\prod_{\{j < k | \sigma_j = \sigma_k\}} \Lambda^{\frac{1}{2}(s_j s_k - 1)} = \prod_{\{j, k | \sigma_j = \sigma_k\}} \Lambda^{\frac{1}{4}(s_j s_k - 1)} = \Lambda^{\frac{1}{4}(s_+^2 - N_+^2 + s_-^2 - N_-^2)}.$$

Therefore, in the limit (8.30), only configurations that minimize $s_+^2 + s_-^2$ will remain. If N_+ and N_- are both even, we have that $s_+^2 + s_-^2$ is minimized for $s_+ = s_- = 0$. In other words, δ_s is replaced by $\delta_{s_+} \delta_{s_-}$. If N_+ and N_- are both odd, it is not possible to have $s_+ = 0$ or $s_- = 0$, and we minimize $s_+^2 + s_-^2$ for the choice $s_+ = -s_- = +1$ and for the choice $s_+ = -s_- = -1$. In that case, δ_s is replaced by $\delta_{s_+ = 1} \delta_{s_- = -1}$ and $\delta_{s_+ = -1} \delta_{s_- = 1}$, respectively. The relative sign of the two terms in the wavefunction is

$$(-1)^{N_+(N_- - 1)/2 - N_+(N_- + 1)/2} = -1. \quad (\text{D.7})$$

Inserting the above observations into (D.3), we obtain (8.33) and (8.34) in the main text.

Wavefunction in the Limit of Large Λ

“ All of physics is either impossible or trivial. It is impossible until you understand it, and then it becomes trivial.

— Ernest Rutherford

To determine the form of the wavefunction (8.4) with coordinates (8.23) in the limit (8.38), we first write the wavefunction as follows

$$\begin{aligned}
 \delta_s \prod_{p=1}^N \chi_{p,s_p} \prod_{j < k} (z_j - z_k)^{\frac{1}{2}(s_j s_k - 1)} &= \delta_s \prod_{p=1}^N \chi_{p,s_p} \prod_{j < k} \left[\cancel{\sigma_{2j} e^{\Lambda f(2j)}} - \sigma_{2k} e^{\Lambda f(2k)} \right]^{(s_{2j} s_{2k} - 1)/2} \\
 &\times \prod_{j < k} \left[\cancel{\sigma_{2j-1} e^{\Lambda f(2j-1)}} - \sigma_{2k-1} e^{\Lambda f(2k-1)} \right]^{(s_{2j-1} s_{2k-1} - 1)/2} \\
 &\times \prod_{j < k} \left[\cancel{\sigma_{2j} e^{\Lambda f(2j)}} - \sigma_{2k-1} e^{\Lambda f(2k-1)} \right]^{(s_{2j} s_{2k-1} - 1)/2} \\
 &\times \prod_{j < k} \left[\cancel{\sigma_{2j-1} e^{\Lambda f(2j-1)}} - \sigma_{2k} e^{\Lambda f(2k)} \right]^{(s_{2j-1} s_{2k} - 1)/2} \\
 &\times \prod_{k=1}^{N/2} \left[\sigma_{2k-1} e^{\Lambda f(2k-1)} - \sigma_{2k} e^{\Lambda f(2k)} \right]^{(s_{2k-1} s_{2k} - 1)/2}.
 \end{aligned} \tag{E.1}$$

For the sake of generality, we shall here assume that the σ_k are general phase factors not restricted to being plus or minus one. Utilizing (8.38), we can ignore the terms that are crossed out in the above expression. Let us define $\tilde{\sigma}(2k)$ and $\tilde{f}(2k)$ such that

$$-\tilde{\sigma}_{2k} e^{\Lambda \tilde{f}(2k)} = -\sigma_{2k} e^{\Lambda f(2k)} + \sigma_{2k-1} e^{\Lambda f(2k-1)}. \tag{E.2}$$

Since $f(2k) \geq f(2k-1)$, we must have $\tilde{f}(2k) \leq f(2k) + \ln(2)/\Lambda$.

With the definition (E.2) we get that (E.1) simplifies to

$$\delta_{\mathbf{s}} \prod_{p=1}^N \chi_{p,s_p} \prod_{j<k} (z_j - z_k)^{\frac{1}{2}(s_j s_k - 1)} \approx \text{constant} \times \delta_{\mathbf{s}} e^{\Lambda F} \prod_{p=1}^N \chi_{p,s_p} \times \prod_{j<k} (-\sigma_k)^{(s_j s_k - 1)/2} \prod_{k=1}^{N/2} \left(\frac{\tilde{\sigma}_{2k}}{\sigma_{2k}} \right)^{(s_{2k-1} s_{2k} - 1)/2}, \quad (\text{E.3})$$

where

$$F \equiv \sum_{k=2}^{N/2} [f(2k-1)s_{2k-1} + f(2k)s_{2k}] \sum_{j=1}^{k-1} (s_{2j-1} + s_{2j}) + \sum_{k=1}^{N/2} \tilde{f}(2k)s_{2k-1}s_{2k}. \quad (\text{E.4})$$

The configurations with the highest weight in the wavefunction are hence those that maximize F under the constraint $\sum_j s_j = 0$. In appendix F, we show that, under the constraint $\sum_j s_j = 0$, F is maximal for all configurations fulfilling $s_{2j-1} + s_{2j} = 0$ for all $j \in \{1, 2, \dots, N/2\}$. We also show that all other configurations with $\sum_j s_j = 0$ have negligible weight, when the approximation (8.38) applies.

To show that the wavefunction is a product of singlets, we additionally need to show that the wavefunction has the right phase factors. The phase of the wavefunction for a given configuration is

$$\prod_{p=1}^N \chi_{p,s_p} \prod_{j<k} (-\sigma_k)^{(s_j s_k - 1)/2} \prod_{k=1}^{N/2} \left(\frac{\tilde{\sigma}_{2k}}{\sigma_{2k}} \right)^{(s_{2k-1} s_{2k} - 1)/2}. \quad (\text{E.5})$$

Utilizing that $s_{2j-1} + s_{2j} = 0$ for all contributing configurations, we get

$$\sum_{j=1}^{k-1} s_j s_k = \begin{cases} -1 & \text{for } k \text{ even} \\ 0 & \text{for } k \text{ odd} \end{cases}, \quad (\text{E.6})$$

and it follows that the latter two products in (E.5) do not depend on the configuration.

From the definition of χ_{p,s_p} , one can check that

$$\chi_{2j-1,+1} \chi_{2j,-1} = -\chi_{2j-1,-1} \chi_{2j,+1}. \quad (\text{E.7})$$

The phase factors of the terms in the wavefunction are hence precisely those for a product of singlets.

Derivation of an Inequality

” *The true laboratory is the mind, where behind illusions we uncover the laws of truth.*

— Jagadish Chandra Bose

To show that precisely the configurations with $s_{2j-1} + s_{2j} = 0$ for all $j \in \{1, 2, \dots, N/2\}$ maximize F under the constraint $\sum_j s_j = 0$, we first note that

$$\begin{aligned}
 F &= \sum_{k=2}^{N/2} [f(2k-1)s_{2k-1} + f(2k)s_{2k}] \sum_{j=1}^{k-1} (s_{2j-1} + s_{2j}) + \sum_{k=1}^{N/2} \tilde{f}(2k)s_{2k-1}s_{2k} \\
 &= \frac{1}{2} \sum_{k=2}^{N/2} [f(2k) + f(2k-1)] (s_{2k} + s_{2k-1}) \sum_{j=1}^{k-1} (s_{2j-1} + s_{2j}) + \sum_{k=1}^{N/2} \tilde{f}(2k)(s_{2k-1}s_{2k} + 1) \\
 &\quad + \frac{1}{2} \sum_{k=2}^{N/2} [f(2k) - f(2k-1)] (s_{2k} - s_{2k-1}) \sum_{j=1}^{k-1} (s_{2j-1} + s_{2j}) - \sum_{k=1}^{N/2} \tilde{f}(2k).
 \end{aligned}$$

With this expression, it is natural to group the spins together in pairs. We define

$$t_j = \frac{1}{2}(s_{2j-1} + s_{2j}), \quad j \in \{1, 2, \dots, N/2\}. \quad (\text{F.1})$$

We note that t_j can take the values -1 , 0 , or $+1$. We shall refer to these as negative defect, no defect, and positive defect, respectively. Note also that the condition $\sum_{j=1}^N s_j = 0$ translates into $\sum_{j=1}^{N/2} t_j = 0$, so for a given choice of configuration, the number of positive defects must equal the number of negative defects. Let us consider a configuration with defects at $a_1 < a_2 < \dots < a_D$, where $a_j \in \{1, 2, \dots, N/2\}$. The factor $(s_{2k} - s_{2k-1})$ is zero if there is a defect at position k , and can be either plus or minus two if there is no defect. The choice of sign does not affect other parts of the right hand side of (F.1), and we get the largest value of the right hand side if the sign of $(s_{2k} - s_{2k-1})$ always cancels the sign of

$$\sum_{j=1}^{k-1} (s_{2j-1} + s_{2j}). \quad (\text{F.2})$$

We can therefore rewrite (F.1) into

$$\begin{aligned} \frac{1}{2}F + \frac{1}{2} \sum_{k=1}^{N/2} \tilde{f}(2k) \leq & \sum_{k=2}^{N/2} [f(2k) + f(2k-1)] t_k \sum_{j=1}^{k-1} t_j + \sum_{k=1}^{N/2} \tilde{f}(2k) |t_k| \\ & + \sum_{k=2}^{N/2} [f(2k) - f(2k-1)] (1 - |t_k|) \left| \sum_{j=1}^{k-1} t_j \right|. \end{aligned} \quad (\text{F.3})$$

We note that the right hand side of this expression is zero if no defects are present.

We now pair up the positive and negative defects in an iterative process as follows. In each iteration step, we pair a_q with a_p according to the following rules:

1. q is the lowest possible number such that a_q is a defect that has not yet been paired.
2. p is the lowest possible number such that
 - a_p is a defect that has not yet been paired
 - $t_{a_p} = -t_{a_q}$
 - $\sum_{x=q+1}^{p-1} t_{a_x} = 0$

We repeat this process until all defects have been paired. An example is shown in Fig. F.1

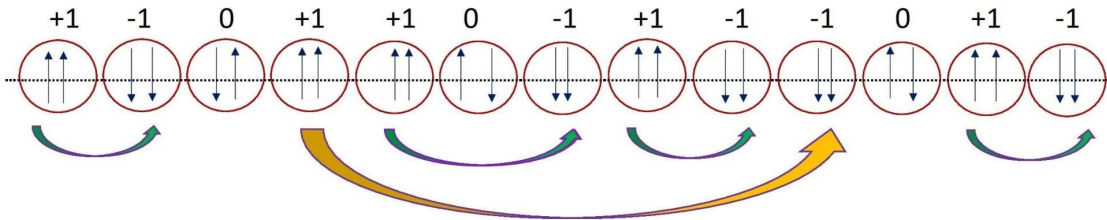


Figure F.1.: Example of the pairing of spins and defects used in the derivation. The figure shows the spins $1, 2, \dots, N$ in the wavefunction (8.4). Each spin is shown as a black arrow. An arrow pointing up or down represents the spin state $s_j = +1$ or $s_j = -1$. The red circles illustrate the pairing of neighboring spins, as for example spin 1 with spin 2, spin 3 with spin 4, \dots , spin $N-1$ with spin N . If the neighboring spins are both up, this leads to a positive defect, which is labeled as $+1$, if the neighboring spins are both down, this leads to a negative defect, which is labeled as -1 , and if one spin is up and one is down, it leads to a neutral site with no defect, which is labeled as 0 . Defects with opposite signs are then paired. We first pair the defects, for which the two defects are neighbors or only have neutral sites between them. These pairs are marked with the four green arrows. We then pair defects, for which the two defects are neighbors if we ignore neutral sites and defects that we have already paired. There is one such pair in the figure, and it is marked with a yellow arrow. We continue this procedure until all defects have been paired.

Unless there are no defects in the system, there will always be at least one value of p for which a_p and a_{p+1} have been paired. Let us first consider such a pair. We introduce the notation

$$v_p = \sum_{j=1}^{a_p-1} t_j = \sum_{j=1}^{p-1} t_{a_j}. \quad (\text{F.4})$$

We note that $v_{p+1} = v_p + t_{a_p}$. With the choice of pairing we have made, v_{p+1} is nonzero and v_{p+1} and $t_{a_{p+1}}$ have opposite signs. Since v_{p+1} and v_p are integers fulfilling $|v_{p+1} - v_p| = 1$, v_p is either zero or has the same sign as v_{p+1} . Furthermore, since $t_{a_p} = -t_{a_{p+1}}$, it also follows that t_{a_p} and v_p have the same sign if v_p is nonzero. Therefore

$$|v_{p+1}| = |v_p + t_{a_p}| = |v_p| + 1. \quad (\text{F.5})$$

It follows that

$$t_{a_p} v_p = |t_{a_p}| |v_p| = |v_p|, \quad (\text{F.6})$$

$$t_{a_{p+1}} v_{p+1} = -|t_{a_{p+1}}| |v_{p+1}| = -|v_p| - 1. \quad (\text{F.7})$$

Utilizing this result, we find that the terms on the right hand side of (F.3), which have $k \in \{a_p, a_p + 1, \dots, a_{p+1}\}$, add up to

$$\begin{aligned} & \sum_{k=a_p}^{a_{p+1}} [f(2k) + f(2k-1)] t_k \sum_{j=1}^{k-1} t_j + \sum_{k=a_p}^{a_{p+1}} \tilde{f}(2k) |t_k| + \sum_{k=a_p}^{a_{p+1}} [f(2k) - f(2k-1)] (1 - |t_k|) \left| \sum_{j=1}^{k-1} t_j \right| \\ &= [f(2a_p) + f(2a_p - 1)] |v_p| - [f(2a_{p+1}) + f(2a_{p+1} - 1)] (|v_p| + 1) \\ &+ \tilde{f}(2a_p) + \tilde{f}(2a_{p+1}) + \sum_{k=a_p+1}^{a_{p+1}-1} [f(2k) - f(2k-1)] (|v_p| + 1) \\ &= \tilde{f}(2a_p) - f(2a_p) + \tilde{f}(2a_{p+1}) - f(2a_{p+1}) - [f(2a_{p+1}) - f(2a_p - 1)] |v_p| \\ &- \sum_{k=a_p}^{a_{p+1}-1} [f(2k+1) - f(2k)] (|v_p| + 1) \end{aligned} \quad (\text{F.8})$$

So far we have not made assumptions about \tilde{f} . For the case of interest here, however, we know that

$$\tilde{f}(2a_p) - f(2a_p) \text{ and } \tilde{f}(2a_{p+1}) - f(2a_{p+1}) \quad (\text{F.9})$$

are both at most $\ln(2)/\Lambda$. On the other hand, we know due to (8.38) that the last term on the right hand side of (F.8) is much more negative than $-2\ln(2)/\Lambda$ even for $|v_p| = 0$. Hence the right hand side of (F.8) is negative.

We then repeat the same computation for all other pairs of defects a_q and a_p for which $|p - q| = 1$. When we have done that, we remove all defects from the set $\{a_1, a_2, \dots, a_D\}$ that we have already taken into account and repeat the same computations for the pairs of defects, for which the defects in the pair are neighbors in the new set. We have shown an example as the pair marked with the yellow arrow in Fig. F.1. The computation is again

the same as above, except that some values of k between a_q and a_p are omitted from the sums, since we have already taken them into account. This does, however, not change the conclusion that the result is negative. We repeat this procedure until all defect pairs have been taken into account. Since the contribution from each pair is negative, we conclude that

$$F \leq - \sum_{k=1}^{N/2} \tilde{f}(2k), \quad (\text{F.10})$$

and equality is only obtained if there are no defects, that is if

$$s_{2j-1} + s_{2j} = 0 \text{ for all } j \in \{1, 2, \dots, N/2\}. \quad (\text{F.11})$$

It also follows from the above derivation and (8.38) that the next highest value of $e^{\Lambda F}$ is much lower than the highest value of $e^{\Lambda F}$, so only configurations fulfilling $s_{2j-1} + s_{2j} = 0$ contribute significantly to the wavefunction.

Let us finally comment that the result (F.11) is valid independent of (8.38) if $f(N) \geq f(N-1) > f(N-2) \geq f(N-3) > \dots \geq f(1)$ and $\tilde{f}(2k) \leq f(2k)$ for all k . The particular case $\tilde{f}(2k) = f(2k)$ leads to

$$\sum_{j < k} f(k) s_j s_k \leq - \sum_{k=1}^{N/2} f(2k) \quad \text{for} \quad \sum_j s_j = 0, \quad (\text{F.12})$$

with equality obtained only for spin configurations fulfilling $s_{2j-1} + s_{2j} = 0$.

Bibliography

- [1] Ian Affleck, Tom Kennedy, Elliott H Lieb, and Hal Tasaki. “Valence bond ground states in isotropic quantum antiferromagnets”. In: *Condensed Matter Physics and Exactly Soluble Models*. Springer, 1988, pp. 253–304.
- [2] Adhip Agarwala, Shriya Pai, and Vijay B. Shenoy. “Fractalized Metals”. In: *arXiv preprint arXiv:1803.01404* (2018).
- [3] Y. Aharonov and D. Bohm. “Significance of Electromagnetic Potentials in the Quantum Theory”. In: *Phys. Rev.* 115 (3 1959), pp. 485–491. DOI: 10.1103/PhysRev.115.485. URL: <https://link.aps.org/doi/10.1103/PhysRev.115.485>.
- [4] M. Aidelsburger, M. Atala, M. Lohse, J. T. Barreiro, B. Paredes, and I. Bloch. “Realization of the Hofstadter Hamiltonian with Ultracold Atoms in Optical Lattices”. In: *Phys. Rev. Lett.* 111 (18 2013), p. 185301. DOI: 10.1103/PhysRevLett.111.185301. URL: <https://link.aps.org/doi/10.1103/PhysRevLett.111.185301>.
- [5] R Ammann, B Grunbaum, and G. C. Shephard. “Aperiodic Tiles”. In: *Discrete Comput. Geom.* 8 (1992).
- [6] P.W. Anderson. “Resonating valence bonds: A new kind of insulator?” In: *Materials Research Bulletin* 8.2 (1973), pp. 153 –160. ISSN: 0025-5408. DOI: [https://doi.org/10.1016/0025-5408\(73\)90167-0](https://doi.org/10.1016/0025-5408(73)90167-0). URL: <http://www.sciencedirect.com/science/article/pii/0025540873901670>.
- [7] Eric C. Andrade, Jose A. Hoyos, Stephan Rachel, and Matthias Vojta. “Cluster-Glass Phase in Pyrochlore XY Antiferromagnets with Quenched Disorder”. In: *Phys. Rev. Lett.* 120 (9 2018), p. 097204. DOI: 10.1103/PhysRevLett.120.097204. URL: <https://link.aps.org/doi/10.1103/PhysRevLett.120.097204>.
- [8] Ronaldo N. Araujo and Eric C. Andrade. “Conventional superconductivity in quasicrystals”. In: *Phys. Rev. B* 100 (1 2019), p. 014510. DOI: 10.1103/PhysRevB.100.014510. URL: <https://link.aps.org/doi/10.1103/PhysRevB.100.014510>.
- [9] Eddy Ardonne and German Sierra. “Chiral correlators of the ising conformal field theory”. In: *Journal of Physics A: Mathematical and Theoretical* 43.50 (2010), p. 505402. URL: <http://stacks.iop.org/1751-8121/43/i=50/a=505402>.
- [10] Daniel Arovas, J. R. Schrieffer, and Frank Wilczek. “Fractional Statistics and the Quantum Hall Effect”. In: *Phys. Rev. Lett.* 53 (7 1984), pp. 722–723. DOI: 10.1103/PhysRevLett.53.722. URL: <https://link.aps.org/doi/10.1103/PhysRevLett.53.722>.

- [11] Daniel Arovas, J. R. Schrieffer, and Frank Wilczek. “Fractional Statistics and the Quantum Hall Effect”. In: *Phys. Rev. Lett.* 53 (7 1984), pp. 722–723. DOI: 10.1103/PhysRevLett.53.722. URL: <https://link.aps.org/doi/10.1103/PhysRevLett.53.722>.
- [12] Shou-Cheng Zhang B. Andrei Bernevig Taylor L. Hughes. “Quantum Spin Hall Effect and Topological Phase Transition in HgTe Quantum Wells”. In: *Science* 314 (5806 2006), pp. 1757–1761. DOI: 10.1126/science.1133734.
- [13] Nielsen Anne E B and German Sierra. “Bosonic fractional quantum Hall states on the torus from conformal field theory”. In: *Journal of Statistical Mechanics: Theory and Experiment* 2014.4 (2014), P04007. DOI: 10.1088/1742-5468/2014/04/P04007. URL: <http://stacks.iop.org/1742-5468/2014/i=4/a=P04007>.
- [14] Michael Baake and Uwe Grimm. *Aperiodic order*. Vol. 1. Cambridge University Press, 2013.
- [15] Leon Balents. “Spin liquids in frustrated magnets”. In: *Nature* 464 (7286 2010). DOI: 10.1038/nature08917. URL: <https://doi.org/10.1038/nature08917>.
- [16] Ajit C. Balram and J. K. Jain. “Exact results for model wave functions of anisotropic composite fermions in the fractional quantum Hall effect”. In: *Phys. Rev. B* 93 (7 2016), p. 075121. DOI: 10.1103/PhysRevB.93.075121. URL: <https://link.aps.org/doi/10.1103/PhysRevB.93.075121>.
- [17] M. Baraban, G. Zikos, N. Bonesteel, and S. H. Simon. “Numerical Analysis of Quasiholes of the Moore-Read Wave Function”. In: *Phys. Rev. Lett.* 103 (7 2009), p. 076801. DOI: 10.1103/PhysRevLett.103.076801. URL: <https://link.aps.org/doi/10.1103/PhysRevLett.103.076801>.
- [18] MT Batchelor, J De Gier, and Mark Maslen. “Exactly solvable $su(N)$ mixed spin ladders”. In: *Journal of Statistical Physics* 102.3-4 (2001), pp. 559–566.
- [19] Jonas Becker and Stefan Wessel. “Diagnosing Fractionalization from the Spin Dynamics of Z_2 Spin Liquids on the Kagome Lattice by Quantum Monte Carlo Simulations”. In: *Phys. Rev. Lett.* 121 (7 2018), p. 077202. DOI: 10.1103/PhysRevLett.121.077202. URL: <https://link.aps.org/doi/10.1103/PhysRevLett.121.077202>.
- [20] F. P. N. Beenker. “Algebraic theory of non-periodic tilings of the plane by two simple building blocks: a square and a rhombus”. In: *TH-Report* 82 (1982).
- [21] G. Ben-Shach, C. R. Laumann, I. Neder, A. Yacoby, and B. I. Halperin. “Detecting Non-Abelian Anyons by Charging Spectroscopy”. In: *Phys. Rev. Lett.* 110 (10 2013), p. 106805. DOI: 10.1103/PhysRevLett.110.106805. URL: <https://link.aps.org/doi/10.1103/PhysRevLett.110.106805>.
- [22] Emil J. Bergholtz and Zhao Liu. “Topological flat band models and fractional Chern insulator”. In: *Int. J. Mod. Phys. B* 27 (2013), p. 1330017.
- [23] B. A. Bernevig, D. Giuliano, and R. B. Laughlin. “Coordinate representation of the two-spinon wave function and spinon interaction in the Haldane-Shastry model”. In: *Phys. Rev. B* 64 (2 2001), p. 024425. DOI: 10.1103/PhysRevB.64.024425. URL: <https://link.aps.org/doi/10.1103/PhysRevB.64.024425>.

- [24] B. Andrei Bernevig and F. D. M. Haldane. “Clustering Properties and Model Wave Functions for Non-Abelian Fractional Quantum Hall Quasielectrons”. In: *Phys. Rev. Lett.* 102 (6 2009), p. 066802. DOI: 10.1103/PhysRevLett.102.066802. URL: <https://link.aps.org/doi/10.1103/PhysRevLett.102.066802>.
- [25] B. Andrei Bernevig and N. Regnault. “Anatomy of Abelian and Non-Abelian Fractional Quantum Hall States”. In: *Phys. Rev. Lett.* 103 (20 2009), p. 206801. DOI: 10.1103/PhysRevLett.103.206801. URL: <https://link.aps.org/doi/10.1103/PhysRevLett.103.206801>.
- [26] B. Andrei Bernevig and N. Regnault. “Emergent many-body translational symmetries of Abelian and non-Abelian fractionally filled topological insulators”. In: *Phys. Rev. B* 85 (7 2012), p. 075128. DOI: 10.1103/PhysRevB.85.075128. URL: <https://link.aps.org/doi/10.1103/PhysRevB.85.075128>.
- [27] B. Andrei Bernevig and Shou-Cheng Zhang. “Quantum Spin Hall Effect”. In: *Phys. Rev. Lett.* 96 (10 2006), p. 106802. DOI: 10.1103/PhysRevLett.96.106802. URL: <https://link.aps.org/doi/10.1103/PhysRevLett.96.106802>.
- [28] Waheb Bishara, Parsa Bonderson, Chetan Nayak, Kirill Shtengel, and J. K. Slingerland. “Interferometric signature of non-Abelian anyons”. In: *Phys. Rev. B* 80 (15 2009), p. 155303. DOI: 10.1103/PhysRevB.80.155303. URL: <https://link.aps.org/doi/10.1103/PhysRevB.80.155303>.
- [29] Immanuel Bloch, Jean Dalibard, and Wilhelm Zwerger. “Many-body physics with ultracold gases”. In: *Rev. Mod. Phys.* 80 (3 2008), pp. 885–964. DOI: 10.1103/RevModPhys.80.885. URL: <https://link.aps.org/doi/10.1103/RevModPhys.80.885>.
- [30] Parsa Bonderson, Michael Freedman, and Chetan Nayak. “Measurement-Only Topological Quantum Computation”. In: *Phys. Rev. Lett.* 101 (1 2008), p. 010501. DOI: 10.1103/PhysRevLett.101.010501. URL: <https://link.aps.org/doi/10.1103/PhysRevLett.101.010501>.
- [31] Parsa Bonderson, Victor Gurarie, and Chetan Nayak. “Plasma analogy and non-Abelian statistics for Ising-type quantum Hall states”. In: *Phys. Rev. B* 83 (7 2011), p. 075303. DOI: 10.1103/PhysRevB.83.075303. URL: <https://link.aps.org/doi/10.1103/PhysRevB.83.075303>.
- [32] E. Brouns, J. W. Visser, and P. M. De Wolff. “An anomaly in the crystal structure of Na₂CO₃”. In: *Acta Crystallographica* 17.5 (1964), pp. 614–614. DOI: 10.1107/S0365110X64001426.
- [33] N.G. de Bruijn. “Algebraic theory of Penrose’s non-periodic tilings of the plane. II”. In: *Indagationes Mathematicae (Proceedings)* 84.1 (1981), pp. 53–66. ISSN: 1385-7258. DOI: [https://doi.org/10.1016/1385-7258\(81\)90017-2](https://doi.org/10.1016/1385-7258(81)90017-2). URL: <http://www.sciencedirect.com/science/article/pii/S1385725881900172>.
- [34] Paola Brunori, Paola Magrone, and Laura Tedeschini Lalli. *Imperial Porphyry and Golden Leaf: Sierpinski Triangle in a Medieval Roman Cloister*. Vol. 809. Springer, 2018. DOI: https://doi.org/10.1007/978-3-319-95588-9_49.

- [35] Marta Brzezinska, Ashley M Cook, and Titus Neupert. “Topology in the Sierpinski-Hofstadter problem”. In: *Phys. Rev. B* 98.20 (2018), p. 205116.
- [36] Pasquale Calabrese and John Cardy. “Entanglement entropy and conformal field theory”. In: *Journal of Physics A: Mathematical and Theoretical* 42 (2009), p. 504005.
- [37] Pasquale Calabrese and John Cardy. “Entanglement entropy and quantum field theory”. In: *Journal of Statistical Mechanics: Theory and Experiment* 2004.06 (2004), P06002.
- [38] Y-H Chan and L-M Duan. “Evidence of a spin liquid with hard-core bosons in a square lattice”. In: *New Journal of Physics* 14 (2012), p. 113039. DOI: 10.1088/1367-2630/14/11/113039.
- [39] Hitesh J. Changlani, Dmitrii Kochkov, Krishna Kumar, Bryan K. Clark, and Eduardo Fradkin. “Macroscopically Degenerate Exactly Solvable Point in the Spin-1/2 Kagome Quantum Antiferromagnet”. In: *Phys. Rev. Lett.* 120 (11 2018), p. 117202. DOI: 10.1103/PhysRevLett.120.117202. URL: <https://link.aps.org/doi/10.1103/PhysRevLett.120.117202>.
- [40] Ji-Yao Chen, Laurens Vanderstraeten, Sylvain Capponi, and Didier Poilblanc. “Non-Abelian chiral spin liquid in a quantum antiferromagnet revealed by an iPEPS study”. In: *arXiv preprint arXiv:1807.04385* (2018).
- [41] Rui Chen, Chui-Zhen Chen, Jin-Hua Gao, Bin Zhou, and Dong-Hui Xu. “Higher-Order Topological Insulators in Quasicrystals”. In: *arXiv preprint arXiv:1904.09932* (2019).
- [42] Meng Cheng, Victor Galitski, and S. Das Sarma. “Nonadiabatic effects in the braiding of non-Abelian anyons in topological superconductors”. In: *Phys. Rev. B* 84 (10 2011), p. 104529. DOI: 10.1103/PhysRevB.84.104529. URL: <https://link.aps.org/doi/10.1103/PhysRevB.84.104529>.
- [43] J. I. Cirac and P. Zoller. “Quantum Computations with Cold Trapped Ions”. In: *Phys. Rev. Lett.* 74 (20 1995), pp. 4091–4094. DOI: 10.1103/PhysRevLett.74.4091. URL: <https://link.aps.org/doi/10.1103/PhysRevLett.74.4091>.
- [44] J. Ignacio Cirac and German Sierra. “Infinite matrix product states, conformal field theory, and the Haldane-Shastry model”. In: *Phys. Rev. B* 81 (10 2010), p. 104431. DOI: 10.1103/PhysRevB.81.104431. URL: <https://link.aps.org/doi/10.1103/PhysRevB.81.104431>.
- [45] Nigel R. Cooper and Jean Dalibard. “Reaching Fractional Quantum Hall States with Optical Flux Lattices”. In: *Phys. Rev. Lett.* 110 (18 2013), p. 185301. DOI: 10.1103/PhysRevLett.110.185301. URL: <https://link.aps.org/doi/10.1103/PhysRevLett.110.185301>.
- [46] Jonathan D’Emidio, Matthew S. Block, and Ribhu K. Kaul. “Renyi entanglement entropy of critical SU(N) spin chains”. In: *Phys. Rev. B* 92 (5 2015), p. 054411. DOI: 10.1103/PhysRevB.92.054411. URL: <https://link.aps.org/doi/10.1103/PhysRevB.92.054411>.

- [47] Kai Sun D.N. Sheng Zheng-Cheng Gu and L. Sheng. “Fractional quantum Hall effect in the absence of Landau levels”. In: *Nature Communications* (2011). DOI: 10.1038/ncomms1380.
- [48] Frank Wilczek Daniel P. Arovas Robert Schrieffer and A. Zee. “STATISTICAL MECHANICS OF ANYONS”. In: (2002), pp. 238–247. URL: https://doi.org/10.1142/9789812777041_0027.
- [49] S. Das Sarma, G. Gervais, and Xiaoqing Zhou. “Energy gap and spin polarization in the $5/2$ fractional quantum Hall effect”. In: *Phys. Rev. B* 82 (11 2010), p. 115330. DOI: 10.1103/PhysRevB.82.115330. URL: <https://link.aps.org/doi/10.1103/PhysRevB.82.115330>.
- [50] Sankar Das Sarma, Michael Freedman, and Chetan Nayak. “Topologically Protected Qubits from a Possible Non-Abelian Fractional Quantum Hall State”. In: *Phys. Rev. Lett.* 94 (16 2005), p. 166802. DOI: 10.1103/PhysRevLett.94.166802. URL: <https://link.aps.org/doi/10.1103/PhysRevLett.94.166802>.
- [51] J De Gier and MT Batchelor. “Magnetization plateaus in a solvable 3-leg spin ladder”. In: *Phys. Rev. B* 62.6 (2000), R3584.
- [52] Santanu Dey, Eric C. Andrade, and Matthias Vojta. “Destruction of long-range order in non-collinear two-dimensional antiferromagnets by random-bond disorder”. In: *arXiv:1907.08208* (2019).
- [53] H. T. Diep. *Frustrated Spin Systems*. World Scientific Publishing Co. Pte. Ltd., 2004.
- [54] DV Dmitriev, V Ya Krivnov, and AA Ovchinnikov. “Exactly solvable spin ladder model with degenerate ferromagnetic and singlet states”. In: *The European Physical Journal B-Condensed Matter and Complex Systems* 14.1 (2000), pp. 91–97.
- [55] M Dolev, M Heiblum, V Umansky, A Stern, and D Mahalu. “Observation of a quarter of an electron charge at the $\nu = 5/2$ quantum Hall state”. In: *Nature* 452 (2008).
- [56] J Dukelsky, S Pittel, and G Sierra. “Colloquium: Exactly solvable Richardson-Gaudin models for many-body quantum systems”. In: *Reviews of modern physics* 76.3 (2004), p. 643.
- [57] Callum W. Duncan, Sourav Manna, and Anne E. B.e Nielsen. “Topological models in quasicrystalline lattices”. In: *arXiv preprint arXiv:1912.09568* (2019).
- [58] Sébastien Dusuel, Michael Kamfor, Román Orús, Kai Phillip Schmidt, and Julien Vidal. “Robustness of a Perturbed Topological Phase”. In: *Phys. Rev. Lett.* 106 (10 2011), p. 107203. DOI: 10.1103/PhysRevLett.106.107203. URL: <https://link.aps.org/doi/10.1103/PhysRevLett.106.107203>.
- [59] D Eloy and JC Xavier. “Entanglement entropy of the low-lying excited states and critical properties of an exactly solvable two-leg spin ladder with three-spin interactions”. In: *Phys. Rev. B* 86.6 (2012), p. 064421.

- [60] B. Estienne, Z. Papić, N. Regnault, and B. A. Bernevig. “Matrix product states for trial quantum Hall states”. In: *Phys. Rev. B* 87 (16 2013), p. 161112. DOI: 10.1103/PhysRevB.87.161112. URL: <https://link.aps.org/doi/10.1103/PhysRevB.87.161112>.
- [61] Mark Fannes, Bruno Nachtergaele, and Reinhard F Werner. “Finitely correlated states on quantum spin chains”. In: *Communications in mathematical physics* 144.3 (1992), pp. 443–490.
- [62] Carlos Fernandez-Gonzalez, Norbert Schuch, Michael M Wolf, J Ignacio Cirac, and David Perez-Garcia. “Frustration Free Gapless Hamiltonians for Matrix Product States”. In: *Communications in Mathematical Physics* 333.1 (2015), pp. 299–333.
- [63] Eduardo Fradkin, Chetan Nayak, Alexei Tsvelik, and Frank Wilczek. “A chernsimons effective field theory for the pfaffian quantum hall state”. In: *Nuclear Physics B* 516.3 (1998), pp. 704–718. ISSN: 0550-3213. DOI: [https://doi.org/10.1016/S0550-3213\(98\)00111-4](https://doi.org/10.1016/S0550-3213(98)00111-4). URL: <http://www.sciencedirect.com/science/article/pii/S0550321398001114>.
- [64] Philippe Francesco, Pierre Mathieu, and David Senechal. “Conformal Field Theory”. In: *Springer-Verlag New York* (1997).
- [65] Jean-Noël Fuchs, Rémy Mosseri, and Julien Vidal. “Landau levels in quasicrystals”. In: *Phys. Rev. B* 98 (16 2018), p. 165427. DOI: 10.1103/PhysRevB.98.165427. URL: <https://link.aps.org/doi/10.1103/PhysRevB.98.165427>.
- [66] Jean-Noël Fuchs and Julien Vidal. “Hofstadter butterfly of a quasicrystal”. In: *Phys. Rev. B* 94 (20 2016), p. 205437. DOI: 10.1103/PhysRevB.94.205437. URL: <https://link.aps.org/doi/10.1103/PhysRevB.94.205437>.
- [67] Yuval Gefen, Benoit B. Mandelbrot, and Amnon Aharony. “Critical Phenomena on Fractal Lattices”. In: *Phys. Rev. Lett.* 45 (11 1980), pp. 855–858. DOI: 10.1103/PhysRevLett.45.855. URL: <https://link.aps.org/doi/10.1103/PhysRevLett.45.855>.
- [68] Yuval Gefen, Yigal Meir, Benoit B. Mandelbrot, and Amnon Aharony. “Geometric Implementation of Hypercubic Lattices with Noninteger Dimensionality by Use of Low Lacunarity Fractal Lattices”. In: *Phys. Rev. Lett.* 50 (3 1983), pp. 145–148. DOI: 10.1103/PhysRevLett.50.145. URL: <https://link.aps.org/doi/10.1103/PhysRevLett.50.145>.
- [69] Ivan Glasser, J Ignacio Cirac, German Sierra, and Anne E B Nielsen. “Exact parent hamiltonians of bosonic and fermionic Moore-Read states on lattices and local models”. In: *New Journal of Physics(Fast Track)* 17.8 (2015), p. 082001. URL: <http://stacks.iop.org/1367-2630/17/i=8/a=082001>.
- [70] Ivan Glasser, J. Ignacio Cirac, Germán Sierra, and Anne E. B. Nielsen. “Lattice effects on Laughlin wave functions and parent Hamiltonians”. In: *Phys. Rev. B* 94 (24 2016), p. 245104. DOI: 10.1103/PhysRevB.94.245104. URL: <https://link.aps.org/doi/10.1103/PhysRevB.94.245104>.

- [71] Ivan Glasser, J. Ignacio Cirac, Germán Sierra, and Anne E. B. Nielsen. “Lattice effects on Laughlin wave functions and parent Hamiltonians”. In: *Phys. Rev. B* 94 (24 2016), p. 245104. DOI: 10.1103/PhysRevB.94.245104. URL: <https://link.aps.org/doi/10.1103/PhysRevB.94.245104>.
- [72] N. Goldman, J. C. Budich, and P. Zoller. “Topological quantum matter with ultracold gases in optical lattices”. In: *Nature Physics* 12.639 (2016).
- [73] Shou-Shu Gong, Wei Zhu, D. N. Sheng, Olexei I. Motrunich, and Matthew P. A. Fisher. “Plaquette Ordered Phase and Quantum Phase Diagram in the Spin- $\frac{1}{2}$ J_1-J_2 Square Heisenberg Model”. In: *Phys. Rev. Lett.* 113 (2 2014), p. 027201. DOI: 10.1103/PhysRevLett.113.027201. URL: <https://link.aps.org/doi/10.1103/PhysRevLett.113.027201>.
- [74] M. G. Gonzalez, F. T. Lisandrini, G. G. Blesio, A. E. Trumper, C. J. Gazza, and L. O. Manuel. “Correlated Partial Disorder in a Weakly Frustrated Quantum Antiferromagnet”. In: *Phys. Rev. Lett.* 122 (1 2019), p. 017201. DOI: 10.1103/PhysRevLett.122.017201. URL: <https://link.aps.org/doi/10.1103/PhysRevLett.122.017201>.
- [75] Eliska Greplova, Agnes Valenti, Gregor Boschung, Frank Schäfer, Niels Lörch, and Sebastian Huber. “Unsupervised identification of topological order using predictive models”. In: *arXiv preprint arXiv:1910.10124* (2019).
- [76] Adolfo G. Grushin, Johannes Motruk, Michael P. Zaletel, and Frank Pollmann. “Characterization and stability of a fermionic $\nu = 1/3$ fractional Chern insulator”. In: *Phys. Rev. B* 91 (3 2015), p. 035136. DOI: 10.1103/PhysRevB.91.035136. URL: <https://link.aps.org/doi/10.1103/PhysRevB.91.035136>.
- [77] Victor Gurarie and Chetan Nayak. “A plasma analogy and berry matrices for non-abelian quantum hall states”. In: *Nuclear Physics B* 506.3 (1997), pp. 685–694. ISSN: 0550-3213. DOI: [https://doi.org/10.1016/S0550-3213\(97\)00612-3](https://doi.org/10.1016/S0550-3213(97)00612-3). URL: <http://www.sciencedirect.com/science/article/pii/S0550321397006123>.
- [78] Zachary NC Ha. *Quantum many-body systems in one dimension*. Vol. 12. World Scientific, 1996.
- [79] M. Hafezi, A. S. Sorensen, E. Demler, and M. D. Lukin. “Fractional quantum Hall effect in optical lattices”. In: *Phys. Rev. A* 76 (2 2007), p. 023613. DOI: 10.1103/PhysRevA.76.023613. URL: <https://link.aps.org/doi/10.1103/PhysRevA.76.023613>.
- [80] F. D. M. Haldane. “Exact Jastrow-Gutzwiller resonating-valence-bond ground state of the spin-1/2 antiferromagnetic Heisenberg chain with $1/r^2$ exchange”. In: *Phys. Rev. Lett.* 60 (7 1988), pp. 635–638. DOI: 10.1103/PhysRevLett.60.635. URL: <http://link.aps.org/doi/10.1103/PhysRevLett.60.635>.
- [81] F. D. M. Haldane. “Model for a Quantum Hall Effect without Landau Levels: Condensed-Matter Realization of the “Parity Anomaly””. In: *Phys. Rev. Lett.* 61 (18 1988), pp. 2015–2018. DOI: 10.1103/PhysRevLett.61.2015. URL: <https://link.aps.org/doi/10.1103/PhysRevLett.61.2015>.

- [82] F Duncan M Haldane. “Continuum dynamics of the 1-D Heisenberg antiferromagnet: identification with the O(3) nonlinear sigma model”. In: *Physics Letters A* 93.9 (1983), pp. 464–468.
- [83] FDM Haldane. “Luttinger liquid theory of one-dimensional quantum fluids. I. Properties of the Luttinger model and their extension to the general 1D interacting spinless Fermi gas”. In: *Journal of Physics C: Solid State Physics* 14.19 (1981), p. 2585.
- [84] T. H. Hansson, C.-C. Chang, J. K. Jain, and S. Viefers. “Composite-fermion wave functions as correlators in conformal field theory”. In: *Phys. Rev. B* 76 (7 2007), p. 075347. DOI: 10.1103/PhysRevB.76.075347. URL: <https://link.aps.org/doi/10.1103/PhysRevB.76.075347>.
- [85] T. H. Hansson, C.-C. Chang, J. K. Jain, and S. Viefers. “Conformal Field Theory of Composite Fermions”. In: *Phys. Rev. Lett.* 98 (7 2007), p. 076801. DOI: 10.1103/PhysRevLett.98.076801. URL: <https://link.aps.org/doi/10.1103/PhysRevLett.98.076801>.
- [86] T. H. Hansson, M. Hermanns, N. Regnault, and S. Viefers. “Conformal Field Theory Approach to Abelian and Non-Abelian Quantum Hall Quasielectrons”. In: *Phys. Rev. Lett.* 102 (16 2009), p. 166805. DOI: 10.1103/PhysRevLett.102.166805. URL: <https://link.aps.org/doi/10.1103/PhysRevLett.102.166805>.
- [87] T. H. Hansson, M. Hermanns, and S. Viefers. “Quantum Hall quasielectron operators in conformal field theory”. In: *Phys. Rev. B* 80 (16 2009), p. 165330. DOI: 10.1103/PhysRevB.80.165330. URL: <https://link.aps.org/doi/10.1103/PhysRevB.80.165330>.
- [88] M. Z. Hasan and C. L. Kane. “Colloquium: Topological insulators”. In: *Rev. Mod. Phys.* 82 (4 2010), pp. 3045–3067. DOI: 10.1103/RevModPhys.82.3045. URL: <https://link.aps.org/doi/10.1103/RevModPhys.82.3045>.
- [89] Matthew B. Hastings, Iván Gonzalez, Ann B. Kallin, and Roger G. Melko. “Measuring Renyi Entanglement Entropy in Quantum Monte Carlo Simulations”. In: *Phys. Rev. Lett.* 104 (15 2010), p. 157201. DOI: 10.1103/PhysRevLett.104.157201. URL: <https://link.aps.org/doi/10.1103/PhysRevLett.104.157201>.
- [90] W. K. Hastings. “Monte Carlo sampling methods using Markov chains and their applications”. In: *Biometrika* 57 (1 1970), pp. 97–109. DOI: <https://doi.org/10.1093/biomet/57.1.97>.
- [91] Yin-Chen He, Michael P. Zaletel, Masaki Oshikawa, and Frank Pollmann. “Signatures of Dirac Cones in a DMRG Study of the Kagome Heisenberg Model”. In: *Phys. Rev. X* 7 (3 2017), p. 031020. DOI: 10.1103/PhysRevX.7.031020. URL: <https://link.aps.org/doi/10.1103/PhysRevX.7.031020>.

- [92] J. S. Helton, K. Matan, M. P. Shores, E. A. Nytko, B. M. Bartlett, Y. Yoshida, Y. Takano, A. Suslov, Y. Qiu, J.-H. Chung, D. G. Nocera, and Y. S. Lee. “Spin Dynamics of the Spin-1/2 Kagome Lattice Antiferromagnet $\text{ZnCu}_3(\text{OH})_6\text{Cl}_2$ ”. In: *Phys. Rev. Lett.* 98 (10 2007), p. 107204. DOI: 10.1103/PhysRevLett.98.107204. URL: <https://link.aps.org/doi/10.1103/PhysRevLett.98.107204>.
- [93] Egil V. Herland, Egor Babaev, Parsa Bonderson, Victor Gurarie, Chetan Nayak, and Asle Sudbo. “Screening properties and phase transitions in unconventional plasmas for Ising-type quantum Hall states”. In: *Phys. Rev. B* 85 (2 2012), p. 024520. DOI: 10.1103/PhysRevB.85.024520. URL: <https://link.aps.org/doi/10.1103/PhysRevB.85.024520>.
- [94] M. Hermanns, A. Chandran, N. Regnault, and B. Andrei Bernevig. “Haldane statistics in the finite-size entanglement spectra of $1/m$ fractional quantum Hall states”. In: *Phys. Rev. B* 84 (12 2011), p. 121309. DOI: 10.1103/PhysRevB.84.121309. URL: <https://link.aps.org/doi/10.1103/PhysRevB.84.121309>.
- [95] Douglas R. Hofstadter. “Energy levels and wave functions of Bloch electrons in rational and irrational magnetic fields”. In: *Phys. Rev. B* 14 (6 1976), pp. 2239–2249. DOI: 10.1103/PhysRevB.14.2239. URL: <https://link.aps.org/doi/10.1103/PhysRevB.14.2239>.
- [96] Christoph Holzhey, Finn Larsen, and Frank Wilczek. “Geometric and renormalized entropy in conformal field theory”. In: *Nuclear Physics B* 424.3 (1994), pp. 443–467.
- [97] David Hsieh, Dong Qian, Lewis Wray, YuQi Xia, Yew San Hor, Robert Joseph Cava, and M Zahid Hasan. “A topological Dirac insulator in a quantum spin Hall phase”. In: *Nature* 452.7190 (2008), p. 970. DOI: 10.1038/nature06843.
- [98] Wen-Jun Hu, Shou-Shu Gong, Wei Zhu, and D. N. Sheng. “Competing spin-liquid states in the spin- $\frac{1}{2}$ Heisenberg model on the triangular lattice”. In: *Phys. Rev. B* 92 (14 2015), p. 140403. DOI: 10.1103/PhysRevB.92.140403. URL: <https://link.aps.org/doi/10.1103/PhysRevB.92.140403>.
- [99] Huaqing Huang and Feng Liu. “Quantum Spin Hall Effect and Spin Bott Index in a Quasicrystal Lattice”. In: *Phys. Rev. Lett.* 121 (12 2018), p. 126401. DOI: 10.1103/PhysRevLett.121.126401. URL: <https://link.aps.org/doi/10.1103/PhysRevLett.121.126401>.
- [100] Huaqing Huang and Feng Liu. “Theory of spin Bott index for quantum spin Hall states in nonperiodic systems”. In: *Phys. Rev. B* 98 (12 2018), p. 125130. DOI: 10.1103/PhysRevB.98.125130. URL: <https://link.aps.org/doi/10.1103/PhysRevB.98.125130>.
- [101] Roni Ilan, Eytan Grosfeld, Kareljan Schoutens, and Ady Stern. “Experimental signatures of non-Abelian statistics in clustered quantum Hall states”. In: *Phys. Rev. B* 79 (24 2009), p. 245305. DOI: 10.1103/PhysRevB.79.245305. URL: <https://link.aps.org/doi/10.1103/PhysRevB.79.245305>.
- [102] Askar A Iliasov, Mikhail I Katsnelson, and Shengjun Yuan. “Power-law energy level spacing distributions in fractals”. In: *Phys. Rev. B* 99.7 (2019), p. 075402.

- [103] V. I. Inozemtsev. “On the connection between the one-dimensional $S=1/2$ Heisenberg chain and Haldane-Shastry model”. In: *Journal of Statistical Physics* 59.5 (1990), pp. 1143–1155. ISSN: 1572-9613. DOI: 10.1007/BF01334745. URL: <https://doi.org/10.1007/BF01334745>.
- [104] Yasir Iqbal, Wen-Jun Hu, Ronny Thomale, Didier Poilblanc, and Federico Becca. “Spin liquid nature in the Heisenberg $J_1 - J_2$ triangular antiferromagnet”. In: *Phys. Rev. B* 93 (14 2016), p. 144411. DOI: 10.1103/PhysRevB.93.144411. URL: <https://link.aps.org/doi/10.1103/PhysRevB.93.144411>.
- [105] Yasir Iqbal, Tobias Muller, Pratyay Ghosh, Michel J. P. Gingras, Harald O. Jeschke, Stephan Rachel, Johannes Reuther, and Ronny Thomale. “Quantum and Classical Phases of the Pyrochlore Heisenberg Model with Competing Interactions”. In: *Phys. Rev. X* 9 (1 2019), p. 011005. DOI: 10.1103/PhysRevX.9.011005. URL: <https://link.aps.org/doi/10.1103/PhysRevX.9.011005>.
- [106] J. K. Jain. “Composite-fermion approach for the fractional quantum Hall effect”. In: *Phys. Rev. Lett.* 63 (2 1989), pp. 199–202. DOI: 10.1103/PhysRevLett.63.199. URL: <https://link.aps.org/doi/10.1103/PhysRevLett.63.199>.
- [107] Ted Janssen, Gervais Chapuis, and Marc De Boissieu. *Aperiodic Crystals: From Modulated Phases to Quasicrystals: Structure and Properties*. Oxford University Press, 2018.
- [108] Blazej Jaworowski, Nicolas Regnault, and Zhao Liu. “Characterization of quasiholes in two-component fractional quantum hall states and fractional Chern insulators in $|C| = 2$ flat bands”. In: *arXiv:1810.03458* (2018).
- [109] Gun Sang Jeon, Kenneth L. Graham, and Jainendra K. Jain. “Fractional Statistics in the Fractional Quantum Hall Effect”. In: *Phys. Rev. Lett.* 91 (3 2003), p. 036801. DOI: 10.1103/PhysRevLett.91.036801. URL: <https://link.aps.org/doi/10.1103/PhysRevLett.91.036801>.
- [110] Gun Sang Jeon and J. K. Jain. “Thermodynamic behavior of braiding statistics for certain fractional quantum Hall quasiparticles”. In: *Phys. Rev. B* 81 (3 2010), p. 035319. DOI: 10.1103/PhysRevB.81.035319. URL: <https://link.aps.org/doi/10.1103/PhysRevB.81.035319>.
- [111] Gun Sang Jeon and Jainendra K. Jain. “Nature of quasiparticle excitations in the fractional quantum Hall effect”. In: *Phys. Rev. B* 68 (16 2003), p. 165346. DOI: 10.1103/PhysRevB.68.165346. URL: <https://link.aps.org/doi/10.1103/PhysRevB.68.165346>.
- [112] Hong-Chen Jiang, Zhenghan Wang, and Leon Balents. “Identifying topological order by entanglement entropy”. In: *Nature Physics* 8 (2012), 902–905. URL: <https://doi.org/10.1038/nphys2465>.
- [113] Hong-Chen Jiang, Hong Yao, and Leon Balents. “Spin liquid ground state of the spin- $\frac{1}{2}$ square J_1 - J_2 Heisenberg model”. In: *Phys. Rev. B* 86 (2 2012), p. 024424. DOI: 10.1103/PhysRevB.86.024424. URL: <https://link.aps.org/doi/10.1103/PhysRevB.86.024424>.

- [114] Dean Johnstone, Patrik Ohberg, and Callum W. Duncan. “Mean-field phases of an ultracold gas in a quasicrystalline potential”. In: *arXiv preprint arXiv:1904.12870* (2019).
- [115] V. Kalmeyer and R. B. Laughlin. “Equivalence of the resonating-valence-bond and fractional quantum Hall states”. In: *Phys. Rev. Lett.* 59 (18 1987), pp. 2095–2098. DOI: 10.1103/PhysRevLett.59.2095. URL: <https://link.aps.org/doi/10.1103/PhysRevLett.59.2095>.
- [116] V. Kalmeyer and R. B. Laughlin. “Equivalence of the resonating-valence-bond and fractional quantum Hall states”. In: *Phys. Rev. Lett.* 59 (18 1987), pp. 2095–2098. DOI: 10.1103/PhysRevLett.59.2095. URL: <http://link.aps.org/doi/10.1103/PhysRevLett.59.2095>.
- [117] C. L. Kane and E. J. Mele. “Quantum Spin Hall Effect in Graphene”. In: *Phys. Rev. Lett.* 95 (22 2005), p. 226801. DOI: 10.1103/PhysRevLett.95.226801. URL: <https://link.aps.org/doi/10.1103/PhysRevLett.95.226801>.
- [118] C. L. Kane and E. J. Mele. “ Z_2 Topological Order and the Quantum Spin Hall Effect”. In: *Phys. Rev. Lett.* 95 (14 2005), p. 146802. DOI: 10.1103/PhysRevLett.95.146802. URL: <https://link.aps.org/doi/10.1103/PhysRevLett.95.146802>.
- [119] Eliot Kapit, Paul Ginsparg, and Erich Mueller. “Non-Abelian Braiding of Lattice Bosons”. In: *Phys. Rev. Lett.* 108 (6 2012), p. 066802. DOI: 10.1103/PhysRevLett.108.066802. URL: <https://link.aps.org/doi/10.1103/PhysRevLett.108.066802>.
- [120] Eliot Kapit and Erich Mueller. “Exact Parent Hamiltonian for the Quantum Hall States in a Lattice”. In: *Phys. Rev. Lett.* 105 (21 2010), p. 215303. DOI: 10.1103/PhysRevLett.105.215303. URL: <https://link.aps.org/doi/10.1103/PhysRevLett.105.215303>.
- [121] Torsten Karzig, Christina Knapp, Roman M. Lutchyn, Parsa Bonderson, Matthew B. Hastings, Chetan Nayak, Jason Alicea, Karsten Flensberg, Stephan Plugge, Yuval Oreg, Charles M. Marcus, and Michael H. Freedman. “Scalable designs for quasiparticle-poisoning-protected topological quantum computation with Majorana zero modes”. In: *Phys. Rev. B* 95 (23 2017), p. 235305. DOI: 10.1103/PhysRevB.95.235305. URL: <https://link.aps.org/doi/10.1103/PhysRevB.95.235305>.
- [122] Ahmet Keles and Erhai Zhao. “Absence of Long-Range Order in a Triangular Spin System with Dipolar Interactions”. In: *Phys. Rev. Lett.* 120 (18 2018), p. 187202. DOI: 10.1103/PhysRevLett.120.187202. URL: <https://link.aps.org/doi/10.1103/PhysRevLett.120.187202>.
- [123] SN Kempkes, MR Slot, SE Freney, SJM Zevenhuizen, D Vanmaekelbergh, I Swart, and C Morais Smith. “Design and characterization of electrons in a fractal geometry”. In: *Nat. Phys.* 15.2 (2019), p. 127.
- [124] A Kitaev. “Fault-tolerant quantum computation by anyons”. In: *Ann. of Phys.* 303 (2003), p. 2. DOI: [https://doi.org/10.1016/S0003-4916\(02\)00018-0](https://doi.org/10.1016/S0003-4916(02)00018-0).

- [125] A.Yu. Kitaev. “Fault-tolerant quantum computation by anyons”. In: *Annals of Physics* 303 (2003), pp. 2–30. DOI: [https://doi.org/10.1016/S0003-4916\(02\)00018-0](https://doi.org/10.1016/S0003-4916(02)00018-0). URL: <http://www.sciencedirect.com/science/article/pii/S0003491602000180>.
- [126] Alexei Kitaev. “Anyons in an exactly solved model and beyond”. In: *Annals of Physics* 321.1 (2006). January Special Issue, pp. 2–111. ISSN: 0003-4916. DOI: <https://doi.org/10.1016/j.aop.2005.10.005>. URL: <http://www.sciencedirect.com/science/article/pii/S0003491605002381>.
- [127] Alexei Kitaev and John Preskill. “Topological Entanglement Entropy”. In: *Phys. Rev. Lett.* 96 (11 2006), p. 110404. DOI: 10.1103/PhysRevLett.96.110404. URL: <https://link.aps.org/doi/10.1103/PhysRevLett.96.110404>.
- [128] Alexei Kitaev and John Preskill. “Topological Entanglement Entropy”. In: *Phys. Rev. Lett.* 96 (11 2006), p. 110404. DOI: 10.1103/PhysRevLett.96.110404. URL: <https://link.aps.org/doi/10.1103/PhysRevLett.96.110404>.
- [129] J Kjall, E Ardonne, V Dwivedi, M Hermanns, and T H Hansson. “Matrix product state representation of quasielectron wave functions”. In: *Journal of Statistical Mechanics: Theory and Experiment* 2018.5 (2018), p. 053101. URL: <http://stacks.iop.org/1742-5468/2018/i=5/a=053101>.
- [130] K. v. Klitzing, G. Dorda, and M. Pepper. “New Method for High-Accuracy Determination of the Fine-Structure Constant Based on Quantized Hall Resistance”. In: *Phys. Rev. Lett.* 45 (6 1980), pp. 494–497. DOI: 10.1103/PhysRevLett.45.494. URL: <https://link.aps.org/doi/10.1103/PhysRevLett.45.494>.
- [131] Maciej Koch-Janusz, Michael Levin, and Ady Stern. “Exactly soluble lattice models for non-Abelian states of matter in two dimensions”. In: *Phys. Rev. B* 88 (11 2013), p. 115133. DOI: 10.1103/PhysRevB.88.115133. URL: <https://link.aps.org/doi/10.1103/PhysRevB.88.115133>.
- [132] V. E. Korepin. “Universality of Entropy Scaling in One Dimensional Gapless Models”. In: *Phys. Rev. Lett.* 92 (9 2004), p. 096402. DOI: 10.1103/PhysRevLett.92.096402. URL: <https://link.aps.org/doi/10.1103/PhysRevLett.92.096402>.
- [133] Yaacov E. Kraus, Yoav Lahini, Zohar Ringel, Mor Verbin, and Oded Zilberberg. “Topological States and Adiabatic Pumping in Quasicrystals”. In: *Phys. Rev. Lett.* 109 (10 2012), p. 106402. DOI: 10.1103/PhysRevLett.109.106402. URL: <https://link.aps.org/doi/10.1103/PhysRevLett.109.106402>.
- [134] Yaacov E. Kraus, Zohar Ringel, and Oded Zilberberg. “Four-Dimensional Quantum Hall Effect in a Two-Dimensional Quasicrystal”. In: *Phys. Rev. Lett.* 111 (22 2013), p. 226401. DOI: 10.1103/PhysRevLett.111.226401. URL: <https://link.aps.org/doi/10.1103/PhysRevLett.111.226401>.
- [135] Yaacov E. Kraus and Oded Zilberberg. “Topological Equivalence between the Fibonacci Quasicrystal and the Harper Model”. In: *Phys. Rev. Lett.* 109 (11 2012), p. 116404. DOI: 10.1103/PhysRevLett.109.116404. URL: <https://link.aps.org/doi/10.1103/PhysRevLett.109.116404>.

- [136] Roman Krmar, Jozef Genzor, Yoju Lee, Hana Cencarikova, Tomotoshi Nishino, and Andrej Gendiar. “Tensor-network study of a quantum phase transition on the Sierpinski fractal”. In: *Phys. Rev. E* 98 (6 2018), p. 062114. DOI: 10.1103/PhysRevE.98.062114. URL: <https://link.aps.org/doi/10.1103/PhysRevE.98.062114>.
- [137] Koji Kudo, Haruki Watanabe, Toshikaze Kariyado, and Yasuhiro Hatsugai. “Many-Body Chern Number without Integration”. In: *Phys. Rev. Lett.* 122 (14 2019), p. 146601. DOI: 10.1103/PhysRevLett.122.146601. URL: <https://link.aps.org/doi/10.1103/PhysRevLett.122.146601>.
- [138] Ville Lahtinen and Jiannis K. Pachos. “A Short Introduction to Topological Quantum Computation”. In: *SciPost Phys.* 3 (3 2017), p. 021. DOI: 10.21468/SciPostPhys.3.3.021. URL: <https://scipost.org/10.21468/SciPostPhys.3.3.021>.
- [139] Li-Jun Lang, Xiaoming Cai, and Shu Chen. “Edge States and Topological Phases in One-Dimensional Optical Superlattices”. In: *Phys. Rev. Lett.* 108 (22 2012), p. 220401. DOI: 10.1103/PhysRevLett.108.220401. URL: <https://link.aps.org/doi/10.1103/PhysRevLett.108.220401>.
- [140] R. B. Laughlin. “Anomalous Quantum Hall Effect: An Incompressible Quantum Fluid with Fractionally Charged Excitations”. In: *Phys. Rev. Lett.* 50 (18 1983), pp. 1395–1398. DOI: 10.1103/PhysRevLett.50.1395. URL: <https://link.aps.org/doi/10.1103/PhysRevLett.50.1395>.
- [141] J. M. Leinaas and J. Myrheim. “On the theory of identical particles”. In: *Nuovo Cim.* B37 (1977), pp. 1–23. DOI: 10.1007/BF02727953.
- [142] Michael Levin and Xiao-Gang Wen. “Detecting Topological Order in a Ground State Wave Function”. In: *Phys. Rev. Lett.* 96 (11 2006), p. 110405. DOI: 10.1103/PhysRevLett.96.110405. URL: <https://link.aps.org/doi/10.1103/PhysRevLett.96.110405>.
- [143] Michael Levin and Xiao-Gang Wen. “Detecting Topological Order in a Ground State Wave Function”. In: *Phys. Rev. Lett.* 96 (11 2006), p. 110405. DOI: 10.1103/PhysRevLett.96.110405. URL: <https://link.aps.org/doi/10.1103/PhysRevLett.96.110405>.
- [144] Hui Li and F. D. M. Haldane. “Entanglement Spectrum as a Generalization of Entanglement Entropy: Identification of Topological Order in Non-Abelian Fractional Quantum Hall Effect States”. In: *Phys. Rev. Lett.* 101 (1 2008), p. 010504. DOI: 10.1103/PhysRevLett.101.010504. URL: <https://link.aps.org/doi/10.1103/PhysRevLett.101.010504>.
- [145] Netanel H. Lindner, Erez Berg, Gil Refael, and Ady Stern. “Fractionalizing Majorana Fermions: Non-Abelian Statistics on the Edges of Abelian Quantum Hall States”. In: *Phys. Rev. X* 2 (4 2012), p. 041002. DOI: 10.1103/PhysRevX.2.041002. URL: <https://link.aps.org/doi/10.1103/PhysRevX.2.041002>.
- [146] Jon Links and Angela Foerster. “Solution of a two-leg spin ladder system”. In: *Phys. Rev. B* 62 (1 2000), pp. 65–68. DOI: 10.1103/PhysRevB.62.65. URL: <https://link.aps.org/doi/10.1103/PhysRevB.62.65>.

- [147] Wen-Yuan Liu, Shaojun Dong, Chao Wang, Yongjian Han, Hong An, Guang-Can Guo, and Lixin He. “Gapless spin liquid ground state of the spin- $\frac{1}{2}$ $J_1 - J_2$ Heisenberg model on square lattices”. In: *Phys. Rev. B* 98 (24 2018), p. 241109. DOI: 10.1103/PhysRevB.98.241109. URL: <https://link.aps.org/doi/10.1103/PhysRevB.98.241109>.
- [148] Zhao Liu, Emil J. Bergholtz, and Eliot Kapit. “Non-Abelian fractional Chern insulators from long-range interactions”. In: *Phys. Rev. B* 88 (20 2013), p. 205101. DOI: 10.1103/PhysRevB.88.205101. URL: <https://link.aps.org/doi/10.1103/PhysRevB.88.205101>.
- [149] Zhao Liu, R. N. Bhatt, and Nicolas Regnault. “Characterization of quasiholes in fractional Chern insulators”. In: *Phys. Rev. B* 91 (4 2015), p. 045126. DOI: 10.1103/PhysRevB.91.045126. URL: <https://link.aps.org/doi/10.1103/PhysRevB.91.045126>.
- [150] S. Longhi. “Topological Phase Transition in non-Hermitian Quasicrystals”. In: *Phys. Rev. Lett.* 122 (23 2019), p. 237601. DOI: 10.1103/PhysRevLett.122.237601. URL: <https://link.aps.org/doi/10.1103/PhysRevLett.122.237601>.
- [151] JM Luttinger. “An exactly soluble model of a many-fermion system”. In: *Journal of Mathematical Physics* 4.9 (1963), pp. 1154–1162.
- [152] Hannah M. Price. “Four-dimensional topological lattices without gauge fields”. In: *arXiv preprint arXiv:1806.05263* (2018).
- [153] E. Macaluso, T. Comparin, L. Mazza, and I. Carusotto. “Fusion Channels of Non-Abelian Anyons from Angular-Momentum and Density-Profile Measurements”. In: *Phys. Rev. Lett.* 123 (26 2019), p. 266801. DOI: 10.1103/PhysRevLett.123.266801. URL: <https://link.aps.org/doi/10.1103/PhysRevLett.123.266801>.
- [154] Sourav Manna and Anne E. B. Nielsen. “Chain and ladder models with two-body interactions and analytical ground states”. In: *Phys. Rev. B* 97 (19 2018), p. 195143. DOI: 10.1103/PhysRevB.97.195143. URL: <https://link.aps.org/doi/10.1103/PhysRevB.97.195143>.
- [155] Sourav Manna, N. S. Srivatsa, Julia Wildeboer, and Anne EB Nielsen. “Quasiparticles as Detector of Topological Quantum Phase Transitions”. In: *arXiv preprint arXiv:1909.02046* (2019).
- [156] Sourav Manna, Julia Wildeboer, and Anne E. B. Nielsen. “Quasielectrons in lattice Moore-Read models”. In: *Phys. Rev. B* 99 (4 2019), p. 045147. DOI: 10.1103/PhysRevB.99.045147. URL: <https://link.aps.org/doi/10.1103/PhysRevB.99.045147>.
- [157] Sourav Manna, Julia Wildeboer, German Sierra, and Anne E. B. Nielsen. “Non-Abelian quasiholes in lattice Moore-Read states and parent Hamiltonians”. In: *Phys. Rev. B* 98 (16 2018), p. 165147. DOI: 10.1103/PhysRevB.98.165147. URL: <https://link.aps.org/doi/10.1103/PhysRevB.98.165147>.

- [158] Hirokazu Miyake, Georgios A. Siviloglou, Colin J. Kennedy, William Cody Burton, and Wolfgang Ketterle. “Realizing the Harper Hamiltonian with Laser-Assisted Tunneling in Optical Lattices”. In: *Phys. Rev. Lett.* 111 (18 2013), p. 185302. DOI: 10.1103/PhysRevLett.111.185302. URL: <https://link.aps.org/doi/10.1103/PhysRevLett.111.185302>.
- [159] Roger S. K. Mong, David J. Clarke, Jason Alicea, Netanel H. Lindner, Paul Fendley, Chetan Nayak, Yuval Oreg, Ady Stern, Erez Berg, Kirill Shtengel, and Matthew P. A. Fisher. “Universal Topological Quantum Computation from a Superconductor-Abelian Quantum Hall Heterostructure”. In: *Phys. Rev. X* 4 (1 2014), p. 011036. DOI: 10.1103/PhysRevX.4.011036. URL: <https://link.aps.org/doi/10.1103/PhysRevX.4.011036>.
- [160] Roger S. K. Mong, Michael P. Zaletel, Frank Pollmann, and Zlatko Papić. “Fibonacci anyons and charge density order in the 12/5 and 13/5 quantum Hall plateaus”. In: *Phys. Rev. B* 95 (11 2017), p. 115136. DOI: 10.1103/PhysRevB.95.115136. URL: <https://link.aps.org/doi/10.1103/PhysRevB.95.115136>.
- [161] Elliott W Montroll, Renfrey B Potts, and John C Ward. “Correlations and Spontaneous Magnetization of the Two-Dimensional Ising Model”. In: *Journal of Mathematical Physics* 4.2 (1963), pp. 308–322.
- [162] Gregory Moore and Nicholas Read. “Nonabelions in the fractional quantum Hall effect”. In: *Nuclear Physics B* 360.2 (1991), pp. 362–396. ISSN: 0550-3213. DOI: [https://doi.org/10.1016/0550-3213\(91\)90407-0](https://doi.org/10.1016/0550-3213(91)90407-0).
- [163] Johannes Motruk and Frank Pollmann. “Phase transitions and adiabatic preparation of a fractional Chern insulator in a boson cold-atom model”. In: *Phys. Rev. B* 96 (16 2017), p. 165107. DOI: 10.1103/PhysRevB.96.165107. URL: <https://link.aps.org/doi/10.1103/PhysRevB.96.165107>.
- [164] Rahul M Nandkishore and Michael Hermele. “Fractons”. In: *Annu. Rev. Condens. Matter Phys.* 10 (2019), pp. 295–313.
- [165] Chetan Nayak, Steven H. Simon, Ady Stern, Michael Freedman, and Sankar Das Sarma. “Non-Abelian anyons and topological quantum computation”. In: *Rev. Mod. Phys.* 80 (3 2008), pp. 1083–1159. DOI: 10.1103/RevModPhys.80.1083. URL: <https://link.aps.org/doi/10.1103/RevModPhys.80.1083>.
- [166] Titus Neupert, Luiz Santos, Claudio Chamon, and Christopher Mudry. “Fractional Quantum Hall States at Zero Magnetic Field”. In: *Phys. Rev. Lett.* 106 (23 2011), p. 236804. DOI: 10.1103/PhysRevLett.106.236804. URL: <https://link.aps.org/doi/10.1103/PhysRevLett.106.236804>.
- [167] Titus Neupert, Luiz Santos, Claudio Chamon, and Christopher Mudry. “Fractional Quantum Hall States at Zero Magnetic Field”. In: *Phys. Rev. Lett.* 106 (23 2011), p. 236804. DOI: 10.1103/PhysRevLett.106.236804. URL: <https://link.aps.org/doi/10.1103/PhysRevLett.106.236804>.
- [168] Lenhard L Ng. “Heisenberg model, Bethe Ansatz, and random walks”. PhD thesis. Harvard University, 1996.

- [169] Anne E. B. Nielsen. “Anyon braiding in semi analytical fractional quantum Hall lattice models”. In: *Phys. Rev. B(Rapid Comm.)* 91 (4 2015), p. 041106. DOI: 10.1103/PhysRevB.91.041106. URL: <https://link.aps.org/doi/10.1103/PhysRevB.91.041106>.
- [170] Anne E. B. Nielsen, J. Ignacio Cirac, and German Sierra. “Laughlin Spin-Liquid States on Lattices Obtained from Conformal Field Theory”. In: *Phys. Rev. Lett.* 108 (25 2012), p. 257206. DOI: 10.1103/PhysRevLett.108.257206. URL: <https://link.aps.org/doi/10.1103/PhysRevLett.108.257206>.
- [171] Anne E. B. Nielsen, J. Ignacio Cirac, and German Sierra. “Laughlin Spin-Liquid States on Lattices Obtained from Conformal Field Theory”. In: *Phys. Rev. Lett.* 108 (25 2012), p. 257206. DOI: 10.1103/PhysRevLett.108.257206. URL: <http://link.aps.org/doi/10.1103/PhysRevLett.108.257206>.
- [172] Anne E. B. Nielsen, J. Ignacio Cirac, and German Sierra. “Quantum spin Hamiltonians for the SU(2)_k WZW model”. In: *Journal of Statistical Mechanics: Theory and Experiment* 2011.11 (2011), P11014. DOI: 10.1088/1742-5468/2011/11/P11014. URL: <http://iopscience.iop.org/article/10.1088/1742-5468/2011/11/P11014/meta>.
- [173] Anne E. B Nielsen, German Sierra, and J. Ignacio Cirac. “Local models of fractional quantum Hall states in lattices and physical implementation”. In: *Nature Communications* 4 (2013). DOI: 10.1038/ncomms3864. URL: <http://dx.doi.org/10.1038/ncomms3864>.
- [174] Anne E. B. Nielsen, Germán Sierra, and J. Ignacio Cirac. “Violation of the area law and long-range correlations in infinite-dimensional-matrix product states”. In: *Phys. Rev. A* 83 (5 2011), p. 053807. DOI: 10.1103/PhysRevA.83.053807. URL: <https://link.aps.org/doi/10.1103/PhysRevA.83.053807>.
- [175] Anne EB Nielsen, Ivan Glasser, and Iván D Rodríguez. “Quasielectrons as inverse quasiholes in lattice fractional quantum Hall models”. In: *New J. Phys.* 20.3 (2018), p. 033029. DOI: 10.1088/1367-2630/aab5d0.
- [176] Qian Niu, D. J. Thouless, and Yong-Shi Wu. “Quantized Hall conductance as a topological invariant”. In: *Phys. Rev. B* 31 (6 1985), pp. 3372–3377. DOI: 10.1103/PhysRevB.31.3372. URL: <https://link.aps.org/doi/10.1103/PhysRevB.31.3372>.
- [177] Román Orús. “A practical introduction to tensor networks: Matrix product states and projected entangled pair states”. In: *Annals of Physics* 349 (2014), pp. 117–158. ISSN: 0003-4916. DOI: <https://doi.org/10.1016/j.aop.2014.06.013>. URL: <http://www.sciencedirect.com/science/article/pii/S0003491614001596>.
- [178] Masaki Oshikawa and T. Senthil. “Fractionalization, Topological Order, and Quasiparticle Statistics”. In: *Phys. Rev. Lett.* 96 (6 2006), p. 060601. DOI: 10.1103/PhysRevLett.96.060601. URL: <https://link.aps.org/doi/10.1103/PhysRevLett.96.060601>.
- [179] Shriya Pai and Abhinav Prem. “Topological States on Fractal Lattices”. In: *arXiv preprint arXiv:1907.01558* (2019).

- [180] Biplab Pal, Wei Wang, Sourav Manna, and Anne E. B. Nielsen. “Anyons and Fractional Quantum Hall Effect in Fractal Dimensions”. In: *arXiv preprint arXiv:1907.03193* (2019).
- [181] R. Penrose. *Pentaplexity A Class of Non-Periodic Tilings of the Plane*. Vol. 2. Springer, 1979. DOI: <https://doi.org/10.1007/BF03024384>.
- [182] D. Perez-Garcia, F. Verstraete, M. M. Wolf, and J. I. Cirac. “Matrix Product State Representations”. In: *arXiv:0608197* (2006).
- [183] R de Picciotto, M Reznikov, M Heiblum, V Umansky, G Bunin, and D Mahalu. “Direct observation of a fractional charge”. In: *Nature* 389 (1997). DOI: 10.1038/38241. URL: <http://dx.doi.org/10.1038/382411>.
- [184] Didier Poilblanc. “Investigation of the chiral antiferromagnetic Heisenberg model using projected entangled pair states”. In: *Phys. Rev. B* 96 (12 2017), p. 121118. DOI: 10.1103/PhysRevB.96.121118. URL: <https://link.aps.org/doi/10.1103/PhysRevB.96.121118>.
- [185] E. de Prunelé. “Penrose structures: Gap labeling and geometry”. In: *Phys. Rev. B* 66 (9 2002), p. 094202. DOI: 10.1103/PhysRevB.66.094202. URL: <https://link.aps.org/doi/10.1103/PhysRevB.66.094202>.
- [186] Yang Qi and Meng Cheng. “Classification of symmetry fractionalization in gapped \mathbb{Z}_2 spin liquids”. In: *Phys. Rev. B* 97 (11 2018), p. 115138. DOI: 10.1103/PhysRevB.97.115138. URL: <https://link.aps.org/doi/10.1103/PhysRevB.97.115138>.
- [187] L. N. Pfeiffer R. L. Willett and K. W. West. “Measurement of filling factor $5/2$ quasiparticle interference with observation of charge $e/4$ and $e/2$ period oscillations”. In: *PNAS* 106 (22 2009). DOI: 10.1073/pnas.0812599106.
- [188] M. Raciunas, F. Nur Unal, Egidijus Anisimovas, and Andre Eckardt. “Creating, probing, and manipulating fractionally charged excitations of fractional Chern insulators in optical lattices”. In: *Phys. Rev. A* 98 (6 2018), p. 063621. DOI: 10.1103/PhysRevA.98.063621. URL: <https://link.aps.org/doi/10.1103/PhysRevA.98.063621>.
- [189] R. Rammal and G. Toulouse. “Spectrum of the Schrodinger Equation on a Self-Similar Structure”. In: *Phys. Rev. Lett.* 49 (16 1982), pp. 1194–1197. DOI: 10.1103/PhysRevLett.49.1194. URL: <https://link.aps.org/doi/10.1103/PhysRevLett.49.1194>.
- [190] Sumathi Rao. “Introduction to abelian and non-abelian anyons”. In: *arXiv:1610.09260* (2016).
- [191] N. Read. “Non-Abelian adiabatic statistics and Hall viscosity in quantum Hall states and $p_x + ip_y$ paired superfluids”. In: *Phys. Rev. B* 79 (4 2009), p. 045308. DOI: 10.1103/PhysRevB.79.045308. URL: <https://link.aps.org/doi/10.1103/PhysRevB.79.045308>.
- [192] N. Read and E. Rezayi. “Beyond paired quantum Hall states: Parafermions and incompressible states in the first excited Landau level”. In: *Phys. Rev. B* 59 (12 1999), pp. 8084–8092. DOI: 10.1103/PhysRevB.59.8084. URL: <https://link.aps.org/doi/10.1103/PhysRevB.59.8084>.

- [193] N. Regnault and B. Andrei Bernevig. “Fractional Chern Insulator”. In: *Phys. Rev. X* 1 (2 2011), p. 021014. DOI: 10.1103/PhysRevX.1.021014. URL: <https://link.aps.org/doi/10.1103/PhysRevX.1.021014>.
- [194] N. Regnault and T. Senthil. “Microscopic model for the boson integer quantum Hall effect”. In: *Phys. Rev. B* 88 (16 2013), p. 161106. DOI: 10.1103/PhysRevB.88.161106. URL: <https://link.aps.org/doi/10.1103/PhysRevB.88.161106>.
- [195] Przemysław Repetowicz, Uwe Grimm, and Michael Schreiber. “Exact eigenstates of tight-binding Hamiltonians on the Penrose tiling”. In: *Phys. Rev. B* 58 (20 1998), pp. 13482–13490. DOI: 10.1103/PhysRevB.58.13482. URL: <https://link.aps.org/doi/10.1103/PhysRevB.58.13482>.
- [196] T. Rieth and M. Schreiber. “Identification of spatially confined states in two-dimensional quasiperiodic lattices”. In: *Phys. Rev. B* 51 (22 1995), pp. 15827–15832. DOI: 10.1103/PhysRevB.51.15827. URL: <https://link.aps.org/doi/10.1103/PhysRevB.51.15827>.
- [197] Ivan D Rodriguez and Anne E. B. Nielsen. “Continuum limit of lattice models with Laughlin-like ground states containing quasiholes”. In: *Phys. Rev. B* 92 (12 2015), p. 125105. DOI: 10.1103/PhysRevB.92.125105. URL: <https://link.aps.org/doi/10.1103/PhysRevB.92.125105>.
- [198] S. Sachdev. “Quantum Phase Transitions, 2nd ed. (Cambridge University Press, Cambridge, England, 2011)”. In: ().
- [199] Anders W. Sandvik. “Computational Studies of Quantum Spin Systems”. In: *arXiv:1101.3281* (2011).
- [200] Sankar Das Sarma, Michael Freedman, and Chetan Nayak. “Majorana zero modes and topological quantum computation”. In: *Npj Quantum Information* 1 (2015). DOI: 10.1038/npjqi.2015.1. URL: <http://dx.doi.org/10.1038/npjqi.2015.1>.
- [201] Jay D. Sau, Sumanta Tewari, and S. Das Sarma. “Probing non-Abelian statistics with Majorana fermion interferometry in spin-orbit-coupled semiconductors”. In: *Phys. Rev. B* 84 (8 2011), p. 085109. DOI: 10.1103/PhysRevB.84.085109. URL: <https://link.aps.org/doi/10.1103/PhysRevB.84.085109>.
- [202] Lucile Savary and Leon Balents. “Quantum spin liquids: a review”. In: *Rep. Prog. Phys.* 80 (2017), p. 016502. DOI: <https://doi.org/10.1088/0034-4885/80/1/016502>.
- [203] Jian Shang, Yongfeng Wang, Min Chen, Jingxin Dai, Xiong Zhou, Julian Kuttner, Gerhard Hilt, Xiang Shao, J Michael Gottfried, and Kai Wu. “Assembling molecular Sierpinski triangle fractals”. In: *Nat. Chem.* 7.5 (2015), p. 389.
- [204] Hui Shao, Yan Qi Qin, Sylvain Capponi, Stefano Chesi, Zi Yang Meng, and Anders W. Sandvik. “Nearly Deconfined Spinon Excitations in the Square-Lattice Spin-1/2 Heisenberg Antiferromagnet”. In: *Phys. Rev. X* 7 (4 2017), p. 041072. DOI: 10.1103/PhysRevX.7.041072. URL: <https://link.aps.org/doi/10.1103/PhysRevX.7.041072>.

- [205] B. Sriram Shastry. “Exact solution of an $S = 1/2$ Heisenberg antiferromagnetic chain with long-ranged interactions”. In: *Phys. Rev. Lett.* 60 (7 1988), pp. 639–642. DOI: 10.1103/PhysRevLett.60.639. URL: <http://link.aps.org/doi/10.1103/PhysRevLett.60.639>.
- [206] D. Shechtman, I. Blech, D. Gratias, and J. W. Cahn. “Metallic Phase with Long-Range Orientational Order and No Translational Symmetry”. In: *Phys. Rev. Lett.* 53 (20 1984), pp. 1951–1953. DOI: 10.1103/PhysRevLett.53.1951. URL: <https://link.aps.org/doi/10.1103/PhysRevLett.53.1951>.
- [207] Tokuro Shimokawa and Hikaru Kawamura. “Ripple State in the Frustrated Honeycomb-Lattice Antiferromagnet”. In: *Phys. Rev. Lett.* 123 (5 2019), p. 057202. DOI: 10.1103/PhysRevLett.123.057202. URL: <https://link.aps.org/doi/10.1103/PhysRevLett.123.057202>.
- [208] Peter W Shor. “Fault-tolerant quantum computation”. In: *Proceedings of 37th Conference on Foundations of Computer Science*. IEEE. 1996, pp. 56–65.
- [209] S. L. Sondhi, S. M. Girvin, J. P. Carini, and D. Shahar. “Continuous quantum phase transitions”. In: *Rev. Mod. Phys.* 69 (1 1997), pp. 315–333. DOI: 10.1103/RevModPhys.69.315. URL: <https://link.aps.org/doi/10.1103/RevModPhys.69.315>.
- [210] Anders S. Sorensen, Eugene Demler, and Mikhail D. Lukin. “Fractional Quantum Hall States of Atoms in Optical Lattices”. In: *Phys. Rev. Lett.* 94 (8 2005), p. 086803. DOI: 10.1103/PhysRevLett.94.086803. URL: <https://link.aps.org/doi/10.1103/PhysRevLett.94.086803>.
- [211] Jean-Marie Stephan and Frank Pollmann. “Full counting statistics in the Haldane-Shastry chain”. In: *Phys. Rev. B* 95 (3 2017), p. 035119. DOI: 10.1103/PhysRevB.95.035119. URL: <http://link.aps.org/doi/10.1103/PhysRevB.95.035119>.
- [212] A. Sterdyniak, N. Regnault, and B. A. Bernevig. “Extracting Excitations from Model State Entanglement”. In: *Phys. Rev. Lett.* 106 (10 2011), p. 100405. DOI: 10.1103/PhysRevLett.106.100405. URL: <https://link.aps.org/doi/10.1103/PhysRevLett.106.100405>.
- [213] Guang-Yu Sun, Yan-Cheng Wang, Chen Fang, Yang Qi, Meng Cheng, and Zi Yang Meng. “Dynamical Signature of Symmetry Fractionalization in Frustrated Magnets”. In: *Phys. Rev. Lett.* 121 (7 2018), p. 077201. DOI: 10.1103/PhysRevLett.121.077201. URL: <https://link.aps.org/doi/10.1103/PhysRevLett.121.077201>.
- [214] Kai Sun, Zhengcheng Gu, Hosho Katsura, and S. Das Sarma. “Nearly Flatbands with Nontrivial Topology”. In: *Phys. Rev. Lett.* 106 (23 2011), p. 236803. DOI: 10.1103/PhysRevLett.106.236803. URL: <https://link.aps.org/doi/10.1103/PhysRevLett.106.236803>.
- [215] Bill Sutherland. “Quantum Many-Body Problem in One Dimension: Ground State”. In: *Journal of Mathematical Physics* 12.2 (1971), pp. 246–250.

- [216] Evelyn Tang, Jia-Wei Mei, and Xiao-Gang Wen. “High-Temperature Fractional Quantum Hall States”. In: *Phys. Rev. Lett.* 106 (23 2011), p. 236802. DOI: 10.1103/PhysRevLett.106.236802. URL: <https://link.aps.org/doi/10.1103/PhysRevLett.106.236802>.
- [217] R. Tao and F. D. M. Haldane. “Impurity effect, degeneracy, and topological invariant in the quantum Hall effect”. In: *Phys. Rev. B* 33 (6 1986), pp. 3844–3850. DOI: 10.1103/PhysRevB.33.3844. URL: <https://link.aps.org/doi/10.1103/PhysRevB.33.3844>.
- [218] Sumanta Tewari, S. Das Sarma, Chetan Nayak, Chuanwei Zhang, and P. Zoller. “Quantum Computation using Vortices and Majorana Zero Modes of a $p_x + ip_y$ Superfluid of Fermionic Cold Atoms”. In: *Phys. Rev. Lett.* 98 (1 2007), p. 010506. DOI: 10.1103/PhysRevLett.98.010506. URL: <https://link.aps.org/doi/10.1103/PhysRevLett.98.010506>.
- [219] R. Thomale, A. Sterdyniak, N. Regnault, and B. Andrei Bernevig. “Entanglement Gap and a New Principle of Adiabatic Continuity”. In: *Phys. Rev. Lett.* 104 (18 2010), p. 180502. DOI: 10.1103/PhysRevLett.104.180502. URL: <https://link.aps.org/doi/10.1103/PhysRevLett.104.180502>.
- [220] Csaba Toke and Jainendra K. Jain. “Understanding the $\frac{5}{2}$ Fractional Quantum Hall Effect without the Pfaffian Wave Function”. In: *Phys. Rev. Lett.* 96 (24 2006), p. 246805. DOI: 10.1103/PhysRevLett.96.246805. URL: <https://link.aps.org/doi/10.1103/PhysRevLett.96.246805>.
- [221] Csaba Toke, Nicolas Regnault, and Jainendra K. Jain. “Nature of Excitations of the $\frac{5}{2}$ Fractional Quantum Hall Effect”. In: *Phys. Rev. Lett.* 98 (3 2007), p. 036806. DOI: 10.1103/PhysRevLett.98.036806. URL: <https://link.aps.org/doi/10.1103/PhysRevLett.98.036806>.
- [222] Sin-itiro Tomonaga. “Remarks on Bloch’s method of sound waves applied to many-fermion problems”. In: *Progress of Theoretical Physics* 5.4 (1950), pp. 544–569.
- [223] Arlei Prestes Tonel, Angela Foerster, Jon Links, and Andre Luiz Malvezzi. “Integrable anisotropic spin-ladder model”. In: *Phys. Rev. B* 64 (5 2001), p. 054420. DOI: 10.1103/PhysRevB.64.054420. URL: <https://link.aps.org/doi/10.1103/PhysRevB.64.054420>.
- [224] David Tong. “Lectures on the Quantum Hall Effect”. In: *arXiv:1606.06687v2* (2016). URL: <http://www.damtp.cam.ac.uk/user/tong/qhe.html>.
- [225] Daniel C Tsui, Horst L Stormer, and Arthur C Gossard. “Two-dimensional magnetotransport in the extreme quantum limit”. In: *Physical Review Letters* 48.22 (1982), p. 1559.
- [226] Hirokazu Tsunetsugu, Takeo Fujiwara, Kazuo Ueda, and Tetsuji Tokihiro. “Electronic properties of the Penrose lattice. I. Energy spectrum and wave functions”. In: *Phys. Rev. B* 43 (11 1991), pp. 8879–8891. DOI: 10.1103/PhysRevB.43.8879. URL: <https://link.aps.org/doi/10.1103/PhysRevB.43.8879>.

- [227] Hong-Hao Tu, Anne E B Nielsen, J Ignacio Cirac, and German Sierra. “Lattice Laughlin states of bosons and fermions at filling fractions $1/q$ ”. In: *New Journal of Physics* 16.3 (2014), p. 033025. URL: <http://stacks.iop.org/1367-2630/16/i=3/a=033025>.
- [228] Hong-Hao Tu and German Sierra. “Infinite matrix product states, boundary conformal field theory, and the open Haldane-Shastry model”. In: *Phys. Rev. B* 92 (4 2015), p. 041119. DOI: 10.1103/PhysRevB.92.041119. URL: <https://link.aps.org/doi/10.1103/PhysRevB.92.041119>.
- [229] Kazuki Uematsu and Hikaru Kawamura. “Randomness-Induced Quantum Spin Liquid Behavior in the $s = 1/2$ Random-Bond Heisenberg Antiferromagnet on the Pyrochlore Lattice”. In: *Phys. Rev. Lett.* 123 (8 2019), p. 087201. DOI: 10.1103/PhysRevLett.123.087201. URL: <https://link.aps.org/doi/10.1103/PhysRevLett.123.087201>.
- [230] Laurens Vanderstraeten, Maarten Van Damme, Hans Peter Buchler, and Frank Verstraete. “Quasiparticles in Quantum Spin Chains with Long-Range Interactions”. In: *Phys. Rev. Lett.* 121 (9 2018), p. 090603. DOI: 10.1103/PhysRevLett.121.090603. URL: <https://link.aps.org/doi/10.1103/PhysRevLett.121.090603>.
- [231] Daniel Varjas, Alexander Lau, Kim Pöyhönen, Anton R Akhmerov, Dmitry I Pikulin, and Ion Cosma Fulga. “Topological phases without crystalline counterparts”. In: *arXiv preprint arXiv:1904.07242* (2019).
- [232] Christopher N. Varney, Kai Sun, Victor Galitski, and Marcos Rigol. “Kaleidoscope of Exotic Quantum Phases in a Frustrated XY Model”. In: *Phys. Rev. Lett.* 107 (7 2011), p. 077201. DOI: 10.1103/PhysRevLett.107.077201. URL: <https://link.aps.org/doi/10.1103/PhysRevLett.107.077201>.
- [233] Edo van Veen, Shengjun Yuan, Mikhail I Katsnelson, Marco Polini, and Andrea Tomadin. “Quantum transport in Sierpinski carpets”. In: *Phys. Rev. B* 93.11 (2016), p. 115428.
- [234] L. P. Vivek Venkatachalam, A Yacoby, and K. West. “Local charge of the $\nu = 5/2$ fractional quantum Hall state”. In: *Nature* 469 (2011).
- [235] Taras Verkholyak and Jozef Strevcka. “Quantum phase transitions in the exactly solved spin-1/2 Heisenberg–Ising ladder”. In: *Journal of Physics A: Mathematical and Theoretical* 45.30 (2012), p. 305001.
- [236] G. Vidal, J. I. Latorre, E. Rico, and A. Kitaev. “Entanglement in Quantum Critical Phenomena”. In: *Phys. Rev. Lett.* 90 (22 2003), p. 227902. DOI: 10.1103/PhysRevLett.90.227902. URL: <https://link.aps.org/doi/10.1103/PhysRevLett.90.227902>.
- [237] Julien Vidal, Sébastien Dusuel, and Kai Phillip Schmidt. “Low-energy effective theory of the toric code model in a parallel magnetic field”. In: *Phys. Rev. B* 79 (3 2009), p. 033109. DOI: 10.1103/PhysRevB.79.033109. URL: <https://link.aps.org/doi/10.1103/PhysRevB.79.033109>.

- [238] Julien Vidal, Ronny Thomale, Kai Phillip Schmidt, and Sébastien Dusuel. “Self-duality and bound states of the toric code model in a transverse field”. In: *Phys. Rev. B* 80 (8 2009), 081104(R). DOI: 10.1103/PhysRevB.80.081104. URL: <https://link.aps.org/doi/10.1103/PhysRevB.80.081104>.
- [239] Konrad Viebahn, Matteo Sbroscia, Edward Carter, Jr-Chiun Yu, and Ulrich Schneider. “Matter-Wave Diffraction from a Quasicrystalline Optical Lattice”. In: *Phys. Rev. Lett.* 122 (11 2019), p. 110404. DOI: 10.1103/PhysRevLett.122.110404. URL: <https://link.aps.org/doi/10.1103/PhysRevLett.122.110404>.
- [240] Steurer Walter and Sofia Deloudi. *Crystallography of quasicrystals: concepts, methods and structures*. Vol. 126. Springer Science & Business Media, 2009.
- [241] Jie Wang, Scott D. Geraedts, E. H. Rezayi, and F. D. M. Haldane. “Lattice Monte Carlo for Quantum Hall States on a Torus”. In: *arXiv preprint arXiv:1710.09729* (2017).
- [242] Ling Wang, Didier Poilblanc, Zheng-Cheng Gu, Xiao-Gang Wen, and Frank Verstraete. “Constructing a Gapless Spin-Liquid State for the Spin-1/2 $J_1 - J_2$ Heisenberg Model on a Square Lattice”. In: *Phys. Rev. Lett.* 111 (3 2013), p. 037202. DOI: 10.1103/PhysRevLett.111.037202. URL: <https://link.aps.org/doi/10.1103/PhysRevLett.111.037202>.
- [243] Ling Wang and Anders W. Sandvik. “Critical Level Crossings and Gapless Spin Liquid in the Square-Lattice Spin-1/2 $J_1 - J_2$ Heisenberg Antiferromagnet”. In: *Phys. Rev. Lett.* 121 (10 2018), p. 107202. DOI: 10.1103/PhysRevLett.121.107202. URL: <https://link.aps.org/doi/10.1103/PhysRevLett.121.107202>.
- [244] Y. Wang, S. Subhankar, P. Bienias, M. Lacki, T-C. Tsui, M. A. Baranov, A. V. Gorshkov, P. Zoller, J. V. Porto, and S. L. Rolston. “Dark State Optical Lattice with a Subwavelength Spatial Structure”. In: *Phys. Rev. Lett.* 120 (8 2018), p. 083601. DOI: 10.1103/PhysRevLett.120.083601. URL: <https://link.aps.org/doi/10.1103/PhysRevLett.120.083601>.
- [245] Yan-Cheng Wang, Xue-Feng Zhang, Frank Pollmann, Meng Cheng, and Zi Yang Meng. “Quantum Spin Liquid with Even Ising Gauge Field Structure on Kagome Lattice”. In: *Phys. Rev. Lett.* 121 (5 2018), p. 057202. DOI: 10.1103/PhysRevLett.121.057202. URL: <https://link.aps.org/doi/10.1103/PhysRevLett.121.057202>.
- [246] Yi-Fei Wang, Zheng-Cheng Gu, Chang-De Gong, and D. N. Sheng. “Fractional Quantum Hall Effect of Hard-Core Bosons in Topological Flat Bands”. In: *Phys. Rev. Lett.* 107 (14 2011), p. 146803. DOI: 10.1103/PhysRevLett.107.146803. URL: <https://link.aps.org/doi/10.1103/PhysRevLett.107.146803>.
- [247] Yi-Fei Wang, Hong Yao, Zheng-Cheng Gu, Chang-De Gong, and D. N. Sheng. “Non-Abelian Quantum Hall Effect in Topological Flat Bands”. In: *Phys. Rev. Lett.* 108 (12 2012), p. 126805. DOI: 10.1103/PhysRevLett.108.126805. URL: <https://link.aps.org/doi/10.1103/PhysRevLett.108.126805>.
- [248] Yupeng Wang. “Exact solution of a spin-ladder model”. In: *Phys. Rev. B* 60.13 (1999), p. 9236.

- [249] Christof Weitenberg, Manuel Endres, Jacob F Sherson, Marc Cheneau, Peter Schauß, Takeshi Fukuhara, Immanuel Bloch, and Stefan Kuhr. “Single-spin addressing in an atomic Mott insulator”. In: *Nature* 471.7338 (2011), p. 319.
- [250] X. G. Wen and Q. Niu. “Ground-state degeneracy of the fractional quantum Hall states in the presence of a random potential and on high-genus Riemann surfaces”. In: *Phys. Rev. B* 41 (13 1990), pp. 9377–9396. DOI: 10.1103/PhysRevB.41.9377. URL: <https://link.aps.org/doi/10.1103/PhysRevB.41.9377>.
- [251] Xiao-Gang Wen. “Colloquium: Zoo of quantum-topological phases of matter”. In: *Rev. Mod. Phys.* 89 (4 2017), p. 041004. DOI: 10.1103/RevModPhys.89.041004. URL: <https://link.aps.org/doi/10.1103/RevModPhys.89.041004>.
- [252] Xiao-Gang Wen. “Quantum orders and symmetric spin liquids”. In: *Phys. Rev. B* 65 (16 2002), p. 165113. DOI: 10.1103/PhysRevB.65.165113. URL: <https://link.aps.org/doi/10.1103/PhysRevB.65.165113>.
- [253] Krauth Werner. “Four lectures on computational statistical physics”. In: *arXiv:0901.2496* (2009).
- [254] Tom Westerhout, Edo van Veen, Mikhail I Katsnelson, and Shengjun Yuan. “Plasmon confinement in fractal quantum systems”. In: *Phys. Rev. B* 97.20 (2018), p. 205434.
- [255] Frank Wilczek. “Magnetic Flux, Angular Momentum, and Statistics”. In: *Phys. Rev. Lett.* 48 (1982), pp. 1144–1146. DOI: 10.1103/PhysRevLett.48.1144.
- [256] Julia Wildeboer, Sourav Manna, and Anne E. B. Nielsen. “Anyonic excitations of hardcore anyons”. In: *arXiv preprint arXiv:1711.00845* (2017).
- [257] Julia Wildeboer, Alexander Seidel, and Roger G. Melko. “Entanglement entropy and topological order in resonating valence-bond quantum spin liquids”. In: *Phys. Rev. B* 95 (10 2017), p. 100402. DOI: 10.1103/PhysRevB.95.100402. URL: <https://link.aps.org/doi/10.1103/PhysRevB.95.100402>.
- [258] R. Willett, J. P. Eisenstein, H. L. Störmer, D. C. Tsui, A. C. Gossard, and J. H. English. “Observation of an even-denominator quantum number in the fractional quantum Hall effect”. In: *Phys. Rev. Lett.* 59 (15 1987), pp. 1776–1779. DOI: 10.1103/PhysRevLett.59.1776. URL: <https://link.aps.org/doi/10.1103/PhysRevLett.59.1776>.
- [259] Arkadiusz Wojs, Csaba Toke, and Jainendra K. Jain. “Landau-Level Mixing and the Emergence of Pfaffian Excitations for the $5/2$ Fractional Quantum Hall Effect”. In: *Phys. Rev. Lett.* 105 (9 2010), p. 096802. DOI: 10.1103/PhysRevLett.105.096802. URL: <https://link.aps.org/doi/10.1103/PhysRevLett.105.096802>.
- [260] Yang-Le Wu, B. Andrei Bernevig, and N. Regnault. “Zoology of fractional Chern insulators”. In: *Phys. Rev. B* 85 (7 2012), p. 075116. DOI: 10.1103/PhysRevB.85.075116. URL: <https://link.aps.org/doi/10.1103/PhysRevB.85.075116>.

- [261] Yang-Le Wu, B. Estienne, N. Regnault, and B. Andrei Bernevig. “Braiding Non-Abelian Quasiholes in Fractional Quantum Hall States”. In: *Phys. Rev. Lett.* 113 (11 2014), p. 116801. DOI: 10.1103/PhysRevLett.113.116801. URL: <https://link.aps.org/doi/10.1103/PhysRevLett.113.116801>.
- [262] Yang-Le Wu, B. Estienne, N. Regnault, and B. Andrei Bernevig. “Braiding Non-Abelian Quasiholes in Fractional Quantum Hall States”. In: *Phys. Rev. Lett.* 113 (11 2014), p. 116801. DOI: 10.1103/PhysRevLett.113.116801. URL: <https://link.aps.org/doi/10.1103/PhysRevLett.113.116801>.
- [263] Bo Yang and F. D. M. Haldane. “Nature of Quasielectrons and the Continuum of Neutral Bulk Excitations in Laughlin Quantum Hall Fluids”. In: *Phys. Rev. Lett.* 112 (2 2014), p. 026804. DOI: 10.1103/PhysRevLett.112.026804. URL: <https://link.aps.org/doi/10.1103/PhysRevLett.112.026804>.
- [264] C. N. Yang. “The Spontaneous Magnetization of a Two-Dimensional Ising Model”. In: *Phys. Rev.* 85 (5 1952), pp. 808–816. DOI: 10.1103/PhysRev.85.808. URL: <http://link.aps.org/doi/10.1103/PhysRev.85.808>.
- [265] N. Y. Yao, A. V. Gorshkov, C. R. Laumann, A. M. Läuchli, J. Ye, and M. D. Lukin. “Realizing Fractional Chern Insulators in Dipolar Spin Systems”. In: *Phys. Rev. Lett.* 110 (18 2013), p. 185302. DOI: 10.1103/PhysRevLett.110.185302. URL: <https://link.aps.org/doi/10.1103/PhysRevLett.110.185302>.
- [266] Hangmo Yi. “Quantum critical behavior of the quantum Ising model on fractal lattices”. In: *Phys. Rev. E* 91 (1 2015), p. 012118. DOI: 10.1103/PhysRevE.91.012118. URL: <https://link.aps.org/doi/10.1103/PhysRevE.91.012118>.
- [267] Tsuneya Yoshida, Koji Kudo, and Yasuhiro Hatsugai. “Non-Hermitian fractional quantum Hall states”. In: *Scientific Reports* 9 (16895 2019). DOI: 10.1038/s41598-019-53253-8. URL: <https://doi.org/10.1038/s41598-019-53253-8>.
- [268] Shun-Li Yu, Wei Wang, Zhao-Yang Dong, Zi-Jian Yao, and Jian-Xin Li. “Deconfinement of spinons in frustrated spin systems: Spectral perspective”. In: *Phys. Rev. B* 98 (13 2018), p. 134410. DOI: 10.1103/PhysRevB.98.134410. URL: <https://link.aps.org/doi/10.1103/PhysRevB.98.134410>.
- [269] Mohammad Hossein Zarei. “Ising order parameter and topological phase transitions: Toric code in a uniform magnetic field”. In: *Phys. Rev. B* 100 (12 2019), p. 125159. DOI: 10.1103/PhysRevB.100.125159. URL: <https://link.aps.org/doi/10.1103/PhysRevB.100.125159>.
- [270] Qi-Bo Zeng, Yan-Bin Yang, and Yong Xu. “Topological Phases in Non-Hermitian Aubry-Andre-Harper Models”. In: *arXiv preprint arXiv:1901.08060* (2019).
- [271] Tian-Sheng Zeng and D. N. Sheng. “SU(N) fractional quantum Hall effects in topological flat bands”. In: *arXiv:1710.11526v1* (2017).

- [272] Shu Zhang, Hitesh J. Changlani, Kemp W. Plumb, Oleg Tchernyshyov, and Roderich Moessner. “Dynamical Structure Factor of the Three-Dimensional Quantum Spin Liquid Candidate $\text{NaCaNi}_2\text{F}_7$ ”. In: *Phys. Rev. Lett.* 122 (16 2019), p. 167203. DOI: 10.1103/PhysRevLett.122.167203. URL: <https://link.aps.org/doi/10.1103/PhysRevLett.122.167203>.
- [273] Yuhe Zhang, G. J. Sreejith, N. D. Gemelke, and J. K. Jain. “Fractional Angular Momentum in Cold-Atom Systems”. In: *Phys. Rev. Lett.* 113 (16 2014), p. 160404. DOI: 10.1103/PhysRevLett.113.160404. URL: <https://link.aps.org/doi/10.1103/PhysRevLett.113.160404>.
- [274] Yuhe Zhang, G. J. Sreejith, and J. K. Jain. “Creating and manipulating non-Abelian anyons in cold atom systems using auxiliary bosons”. In: *Phys. Rev. B* 92 (7 2015), p. 075116. DOI: 10.1103/PhysRevB.92.075116. URL: <https://link.aps.org/doi/10.1103/PhysRevB.92.075116>.
- [275] Zheng Zhu, Inti Sodemann, D. N. Sheng, and Liang Fu. “Anisotropy-driven transition from the Moore-Read state to quantum Hall stripes”. In: *Phys. Rev. B* 95 (20 2017), p. 201116. DOI: 10.1103/PhysRevB.95.201116. URL: <https://link.aps.org/doi/10.1103/PhysRevB.95.201116>.
- [276] Zhenyue Zhu, David A. Huse, and Steven R. White. “Unexpected z -Direction Ising Antiferromagnetic Order in a Frustrated Spin-1/2 $J_1 - J_2$ XY Model on the Honeycomb Lattice”. In: *Phys. Rev. Lett.* 111 (25 2013), p. 257201. DOI: 10.1103/PhysRevLett.111.257201. URL: <https://link.aps.org/doi/10.1103/PhysRevLett.111.257201>.
- [277] Zhenyue Zhu, P. A. Maksimov, Steven R. White, and A. L. Chernyshev. “Topology of Spin Liquids on a Triangular Lattice”. In: *Phys. Rev. Lett.* 120 (20 2018), p. 207203. DOI: 10.1103/PhysRevLett.120.207203. URL: <https://link.aps.org/doi/10.1103/PhysRevLett.120.207203>.
- [278] O. S. Zozulya, M. Haque, K. Schoutens, and E. H. Rezayi. “Bipartite entanglement entropy in fractional quantum Hall states”. In: *Phys. Rev. B* 76 (12 2007), p. 125310. DOI: 10.1103/PhysRevB.76.125310. URL: <https://link.aps.org/doi/10.1103/PhysRevB.76.125310>.

Declaration of Authorship

Erklärung :

Hiermit versichere ich, dass ich die vorliegende Arbeit ohne unzulässige Hilfe Dritter und ohne Benutzung anderer als der angegebenen Hilfsmittel angefertigt habe; die aus fremden Quellen direkt oder indirekt bernommenen Gedanken sind als solche kenntlich gemacht. Die Arbeit wurde bisher weder im Inland noch im Ausland in gleicher oder hnlicher Form einer anderen Prüfungsbehörde vorgelegt. Diese Arbeiten wurden unter der Leitung von Dr. Anne E. B. Nielsen und Prof. Dr. Roderich Moessner am Max-Planck-Institut für Physik komplexer Systeme in Dresden durchgeführt. Ich erkläre hiermit, dass keine früheren erfolglosen Promotionsverfahren stattgefunden haben. Ich erkenne die Promotionsordnung der Fakultät für Mathematik und Naturwissenschaften der Technische Universität Dresden an.

Unterschrift :

Ort, Datum :

